Durham E-Theses

Investigation of the grain boundary layer characteristics of donor doped barium titanate ceramics.

Illingsworth, J S.

How to cite:

Illingsworth, J S. (1990) *Investigation of the grain boundary layer characteristics of donor doped barium titanate ceramics.*, Durham theses, Durham University. Available at Durham E-Theses Online: http://etheses.dur.ac.uk/1118/

Use policy

The full-text may be used and/or reproduced, and given to third parties in any format or medium, without prior permission or charge, for personal research or study, educational, or not-for-profit purposes provided that:

- a full bibliographic reference is made to the original source
- a link is made to the metadata record in Durham E-Theses
- the full-text is not changed in any way

The full-text must not be sold in any format or medium without the formal permission of the copyright holders.

Please consult the full Durham E-Theses policy for further details.

Academic Support Office, Durham University, University Office, Old Elvet, Durham DH1 3HP
e-mail: e-theses.admin@dur.ac.uk Tel: +44 0191 334 6107
http://etheses.dur.ac.uk

The copyright of this thesis rests with the author.
No quotation from it should be published without
his prior written consent and information derived
from it should be acknowledged.

INVESTIGATION OF THE GRAIN BOUNDARY LAYER CHARACTERISTICS OF DONOR DOPED BARIUM TITANATE CERAMICS

by

J.S. ILLINGSWORTH BSc., A.M.I.M., M. I. Ceram.

A thesis submitted for the degree of

Doctor of Philosophy in the

University of Durham

September 1990

UNIV DURHAM
25 APR 1991

BEST COPY

AVAILABLE

Variable print quality

ABSTRACT

Donor doped barium titanate ceramics are well known for their Positive Temperature Coefficient of Resistance (PTCR) characteristic above the crystallographic transition temperature, T_c ~130°C, where the material changes from the ferroelectric state to paraelectric. The shape and magnitude of the PTCR characteristic are known to be dependent on the composition and preparation of the ceramic, the presence of impurities, particularly donor dopant concentration and acceptor ions, and the sintering conditions. Thirty years ago Heywang proposed a model based on the presence of two-dimensional resistive grain boundary layers consisting of discrete electron traps located in energy between the conduction and valence bands, to explain the PTCR effect.

Donor doped barium titanate samples were prepared in a number of different ways: the variation of donor concentration, the addition of impurity acceptor ions, reduction of the sintering temperature and variation of the sintering atmosphere. These samples were investigated by examining their microstructure and their electric and dielectric properties, both at room temperature and above the transition. Theoretical analysis of the experimental results, based on the Heywang model, was then performed to investigate the effects of preparation on the grain boundary layer characteristics.

Resistivity - temperature measurements were carried out to find the effect of composition and sintering conditions on the PTCR characteristic and capacitance - temperature measurements demonstrated the effects of donor and acceptor incorporation on the dielectric properties of barium titanate. Grain boundary and grain bulk resistance were separated by means of a.c. impedance methods at room temperature, where the effects of composition and sintering on each were observed. Finally, current - voltage measurements between T_c and the resistivity maximum were made for samples containing different donor concentrations, to examine the current conduction mechanism.

Detailed analysis of the electric and dielectric measurements permitted the effects of composition and sintering on the grain boundary layer characteristics to be determined. Acceptor state densities were estimated using the resistivity - temperature measurements and capacitance - temperature results, between T_c and the resistivity maximum. Resistivity - temperature measurements above the maximum enabled acceptor energies to be estimated. Analysis of the dielectric properties showed that neither the composition nor sintering atmosphere affected the dielectric properties of the grain boundary layers, which were found to obey the Curie-Weiss law above the transition temperature in the same way as the grain bulk. The observed effects of the changes in the preparative conditions to the electric and dielectric properties were explained in terms of the Heywang model and microstructural development, resulting from modifications to the grain boundary layers.

The conduction mechanism was examined by means of current - voltage measurements above the transition temperature and below the resistivity maximum. In contrast to the prediction of Heywang. this was found to be predominantly diffusion limited.

DECLARATION

I declare that the work reported in this thesis, unless otherwise stated, was carried out by the candidate, that it has not previously been submitted for any degree and that it is not currently being submitted for any other degree.

Dr. A. W. Brinkman

Supervisor

J. Illingsworth

Candidate

ACKNOWLEDGEMENTS

My appreciation goes to Dr. A.W. Brinkman, my supervisor, and Dr. H.M. Al-Allak for their invaluable support of my research work. I would also like to thank Drs T. Hashemi and K. Durose and Prof. J. Woods for their advice and helpful discussions during the preparation of this thesis and the technical staff of the School of Engineering and Applied Science for their ever enthusiastic help and assistance whenever necessary. My thanks also go to Elmwood Sensors Ltd., my employers, and especially Mr. P. Thompson, for their financial support and for allowing me the time for writing up. I would also like to express my pleasure at their finding many commercial uses for many of my results.

Thanks also extend to Mrs. K. Seaton and Ms. J. Morgan for their preparation of the drawings and photographs, to Miss. S. Swainston for typing the tables and to Mr. N. Arrowsmith for proof reading.

Finally, I would like to express gratitude to my husband, Tony, and the rest of my family for their encouragement and support, particularly during the writing of this thesis.

CONTENTS

CHAPTER ONE

INTRODUCTION TO BARIUM TITANATE PTCR CERAMICS

Pure barium titanate is a ferroelectric, dielectric material and in its ceramic form finds application within capacitor and piezoelectric technologies. Upon the addition of a small amount of a suitable metal oxide as a donor dopant (e.g. La_2O_3 or Nb_2O_5) the ceramic becomes semiconducting at room temperature and exhibits a very large resistivity rise, of between 3 and 7 orders of magnitude, within a few degrees above its ferroelectric transition temperature, ~130°C. This so-called Positive Temperature Coefficient of Resistance (PTCR) effect finds many applications in the field of sensor and heater technologies; for example, a PTCR device can be used as a self-regulating heater, a temperature switch, a protector against current surges and a reusable fuse. Each application utilizes the steep resistivity increase in some way and each device can be optimised in order to achieve the best performance for its application.

In order to understand this anomalous resistivity behaviour it is important to characterise the various material properties observed in ceramic barium titanate. These may include crystallographic, microstructural, dielectric and electric properties. The effects of such material properties upon the addition of the donor dopant may then be expected to lead to an explanation and a good understanding of the PTCR effect.

1.1 FERROELECTRIC MATERIALS

Crystalline materials are normally classed in terms of their crystallographic structure. The seven crystal systems, which initially describe geometry, are cubic, monoclinic, tetragonal, hexagonal, triclinic, trigonal and monoclinic and may be divided according to their symmetry with regard to a point, into 32 point groups (crystal classes). Eleven of these classes are characterized by the existence of a

centre of symmetry and are called centrosymmetric. Of the 21 nonsymmetric crystal classes, 20 contain one or more polar axes and thus exhibit electrical polarity upon the application of a stress. This is the piezoelelectric effect and is characterized by the flow of charge when the material is subject to stress, the direction of which is reversed upon stress in the opposite direction. Similarly, when an electric field is applied across a piezoelectric, a mechanical displacement is observed.

Half of the piezoelectric crystals have more than one crystal axis along which the dipoles may arrange themselves under an electric field. The remainder have only one such axis and display an additional feature known as spontaneous polarization, where the dipoles continue to exist in the absence of an electric field or mechanical stress. These permanent dipoles are associated with a charge present on the surface of the material, the magnitude of which is dependent on the number of dipoles per unit area (i.e. the magnitude of the spontaneous polarisation). Such charge, however, is undetectable at any one temperature because of the effects of compensation by mobile charges, either in the surrounding medium or in the bulk of the material itself. The magnitude of the spontaneous polarization, and hence the surface charge density, is dependent on temperature. As temperature is changed the variation in charge density, and consequently spontaneous polarization, may be detected. This is the pyroelectric effect and the ten polar crystal classes are also described as pyroelectrics.

Upon reversal of the direction of the applied electric field some pyroelectric materials show changes in the direction of polarization, i.e. the dipoles rotate to align themselves with the direction of the field. The resulting hysteresis between polarization and electric field resembles the hysteresis between field and magnetization of ferromagnets and has led to the adoption of the term 'ferroelectrics' to describe these materials.

One characteristic of ferroelectric materials concerns the compensation of the surface charge arising from the spontaneous polarization. Within the material the

(second order) and depends on the temperature dependence of one of the parameters d and ϕ. For a first order transition, d or ϕ changes discontinuously at T_c and the displacement is imposed suddenly at this temperature, the transition itself taking place within a few degrees of T_c. In contrast, the second order transition is characterized by a continuous function of d or ϕ with temperature and the transition takes place in the vicinity of T_c. According to ferroelectric theory[1.1], the phase transition of a ferroelectric material can be described in terms of the Gibbs elastic function, G_1 and the polarization, P. The temperature dependence of P affects the value of G_1 and leads to the definition of the order of the transition. Where there is a first order transition, at $T \sim T_c$, there are three possible states where G_1 is minimum, i.e. the crystal is stable, at $P = 0$ and $P = +/-P_s$, where P_s is the magnitude of the spontaneous polarization. When $T > T_c$ there is only one such state, where $P = 0$. At T_c all three states have equal energy and the stable state of the crystal can jump between $P = 0$ and $P = P_s$. As temperature is raised the minimum corresponding to $P = 0$ becomes deeper than those with $P = P_s$, indicating that the non-polar phase is more stable than the ferroelectric one. Eventually the two ferroelectric minima disappear and only the paraelectric state is stable. Because of the presence of the metastable minima in G_1 close to T_c, some hysteresis of the transition may be observed, where the minimum temperature of hysteresis is defined as θ, the Curie point. A second order transition is characterized by the gradual change between the presence of two minima of G_1, at $P = +/-P_s$, to one, at $P = 0$. The transition, therefore, is continuous since P_s undergoes a continuous change as temperature is raised through T_c. No hysteresis is observed and the Curie temperature is defined as that at which the two minima of G_1 converge into one, at $P = 0$.

Each type of phase transition may also be described in terms of their dielectric behaviour in the vicinity of T_c. In particular, the behaviour of permittivity, ϵ', and its reciprocal, $1/\epsilon'$, highlight the nature of the transition. Where the phase

change is discontinuous, $1/\epsilon'$ is observed to decrease slowly, in the ferroelectric phase, as T_c is approached. At the Curie temperature $1/\epsilon'$ drops sharply and then, upon further increase of temperature, rises linearly, in accordance with the Curie-Weiss law, shown schematically in figure 1.2.a. The value of θ, the Curie Point, is given by the extrapolated intercept on the temperature axis while C, the Curie constant, is obtained from the gradient of the linear portion. The dielectric behaviour of a material having a continuous phase change, on the other hand, is shown in figure 1.2.b. The value of $1/\epsilon'$ in the ferroelectric phase falls linearly with temperature towards T_c and then rises in accordance with the Curie-Weiss law as temperature is raised further. There is no sudden drop of $1/\epsilon'$ and the Curie temperature, T_c, and Curie point, θ, coincide. The value of the Curie constant is also given by the gradient of the linear portion above T_c.

1.2 BARIUM TITANATE

Ceramic barium titanate, $BaTiO_3$, is a pale yellow, translucent, insulating material and a ferroelectric, belonging to the crystallographic family of perovskites. The family is named after the mineral perovskite, $CaTiO_3$, each member having the same basic, cubic structure. Below its Curie temperature, T_c, ~120°C, barium titanate exhibits properties typical of ferroelectrics, i.e. hysteresis between polarization and electric field, the pyroelectric effect and piezoelectricity. It is different from some other ferroelectric materials because it exhibits three phase changes, two of which take place below the Curie temperature and are minor. Above T_c the cubic perovskite phase, which is centrosymmetric and non-polar, is stable. In crystallographic terms, the cubic perovskite structure may be described as a close-packed arrangement of Ba^{2+} and O^{2-} ions with Ti^{4+} ions in the octahedral interstices, see figure 1.3. Below 120°C the stable phase is tetragonal and polar, where the polar direction is parallel to a cubic ⟨100⟩ direction. The tetragonal phase is often illustrated in terms of the cubic phase, where one

of the cubic axes has been elongated slightly to give a non-symmetric structure with its polar direction parallel to the elongated axis, as shown schematically in figure 1.4.a. Below 5°C a non-symmetric (polar) orthorhombic phase is stable, which has its polar direction parallel to one of the cubic ⟨110⟩ directions. This phase may be illustrated in terms of the cubic phase, where the unit cell has been distorted as shown schematically in figure 1.4.b. Finally, below -90°C the fourth, rhombohedral, phase is prefered. Also being non-symmetric, this too is polar and ferroelectric, where the polar direction is parallel to a cubic ⟨111⟩ direction. The translation of the original cubic unit cell is shown in figure 1.4.c, where each axis has been distorted in comparison to the tetragonal and orthorhombic phases.

Extensive studies of the dielectric and ferroelectric properties of ceramic barium titanate can be found in the literature[1.1–1.3]. In particular, some workers have observed the relative permittivity (ϵ') of barium titanate to be dependent on grain size: a ceramic with grains $\sim 1\mu$m has been reported to have a value of ϵ' $\sim$6000 at room temperature[1.4.1.5], whereas coarse grains have been found to have much lower permittivity ($\sim$1500)[1.6]. In the ferroelectric phase the permittivity is approximately independent of temperature but at the phase transition temperature (T_c) it jumps suddenly by about an order of magnitude. Over the next 40 - 60°C above T_c it falls quickly, and as temperature is further increased it falls more slowly, reaching a value of $\sim$2000 towards 200°C, in accordance with the Curie-Weiss law, $\epsilon' = C/(T - \theta)$. In common with some other members of the perovskite family,[1.1,1.2] the phase change is discontinuous[1.7], as exhibited most clearly by the sharp drop in the value of $1/\epsilon'$ at $\sim$120°C and by the linear behaviour above T_c[1.8–1.10]. Values for C and θ have been reported in the literature for both ceramic and single-crystal $BaTiO_3$, and are affected by the purity and density of the material. The most widely accepted values for C and θ for the ceramic are given by Roberts[1.8] as 1.54×10^5K and 391K (118°C), respectively. The literature[1.1,1.2] cites values for C ranging from 1.5×10^5K to 6.5×10^5K and

θ between 380 and 391K.

The two minor phase changes below 120°C are also discontinuous, as demonstrated by small jumps of relative permittivity at 5°C and -90°C which are followed by ϵ' falling in a similar manner to Curie Weiss behaviour towards the next transition[1.11]. Figure 1.5 shows the behaviour of the relative permittivity of barium titanate as temperature is raised through each transition temperature.

The magnitude of the applied electric field has been reported[1.9,1.10] to affect dielectric and ferroelectric characteristics in the vicinity of T_c. In particular, spontaneous polarization may be induced within the non polar phase at temperatures above 120°C, depending on the magnitude of the field, the effective T_c being increased by 1.2×10^{-3}°C/V[1.9]. Thus the disappearance of the ferroelectric hysteresis is arrested and the position of the relative permittivity maximum is increased. Under very high fields these effects may be observed with some ease, although only a few degrees increase in temperature above T_c can be sustained before the transformation is more favourable and ferroelectric properties disappear.

1.3 DONOR DOPED BARIUM TITANATE

N-type semiconductivity may be induced in ceramic and single crystal barium titanate in one of two ways: the first is by the reduction of some of the Ti^{4+} ions to Ti^{3+}, thereby releasing an electron into donor levels close to the conduction band, by heat-treating the material in a reducing atmosphere. The alternative method is to add a small amount of donor ions which, upon dissolution in the lattice, have valency higher than that of the host ion. Commonly used dopants include La^{3+}, Ho^{3+}, Y^{3+}, which substitute for Ba^{2+} and Ta^{5+}, Nb^{5+}, which are accommodated on Ti^{4+} sites[1.12–1.14]. The incorporation of the donor ions into

the lattice is believed to be described by the following reactions[1.15]:

$$2(1-n)BaTiO_3 + nLa_2O_3 + 2nTiO_2 \leftrightarrow 2Ba_{1-n}La_nTiO_3 + n/2O_2 \qquad (1.1)$$

for lanthanum subsitution for barium ions, and

$$2(1-n)BaTiO_3 + nNb_2O_5 + 2nBaO \leftrightarrow 2BaTi_{1-n}Nb_nO_3 + n/2O_2 \qquad (1.2)$$

when niobium is incorporated onto titanium sites. The extra electron belonging to the dopant ion remains loosely bound and thus is readily excited into the conduction band, leaving a positively charged ion in the lattice. The results of Hall measurements[1.13,1.16,1.17] have been reported, from which the activation energy for conduction has been found to be ~0.1eV. The energy band diagram for semiconducting barium titanate is shown schematically in figure 1.6, where donor levels are situated approximately 0.1eV below the conduction band[1.16–1.19]. Semiconducting barium titanate, whether donor doped or heat-treated in a reducing atmosphere, is dark blue, although only *donor doped ceramic* barium titanate exhibits the PTCR effect at the phase transition temperature. Pure barium titanate annealed in a reducing atmosphere and single crystal donor doped barium titanate retain their low resistivity at all temperatures[1.13,1.20,1.21].

According to equations 1.1 and 1.2, oxygen is evolved during donor incorporation within the sintering process. Drofenik[1.22] has carried out a systematic investigation of the sintering behaviour of donor doped barium titanate ceramics and has reported[1.23] the evolution of oxygen in the quantities represented by these equations during sintering in a vacuum. He also reported that grain growth, which takes place during sintering, is dependent on the atmospheric oxygen partial pressure: the equilibrium constants, K, of equations 1.1 and 1.2 have been shown to be proportional to the oxygen partial pressure, p_{O_2}:

$$K \simeq p_{O_2} exp(\frac{-\Delta G}{RT}) \qquad (1.3)$$

where ΔG is the free energy change during oxygen release, R is the gas constant and T is absolute temperature. Consequently, the sintering process can be seen

to be enhanced under low oxygen pressures, i.e. the grains grow to larger sizes. In air, however, sintering is restricted by the large partial pressure of oxygen. Donor doped barium titanate has been reported to have small grains, in comparison to undoped barium titanate, which then have been observed to be reduced upon increasing the dopant concentration[1.24–1.28]. Evidently, the oxygen released during donor incorporation raises the local partial pressure, thus reducing the equilibrium constant of the reaction equation 1.1 or 1.2 and inhibiting grain growth[1.29].

As well as the reduction of grain size, the incorporation of donor dopant into barium titanate has been reported to exhibit additional effects, mostly regarding electrical and dielectric properties:

a.) As donor concentration is increased towards ~0.4 at%, the colour of the ceramic changes from grey or white to dark blue. Further increasing the amount of dopant results in the return of the grey colour, or a yellow colour[1.26,1.28,1.30].

b.) Accompanying the colour change is an unexpected effect of the resistivity: at low donor concentrations resistivity is reduced, in accordance with semiconductor theory. Above approximately 0.4 at% donor, however, it has been reported widely[1.16–1.19,1.25,1.26,1.28,1.30–1.33] to be increased.

c.) The resistivity of a donor doped barium titanate ceramic has been found to be dependent on the value of the applied voltage. This non-ohmic behaviour is characterised by an exponential reduction in resistivity with increasing applied electric field[1.16,1.18,1.19,1.34–1.39].

d.) The measured capacitance of a sample of donor doped barium titanate has been reported[1.16,1.18,1.19,1.40,1.41] to be more than an order of magnitude higher than that of a sample of undoped barium titanate having similar dimensions.

e.) Conditions of preparation of the ceramic, in particular sintering and cooling, have been observed to affect resistivity. Long sintering times and slow cooling have been shown[1.31,1.38,1.42–1.45] to increase resistivity. Heat-treatment in an atmosphere deficient in oxygen was found[1.19,1.30,1.31,1.42,1.43,1.45,1.46] to have the

effect of significantly lowering the resistivity. Heat-treatment in an oxidizing atmosphere, on the other hand, has been reported to have the effect of increasing resistivity[1.43,1.47].

f.) The addition of very small quantities of ions which have valency less than that of their host ion have been reported to act as acceptors and cause the resistivity to be raised[1.38,1.40,1.41,1.48–1.56]. Typical additional dopants include Mn^{2+}, Fe^{3+} and Al^{3+}, which are incorporated onto Ti^{4+} sites[1.53], for example in the following way when the donor dopant is lanthanum and the acceptor is manganese,

$$(1-p)Ba_{1-n}La_nTiO_3 + pMnCO_3 + pBaO + p/2La_2O_3 \leftrightarrow$$

$$Ba_{1-n}La_nTi_{1-p}Mn_pO_3 + pCO_2 + p/4O_2. \tag{1.4}$$

It is clear that these characteristics are connected with the incorporation of the donor dopant, since they are not observed in undoped barium titanate. A number of models have been proposed over the past 30 years to explain these observed effects and, in particular, to describe the mechanism by which the PTCR effect takes place. These models will be described and discussed in detail in the next chapter.

REFERENCES

1.1 Jona F. and Shirane G., *International Series of Monographs on Solid State Physics*, Volume 1, Ferroelectric Crystals, Ed. Smoluchowski R and Kurti N (Pergamom, New York), 1962.

1.2 Megaw H.D., *Ferroelectricity in Crystals*, (Methuen, London), 1957.

1.3 Mason W.P., *Molecular Science and Molecular Engineering*, Piezoelectric and Ferroelectric Devices, Ed. Von Hippel A. (John Wiley, New York), 1959.

1.4 Jonker G.H. and Noorlander W., Science of Ceramics I, Ed. Steward G.H. (Academic, London), 1962, p.255.

1.5 Martrinea H.T. and Burloot J.C., J. Phys. C: Sol. Stat. Phys., **7**, 3182, 1974.

1.6 Arlt G. and Peusens H., Ferroelectrics, **48**, 213, 1983.

1.7 Drougard M.E. and Young D.R., Phys. Rev., **95**, 1152, 1954.
(As quoted by Megaw, 1957 and Jona & Shirane, 1962)

1.8 Roberts S., Phys. Rev., **75**, 989, 1949.
(As quoted by Megaw, 1957 and Jona & Shirane, 1962)

1.9 Kanzig W. and Maikoff N., Helv. Phys. Acta., **24**, 343, 1951.
(As quoted by Megaw, 1957 and Jona & Shirane, 1962)

1.10 Merz W.J., Phys. Rev., **91**, 513, 1953.
(As quoted by Megaw, 1957 and Jona & Shirane, 1962)

1.11 Merz W.J., J. Phys. Rev., **76**, 1221, 1949.
(As quoted by Megaw, 1957 and Jona & Shirane, 1962)

1.12 Jonker G.H. and Havinga E.E., Mater. Res. Bull., **17**, 345, 1982.

1.13 Murakami T., Nakahara M, Miyashita T. and Ueda S., J. Am. Ceram. Soc., **56**, 291, 1973.

1.14 Schmeltz H., Phys. Stat. Sol., **31**, 121, 1969.

1.15 Drofenik M.H., J. Am. Ceram. Soc., **69**, C8, 1986.

1.16 Saburi O., J. Phys. Soc. Jpn., **14**, 1159, 1959.

1.17 Tennery V.J. and Cook R.L., J. Am. Ceram. Soc., **44**, 187, 1961.

1.18 Heywang W., Sol. Stat. Electron., **3**, 51, 1961.

1.19 Heywang W., J. Am. Ceram. Soc., **47**, 484, 1964.

1.20 Goodman G., J. Am. Ceram. Soc., **46**, 48, 1963.

1.21 Berglund C.N. and Baer W.S., Phys. Rev., **157**, 358, 1967.

1.22 Drofenik M.H., Pejovnik S., Irnanonik L., Mocnik I. and Krasevec V., *Proc 5th Int. Round Table Conference on Sintering*, Sintering - Theory and Practice, Mater. Sci. Monographs, **14**, 361, 1981.

1.23 Drofenik M.H., Popovic A., Irnanonok L., Kolar D. and Krasevec V., J. Am. Ceram. Soc., **65**, C203, 1982.

1.24 Ashida T and Toyoda H., Jpn. J. Appl. Phys., **5**, 269, 1966.

1.25 Murakami T., Miyashita T., Nakahara M and Sekine E., J. Am. Ceram. Soc., **56**, 294, 1973.

1.26 Fukami T. and Tsuchiya H., Jpn. J. Appl. Phys., **18**, 735, 1979.

1.27 Enomoto Y and Yamaji A., Ceram. Bull., **60**, 566, 1981.

1.28 Kleint C.A., Stöpel U. and Rost A., Phys. Stat. Sol. (a), **115**, 165, 1989.

1.29 Drofenik M.H., J. Am. Ceram. Soc., **70**, 311, 1987.

1.30 Kahn M., Ceram. Bull., **50**, 676, 1971.

1.31 Jonker G.H., Sol. Stat. Electron., **7**, 895, 1964.

1.32 Daniels J., Hardtl K.H. and Wernicke R., Philips Tech. Rev., **38**, 73, 1978/79.

1.33 Basu R.N. and Maiti H.S., Trans. Ind. Chem. Soc., **45**, 140, 1986.

1.34 Peria W.T., Bratschun W.R. and Fenity R.D., J. Am. Ceram. Soc., 44, 249, 1961.

1.35 Ikushima H. and Hayakawa S., Jpn. J. Appl. Phys., 4, 328. 1965.

1.36 Mallik G.T. and Emtage P.R., J. Appl. Phys., **39**, 3088. 1968.

1.37 Gerthsen P. and Hoffman B., Sol. Stat. Electron., **16**, 617, 1973.

1.38 Ihrig H. and Puschert W., J. Appl. Phys., **48**, 3081, 1977.

1.39 Nemoto H. and Oda I., J. Am. Ceram. Soc., **63**, 398, 1980.

1.40 Heywang W., J. Mater. Sci., **6**, 1214, 1971.

1.41 Kutty T.R.N. and Murugaraj P., Mater. Res. Bull., **20**, 1473, 1985.

1.42 Ueda I. and Ikegami S., J. Phys. Soc. Jpn., **20**, 546, 1965.

1.43 Jonker G.H., Mater. Res. Bull., **2**, 401, 1967.

1.44 Wernicke R., Phys. Stat. Sol. (a), **47**, 139, 1978.

1.45 Al-Allak H.M., Russell G.J. and Woods J., J. Phys. D: Appl. Phys., **20**, 1645, 1987.

1.46 Igarashi H., Hayakawa S. and Okazaki K., Jpn. J. Appl. Phys., **20**, Suppl.20-4, 135, 1981.

1.47 McChesney J.B. and Potter J.F., J. Am. Ceram. Soc., **48**, 81, 1965.

1.48 Brauer H., Z. Angew. Phys., **23**, 373, 1967.

1.49 Rheme H., Phys. Stat. Sol., **26**, K1, 1968.

1.50 Matsuoka T., Matsuo Y., Sasaki H. and Hayakawa S., J. Am. Ceram. Soc., **55**, 108, 1972.

1.51 Ueoka H., Ferroelectrics, **7**, 351, 1974.

1.52 Ueoka H. amd Yodogawa M., IEEE Trans. Manuf. Tech., **MFT-3**, 77, 1974.

1.53 Ihrig H., J. Phys. C: Sol. Stat. Phys., **11**, 819, 1978.

1.54 Ihrig H., J. Am. Ceram. Soc., **64**, 617, 1981.

1.55 Murugaraj P. and Kutty T.R.N., J. Mater. Sci. Lett., **5**, 171, 1986.

1.56 Cipollini N.E., Sowa J.M., Forbes C.E. and Lynch J.F., *Proc. 6^{th} IEEE Int. Symp. on Applications of Ferroelectrics*, Ed. Wood V. (IEEE, New York), 1986.

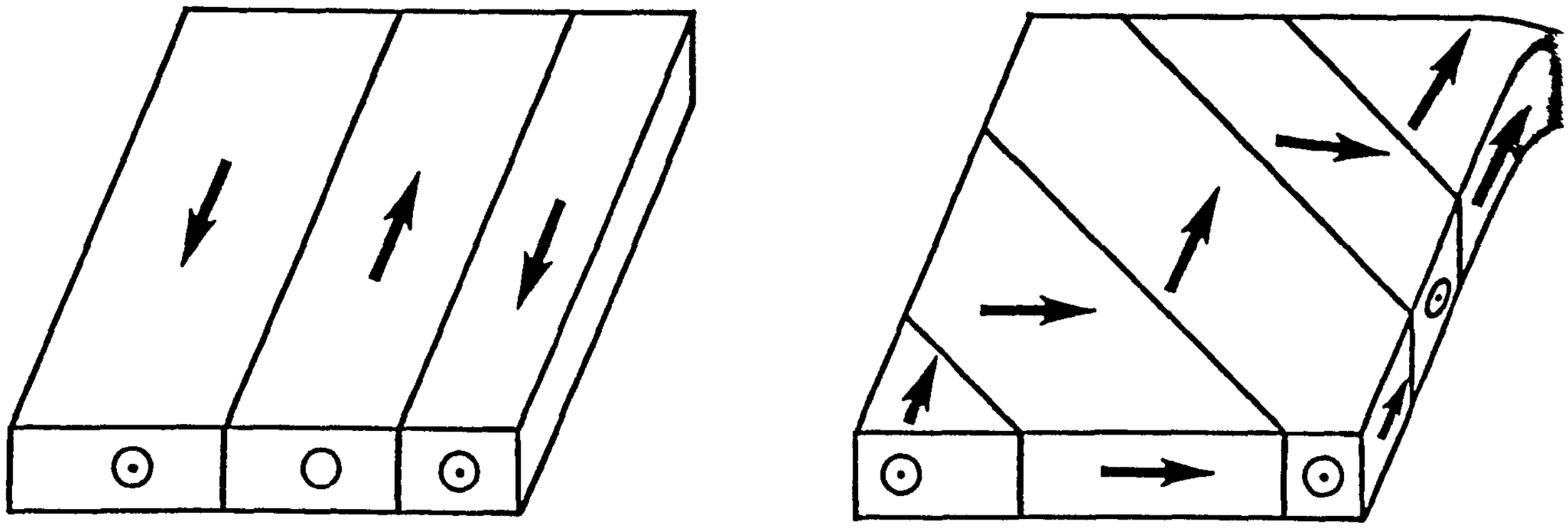

Figure 1.1 Orientation of typical ferroelectric domains.

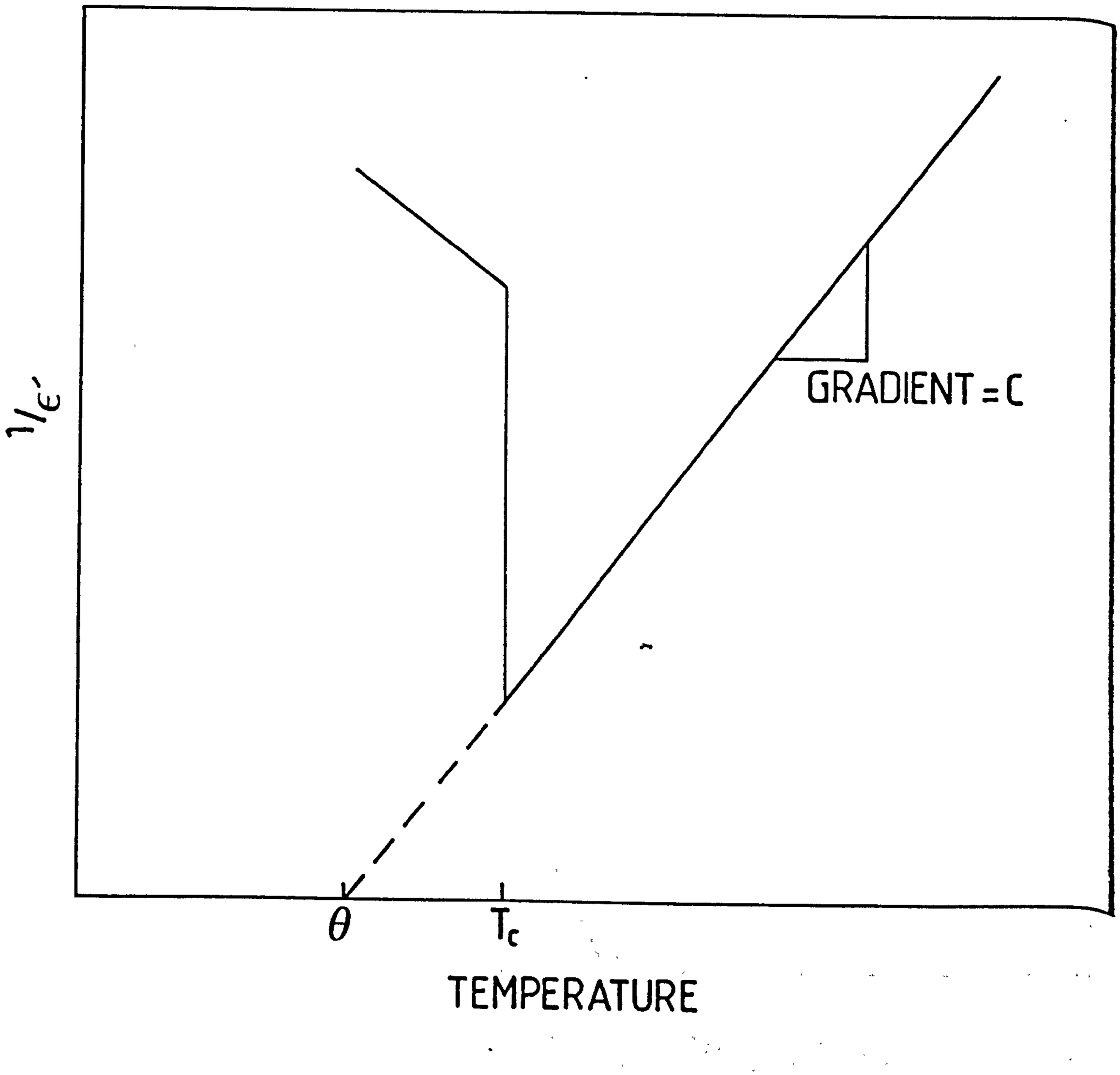

Figure 1.2a Relationship between $1/\epsilon'$ and temperature throughout a discontinuous (first order) phase transition.

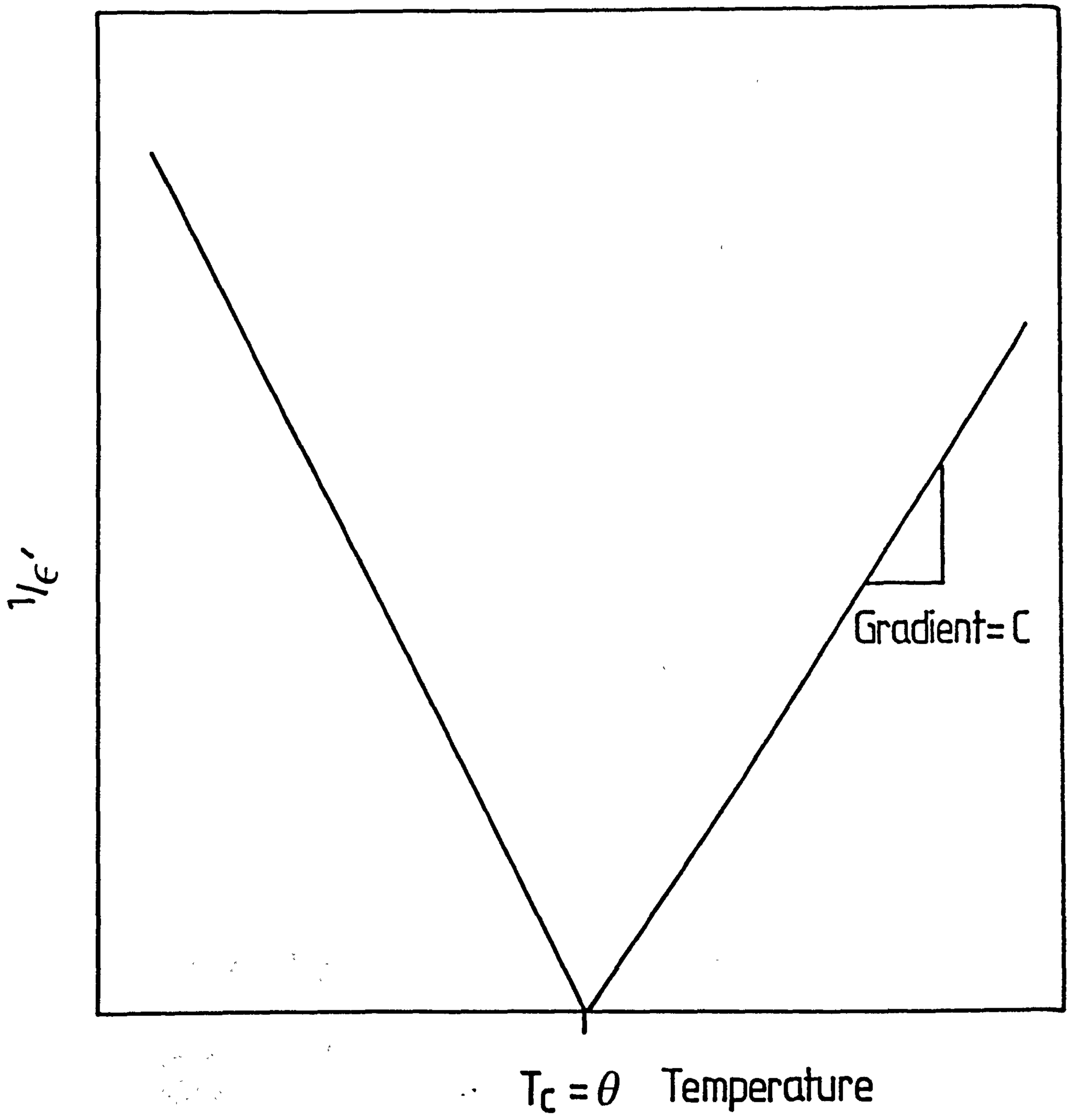

Figure 1.2b Relationship between $1/\epsilon'$ and temperature throughout a continuous (second order) phase transition.

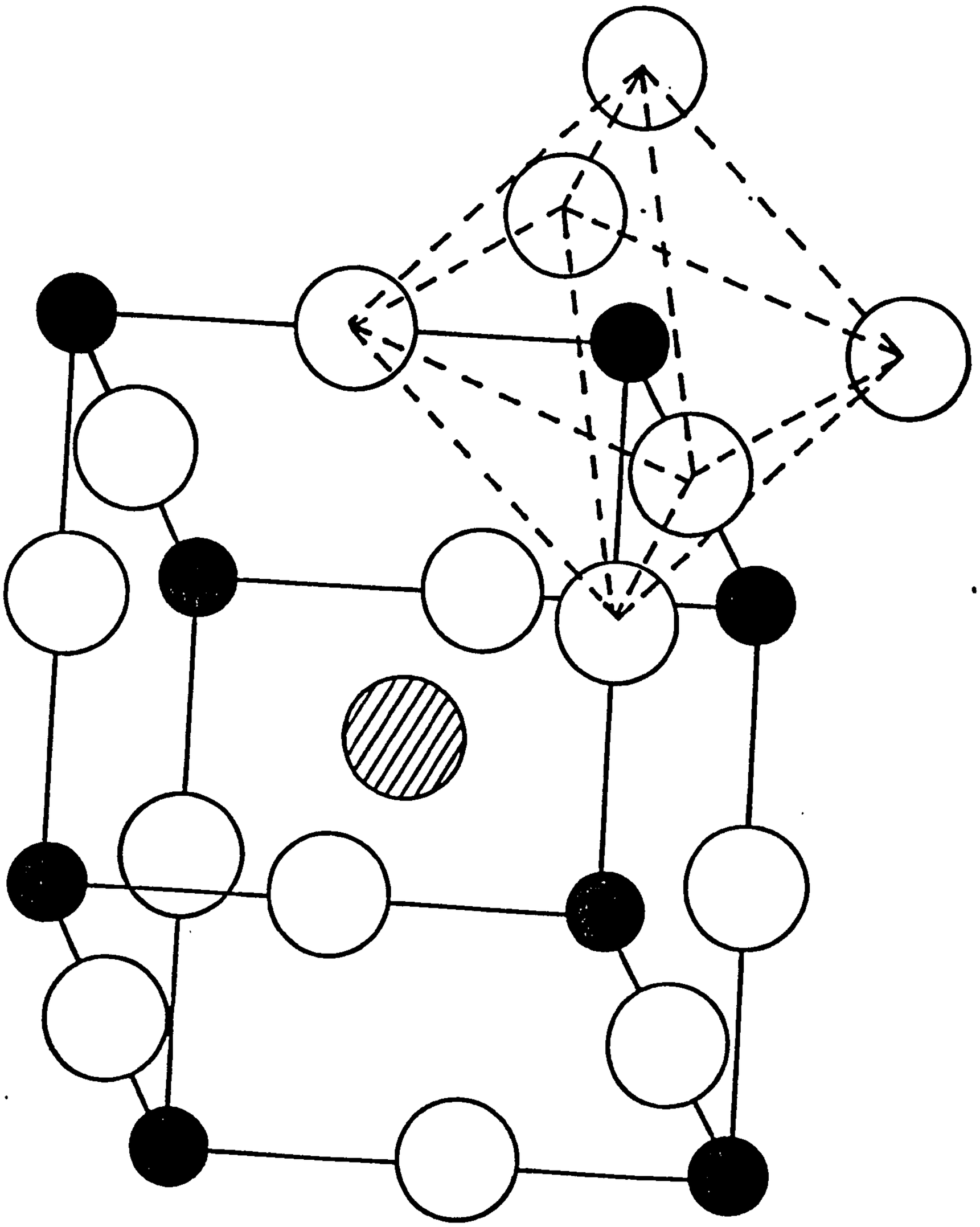

Figure 1.3 Arrangement of the atoms within Perovskite $BaTiO_3$.

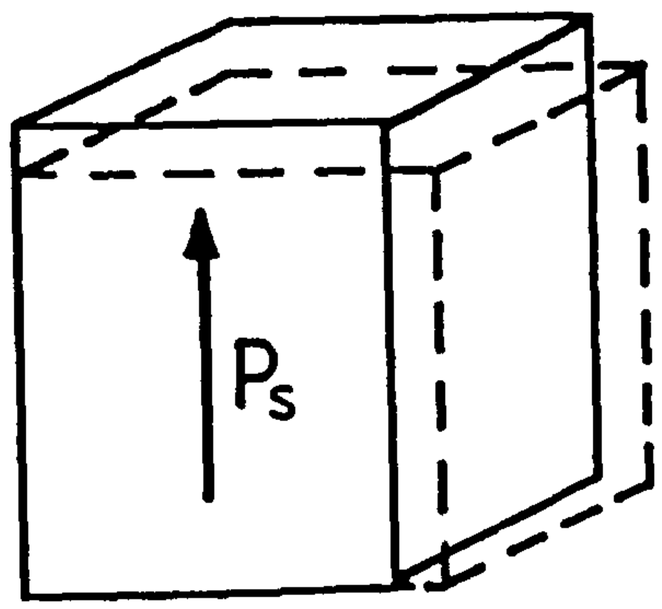

Figure 1.4a Schematic representation of the tetragonal unit cell of $BaTiO_3$, in comparison with the cubic unit cell.

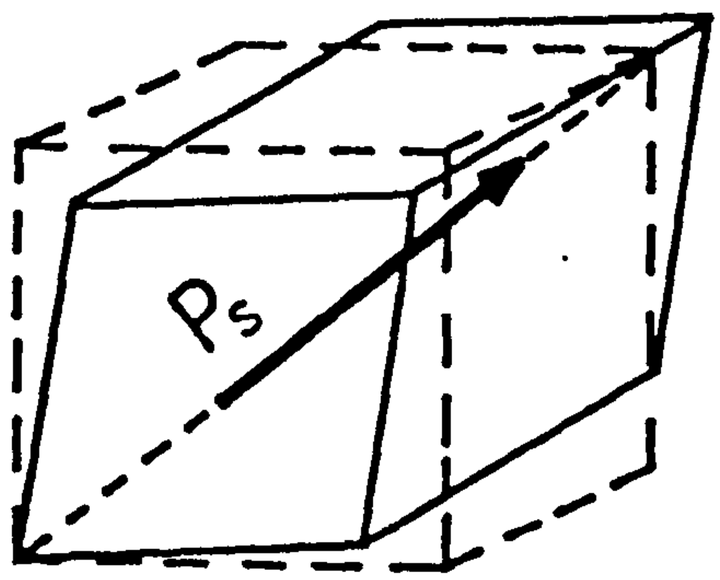

Figure 1.4b Schematic representation of the orthorhombic unit cell of $BaTiO_3$, in comparison with the cubic unit cell.

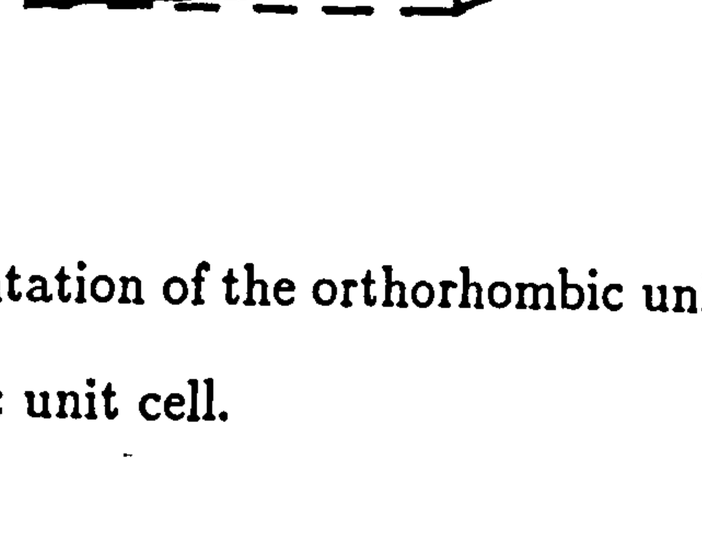

Figure 1.4c Schematic representation of the rhombohedral unit cell of $BaTiO_3$, in comparison with the cubic unit cell.

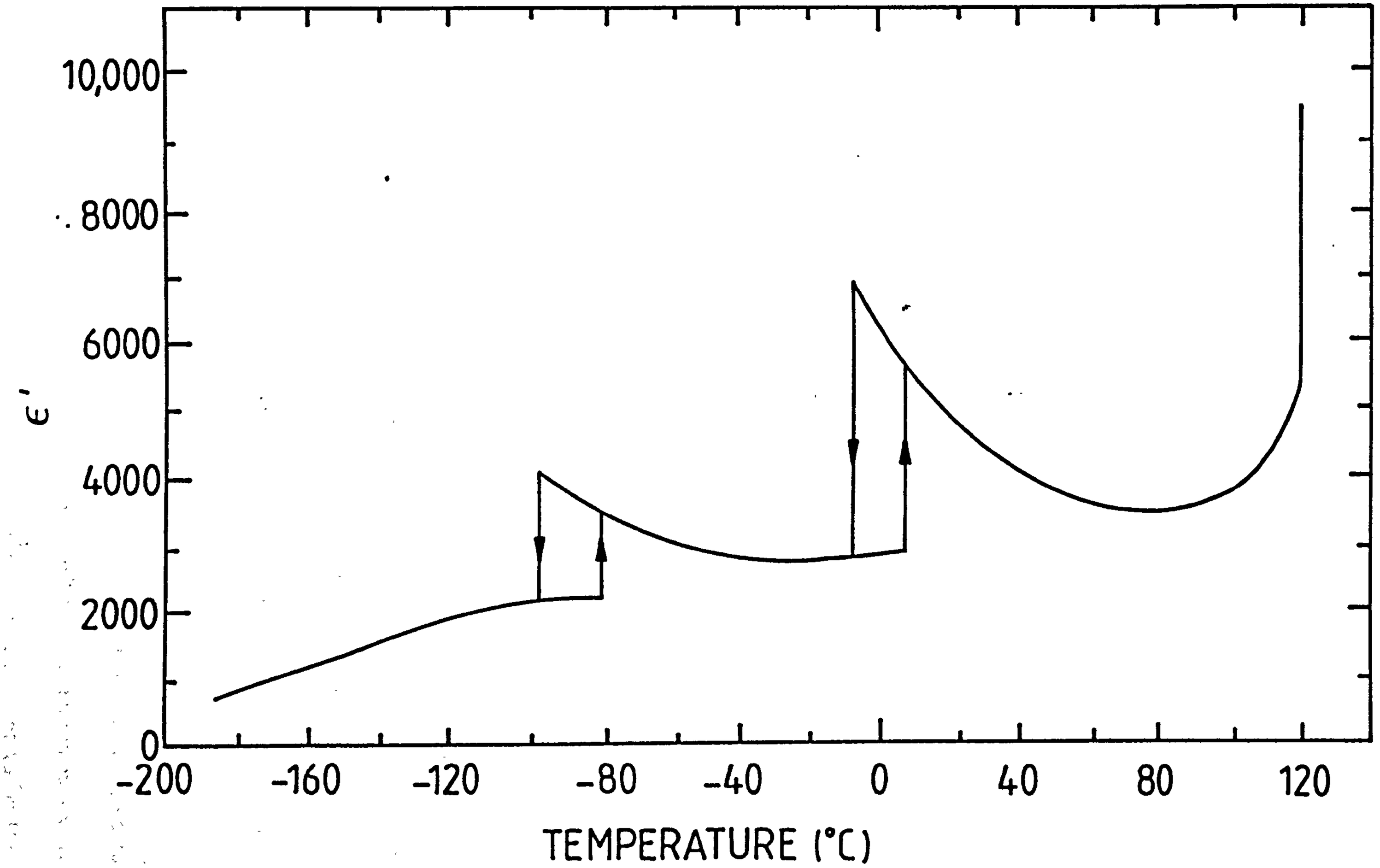

Figure 1.5 Relative permittivity of barium titanate throughout each phase transition.

CHAPTER TWO

THEORY OF THE PTCR EFFECT IN DONOR DOPED $BaTiO_3$ CERAMICS

In the 35 years since Haayman et al[2.1] first observed and patented the anomalous rise in resistivity observed in donor doped barium titanate ceramics in the vicinity of their Curie temperature, ~130°C, much effort has been expended, by many workers, in explaining it. The models proposed as a result of this effort can be divided into two sections: those which assume the PTCR effect to take place at the grain boundaries and those which attribute it to effects within the bulk of the material. The latter group were the first of the models to be proposed[2.2,2.3], but upon further investigations, grain boundary models came to be preferred. In the following sections each of the models will be described and briefly discussed, to show the advantages and shortcomings of each.

2.1. GRAIN BULK MODELS

Saburi[2.2] was one of the first to investigate the PTCR effect in any detail, making many samples with a number of different donor dopants, added in varying quantities. It was concluded that the most efficient ions for donor doping were those which were of similar size to their host ion (Ba^{2+} or Ti^{4+}) and had higher valency (i.e. +3 or +5, respectively). Since the semiconducting samples were dark blue in colour, donor incorporation was assumed to be accompanied by a reduction of some of the Ti^{4+} ions to Ti^{3+} in the following reaction

$$Ba^{2+}Ti^{4+}O_3^{2-} + nDo^{3+} \leftrightarrow Ba^{2+}_{1-n}Do^{3+}_nTi^{4+}_{1-n}Ti^{3+}_nO_3^{2-} \qquad (2.1)$$

where the donor (Do) substitutes onto the Ba site. The donor, in this case, may be for example, La^{3+}, Ho^{3+}, Y^{3+} and the extra electron was considered to be responsible for the conductivity. Hall and thermoelectric measurements were used to show the conductivity to be n-type and the Hall coefficient to be low,

$\sim 10^{-2} cm^3/C$. Arrhenius plots of $\ln\rho$ versus 1/T, where ρ is resistivity and T absolute temperature, were drawn between 200 and 600K, where resistivity was found to decrease in accordance with n-type semiconductivity only at temperatures lower than the Curie temperature and above ~500K. Activation energy for conduction was calculated to be ~0.1eV below the crystallographic transition and ~1.2eV above 500K. Between these temperatures, resistivity was observed to rise by between 2 and 4 orders of magnitude, with a temperature coefficient between 8 and $60\%°C^{-1}$. He attributed this anomaly to the crystallographic phase change, although no mechanism by which it takes place was offered.

Saburi also observed a reduction in the steepness of the PTCR characteristic when the voltage was increased or when an ac voltage was applied and concluded that a two-layer system existed within each grain, based on the equivalent circuit shown in figure 2.1. The parallel resistance and capacitance, R_p and C_p, represented the donor doped barium titanate grain, the values of R_p and C_p being temperature and frequency dependent. This combination was proposed to be in parallel with R_o, a leakage resistance corresponding to the dc resistance of the material. Theoretical calculations using this model gave some agreement with experiment, although no explanation was offered for the physical representation of C_p, R_p and R_o, nor the mechanism by which the resistivity anomaly takes place. In addition, the effects of donor concentration and additional acceptor doping on the resistivity anomaly, as described in section 1.3, were not considered.

Tennery and Cook[2.3] measured the resistivity versus temperature characteristics and the thermoelectric power of a large number of barium titanate ceramics, containing different donor ions in a number of concentrations. They also plotted $\ln\rho$ versus 1/T between room temperature and the temperature of the resistivity maximum and showed that the activation energy for conduction was ~0.1eV in the ferroelectric phase, in agreement with the results of Saburi[2.1]. Using semicon-

ductor theory, i.e. the equation

$$\rho = \frac{1}{n \times e \times \mu} \tag{2.2}$$

where n is the concentration of charge carriers, e is the electronic charge and μ is the mobility of the charge carriers (cm^2V-1s^{-1}), they concluded that the PTCR effect at the transition was due either to a change in the number of charge carriers or of their mobility. They performed Hall and thermoelectric measurements which indicated n-type conductivity in the ferroelectric phase. In addition, thermoelectric measurements, taken while temperature was raised through T_c, were observed to demonstrate a change in sign of the majority charge carriers by means of a change in the direction of the results curve, leading to a negative reading. This was assumed to be the result of a change from n-type conductivity to p-type at the transition. In other words, the crystallographic transition was proposed to be accompanied by a change from electron conduction to holes which was responsible for the large rise in resistivity. As temperature was raised further, the measurements showed a second change, indicating a return to n-type semiconductivity, at ~200°C, which was assumed to be the cause of the resistivity maximum. However, these results have never been confirmed by later work.

This model explains very little of the observations described in section 1.3, in particular the compositional effects of the PTCR characteristic, its voltage and frequency sensitivity and the increased dielectric permittivity upon donor incorporation. In addition, there is no reason proposed for the change in the nature of the charge carriers either at the transition or at the higher temperature.

In recent years, Sinclair and West[2.4.2.5] have undertaken a detailed investigation on donor doped barium titanate ceramics using ac impedance analysis. Measuring impedance, Z, and electric modulus, M (where $M = 1/\epsilon$ and ϵ is permittivity) over a large frequency range as temperature was raised through T_c, complex plane plots of each parameter were generated. Analysis was based on an equivalent circuit representing the grain bulk and a grain boundary layer, each

having different values of resistance but similar capacitance. The impedance plots were shown to highlight the value of the larger resistance whereas each capacitance value was found using the complex modulus diagrams. Plots of the imaginary part of the electric modulus versus frequency were used to obtain the values of both resistances, particularly the smaller one. On measuring each resistance at increasing temperature, they observed PTCR - like behaviour in both the grain boundary and the grain bulk, where the grain boundary exhibited a rise of 4-5 orders of magnitude in comparison with the bulk, which only increased by 3 orders of magnitude. An activation energy for conduction in the grain boundary and grain bulk above the resistance maximum was calculated from Arrhenius plots of ln(1/R) versus 1/T, where 1/R is conductance and T is the absolute temperature. Capacitance - temperature measurements obtained from the complex modulus plots showed that one capacitance obeyed the Curie-Weiss law above T_c, whereas the other was approximately constant with temperature. The Curie-Weiss behaviour was attributed to the bulk of the grains, from which an estimate of the relative permittivity of the barium titanate within the bulk led to the observation that this region occupies only ~20% of the volume of the grain. Since the grain boundary capacitance was proposed to be approximately constant with temperature, it was concluded that this region was made of an inorganic, non-ferroelectric layer having permittivity ~10 and comprising <1% of the volume of the grain. The remaining 80% was proposed to consist of a ferroelectric conductive core, making, in effect, a three-layer system shown schematically in figure 2.2.

This model leaves many of the observations of the PTCR effect (section 1.3) unexplained. It does not propose the nature of the intergranular, non-ferroelectric layer, nor the mechanism by which this region or the grain bulk exhibit a PTCR effect. Neither does it propose any reason for the frequency and voltage sensitivity of the resistance anomaly. Although single crystals of donor doped barium titanate have not been reported to exhibit the PTCR effect[2.6–2.8], Sinclair and

West proposed that a region of the bulk of the grain may exhibit a large resistivity rise, albeit small in comparison with that at the grain boundaries. This, however, was not discussed in the model. In addition, the small capacitance belonging to the conductive grain core would be expected to appear as a third peak in the complex modulus plots, at high frequency, according to their analysis. Such a peak was not observed, although the high frequency regions do not appear to have been investigated thoroughly. Unfortunately, the samples used for this analysis were supplied by an external body, in contrast to common practice, where samples are prepared by the authors. The composition of the samples was mentioned, but no details about the method of preparation, sintering, etc, were given. In other words, there is no information about the nature of the sample, in terms of exact composition or processing, which are known to affect the PTCR characteristic.

2.2. GRAIN BOUNDARY MODELS

The models described in the previous section, which assume the PTCR characteristic to be an effect taking place within the bulk of the barium titanate grains, can be seen not to explain adequately many of the observations described in section 1.3. The following models have attributed the resistivity anomaly to the grain boundaries, which will be seen to explain more sufficiently the observations of donor doped barium titanate ceramics, in particular voltage and frequency sensitivity and the effects of composition and processing.

2.2.1. THE PRESSURE CONTACT MODEL

In constrast to Saburi[2.2] and Tennery and Cook[2.3], Peria and co-workers[2.9] proposed that an equivalent circuit may be used to describe donor doped ceramic barium titanate, which was based on their own observations of this material. Having failed to observe a PTCR effect in single crystal donor doped samples and that the magnitude of the resistance anomaly was reduced upon the appli-

cation of an alternating current, they were the first to suggest that the PTCR characteristic was due to resistive regions at or near the grain boundaries. An equivalent circuit was proposed, consisting of two parallel combinations of resistance and capacitance, in series, see figure 2.3, representing grain boundary and grain bulk properies. Good qualitative agreement with experiment was obtained with suitable values of R_1, C_1, R_2 and C_2 and any inaccuracies between theory and experiment were explained on the grounds that it was unlikely that all of the grain boundaries would have identical properties. The resistance observed when a dc field was applied was assumed to be the sum of R_1 and R_2, but at high frequency the highly resistive grain boundary regions would, according to the equivalent circuit, be shunted by their capacitance and the measured resistance would then be due only to the bulk of the crystallites. Hence the resistance was shown to be frequency-dependent.

Since the contact between grain boundary regions is well known to be non-ohmic i.e. dependent on applied voltage, and affected by external pressure, Peria et al assumed that the intergranular electrical contact was a pressure contact. As the crystallographic transition takes place, the change in the lattice parameters (described in section 1.2), was proposed to cause a large intergranular strain which would induce a change in the pressure-sensitive contact resistance in a similar manner to that observed with metal-semiconductor contacts. Support was obtained for this model by means of the frequency and voltage sensitivity of the PTCR effect and the observed irreproducibility of manufacture of these ceramics. Such a pressure-sensitive PTCR effect, however, would be expected to take place at the same temperature as the transition and in the same discontinuous manner. The resistivity increase is well known to continue over a temperature range of 100°C above T_c, in contradiction to the model. It was proposed that this was due to high field effects within the grain boundary layers, arresting the transition in these regions (as described in section 1.2), thus causing the resistivity rise to take

place over a range of temperatures.

Although this model explains the frequency and voltage dependence of the resistivity anomaly by proposing a two-layer system comprising the grain bulk and grain boundary properties, the nature of the grain boundary layer is not explained. Observations, as described in section 1.3, of the effects of composition, together with the influences of sintering and annealing, are not explained, although the increase in resistivity below T_c at high donor concentrations was attributed to the limit of solubility of the donor ions in $BaTiO_3$. This model suggested that the material within the grain boundary layers has a fixed resistance which is solely dependent on the contact pressure between adjacent grain boundaries. The lattice strain created during the transition results in the formation of large stresses which are relieved by the formation of twins and therefore is unlikely to be sufficient to cause a resistance increase of 3 to 5 orders of magnitude. In fact, piezoresistive effects tend to be linearly dependent on applied pressure, thus requiring an enormous unrelieved stress at the transition. Moreover, were sufficient strain to be induced, the sample would be unlikely to survive. Finally, the temperature range in which the ferroelectric properties can be induced in the cubic phase is very small, of the order of 10°C (section 1.2), so the PTCR effect would be expected to fall within 10°C of the Curie temperature if this model were to describe the resistivity anomaly correctly.

2.2.2. THE SPACE CHARGE LIMITED CURRENT MODEL

Nemoto and Oda[2.10] proposed a simple grain boundary model to explain the current - voltage characteristics as well as the resistivity anomaly in donor doped barium titanate ceramics. They investigated single grain boundaries and the grain bulk of carefully prepared samples and observed the PTCR effect only across grain boundaries, in agreement with those workers who had failed to obtain any significant resistivity increase in single crystal donor doped barium titanate[2.6–2.8].

Current - voltage measurements above the Curie temperature showed ohmic behaviour until the voltage drop across a grain boundary was ~1V, above which they were found to obey approximately Child's law, with $I \simeq V^2$. They concluded that the conduction was described by a space charge limited current (SCLC) within the intergranular second phase, in a similar manner to the device characteristics of a vacuum diode. The SCLC itself was proposed to be limited by electron trapping within the second phase, the traps being thought to decrease the mobility of the conduction electrons and thus increase resistivity, in accordance with equation 2.1. As temperature is raised above T_c, the gradual filling of the traps was considered to cause the resistivity to reach a maximum value. Below the transition, the traps were suggested to be compensated by the spontaneous polarization, in agreement with previous workers[2.11] and hence resistivity was shown to be low.

Despite proposing a model for the PTCR characteristic which also incorporates the observed voltage sensitivity of resistivity, Nemoto and Oda were later found not to have explained the PTCR effect sufficiently. Haanstra and Ihrig[2.12], Knauer[2.13] and Koshek and Kubalek[2.14] all failed to observe a second phase at the grain boundaries. In addition, they did not account for the self-heating of the resistive grain boundaries as voltage was increased. Clearly, this phenomenon affected their measurements and led to inaccurate interpretation of the results. Finally, the nature of the electron traps was not considered, although their presence was associated with the loss of the spontaneous polarization above T_c. But, were they to be associated with this, the resistivtity of a donor doped barium titanate ceramic would be expected to increase sharply at T_c, over a very short temperature range, until all of the traps were full. Moreover, the number of traps would need to be very large in order to reduce elctron mobility sufficiently to cause a resistivity rise of between 3 and 5 orders of magnitude.

2.2.3. THE HEYWANG MODEL

Heywang[2.15,2.16] attributed the PTCR effect to the presence of resistive grain boundary layers, in agreement with Peria et al[2.9]. In contrast to these workers, however, he proposed the resistive layers to arise as a result of the presence of deep electron traps (acceptor states) at the grain surfaces. These negatively charged surface states were proposed to be compensated by the creation of a thin, positively charged depletion layer within the surface of each grain. Describing this effect in terms of energy, Heywang proposed a schematic arrangement as shown in Figure 2.4, where the conduction band is bent upwards, developing Schottky-like potential barriers between the grains. The surface traps were proposed to exist at an energy E_a below the conduction band, which is also below the Fermi level, E_F. The number, N_a, of ionized acceptor states contributes to the extent of the conduction band bending to create a potential barrier of height $e\phi_o$ above the bulk conduction band. The charge carrier (ionized donor) concentration is given by N_d, N_c is the effective density of states (equal to the Ti^{4+} density) and b is the width of the depletion layer on each side of the barrier.

Heywang observed that the PTCR characteristic takes place over the same range of temperature as that at which dielectric relative permittivity falls in accordance with the Curie-Weiss law, $\epsilon' = C/(T - \theta)$, where C is the Curie constant, T is absolute temperature and θ is the Curie constant, and concluded that the two effects were connected. As the temperature is raised above T_c the permittivity, which determines the distribution of electrostatic potential within the grain boundary layer, falls, and the potential barrier is raised. According to Poisson's relation, ϕ_o was given by

$$\phi_o = \frac{eN_d}{2\epsilon_o\epsilon'} \times b^2 \tag{2.3}$$

where e is the electronic charge and ϵ_o is the permittivity of free space. The width of the depletion layer was given by semiconductor theory,

$$b = N_a/2N_d, \tag{2.4}$$

and equation 2.3 may be written in terms of acceptor density and donor concentration,

$$\phi_o = \frac{eN_a^2}{8\epsilon_o\epsilon' N_d}. \tag{2.5}$$

Therefore, as temperature increases, ϕ_o is raised in proportion to $1/\epsilon'$.

The density of the surface acceptor traps was proposed also to be dependent on temperature: as temperature is raised, ϕ_o increases, as shown above but at a particular temperature it can be seen from figure 2.4 that the value of $e\phi_o$ will be high enough to cause the acceptor levels to become close to the Fermi level and so release some of their electrons, i.e. depopulation of the acceptors begins to take place. This, in turn, effectively reduces the value of N_a and hence ϕ_o in accordance with equation 2.5. A dynamic equilibrium is then established, where further rises in temperature lead to a corresponding reduction in the value of N_a and hence the potential barrier height remains essentially constant, at its maximum. The temperature dependence of N_a was given by

$$N_a = \frac{N_{ao}}{1 + exp[(E_F + e\phi_o - E_a)/kT]} \tag{2.6}$$

with

$$E_F = kTln(N_c/N_d), \tag{2.7}$$

where N_{ao} is the total density of surface acceptor states and k is the Boltzmann constant.

The resistance, R_{gb}, of the two adjacent grain boundary layers of figure 2.4 was shown to be exponentially proportional to the height of the potential barrier, in accordance with semiconductor theory:

$$R_{gb} \propto exp(\frac{e\phi_o}{kT}). \tag{2.8}$$

The resistance of a ceramic sample was then given by

$$R = R_o exp(\frac{e\phi_o}{kT}) \tag{2.9}$$

where R_o can be assumed constant and is essentially a multiplication factor for the number of grain boundaries in series within the sample. The resistance of the grain bulk was given by semiconductor physics,

$$R_{bulk} \propto \frac{1}{N_d \times e \times \mu} \tag{2.10}$$

where μ is the mobility of the charge carriers.

As temperature is raised above T_c, the reduction in ϵ' causes the potential barrier height to increase, which is followed exponentially by the resistivity. At a certain temperature, depopulation of the acceptor states takes place, equation 2.6, leading to a maximum value of potential barrier height (estimated to be ~0.5eV) which is accompanied by a maximum in the resistivity. Above this temperature, resistivity is observed to decay exponentially, in accordance with equation 2.8, since ϕ_o is no longer temperature-dependent

$$R = R_o exp(\frac{e\phi_{o(max)}}{kT}). \tag{2.11}$$

The low resistance observed below T_c appears to contradict the Heywang model, since ϵ' of barium titanate is also low. Capacitance measurements of the donor doped material were found to be more than an order of magnitude higher than those belonging to pure barium titanate and the increase was attributed to the presence of thin grain boundary layers. Heywang proposed that the trapped charges across the grain boundary depletion layer created a high electric field which induced high permittivity within the grain boundary layers below the transition temperature. Then, in accordance with equations 2.5 and 2.9, a low resistance was obtained.

The observed reduction of the resistance above T_c with applied voltage was explained by Heywang's model as follows: Assuming the applied voltage to be sufficiently small not to affect the occupation of the surface states, the grain boundary layer was proposed to accommodate all of the voltage drop, causing

the depletion layer to be displaced on one side of the barrier. Figure 2.5 shows schematically the modified potential barrier, where a voltage U per grain boundary has been applied and the displacement of the depletion layers has been represented by the new distances, b_1 and b_2, where

$$b_1 + b_2 = 2b \tag{2.12}$$

and

$$\frac{e^2 N_d}{2\epsilon_o \epsilon'}(b_2^2 - b_1^2) = U. \tag{2.13}$$

The passage of electrons from one side of the barrier to the other is now dependent on the new potential barrier height, $\phi(U)$, given by

$$\phi(U) = \frac{e^2 N_d}{2\epsilon_o \epsilon'} b_1^2. \tag{2.14}$$

From equations 2.12 and 2.13,

$$b_1 - b_2 = \frac{U\epsilon_o \epsilon'}{e^2 N_d b} \tag{2.15}$$

and, subtracting equation 2.12 from equation 2.15, b_1 is obtained:

$$b_1 = b - \frac{U\epsilon_o \epsilon'}{2e^2 N_d b}. \tag{2.16}$$

The modified potential barrier height may now be written,

$$\phi(U) = \frac{e^2 N_d}{2\epsilon_o \epsilon'}(b - \frac{U\epsilon_o \epsilon'}{2e^2 N_d b})^2, \tag{2.17}$$

or, by substituting equation 2.3 into equation 2.17,

$$\phi(U) = \phi_o(1 - \frac{U}{4\phi_o})^2. \tag{2.18}$$

Substituting equation 2.16 into equation 2.9 therefore demonstrates the effect of applied voltage on the PTCR anomaly:

$$R = R_o exp[\frac{e}{kT} \times \phi_o(1 - \frac{U}{4\phi_o})^2], \tag{2.19}$$

where an increase in applied voltage can be seen to reduce the effective potential barrier height and the magnitude of the PTCR characteristic.

It can be seen that equations 2.5, 2.6 and 2.9 can be used to define the resistivity anomaly of a donor doped barium titanate ceramic if N_d, N_a and E_a are known. These factors arise from the composition of the ceramic: N_d is controlled by the number of ionized donor ions and N_a and E_a are controlled by the presence of grain boundary acceptor states. Increasing N_d by increasing the concentration of donor ions causes the potential barrier height, and thus resistance, to be lowered, in accordance with observations described in section 1.3. The rise in resistance upon further increasing the donor concentration was attributed by Heywang[2.17] to be due to compensation of the donors by means of the formation of additional acceptor traps. N_a may itself be increased by the addition of acceptor ions to the composition of the ceramic and may be seen to increase the resistivity and therefore the height of the potential barrier. The energy of the acceptor states below the Fermi level determines the temperature at which depopulation of the traps starts, hence acceptors may be observed to increase both the magnitude of the resistivity anomaly and the temperature range over which it takes place.

Heywang[2.15,2.16] did not make any suggestion of the nature of the grain boundary acceptor traps, except for tentatively attributing them to the presence of impurity ions, having failed to observe a PTCR effect in donor doped ultra pure barium titanate[2.17]. Influences of sintering and processing, as described in section 1.3 were not mentioned, nor was there any proposal regarding the failure to obtain a PTCR characteristic in undoped ceramic barium titanate.

2.2.4. THE JONKER MODIFICATION

While in agreement with Heywang[2.16–2.18] regarding the model for the grain boundary resistance above T_c, Jonker[2.11] did not consider the description for resistivity below T_c to be sufficient. His modification to the Heywang model considers the ferroelectric properties of barium titanate below the transition. Each grain was assumed to be divided into a number of domains which are spontaneously polarized, antiparallel to each other. At the grain boundaries the domains may be considered to end, forming a pattern of positive and negative charges within the depletion layer. Half of these charges compensate the grain boundary acceptors, as shown schematically in figure 2.6, thus eliminating the potential barrier in these regions and creating a conducting path through the grains. Jonker observed a discontinuous jump in resisitvity of between one and three orders of magnitude at T_c, which he attributed to the sudden increase in potential barrier height as a result of the sudden disappearance of the spontaneous polarization. Where such a jump was not observed, the electric field at the grain boundary was assumed to slow the disappearance of the ferroelectric properties.

In summary, the Heywang/Jonker model describes the PTCR resistance anomaly of donor doped barium titanate ceramics in terms of grain boundary layers, the resistance of which is dependent on temperature and controlled by the large change in permittivity above the Curie temperature, T_c. Figure 2.7 shows a typical resistance - temperature characteristic, divided into three temperature zones. Within zone I, where $T < T_c$, the high potential barrier is compensated by the spontaneous polarization and resistance is given by the grain bulk. Close to T_c, where $T > T_c$, zone II, the spontaneous polarization disappears and resistance is governed by the rising potential barrier height. As temperature is increased further, into zone III, where $T \gg T_c$, the energy of the acceptor traps coincides with the Fermi level and depopulation of the traps takes place to create a maximum potential

barrier height. Resistance in this region is controlled only by temperature.

2.2.5. THE DANIELS MODEL

Some years after Jonker added his modification, Daniels and co-workers published a series of articles[2.18–2.22] in which they challenged the Heywang model[2.15]. In a review of their model[2.23], they highlighted some deficiencies of Heywang's, in particular the nature of the grain boundary acceptor states, the absence of the PTCR effect in donor doped single crystal and undoped ceramic barium titanate, the increase in room temperature resistance with high concentrations of donor dopant and the observed sensitivity of the resistance anomaly on sintering and cooling conditions.

They concentrated on the defect chemistry of both pure and donor doped barium titanate ceramics to derive a model based on a three-dimensional insulating zone at the grain surfaces. The Heywang model, where a two-dimensional layer of acceptor traps exists at the grain boundary, was considered to be a limiting case and complementary to Daniels et al.

Daniels and Hardtl[2.18] first investigated the thermodynamics of the defects which they considered to affect the electrical properties of ceramic donor doped barium titanate. They measured the conductivity of samples containing up to 2.0 at%La at high temperature and observed three distinct regions of conductivity as oxygen partial pressure was reduced from 10^0 to 10^{-12} atmospheres. Undoped barium titanate was observed to be n-type semiconducting only below $\sim 10^{-3}$ atmospheres and p-type at higher oxygen concentrations. In comparison, donor doped barium titanate exhibited n-type conductivity at every oxygen partial pressure.

They assumed the only defects present in donor doped barium titanate ceramics to be uncharged, singly or doubly negatively charged barium vacancies, (V_{Ba}, $V_{Ba'}$, $V_{Ba''}$), neutral, singly or doubly positively charged oxygen vacancies (Vo,

$V\dot{o}$, $V\ddot{o}$) and singly positively charged donor ions, $L\dot{a}$. The presence of titanium vacanies was considered unlikely since excess TiO_2 is commonly added for the purpose of liquid phase sintering (see section 3.1). Other defects, such as clusters of defects and interstitial atoms were considered to have a negligible effect on the electrical properties. The following electroneutrality equation was derived:

$$n + [V_{Ba'}] + 2[V_{Ba''}] = p + [V\dot{o}] + 2[V\ddot{o}] + [L\dot{a}] \tag{2.20}$$

where n is the concentration of conduction electrons and p is the concentration of holes. Analysis of the equilibrium conditions regarding each defect yielded relations between electron concentration, oxygen partial pressure, donor concentration and the equilibrium constants for the creation of each defect. The concentration of each defect was calculated as oxygen partial pressure was changed and the defect chemistry of pure and donor doped barium titanate was determined. Using the defect chemistry and the conductivity measurements, Daniels and Hardtl proposed the nature of the defects responsible for conductivity at each oxygen partial pressure. The conductivity of pure barium titanate, heat-treated in a reducing atmosphere to induce n-type conductivity, was found to be controlled only by the presence of donor-like oxygen vacancies. The donor doped material, on the other hand, was found to be controlled by three different mechanisms, depending on the oxygen partial pressure at equilibrium: close to atmospheric pressure,

$$2[V_{Ba''}] \simeq [L\dot{a}], \tag{2.21}$$

at intermediate oxygen concentrations,

$$n \simeq [L\dot{a}], \tag{2.22}$$

and at the lowest pressures,

$$n \simeq [V\dot{o}], \tag{2.23}$$

where the square brackets indicate defect concentrations. In other words, at very low oxygen partial pressures, the number of oxygen vacancies, which is far greater

than that of the donor ions, determines the conductivity. At intermediate pressures there is electronic compensation of the donor ions, i.e. each donor ion releases an electron into the conduction band. Close to atmospheric conditions, the donor ions are compensated by barium vacancies which act as acceptors and lower the free electron concentration.

The energy of each defect, with reference to the conduction and valence bands, was then calculated. Energy levels attributed to the singly charged oxygen vacancies and lanthanum ions were found to lie within 0.1eV of the conduction band, demonstrating their behaviour as donors, whereas the remaining defects had energy levels between the Fermi level and the valence band, highlighting their nature as acceptors. The band diagram they calculated is shown schematically in figure 2.8.

Wernicke[2.21,2.24] followed the thermodynamic investigation by studying the kinetics of equilibrium of each defect. Clearly, the restoration of equilibrium in, say a grain of donor doped barium titanate, is dependent on the diffusion of the slowest defect. By monitoring the defect chemistry of a sample of donor doped ceramic barium titanate, oxygen vacancies were found to diffuse rapidly at high temperature, from the surface of the sample into the bulk. Barium vacancies, on the other hand, move very slowly and were found to diffuse into the grain from the grain boundaries. It was proposed that barium vacancies are created at the grain boundaries as a result of the titania-rich second phase, for example in the following way:

$$BaTi_3O_7 + 2Ba_{lattice} + 2O_{lattice} \leftrightarrow 3BaTiO_3 + 2V_{Ba} + 2V_o, \qquad (2.24)$$

from where they diffuse into the grain bulk.

Having obtained the defect chemistry at high temperatures, where samples were assumed to be in equilibrium, Wernicke[2.24] calculated the change in defect chemistry upon cooling (typically between 3 and 10°C/min), where samples could

not be assumed to be in equilibrium. At high temperatures (>1100°C) restoration of equilibrium is possible, since even the slow moving barium vacanices have sufficient thermal energy to diffuse through the grains. As temperature is lowered, however, the rate of diffusion slows exponentially and the barium vacancies in particular are frozen. The oxygen vacancies, however, are still mobile at lower temperatures. Thus, although according to equation 2.24 both barium and oxygen vacancies are created at the grain boundaries at temperatures less than ~1100°C, only the oxygen vacancies can diffuse away. Thus a region close to the grain boundaries will develop which will be rich in acceptor-like barium vacancies. Wernicke described the nature of the grain boundary zone as a diffusion front of barium vacancies which penetrates into the bulk of the grain, losing speed as temperature is reduced. The concentration of barium vacancies within the zone is high enough to compensate the donor ions and this region is therefore insulating. The thickness of the zone is dependent on the rate of cooling and its room temperature resistivity was estimated between 10 and 100Ωcm, resulting in an n-i-n structure at adjacent grains. The bulk of the grains was considered to be conducting since the concentration of barium vacancies here is too low to compensate all of the donor ions Heywang's grain boundary potential barrier, drawn schematically in figure 2.4, was modified, as shown in figure 2.9, to account for the width of the depletion zone upon cooling. It was then proposed that the resistance of the donor doped barium titanate was the weighted average of the grain boundary zone and grain bulk resistances.

In agreement with the hypothesis of Jonker[2.11], conductivity below the Curie temperature was explained by the compensation of the positively charged depletion zone by the spontaneous polarization. Above T_c, the Heywang[2.15,2.16] model was adopted to describe the mathematics of the resistance anomaly, with a maximum potential barrier height of ~1eV[2.22].

The deficiencies of the Heywang model were addressed[2.22,2.23]: the nature of

the grain boundary acceptor states had been shown to be doubly ionized barium vacancies. Single crystal donor doped and undoped ceramic barium titanate were shown to contain insufficient grain boundary acceptor traps for a potential barrier to exist and the PTCR effect is not observed. Wernicke[2.24] calculated the width of the depletion zone to be between 1 and 3μm, depending on the cooling rate. The reduction in grain size at high donor concentrations then corresponds to an increased resistive effect of the insulating grain boundary zone. Highly doped barium titanate, whose grains are of the order of 3μm, was considered to be fully insulating as a result of the complete penetration of the barium vacancy-rich zone throughout the grain bulk. Finally, sintering and cooling conditions were shown to affect the width of the depletion zone and hence the PTCR characteristic.

Despite modifying and extending the understanding of the PTCR effect and the nature of the grain boundary acceptor traps in particular, some of the Daniels model is contradictory to observations described by other workers. Heywang failed to observe any significant PTCR effect in donor doped ultra-pure barium titanate[2.17], although the Daniels model would predict a typcial effect with such a precursor. Jonker[2.11] observed a heightening of the resistance anomaly when he annealed samples in halogen gases, to which he attributed an increase in the value of N_a in equation 2.5. He also observed an increase in resistance when samples were sintered in high oxygen concentrations and suggested that this was due to an increase in acceptor state density at the grain boundaries. According to Daniels, no change would be expected, since the only acceptor states are barium vacancies and their concentration is due only to their defect chemistry which is dependent on cooling rate alone. Quenching donor doped barium titanate samples from high temperature (>1200°C), according to Daniels, would result in the freezing of the high temperature defect chemistry and the presence of no depletion zone since there will have been no time for diffusion to take place. Samples would, therefore, be expected to be conducting, with no PTCR effect. The literature

reports samples quenched from >1200°C, where a modified PTCR characteristic was observed[2.25,2.26]. This model also makes very little explanation for the effects of composition, as described in section 1.3, where the addition of acceptor ions is well known to heighten the PTCR characteristic. They proposed tentatively that acceptor ions cause an increase in the width of the depletion zone, and hence increase its resistance[2.22], although the exact means by which this takes place was not covered. The increased effect of the insulating depletion zone to account for high room temperature resistance of highly doped barium titanate is not an adequate explanation since results have been reported[2.27] where such samples have exhibited a modified PTCR effect which is sensitive to both frequency and voltage. Were the entire grain to be insulating, no PTCR effect would be expected.

2.2.6. THE DURHAM MODIFICATION

More recently, Al-Allak and co-workers[2.27] published a modification to the Daniels model, following an extensive study on the effect of annealing on donor doped ceramic barium titanate. They annealed samples in air at 1220°C for between 20 minutes and 27 hours, finding the PTCR characteristic to be substantially modified as annealing time progressed. Although the grains of their samples were small, impedance analysis proved that, even after 27 hours' anneal, none of the grains had been made completely insulating by the diffusion of barium vacancies, in contradiction to the Daniels model[2.23]. Samples annealed for the longest period were heat-treated in N_2 at the annealing temperature for 3 hours, whereupon no PTCR effect was observed. Reoxidation in air at the same temperature and for the same length of time then took place, after which the samples were observed to have similar resistivity - temperature characteristics as the as- annealed ones. They argued that, according to the Daniels model, the barium vacancies would have been destroyed during the reducing treatment and recreated during reoxidation. The samples would then have exhibited PTCR curves similar to sam-

ples annealed only for 3 hours. Al-Allak and co-workers proposed that, during reduction, oxygen vacancies are formed, which coexist with the barium vacancies at the grain boundaries. The concentration of barium vacancies is not affected during each of the post-annealing heat-treatments because of their low diffusivity. At room temperature the oxygen vacancies are ionized and act as donors, reducing the resistivity and eliminating the PTCR effect. After reoxidation in air, they are destroyed and the effect of the barium vacancies is again prominent. The barium vacancies were considered, not to form a diffusion front, but to exist within a thin grain boundary region, similar to that proposed by Heywang[2.15,2.16]. Earlier work by Koschek and Kubalek[2.14] appears to support this modification. These workers investigated the grain boundaries of donor doped barium titanate ceramics sintered for different lengths of time using cathodoluminescence and found spectra at the grain boundaries corresponding to thin layers, even for those samples sintered for the maximum time. After analysis of the cathodoluminescence spectra, they proposed the grain boundary layers to be rich in doubly ionized barium vacancies and singly ionized oxygen vacancies. Al-Allak and co-workers later proposed the nature of the grain boundary acceptors to be a combination of impurity metal ions, barium vacancies and adsorbed atomic oxygen[2.28].

2.3. OBJECTIVES OF THE PROJECT

The purpose of the work described in this thesis was to investigate the validity of the most widely accepted model, that of Heywang[2.15–2.17], versus the validity of the model proposed by Daniels and co-workers[2.18–2.23]. Different sets of samples were prepared and investigated by performing various experiments, to investigate the effects of composition and processing on the PTCR effect at the grain boundaries. Firstly, the effect of donor concentration was studied, whereupon it was found that the amount of dopant and the temperature at which sintering took place were of prime importance to the grain boundary acceptor state density and

hence to the PTCR characteristic. Following from this, the effect of the deliberate addition of ions known to act as acceptors was carried out and the characteristics of the grain boundaries investigated. The purpose of this was to confirm the addition of the extra dopant as an acceptor and to determine the way in which it took effect. Finally, samples were sintered in different oxygen - containing atmospheres to examine the effect of the number of adsorbed oxygen atoms on the grain boundary properties and the PTCR characteristic. All of the results were analysed in terms of the theory in order to gain an understanding of the PTCR effect at the grain boundaries of donor doped barium titanate ceramics.

REFERENCES

2.1 Haayman P.W., Dam R.W. and Klassens H.A., Ger. Pat. 929 350, 1955.

2.2 Saburi O., J. Phys. Soc. Jpn., **14**, 1159, 1959.

2.3 Tennery V.J. and Cook R.L., J. Am. Ceram. Soc., **44**, 187, 1961.

2.4 Sinclair D.C. and West A.R., J. Mater. Sci. Lett., **7**, 823, 1961.

2.5 Sinclair D.C. and West A.R., J. Appl. Phys., bf 66, 3850, 1989.

2.6 Goodman G., J. Am. Ceram. Soc., **46**, 48, 1963.

2.7 Berglund C.N. and Baer W.S., Phys. Rev., **157**, 358, 1967.

2.8 Murakami T., Nakahara M., Miyashita T. and Ueda S., J. Am. Ceram. Soc., **56**, 291, 1973.

2.9 Peria W.T., Bratschun W.R. and Fenity R.D., J. Am. Ceram. Soc., **44**, 249, 1961.

2.10 Nemoto H. and Oda I., J. Am. Ceram. Soc., **63**, 398, 1980.

2.11 Jonker G.H., Sol. Stat. Electron., **7**, 895, 1964.

2.12 Haanstra H.B. and Ihrig H., J. Am. Ceram. Soc., **63**, 288, 1980.

2.13 Knauer U., Phys. Stat. Sol. (a), **65**, K109, 1981.

2.14 Koschek G. and Kubalek E., J. Am. Ceram. Soc., **68**, 582, 1985.

2.15 Heywang W., Sol. Stat. Electron., **3**, 51, 1961.

2.16 Heywang W., J. Am. Ceram. Soc., **47**, 484, 1964.

2.17 Heywang W., J. Mater. Sci., **6**, 1214, 1971.

2.18 Daniels J. and Härdtl K.H., Phil. Res. Rep., **31**, 489, 1976.

2.19 Daniels J., *ibid*, **31**, 505, 1976.

2.20 Hennings D., *ibid*, **31**, 516, 1976.

2.21 Wernicke R., *ibid*, **31**, 526, 1976.

2.22 Daniels J. and Wernicke R., *ibid*, **31**, 544, 1976.

2.23 Daniels J., Härdtl K.H. and Wernicke R., Phil. Tech. Rev., **38**, 73, 1978/79.

2.24 Wernicke R., Phys. Stat. Sol. (a), **47**, 139, 1978.

2.25 Ueoka H., Ferroelectrics, **7**, 351, 1974.

2.26 Ueoka H. and Yodogawa M., IEEE Trans. Manuf. Tech., **MTF-3**, 77, 1974.

2.27 Al-Allak H.M., Russell G.J. and Woods J., J. Phys. D: Appl. Phys., **20**, 1645, 1987.

2.28 Al-Allak H.M., Brinkman A.W., Russell G.J. and Woods J., J. Appl. Phys., **63**, 4530, 1988.

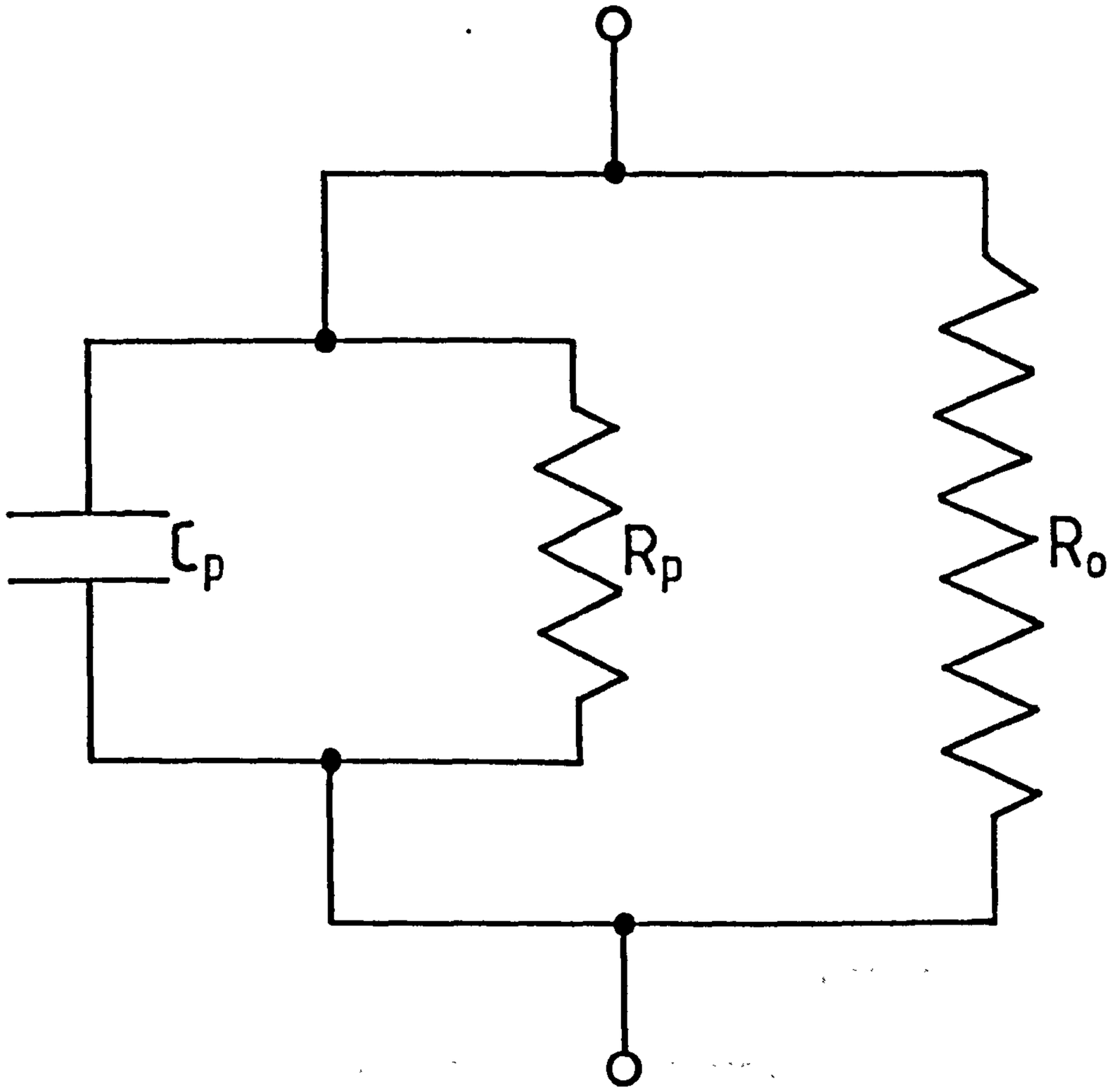

Figure 2.1 Equivalent circuit for PTCR barium titanate, after Saburi[2.2].

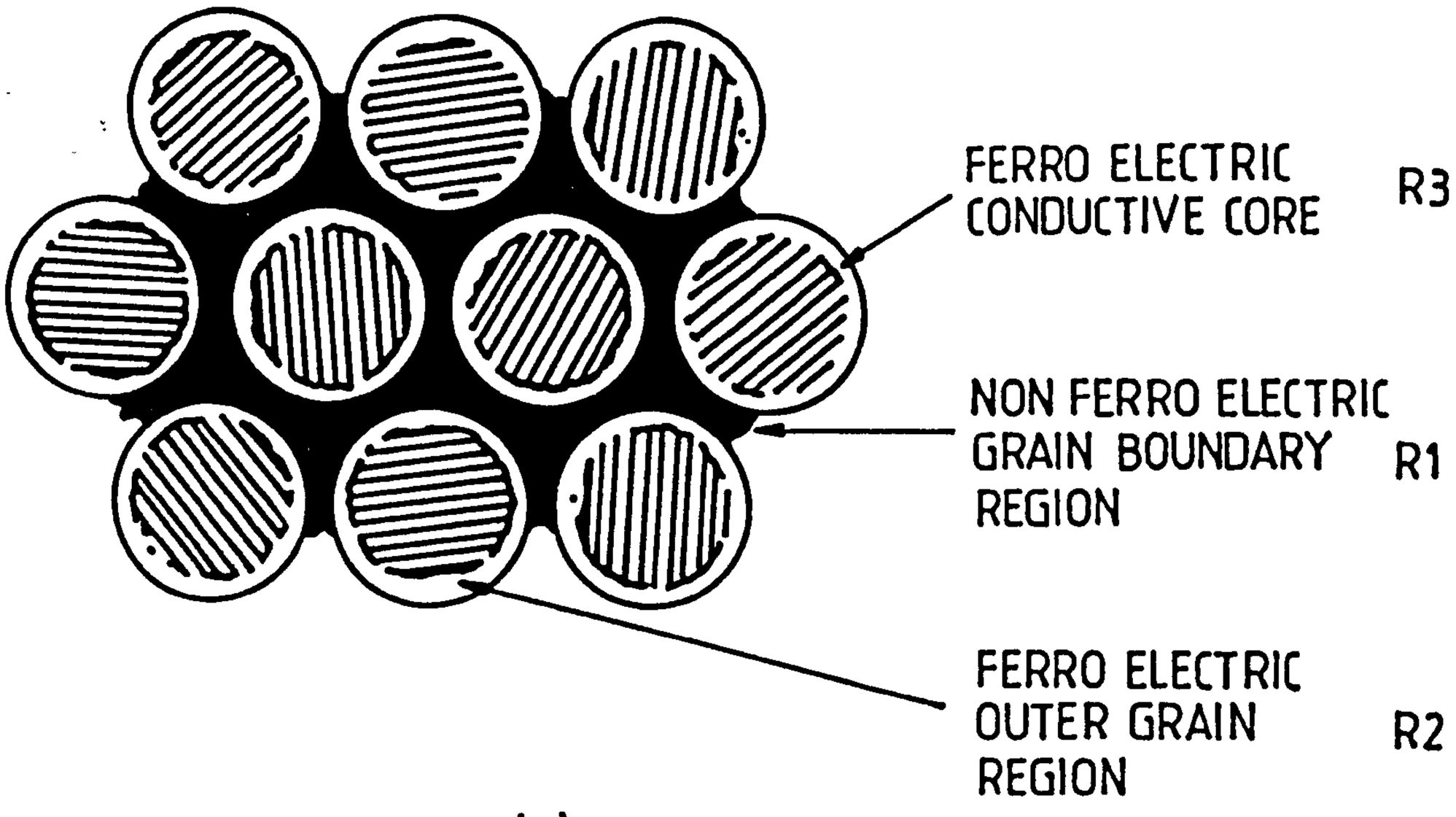

(a)

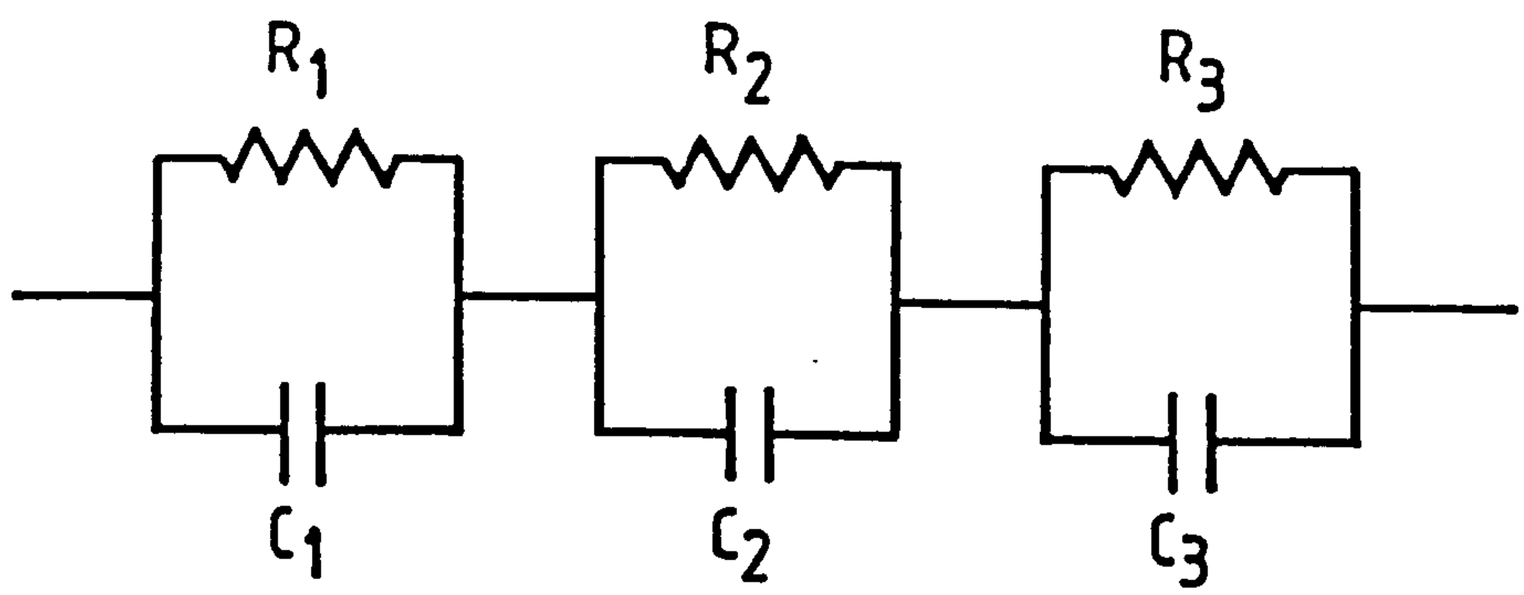

(b)

Figure 2.2 Three-layer model proposed by Sinclair and West[2.4,2.5].

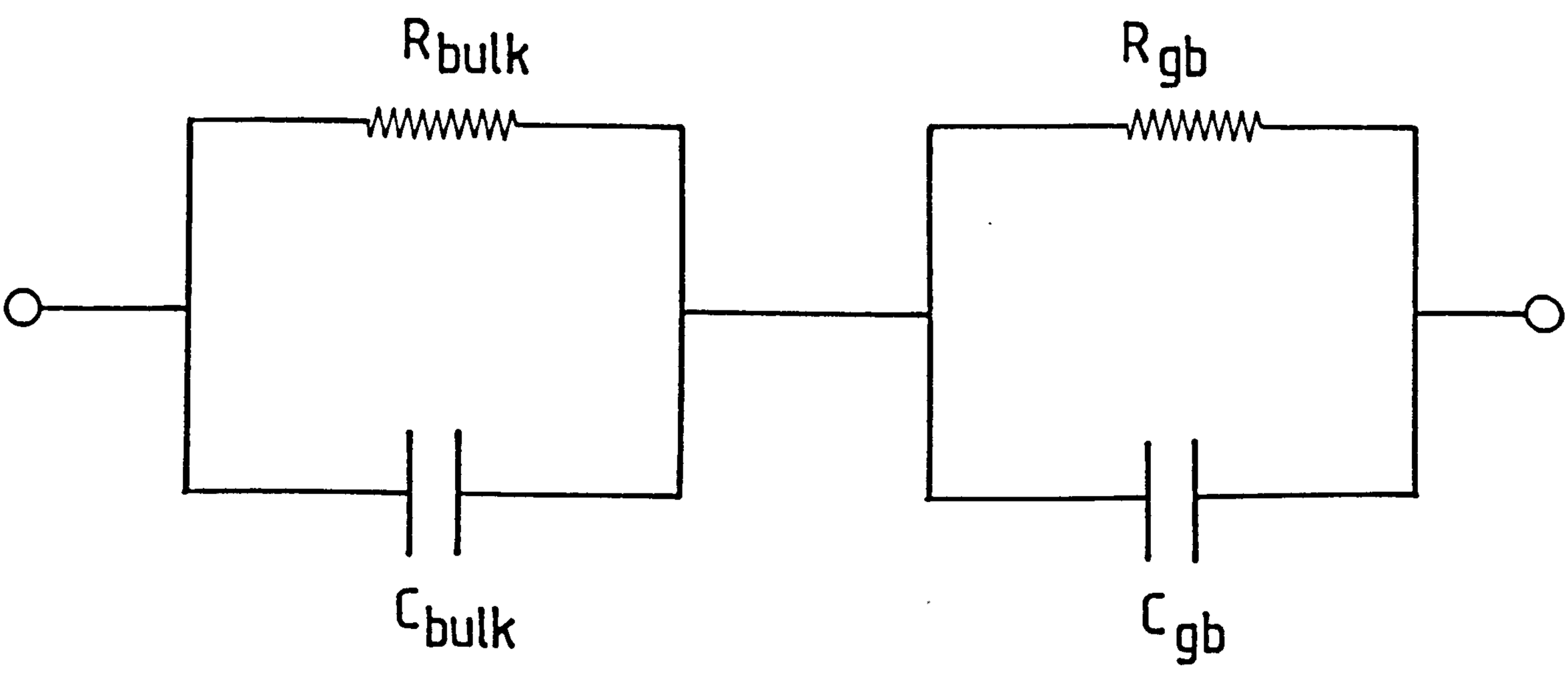

Figure 2.3 Equivalent circuit for the two-layer system, after Peria et al[2.9].

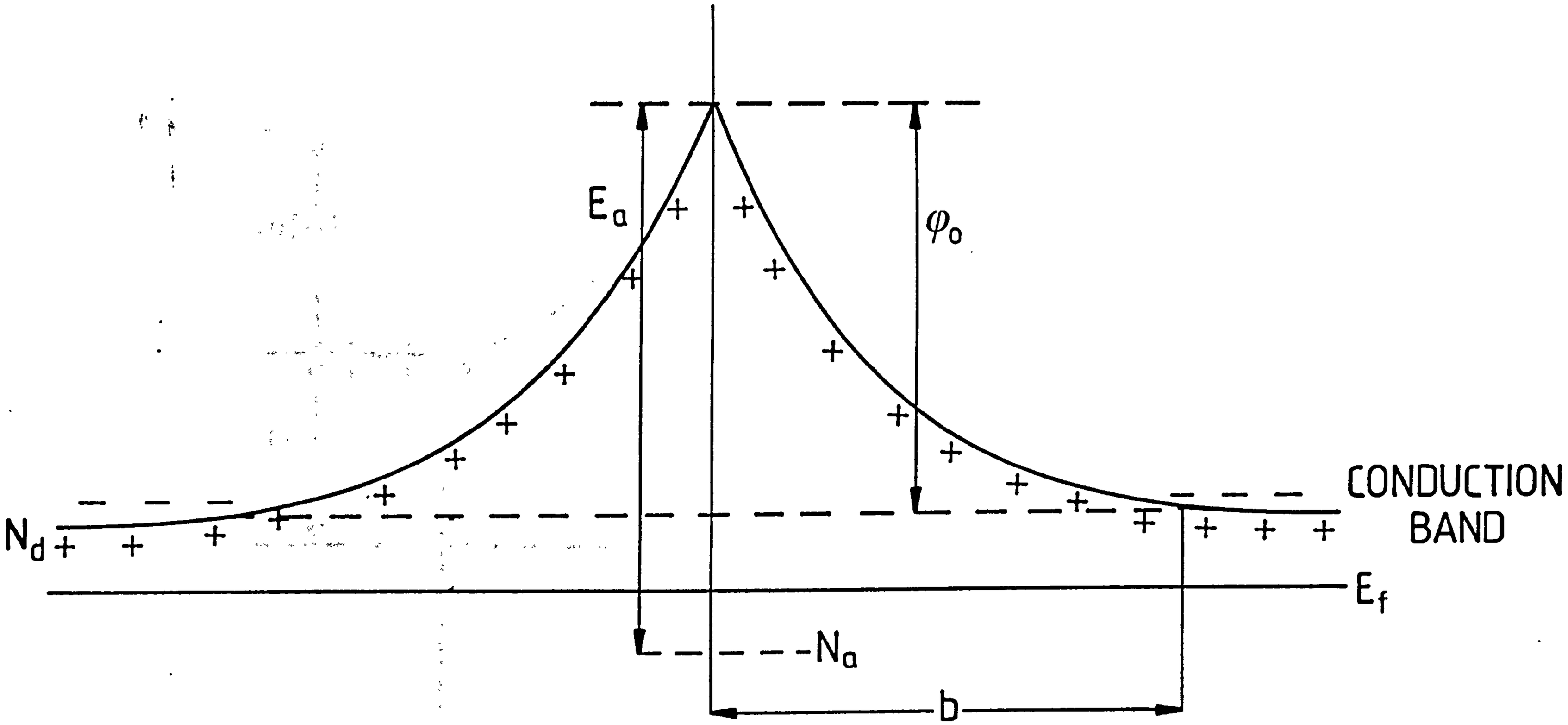

Figure 2.4 Grain boundary Schottky barrier proposed by Heywang[2.15].

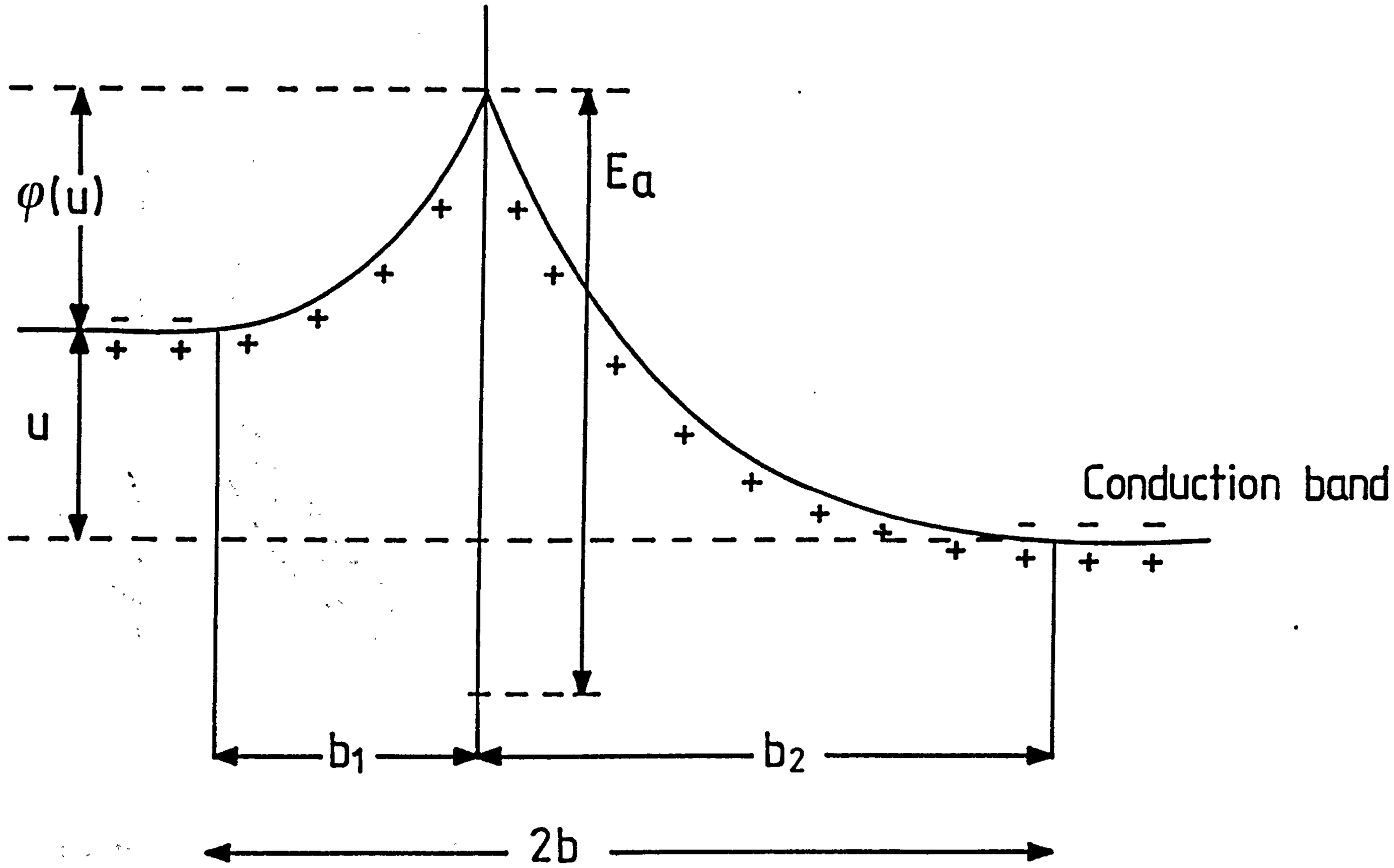

Figure 2.5 Modified potential barrier upon application of voltage U per grain boundary.

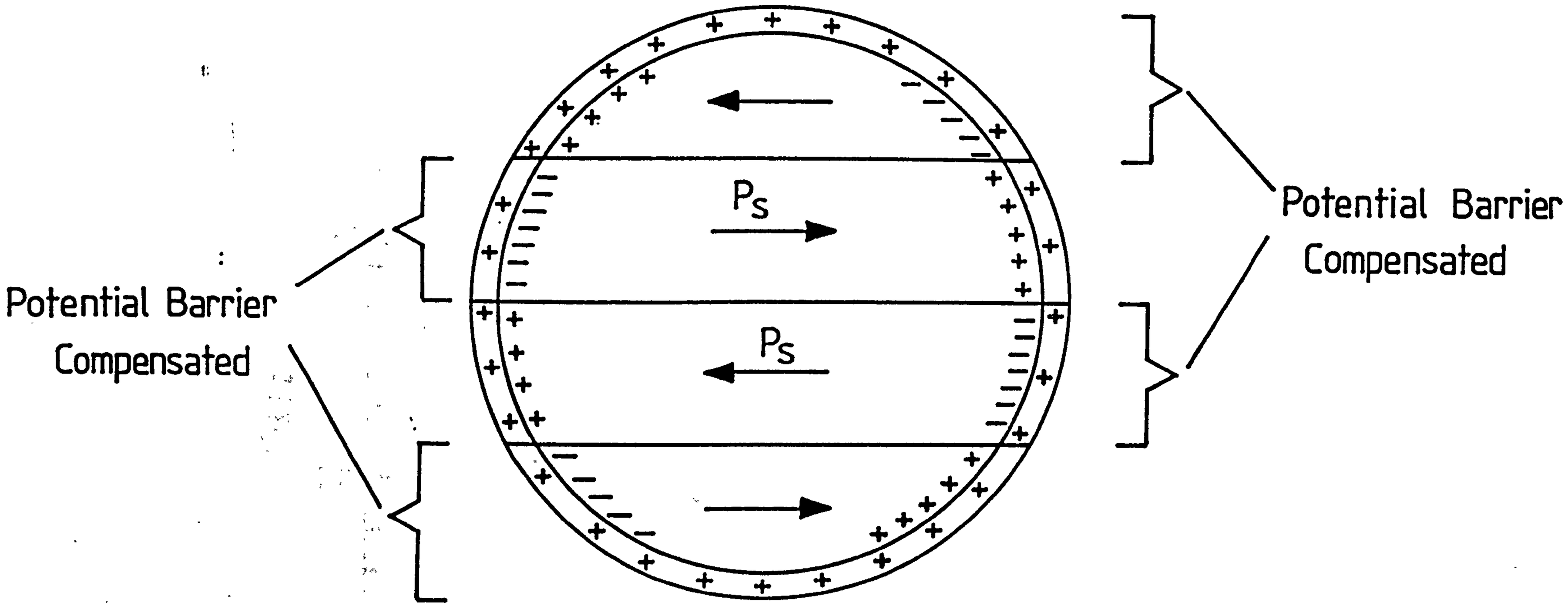

Figure 2.6 Compensation of the grain boundary potential barrier below T_c, after Jonker[2.11].

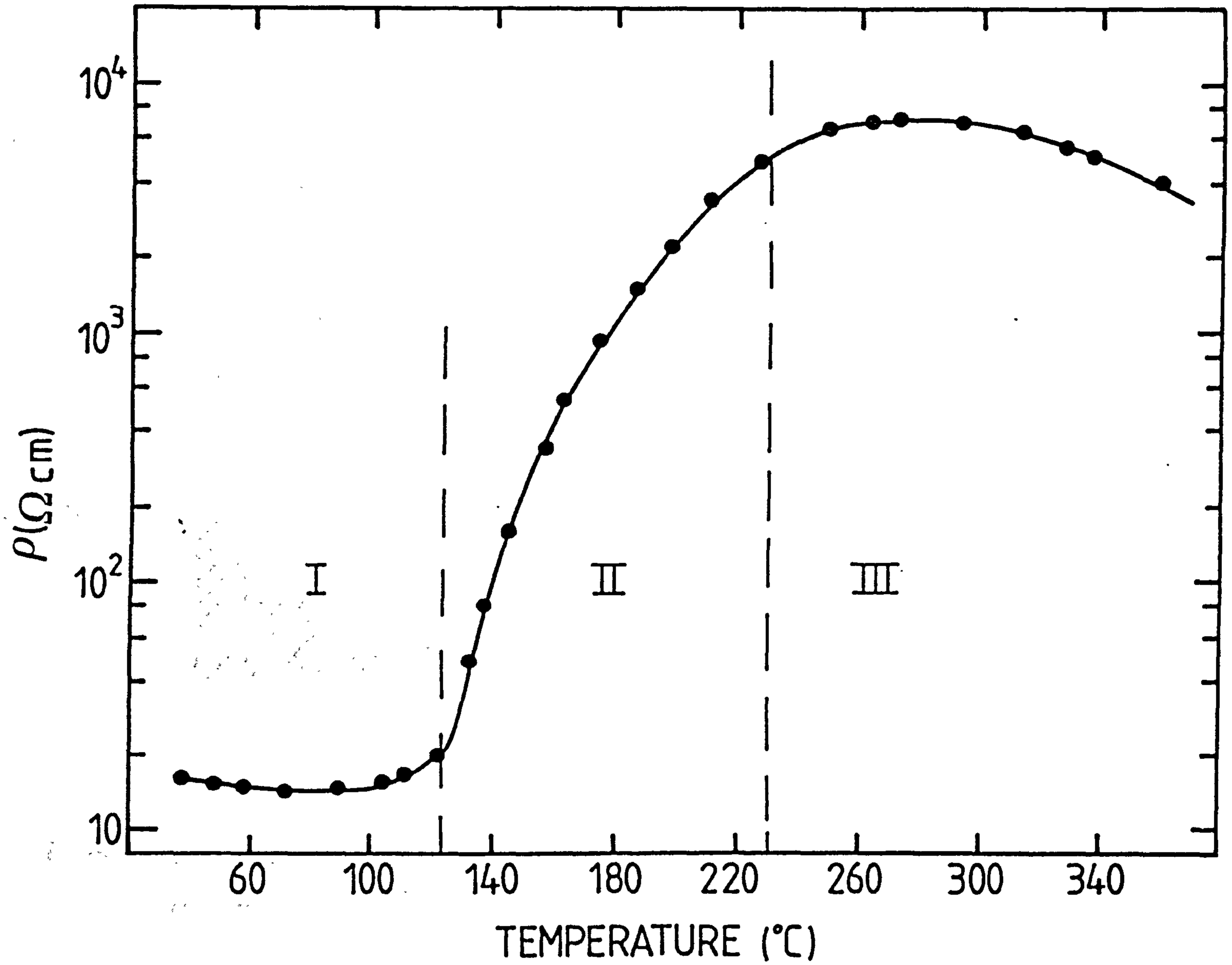

Figure 2.7 Typical PTCR resistivity-temperature characteristic.

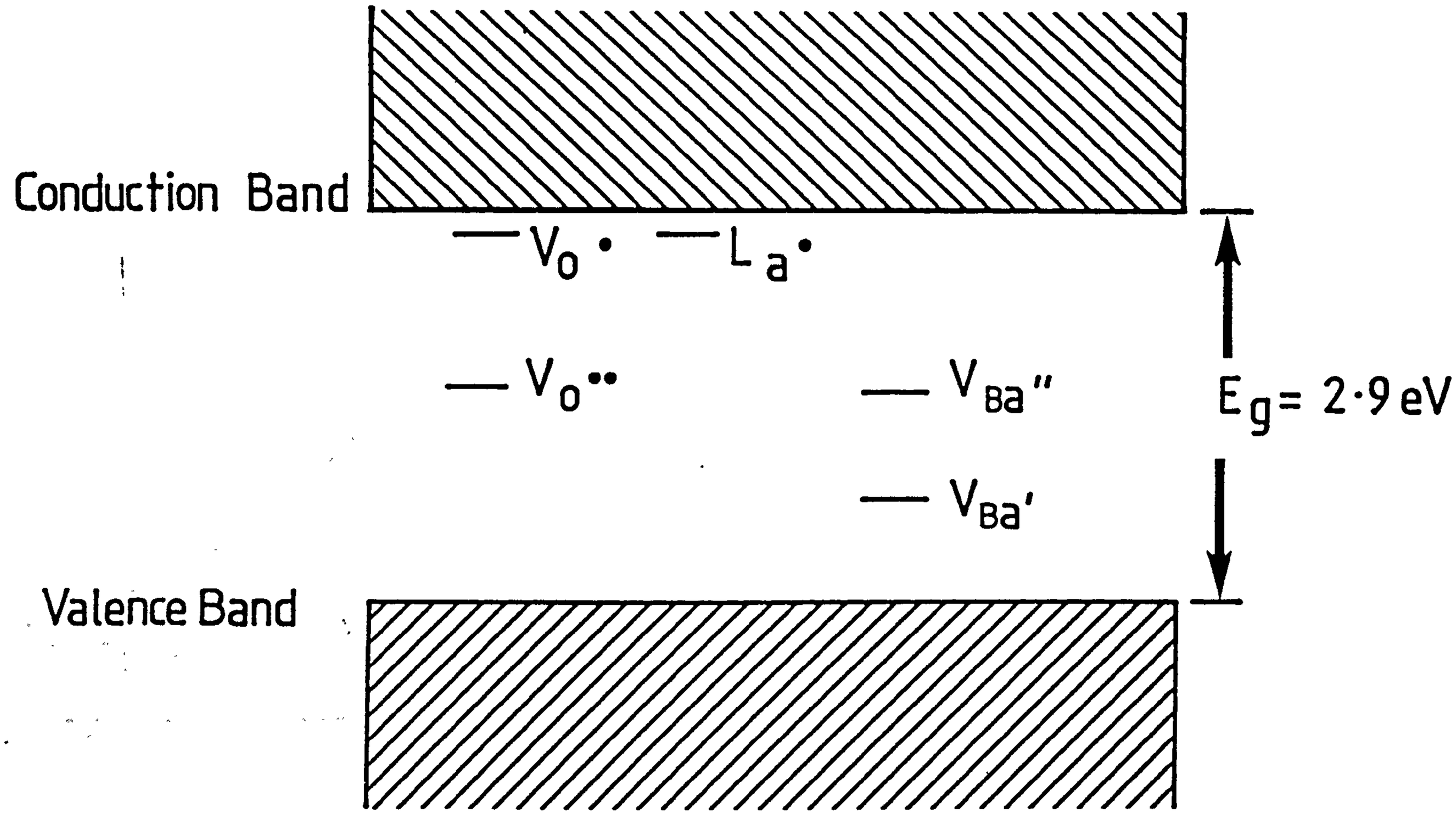

Figure 2.8 Energy level diagram for donor doped barium titanate ceramic, after Daniels et al[2.23].

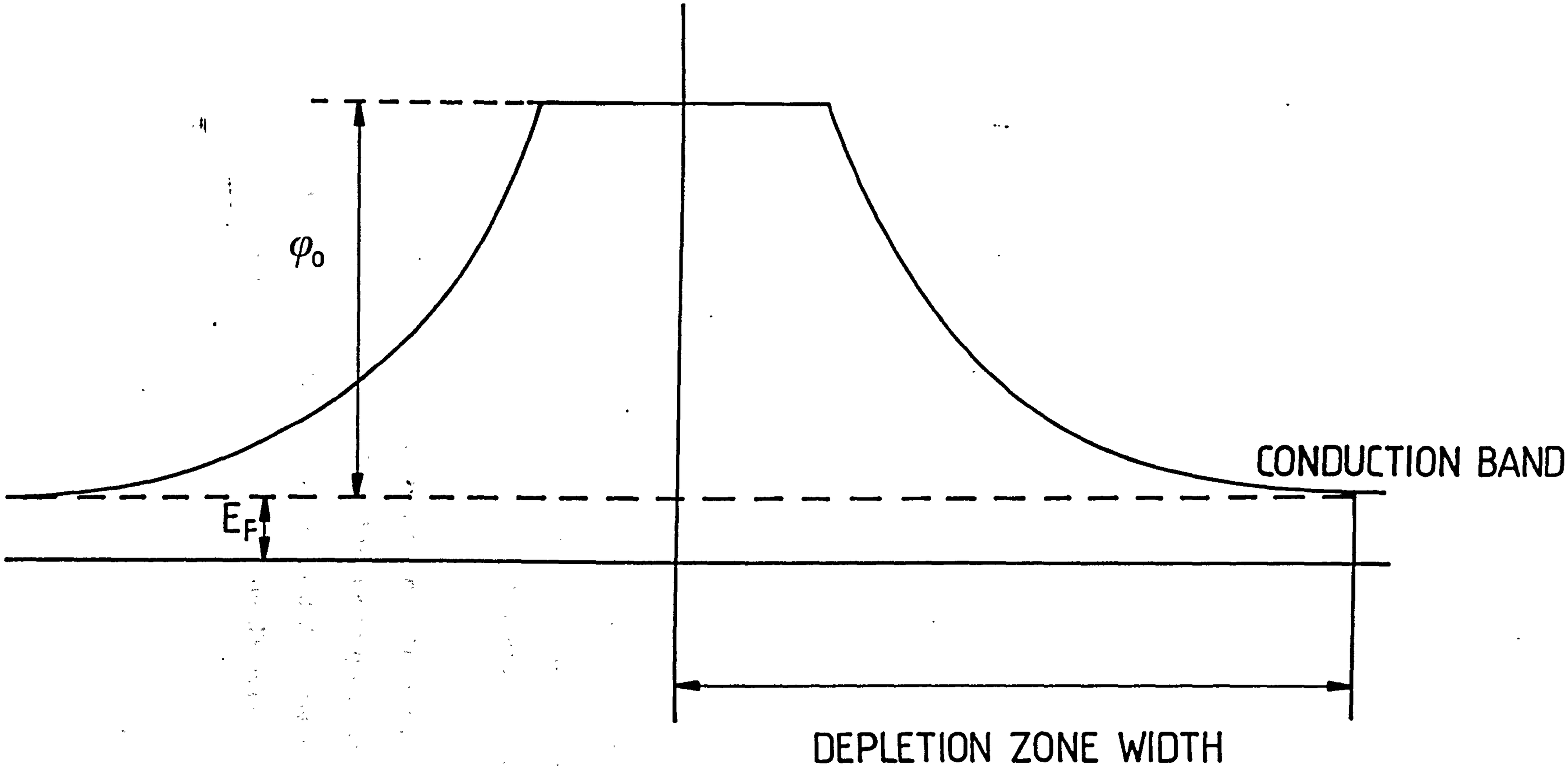

Figure 2.9 Modified grain boundary potential barrier, proposed by Daniels et al[2.23]

CHAPTER THREE

EXPERIMENTAL TECHNIQUES

Semiconducting barium titanate ceramics were prepared by incorporating small amounts of donor (impurity) ions to barium titanate powder. Following a conventional ceramic processing route, samples were heat-treated to dissolve the donor ions into the barium titanate lattice and to induce densification and grain growth. The blue ceramics which were obtained were examined using the scanning electron microscope and energy dispersive x-ray analysis to determine their microstructure and composition. Electric and dielectric measurements were carried out for the purposes of classification and investigation of the electrical properties of the material. Resistance and capacitance were measured as temperature was raised through the Curie temperature, from which resistivity and relative permittivity - temperature characteristics were obtained. The non-ohmic nature of this material, both below and above the Curie temperature, was investigated by measuring the current as voltage was increased. Finally, ac impedance measurements at room temperature were used to separate the resistance attributable to the grain bulk from that due to the grain boundary of the donor doped barium titanate material.

Having collected these results, the Heywang model was utilized to analyze them. Simple algebraic rearrangement of the model allowed the characteristics of the grain boundary acceptor traps and the height of the grain boundary potential barrier to be calculated.

The following sections of this chapter describe the experimental techniques used in the preparation of the samples and their subsequent microstructural and electrical characterization. Methods of analysis of these results are described in later chapters, where they are more relevant to the discussion.

3.1. Sample Preparation - Powder Processing

Semiconducting barium titanate ceramics were prepared using a conventional route[3.1,3.2], shown schematically in figure 3.1. The powders were weighed and ball milled together in a polyethylene jar, where the mixing media were agate balls and deionized water, for 12 hours. The resulting slurry was filtered and dried to give a powder cake which was crushed to a fine powder in a glass pestle and mortar. Binder solution containing equal proportions of 5% solutions of PVA and glucose were mixed with the powder and the paste was dried in an air oven at 70°C. The mixture was then crushed once again and passed through sieves having apertures of 500 and 90μm, where those granules which remained on the finer sieve were collected for use. Small pellets 4mm in diameter and ~1mm thick were pressed under a load of 600kg in a carbide die.

Holmium oxide, Ho_2O_3, was chosen as the donor dopant because the Ho^{3+} ion is similar in size to the Ba^{2+} ion and will easily substitute for barium in the lattice. Where acceptor doping was to take place, $MnCO_3$ was added, since the Mn^{2+} ion has been reported[3.3] to act as an acceptor, substituting onto Ti^{4+} sites. The process of sintering was aided by the addition of a small amount of SiO_2 (0.9mol%) or Si_3N_4 (0.3mol%) and 0.5mol% excess TiO_2 which combine at high temperatures to form a liquid phase. Upon cooling the second phase may be found between grains or segregated to the surface of the sample[3.4–3.7] and is believed[3.8] not to have a significant effect on the PTCR characteristic. For most investigations the precursor powder was a commercial grade of high purity barium titanate but in some investigations barium titanate was prepared from $BaCO_3$ and TiO_2. In these cases extra processing stages were necessary, as shown in figure 3.1: after milling, filtering and drying, the powder was calcined in an alumina crucible to induce the solid state reaction between the $BaCO_3$ and TiO_2 but to prevent any densification or grain growth. The powder was then returned to the ball mill where it was mixed a second time for a further 12 hours to break down

any agglomerates which may have formed during calcination and to mix together any non-stoichiometric phases. The slurry was then filtered and dried, after which processing continued as usual.

It is well known that ceramics are sensitive to their processing[3.9,3.10], particularly when their characteristics are dependent on small changes in composition, such as in the case for donor doped barium titanate ceramics. Control of composition was maintained throughout processing by the careful choice of equipment and by maintaining a consistent method. The jar in which the powders were mixed was made of polyethylene, which is completely combustible, and the mixing balls were agate, a very hard form of SiO_2. Any contamination from milling, therefore, would affect only the second phase composition and since milling time was consistent, the small amount of SiO_2 added was the same in each mix. All equipment at all stages was thoroughly washed with deionized water to ensure cleanliness and the powders, before and after mixing, were covered to minimise dust from the environment.

3.2. Sample Preparation - Sintering

Pure barium titanate has been found to sinter at temperatures between 1150 and 1250°C, depending on the stoichiometry[3.11–3.14]. The addition of donor dopant, however, tends to increase the sintering temperature towards 1350°C, as a result of the grain growth inhibiting effect of the dopant ions[3.15–3.23]. The samples used in the present experiments were sintered in either a Vecstar VH2 1600°C muffle furnace or a Lenton Thermal Designs 1600°C tube furnace. Both were used to sinter samples in air but where sintering atmosphere was to be controlled, the tube furnace, which had been adapted for this purpose, was used, with mixtures of O_2 and N_2 flowing at a rate upto 1.5 l/min.

Problems often associated with handling samples after the binder has been burnt away were removed by choosing sintering regimes where it was burnt away

during the first stage of heat-treatment. Figure 3.2 shows a typical sintering cycle, showing each stage of the heat-treatment process. Binder removal was carried out at 500°C for 90 minutes, heating slowly to avoid any disruption of the particles during early binder burn-off, in air or in a mixture of 20%O_2/80%N_2, where subsequent sintering was to be carried out in an atmosphere containing less than 20% oxygen. Before the next stage, the gas mixture was set to the new desired composition and the furnace purged for 30 minutes. In stage two the temperature was raised quickly to the maximum, sintering temperature. Typical heating rates employed were 600 or 900°C/hour. The sintering temperature, rather than the time, has been shown to have a greater effect on the microstructure of these ceramics[3.24–3.26], in common with experience with other ceramic and metallic materials. The process of grain growth and densification may be described, empirically, as

$$d = f_1(T) + f_2(t) \tag{3.1}$$

where d is the grain size, T is sintering temperature, t is sintering time. f_1 is commonly an exponential function, incorporating an activation energy for the densification and grain growth processes and f_2 usually contains a power of t between 0.1 and 0.5[3.27]. Basu and Maiti[3.24] observed no significant change in grain size when sintering time was varied between 20 and 600 minutes, in agreement with Yoneda et al[3.26], who found that the sintering temperature affected grain size to a very great extent, the average diameter being $\sim 4\mu$m when sintering was carried out at 1280°C and $>10\mu$m when this was raised to 1340°C. In other words, it appears that sintering time is much less important to the development of the microstructure than the sintering temperature and that $f_1(T)$ is the dominating factor in equation 3.1. Basu and Maiti[3.24], however, also observed that the time for which the sample was held at the sintering temperature did affect the electrical characteristics; in particular, room temperature resistivity was increased and the PTCR resistivity anomaly was steeper, with the maximum resistivity occuring

at lower temperatures as sintering time lengthened. These observations highlight the need to maintain as much control as possible by preparing each sample in the same way. Sintering typically took place at 1350-1460°C for 60 minutes.

The third stage of sintering was that of cooling. During this procedure it is assumed that no further significant microstructural development takes place, but that the grain boundary layer is affected. It is generally thought[3.6,3.24,3.28–3.31] that the cooling process is of particular importance for the development of the resistive grain boundary layer. Wernicke[3.28] and Daniels et al[3.29] (see also Chapter 2.2) suggested that this is due to the inward diffusion of barium vacancies from the grain surfaces which act as acceptors, compensating the donors and creating a resistive grain boundary layer. Samples were cooled, typically at a rate of 300°C/hour, to 800°C and thereafter at the natural cooling rate of the furnace. According to Daniels and co-workers[3.29], the diffusivity of barium vacancies below 800°C becomes negligible and no further diffusion can take place and there is no need for controlled cooling below this temperature. In some cases, cooling was interrupted to include an annealing stage, at a temperature at which grain growth and densification do not occur, typically ~1200°C, for 5 hours.

3.3. Microstructural Characterization

3.3.1. Scanning Electron Microscopy

Samples were examined using a Cambridge Instruments S600 scanning electron microscope (SEM), in secondary electron emission mode. In the SEM an electron beam ~100Å in diameter is scanned across an area of the sample under investigation. A small proportion of the beam is reflected elastically from the surface (backscattered electrons). The rest undergo inelastic collisions, resulting in the generation of secondary electrons which are able to escape from upto 500Å below the surface. It is these secondary electrons which are used in routine topographic imaging.

The surfaces of samples which were examined using SEM in either the as-fired state, where the sample was removed from the furnace and immediately set onto an aluminium stub, taking care to keep the top surface uppermost, or as polished and etched cross-sections. The latter method is the one most commonly used in the study of ceramic microstructures, although there are a number of associated problems. Samples were prepared by polishing the as-fired surface using emery paper or coarse alumina grit until the region of the sample to be examined was reached, typically the centre. This surface was then polished using progressively finer alumina grit, and finally using 1μm diamond paste. Etching took place in order to allow the distinction between the grains by either chemically or thermally dissolving the grain boundaries, using a solution of 5%HF in HNO_3 or heat-treatment to 1200°C, respectively. The limitations of this method of preparing samples for microscopy are that the polishing procedure is very time consuming and that the sample may be damaged by grain pull-out. The advantages, however, are that voids, intergranular phases and the structure with which the grains fit together may be observed. Samples where grains have been pulled away, however, may give the appearance of being more porous than they actually are, and the average grain size is difficult to determine, since there is no certainty that the grains have been cut across their diameters. Examining as-fired surfaces, however, is less time consuming since no preparation is required, grain size and distribution are easily determined because whole grains are available and the porosity can be estimated from observations of open pores.

The purpose of examining samples with the SEM throughout this work was to observe the microstructure of each sample and then to obtain average grain size, shape and distribution. In addition, the presence of any second phase on the surface was detected and observed. Hence, most of the microscopy was performed using as-fired surfaces.

3.3.2. Energy Dispersive X-ray Analysis

A Link Systems 860 energy dispersive x-ray (EDX) analyser, fitted to the Cambridge Instruments S600 microscope, was used to determine the chemical composition of samples. X-ray microanalysis is possible in the SEM as a result of the formation of characteristic x-rays from the sample when it is bombarded by the electron beam. The primary electrons eject core (and other) electrons (secondary electrons) and subsequent relaxations from higher energy levels into the empty states are accompanied by the emission of x-rays. For example, when an electron has been ejected from the K orbital, electrons from the L, M and higher shells may relax into the K shell. Those which do so from the L orbital emit Kα x-rays and those from the M orbital emit Kβ radiation. The frequency, ν, of each type of x-ray is given by Moseley's law,

$$\sqrt{\nu} = C(Z - \sigma) \tag{3.2}$$

where C is a constant, Z is the atomic number and σ is a screening factor. Evidently elemental analysis is possible if the energy of the x-rays can be measured. Furthermore, the electron beam of the SEM (~10nm in width) may be positioned onto features of the sample, observed using secondary electron imaging, enabling analysis of sub-micron features.

The EDX analyser is comprised of a liquid nitrogen cooled lithium-drifted silicon reverse biassed p-n junction. The x-rays fall onto the depletion region of the junction, where energy transfer takes place to form electron-hole pairs. Since only 3.8eV is required to make each pair, which is much less than the energy of the x-rays, a large number of pairs are generated. The magnitude of the resulting pulse of electrical current is proportional to the number of electron-hole pairs created which is, in turn, proportional to the energy of the x-rays. The number of current pulses and their magnitudes are sorted using a multichannel analyser, where the bar charts of energy versus magnitude are displayed on a screen. The energies may then be compared with those stored in a computer memory, for

elemental identification. From equation 3.2 it can be seen that the frequency of the characteristic x-rays decreases as the square of the atomic number and since long wavelength x-rays are more strongly absorbed in most media, lighter elements are less easily detected by EDX. Elements having atomic number less than 11 (Na) could not be detected with this analyzer. In addition, the signal/noise ratio of the detection system is ~ 50, which imposes a detection limit on any element of ~2%.

EDX analysis was performed on as-fired as well as polished and etched surfaces, in order to find the composition of grains and any intergranular phases. Other features on the surface, e.g. dust particles or spots of impurities, were also examined using this technique. It was not possible, however, to detect any differences in dopant concentration at grain boundaries as a result of the detection limit.

3.4. Electrical Measurements

3.4.1. Resistivity - Temperature Measurements

Resistance was measured using a technique controlled by a BBC microcomputer; figure 3.3 is a diagram of the experimental arrangement. A two-probe measurement was used since the contact resistance was assumed to be negligible. Up to 10 samples were placed into the air oven, the temperature of which was controlled by the BBC microcomputer via a Eurotherm temperature controller. At each set temperature a voltage of 2V was applied to each sample in turn, where the current passing through the samples was measured on the multimeter. The applied voltage was chosen so that no self-heating of the samples would take place, at the same time as obtaining a sufficiently accurate value of current. Resistance and resistivity were calculated and stored by the microcomputer. The oven temperature was raised to each set point at a rate of ~3°C/min and held for a further 3 minutes to ensure an even sample temperature.

Samples were prepared for resistivity measurements by means of gentle polishing to ensure flat surfaces and to obtain samples of approximately the same thickness (typically ~1mm). Ohmic contacts were made by rubbing an alloy of indium/gallium in the ratio of 2:1 by weight onto the flat surfaces. This material was chosen since both metals have low work functions ensuring the absence of any electron barriers at the contact. In addition, the gallium has a relatively high oxygen affinity (i.e. it is an oxygen getter) and removes surface oxygen which otherwise causes a resistive depletion layer at the contact region. For the purposes of the resistance measurements, four or five samples of each batch were measured at a time, to ensure the reproducibility of the results and to determine the amount of experimental scatter.

3.4.2. Current - Voltage Measurements

The purpose of these measurements was to investigate the non-ohmic effect of increasing electrical field on the resistance. Figure 3.4 shows the arrangment of the apparatus for these experiments. Single short pulses (~1.5ms) of the set voltage were applied across the sample, which was placed in series with a resistance of known value. The voltages across the resistor and the sample were measured using the digital storage oscilloscope and used to calculate the current through the circuit and thus the resisitivty of the sample under the applied electric field. Because high fields were necessary, samples were polished using emery paper to ~0.7mm thickness, to facilitate the application of the field with a suitable voltage supply. These measurements were made above the Curie temperature, in order to remove the effects of the spontaneous polarisation below T_c. For the purpose of this, the samples were placed in a small, heated capsule, controlled with a Eurotherm 810 temperature controller.

According to the Heywang model[3.32,3.33], when a voltage, U, is applied across the grain boundary potential barrier, the space charge region is moved in propor-

tion to U, as shown in figure 2.5. The resulting new potential barrier is given by equation 2.18,

$$\phi(U) = \phi_o(1 - U/4\phi_o)^2,$$

which, in turn reduces the resistivity of the grain boundary layer in accordance with equation 2.9. Analysis of the reduction of resistivity, and the current density across each grain boundary layer, of a sample can be used to obtain an estimated value of ϕ_o at the measuring temperature.

3.5. Dielectric Measurements

3.5.1. Capacitance - Temperature Measurements

Capacitance was measured at a fixed frequency of 30kHz using a Marconi TF1313A ac bridge. Samples were placed in a heated capsule and connected to the bridge with short, air insulated leads which had negligible impedance, figure 3.5. Sample temperature was controlled between ambient and ~360°C with a Eurotherm 810 temperature controller. Measurements were only made after the sample had been maintained at the set point for a few minutes, to ensure an even temperature distribution.

Figure 3.6 shows the mechanism by which capacitance was measured with the ac bridge. The bridge was constructed of four impedances, Z_1 and Z_2 being pure resistances and Z_3 and Z_s equivalent to parallel combinations of resistance, R_3 and R_s, and capacitance, C_3 and C_s, respectively and represent the bridge characteristic and the sample. At balance, the impedances are such that no trace is observed on the oscilliscope, giving, from elementary circuit theory,

$$\frac{Z_1}{Z_1 + Z_s} = \frac{Z_2}{Z_2 + Z_3} \tag{3.3}$$

since $Z_1 = R_1$, $Z_2 = R_2$, $Z_3 = R_3/(1 + j\omega C_3 R_3)$ and $Z_s = R_s/(1 + j\omega C_s R_s)$, equation 3.3 can be written,

$$\frac{R_1(1 + j\omega C_s R_s)}{R_1 + R_s + j\omega C_s R_s R_1} = \frac{R_2(1 + j\omega C_3 R_3)}{R_2 + R_3 + j\omega C_3 R_3 R_2} \tag{3.4}$$

which, upon simplification and separation of the real and imaginary parts, gives an expression for the equivalent parallel capacitance of the sample:

$$C_s = R_2 \times C_3/R_1. \tag{3.5}$$

The parameter C_3/R_1 is a constant factor which is taken into account on the dial of the balancing resistor, R_2. In other words, the dial is graduated in such a way that the value of C_s can be read directly. The resistance, R_3, was obtained using an external variable resistor connected to the bridge, automatically in parallel with C_3, which is within the bridge. The bridge's own balance for R_3 was not used since this gave the loss tangent of the sample, which was not required.

Thin samples were needed for capacitance-temperature measurements to avoid any effects of fringing of the electric field at the sample edges. According to ASTM D150/87[3.34] for disc electrodes without a guard ring, i.e. where the diameter of the electrodes is that of the sample, and the electrode thickness is much smaller than the sample thickness, t, the fringing capacitance, C_e, is given by

$$C_e = (0.0087 - 0.00252\ ln(t)\ ) \times P \tag{3.6}$$

where P is a constant, related to the sample dimensions: $P = \pi \times (d + t)$, where d is the sample diameter. The fringing capacitance is a parallel capacitance which adds directly to the apparent sample capacitance if it is not negligible, thereby introducing inaccuracies into the measurements. Samples for the present experiments were ~0.7mm thick and were 4mm in diameter, giving C_e ~0.1pF. This is over three orders of magnitude lower than typical sample capacitances (which were of the order of μF) and so the fringing capacitance was ignored for the duration of the measurements.

Ohmic electrodes were obtained, as described previously, with In/Ga alloy rubbed onto the flat surfaces. The capacitance measurements were used to calculate sample, or apparent, permittivity, ϵ'_{app}, using the formula,

$$\epsilon'_{app} = C_s \times \frac{t}{\epsilon_o A} \tag{3.7}$$

where A is the area of the electrodes. For most investigations, two samples from each batch were measured to ensure reproducibility.

3.5.2. A.c. Impedance measurements

According to ac theory, plots of the real part of ac impedance versus the imaginary part permit the separation of the grain bulk and grain boundary resistance of donor doped barium titanate ceramics, in accordance with a simple model. Ac impedance measurements were carried out at room temperature at frequencies upto 50MHz using the ac bridge and a Hewlett-Packard HP4342A Q-meter. The ac bridge was employed between ~100Hz and 40kHz, where the equivalent parallel resistance and capacitance of the sample were obtained in the same way as described in paragraph 3.5.1. One adjustment was made to the balancing resistors: R_3 was measured by means of an internal resistor, the dial giving the value of Q ($1/\tan\delta$, the dielectric loss factor) at balance. For the purpose of the impedance measurements, however, a series connection of resistance and capacitance was required, although only the parallel equivalent values could be measured using the ac bridge. The series equivalent values were calculated from the parallel results in the following way: impedances of the parallel and series equivalent circuits, Z_p and Z_s, respectively, are described in terms of R_p, C_p, R_s and C_s, the resistance and capacitance of each circuit, respectively. Z_p is equivalent to Z_s since each circuit is used to describe the same sample. Hence,

$$Z_p = \frac{R_p}{1 + j\omega C_p} = \frac{R_p(1 - j\omega C_p R_p)}{1 + \omega^2 C_p^2 R_p^2} \tag{3.8}$$

and

$$Z_s = R_s + \frac{1}{j\omega C_s} \tag{3.9}$$

where $\omega = 2\pi f$ and f is the frequency of the applied ac voltage. Since Q, for a parallel connection, is defined as $Q = \omega\ R_p\ C_p$, equation 3.8 can be written

$$Z_p = \frac{R_p}{1 + Q^2} - j\frac{Q^2}{\omega C_p(1 + Q^2)} \tag{3.10}$$

Since $Z_p = Z_s$, then

$$R_s = R_p(\frac{1}{1+Q^2}) \tag{3.11}$$

and

$$C_s = C_p\frac{(1+Q^2)}{Q^2}. \tag{3.12}$$

In series connection, Q is also defined as $Q = X_s/R_s$, where X_s is the series reactance, so

$$X_s = Q \times R_s. \tag{3.13}$$

At each frequency a balance is obtained with a unique combination of C_p and Q, hence R_s and X_s can be obtained.

Measurements at higher frequencies were made using the Q-meter, also assuming series connection of resistance and capacitance. Figure 3.7 is a schematic diagram of the Q-meter, which operates on the principle of resonance between the inductor, L, and the Q-meter or the inductance, Q-meter and sample in series. Measurements are taken in the following way: firstly the Q and C values of the meter alone, in series with the inductor, are obtained by shorting across the sample and tuning the variable capacitor, C_m, to give maximum deflection on the meter. The sample is then included into the circuit, where C_m is adjusted again, to obtain resonance. If C_1 and Q_1 are the values of capacitance and Q of the meter alone and C_2 and Q_2 are those when the sample is added, the equivalent series resistance, R_s, and Q of the sample are obtained using the equations

$$Q = \frac{Q_1Q_2(C_1 - C_2)}{C_1Q_1 - C_2Q_2} \tag{3.14}$$

$$R_s = \frac{(C_1/C_2)Q_1 - Q_2}{\omega C_1Q_1Q_2} \tag{3.15}$$

X_s is then obtained from equation 3.13.

For optimum operation of the Q-meter it is necessary to find as large as possible a value for C_1 - C_2 to obtain an accurate value for Q. As a result, measurements of Q were subject to inaccuracies at low frequencies (<100Hz) because values of

(C_1 - C_2) were generally small, particularly with conducting samples (R <100Ω), as was often the case.

According to Basu & Maiti[3.24], impedance plots of X_s versus R_s permit the separation of the grain bulk and grain boundary resistance. The grain bulk and boundary may each be modelled as a parallel combination of resistance and capacitance, making a two-layer equivalent circuit, as shown in figure 3.8, having R_{bulk}, C_{bulk}, R_{gb} and C_{gb}, respectively. Since the grain bulk may be assumed to have negligible dielectric effect because it is conductive, C_{bulk} may be ignored. The impedance, Z, of the equivalent circuit is then given by

$$Z = R_{bulk} + \frac{R_{gb}}{1 + j\omega C_{gb} R_{gb}}. \tag{3.16}$$

Multiplying the second term in equation 3.16 by its complex conjugate gives

$$Z = R_{bulk} + \frac{R_{gb}}{1 + \omega^2 C_{gb}^2 R_{gb}^2} - j\frac{\omega C_{gb} R_{gb}}{1 + \omega^2 C_{gb}^2 R_{gb}^2}. \tag{3.17}$$

It can be seen from the theory relating to the impedance measurements that the real and imaginary parts of Z are equivalent to R_s and X_s, respectively. Thus,

$$R_s = R_{bulk} + \frac{R_{gb}}{1 + \omega^2 C_{gb}^2 R_{gb}^2} \tag{3.18}$$

and

$$X_s = \frac{\omega C_{gb} R_{gb}}{1 + \omega^2 C_{gb}^2 R_{gb}^2} \tag{3.19}$$

As frequency changes it is evident that the values of R_s and X_s are affected: at low frequency, $\omega \rightarrow 0$ so $R_s \rightarrow R_{bulk} + R_{gb}$ and $X_s \rightarrow 0$. On the other hand, at very high frequency, $\omega \rightarrow \infty$ so $R_s \rightarrow R_{bulk}$ and X_s again $\rightarrow 0$. The values of R_{bulk} and R_{gb} can be obtained from the intercepts on the real axis, at high and low frequency, respectively.

3.6. Theoretical prediction of the PTCR characteristic

According to the Heywang model[3.32,3.33] the grain boundary potential barrier height, $\phi_o(T)$, is given by equation 2.5,

$$\phi_o(T) = \frac{eN_a(T)^2}{8\epsilon_o\epsilon' N_d}$$

where e is the electronic charge, $N_a(T)$ is the density of ionized surface acceptor traps, ϵ_o is the permittivity of free space, ϵ' is the relative permittivity of the material in the grain boundary layer and N_d is the charge carrier concentration. The surface traps exist at an energy, E_a, below the Fermi level, E_F and according to Heywang the density of the surface states is dependent on the difference between the potential barrier height and the depth of the acceptor traps, equation 2.6,

$$N_a(T) = \frac{N_{ao}}{1 + exp[(e\phi_o(T) + E_F - E_a)/kT]}$$

where N_{ao} is the initial density of surface traps, k is the Boltzmann constant and T is absolute temperature. The Fermi level is given, in semiconductor physics, as

$$E_F = kTln(N_d/N_c) \tag{3.20}$$

where N_c is the effective density of carrier states (equivalent to the Ti^{4+} concentration[3.35], $1.56 \times 10^{22}cm^{-3}$, equivalent to the concentration of sites upon which electron transfer takes place[3.36].

As temperature is raised above the Curie temperature, T_c, the permittivity of the grain boundary layers decreases in accordance with the Curie-Wiess law,

$$\epsilon' = C/(T - \theta) \tag{3.21}$$

where C is the Curie constant and θ is the Curie point, thus raising the potential barrier height. As $\phi_o(T)$ increases with temperature the energy of the acceptor traps begins to approach the Fermi level and depopulation of the acceptor traps begins to take place. This in turn reduces $\phi_o(T)$ in accordance with equation

2.5 and counteracts the effect of the reducing permittivity. Thus, a dynamic equilibrium is obtained between $N_a(T)$ and ϵ', which results in a saturation value of ϕ_o and a maximum value of resistivity.

Theoretical modelling of the PTCR characteristic was carried out using a program available on the Archimedes computer, which solved equations 2.5 and 2.6 numerically to obtain values of $\phi_o(T)$ between 400 and 600K. The permittivity of the grain boundary layer material was assumed to obey the Curie-Weiss law at all temperatures above T_c. N_d was obtained using results from the impedance measurements, as described in section 5.4 (equation 5.26) and E_a and N_{ao} were either estimated or determined from experimental results. Having determined $\phi_o(T)$ at each temperature, the computer was programmed to calculate values of resistivity using the equation,

$$\rho(T) = (N_d e\mu)^{-1} \times [\frac{(1 + zb(T)kT}{e\phi_o(T))} \times exp(\frac{e\phi_o(T)}{kT})] \qquad (3.22)$$

where z is the number of grains per cm and b is the width of the grain boundary layer.

Theoretical modelling was carried out to investigate the effects of acceptor trap energy and density on the PTCR characteristic and to predict or verify experimental observations.

REFERENCES

3.1 Ichinose N., 'Introduction to Fine Ceramics', (John Wiley and Sons, New York, 1987), p.16.

3.2 Moulson A.J. and Herbert J.M., 'Electroceramics', (Chapman and Hall, London, 1990), p.88.

3.3 Ihrig H., J. Am. Ceram, Soc., 64, 617, 1981.

3.4 Kingery W.D., Bowen H.K. and Uhlmann D.R., 'Introduction to Ceramics', (John Wiley and Sons, New York, 1976), p.498.

3.5 Udayakumar K.R., Brooks K.G., Taylor J.A.T. and Amarakoon V.R.W., Ceram. Eng. Prod. Sci., 8, 1035, 1987.

3.6 Al-Allak H.M., Russell G.J. and Woods J., J. Phys. D: Appl. Phys., 20, 1645, 1987.

3.7 Al-Allak H.M., Brinkman A.W., Russell G.J., Roberts A.W. and Woods J., J. Phys. D: Appl. Phys., 21. 1226, 1988.

3.8 Cheng H.F., J. Appl. Phys., 66, 1382. 1989.

3.9 Messer P.F., Trans. J. Brit. Ceram. Soc., 82, 156, 1983.

3.10 Messer P.F., 'A Systematic Approach to Ceramic Processing', unpublished.

3.11 Jonker G.H. and Noorlander W., Science of Ceramics I, ed. G.H. Steward, (Academic, London, 1962), p.255.

3.12 Matsuo Y. and Sasaki H., J. Am. Ceram. Soc., 54, 471, 1971.

3.13 Ueyama T., Yamara S. and Kaneko N., Jpn. J. Appl. Phys., 26, Suppl. 26-2, 139, 1987.

3.14 Hennings D., Janssen R. and Reynen P., J. Am. Ceram. Soc., 70, 23, 1987.

3.15 Drofenik M., Pejovnik S., Irmanonik L., Mocnik I. and Krasevec V., 'Sintering - Theory and Practice ', Proceedings of the 5^{th} International Round Table Conference on Sintering, Yugoslavia, 7-10 September, 1981, Mater. Sci. Monographs, Ed. D. Kolar, S. Pejovnik and M.M. Rustic, (Elsevier, Amsterdam, 1982), p.343.

3.16 Drofenik M., Popvic A. and Kolar D., Ceram. Bull., **63**, 702, 1984.

3.17 Drofenik M., J. Am. Ceram. Soc., **69**, C8, 1986..

3.18 Drofenik M., J. Am. Ceram. Soc., **70**, 311, 1987.

3.19 Lubitz K., 'Sintering - Theory and Practice', Proceedings of the 5^{th} International Round Table Conference on Sintering, Yugoslavia, 7-10 September, 1981, Mater. Sci. Monographs, Ed. D. Kolar, S. Pejovnik and M.M. Rustic, (Elsevier, Amsterdam, 1982), p.343.

3.20 Zajc I. and Drofenik M., Br.Ceram. Trans. J., **88**, 223, 1989.

3.21 Murakami T., Nakahara M., Miyashita T. and Ueda S., J. Am. Ceram. Soc., **56**, 294, 1973.

3.22 Fukami T. and Tsuchiya H., Jpn. J. Appl. Phys., **18**, 735, 1979.

3.23 Kleint C.A., Stöpel U. and Rost A., Phys. Stat. Sol. (a), **115**, 165, 1989.

3.24 Basu R.N. and Maiti H.S., Mater. Lett., **5**, 99, 1987.

3.25 Chiou B.S., Koh C.M. and Duh J.C., J. Mater. Sci., **22**, 2893, 1987.

3.26 Yoneda Y., Kato H. and Sasaki H., J. Am. Ceram. Soc., **59**, 531, 1976.

3.27 Kingery W.D., Bowen H.K. and Uhlmann D.R., 'Introduction to Ceramics ', (John Wiley and Sons, New York, 1976), p.452.

3.28 Wernicke R., Phys. Stat. Sol. (a), **47**, 139, 1978.

3.29 Daniels J., Härdtl K.H. and Wernicke R., Phil. Tech. Rev., **38**, 73, 1978/79.

3.30 Ihrig H. and Puschert W., J. Appl. Phys., **48**, 3081, 1977.

3.31 Ueda I. and Ikegami S., J. Phys. Soc. Jpn., **20**, 546, 1965.

3.32 Heywang W., Sol. Stat. Electron., **3**, 51, 1961.

3.33 Heywang W., J. Am. Ceram. Soc., **47**, 484, 1964.

3.34 American Standards for Testing Materials D150, 1987. *Fringing capacitance for electrodes without a guard ring.*

3.35 Saburi O., J. Phys. Soc. Jpn., **14**, 1159, 1959.

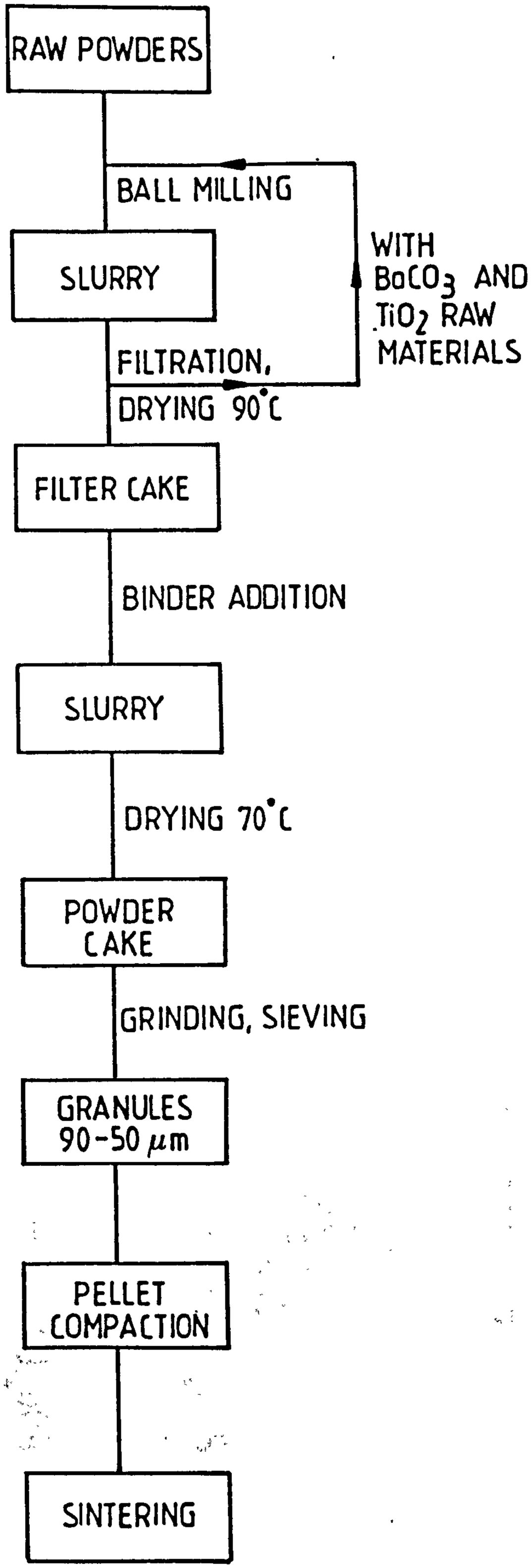

Figure 3.1 Mixed oxide route for ceramic processing.

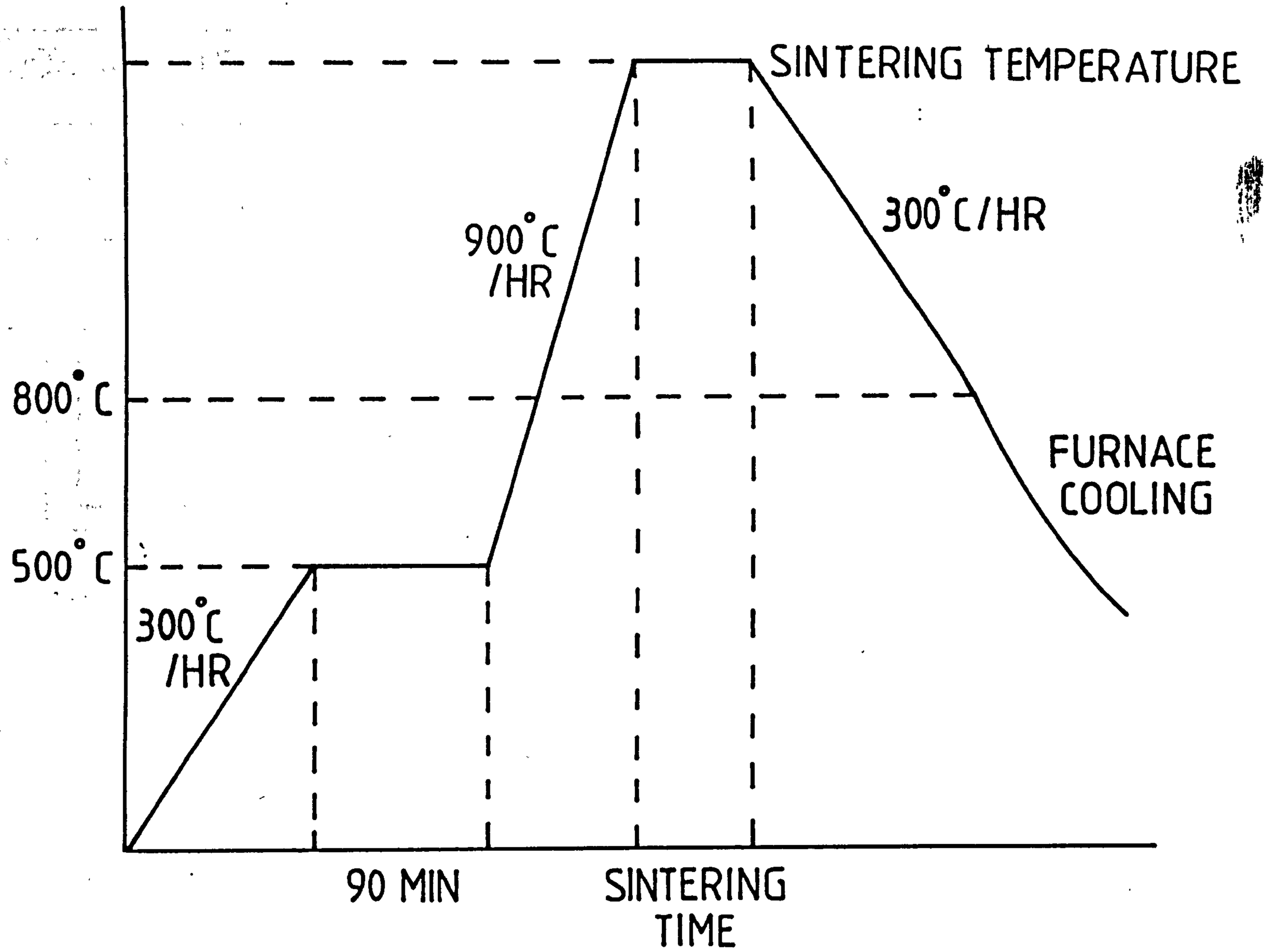

Figure 3.2 Typical sintering regime of T versus time

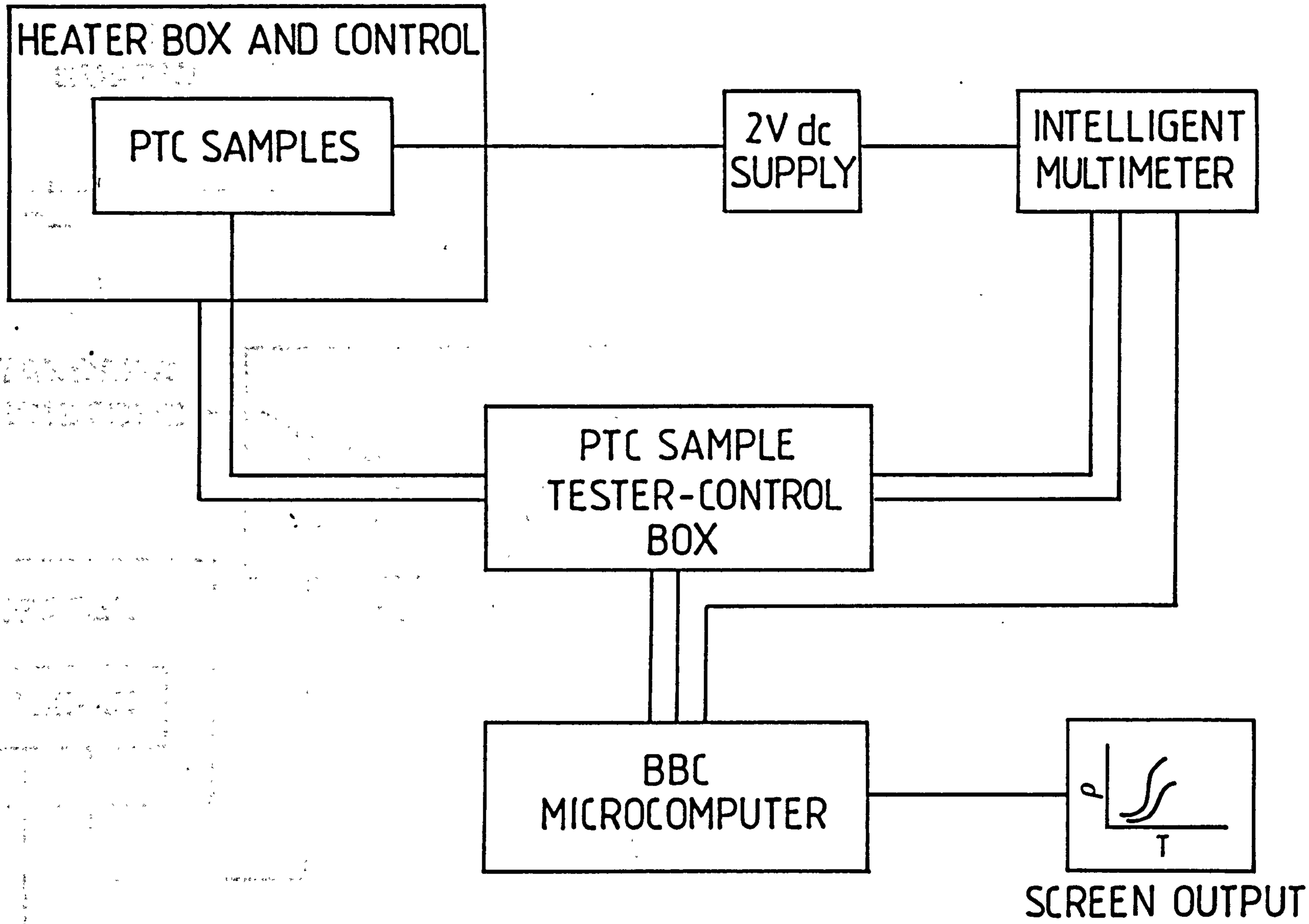

Figure 3.3 Resistivity - temperature measuring system.

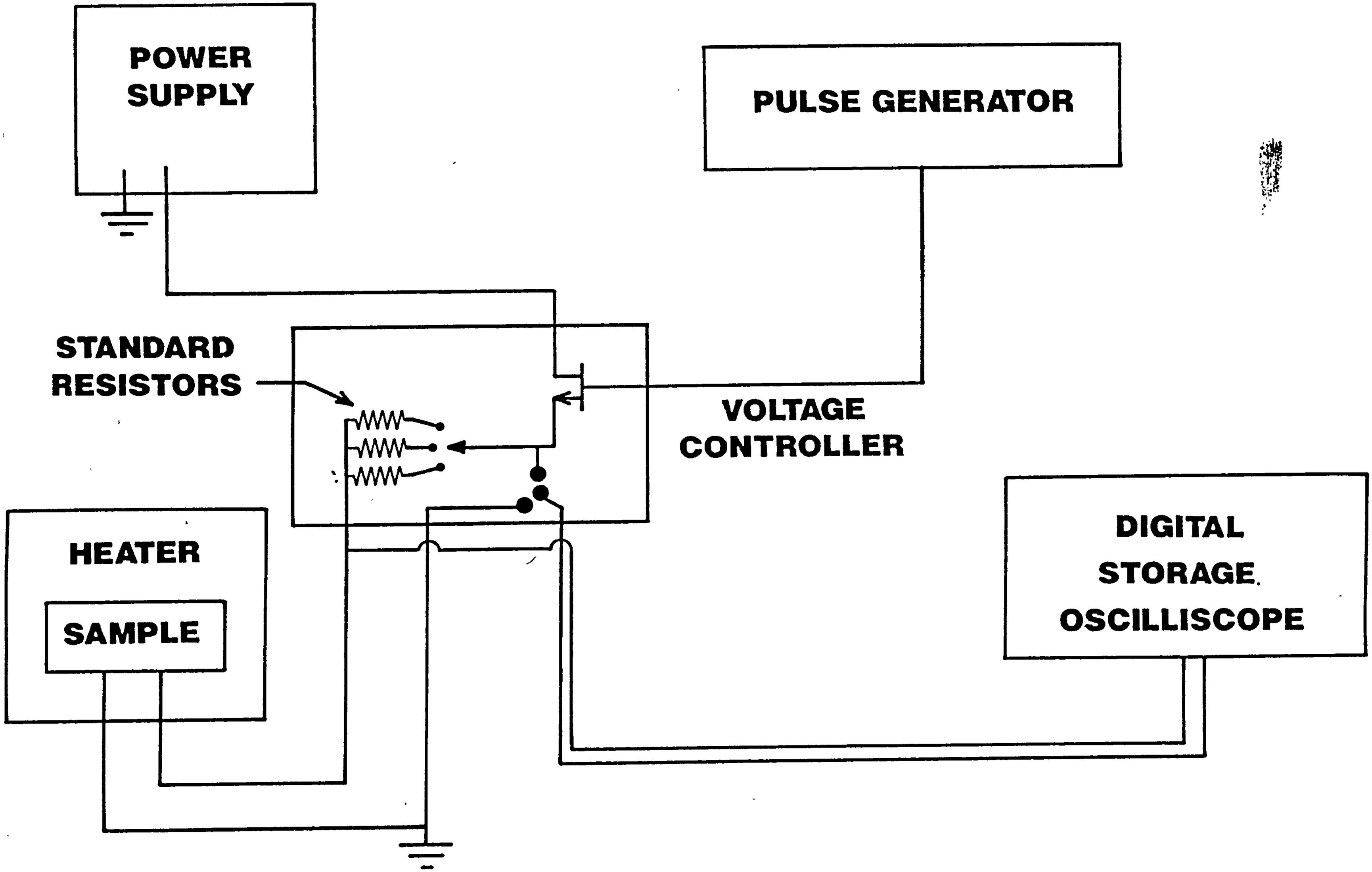

Figure 3.4 Apparatus for current - voltage measurements.

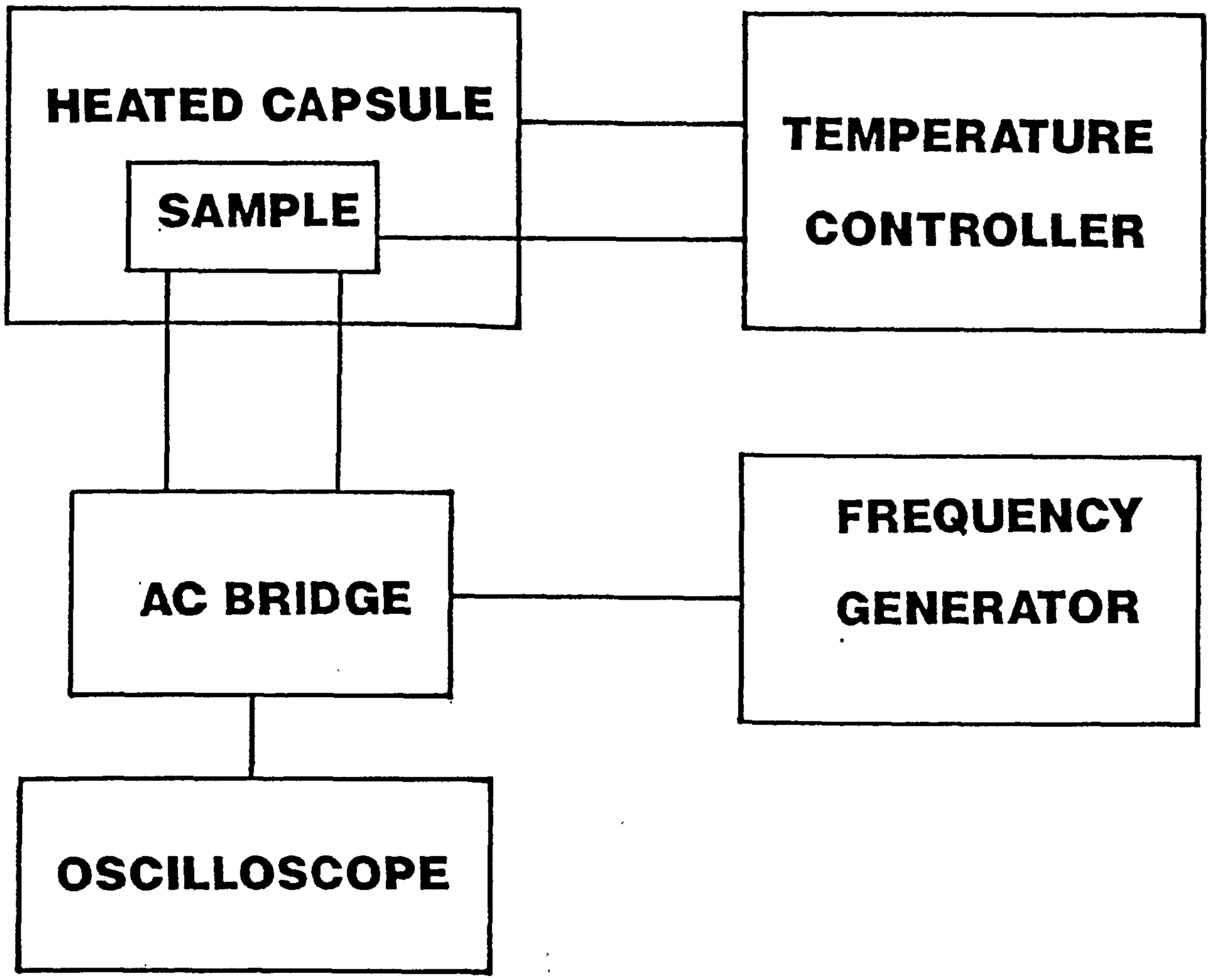

Figure 3.5 Apparatus for capacitance - temperature measurements.

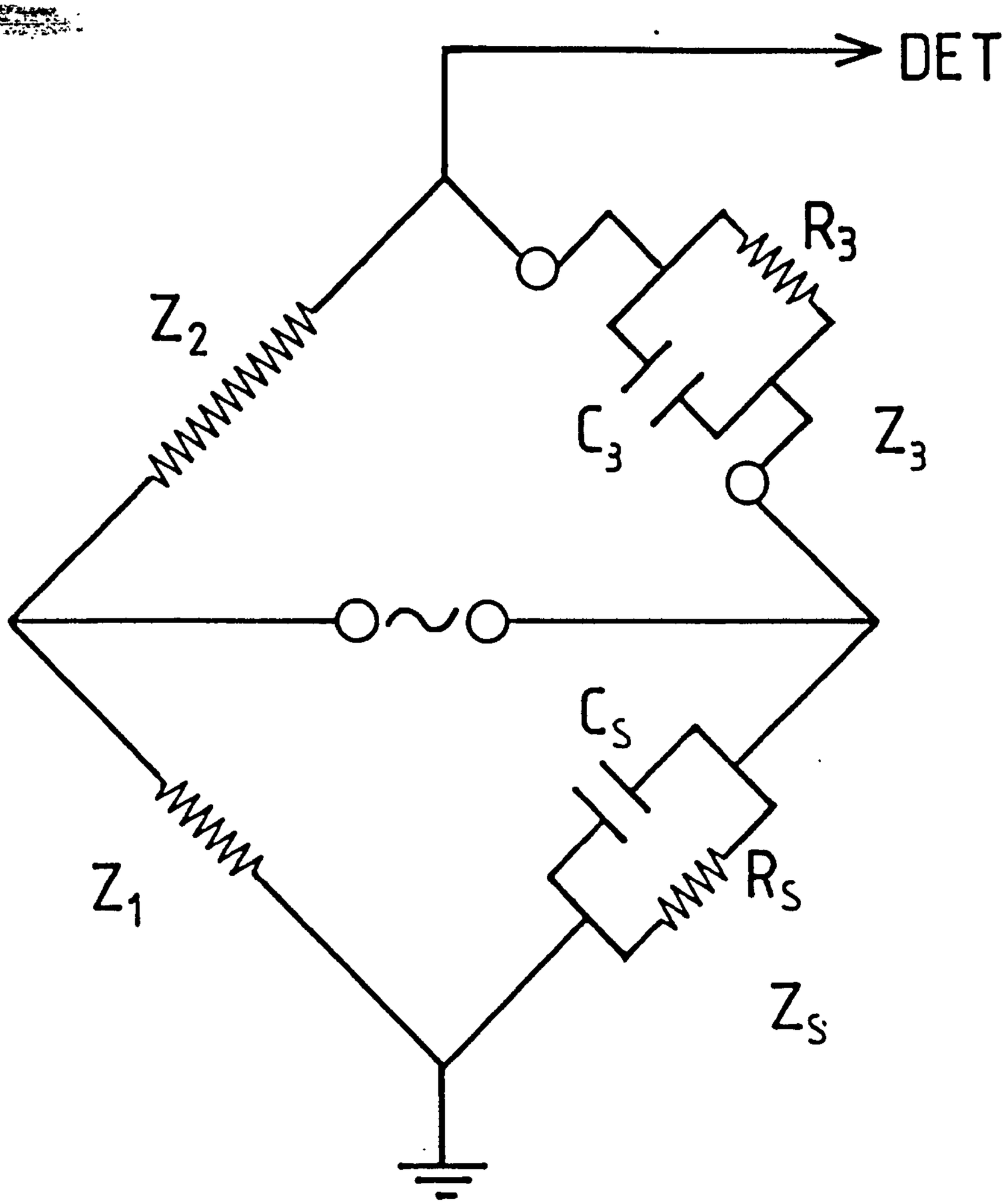

Figure 3.6 Equivalent circuit for the a.c. bridge.

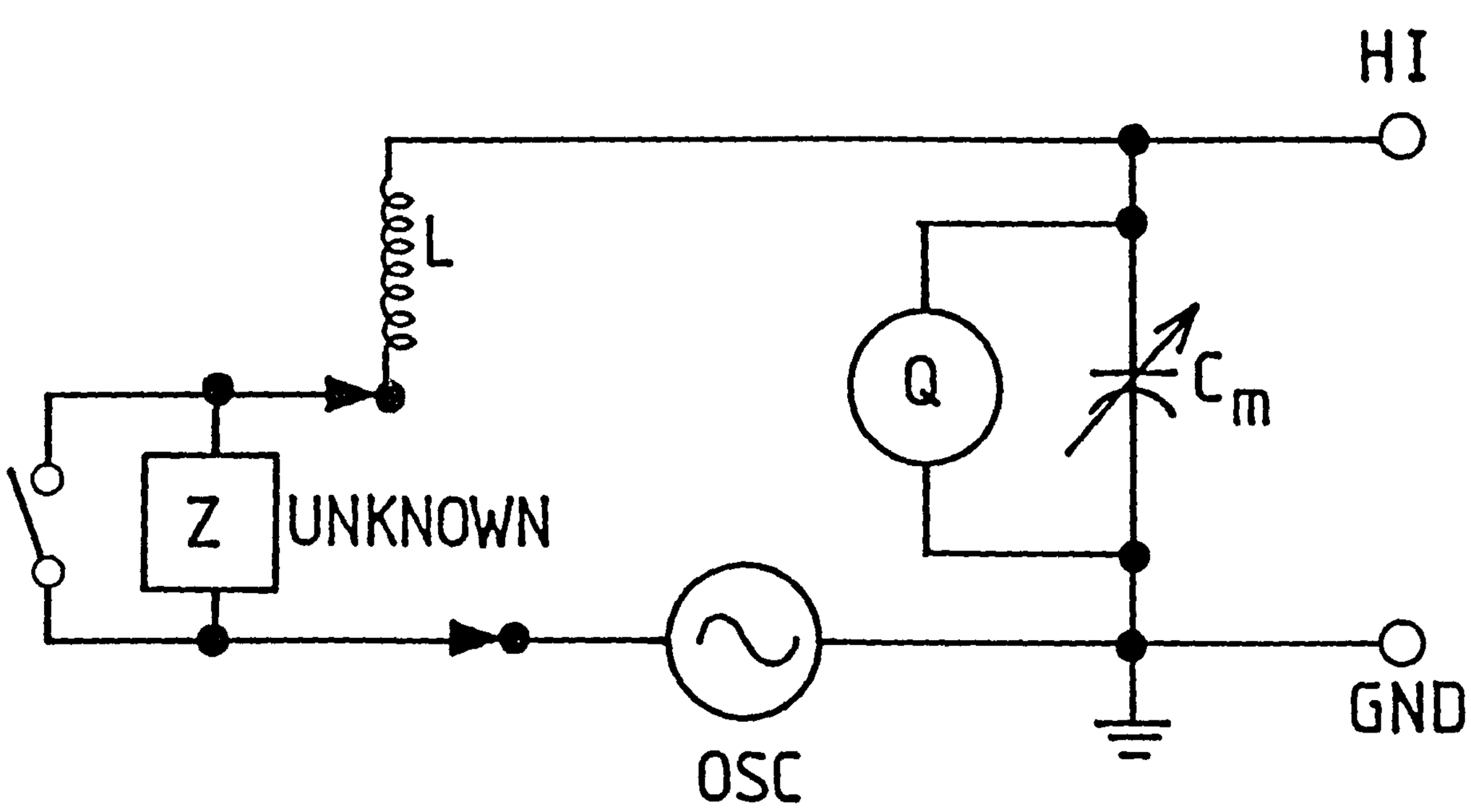

Figure 3.7 Equivalent circuit for the Q-meter.

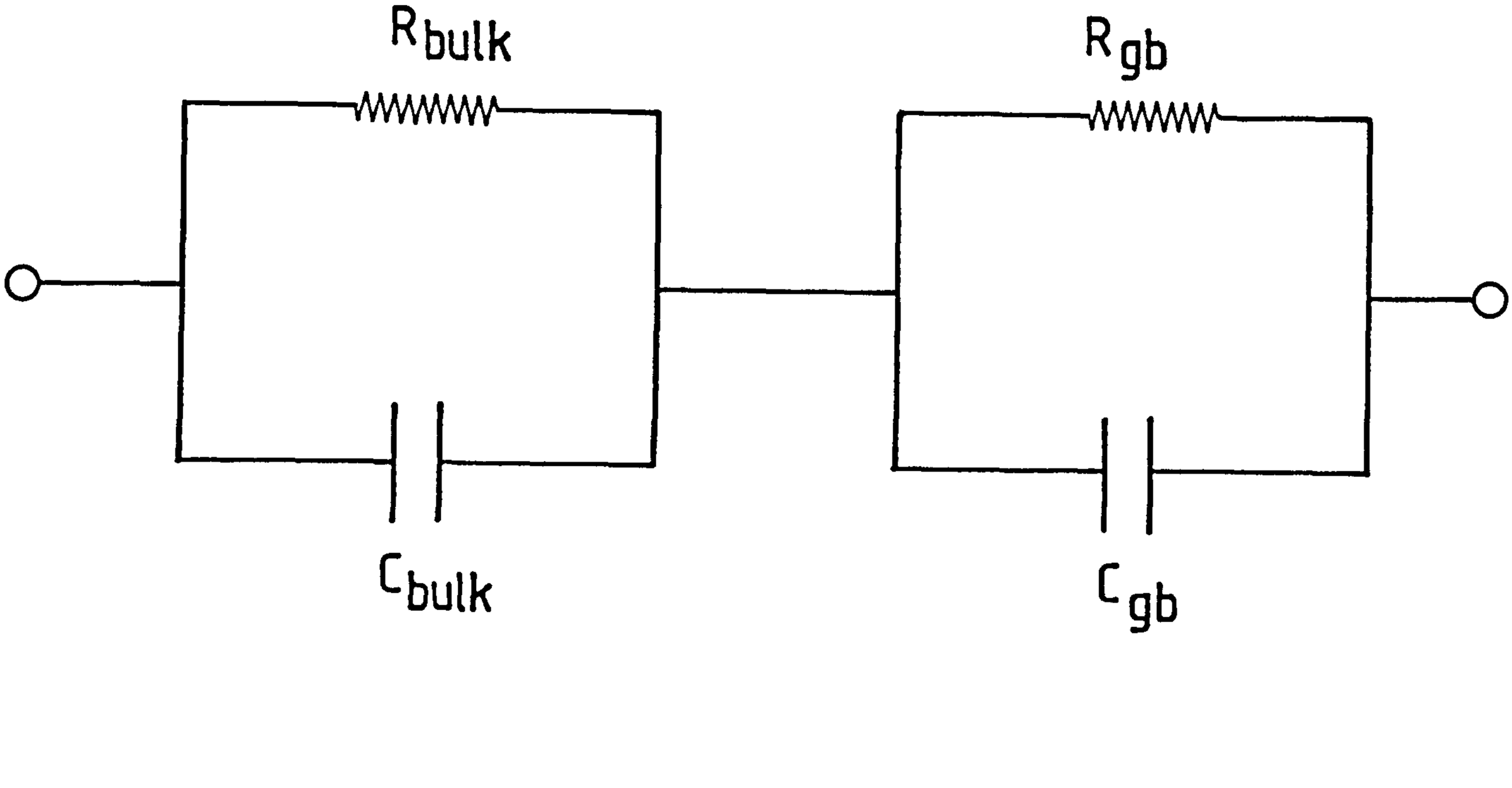

Figure 3.8 Equivalent circuit of PTCR barium titanate ceramics.

CHAPTER FOUR

INVESTIGATION OF THE EFFECT OF DONOR DOPANT CONCENTRATION

Despite much literature regarding the effect of donor dopant concentration on barium titanate PTCR ceramics, the relationship between donor concentration and the observed characteristics has not been fully explained. Several reports, mostly concerning room temperature effects such as resistivity and microstructure, have been published, from which limited theoretical proposals have been put forward. A complete picture of the effect of dopant concentration, however, has never yet been established. The study described in this chapter has examined aspects of donor dopant incorporation into polycrystalline barium titanate and has looked at a model regarding the effects of donor concentration on the grain boundary characteristics, such as resistivity, the potential barrier and acceptor state density.

4.1. SAMPLE PREPARATION

Samples were prepared by ball milling powders of Mandoval $BaTiO_3$, Ho_2O_3, SiO_2 and TiO_2 for 12 hours in a polyethylene mill using deionized water and agate media. The proportions of each ingredient were chosen such that each mix would contain 0.9mol% SiO_2 and 0.5mol%TiO_2 (which form the liquid phase during sintering), between 0.05 and 1.8 at% holmium ions and the same amount of TiO_2, to give stoichiometric $Ba_{1-n}Ho_nTiO_2$, where n is the mole fraction of donor dopant added. The exact concentrations of holmium added were: 0.05, 0.1, 0.2, 0.3, 0.4, 0.5, 0.55, 0.6, 0.8, 1.0, 1.2, 1.4, 1.6 and 1.8 at%. After the addition of binder, pellets were pressed in the usual manner and ~10 samples of each composition were sintered in the muffle furnace, at 1460°C for 60 minutes, followed by slow cooling (300°C/hour) to 800°C and, finally, furnace cooling to room temperature.

As-fired surfaces were examined in the Scanning Electron Microscope (SEM) to investigate their microstructure and any surface features (segregated second phase and impurities) were analyzed using the Energy Dispersive X-ray (EDX) attachment. Average grain size was calculated using an area count method of at least 200 grains and assuming them to be cubic.

For electrical investigations, the as-fired samples were polished slightly to flatten their surfaces and electrodes of In/Ga alloy were applied. The resistivity of five nominally identical samples was measured using the R-T plotter, between 40 and ~450°C. Average resistivity was then calculated, together with the variation between samples, to check reproducibility between the nominally identical samples.

Thin samples (~0.5mm thick) were prepared for the dielectric measurements (capacitance and impedance plots) in order to eliminate any effects of fringing of the electric field across the samples. In/Ga alloy was also used for the electrodes and, for the purposes of reproducibility, two samples of each composition were measured. The same samples were used for the current-voltage measurements, to enable large fields to be applied using a standard laboratory power supply. These measurements were carried out at 170°C, where sample resistance was approaching the maximum value for all compositions and hence the grain boundary potential barrier height was large.

4.2. EXPERIMENTAL RESULTS

4.2.1. Microstructure

The as-fired surfaces of all of the samples demonstrated the occurrence of densification and grain growth during sintering. Simple density measurements revealed them all to have obtained $\geq$92% of the theoretical density.

Samples containing the lowest amounts of donor dopant (<0.1 at%Ho) were blue-grey in colour and appeared shiny, suggesting the presence of a glassy (reflec-

tive) surface phase. Those containing between 0.2 and 1.4 at%Ho were dark blue in colour and had a matt-like appearance. The most heavily doped samples (containing >1.4 at%Ho) became lighter, similar in colour to the very lightly doped samples, being blue-grey but, in contrast, were matt in appearance.

The average grain sizes of samples of each composition were estimated, whereupon it was found that, as donor concentration was increased from 0.05 - 1.8 at%Ho, there was approximately an order of magnitude reduction in grain size. This is demonstrated in figure 4.1, where average grain size is plotted versus donor concentration. The average grain size can be seen to fall quickly in samples doped with upto 0.6 at%Ho, from 32μm with 0.05 at%Ho concentration, to ~10μm for doping levels of 0.6 at%Ho. Above this level, the grains reduced in size more slowly with donor concentration, with the most highly doped samples (containing 1.8at%Ho) having grains 4μm in size. Figure 4.2 is a scanning electron micrograph of a sample containing 0.05 at%Ho, where the grains are in excess of 30μm in size. The most lightly doped samples were also found to contain a large number of second phase features on the surface which appeared as irregular shapes, e.g. needles and spheroids, as can be seen in figure 4.3, which is a region of the surface of the sample doped with 0.1 at%Ho. Elemental analysis using EDX revealed these features to be rich in silicon and titanium, the constituents of the second phase additions to the formulation. Their presence in the irregularly shaped features additionally suggests that they are glassy in nature, i.e. they result from the segregation of the second phase (sintering aids) to the surface of the sample. From figure 4.2 it can be seen that the large, flat grains fit very closely together, with very little intergranular space for the second phase to fill. Consequently it is expelled from within the ceramic, onto the surface. Clearly, these glassy second phase features lend the material its shiny appearance.

As the grain size was reduced with increasing donor concentration, the shape of the grains was also affected. This gradually changed from being large and flat in

samples containing <0.2 at%Ho, to more rounded, pebble-like shapes in samples doped with >0.8 at%Ho. In addition, they became less regularly sized, with some grains in a typical sample containing >0.8 at%Ho as large as 20μm and others ~2μm in size. Figure 4.4 is a scanning electron micrograph of a sample doped with 1.2 at%Ho, where rounded, irregularly sized grains ranging from 10-20μm to <5μm can be seen. These samples had very much fewer surface second phase features, presumably because the interstices between grains were larger and more numerous as a result of the irregular size and rounded shape of the grains, thereby affording more space for the second phase to fit.

4.2.2. Resistive behaviour

Samples containing the lowest amounts of donor dopant (<0.1 at%Ho) had relatively high resistivity at room temperature, in the region of 300-500Ωcm. As donor concentration was increased between 0.2 and 1.4 at%Ho, room temperature resistivity was observed initially to fall monatonically, to 20 - 100Ωcm. As doping levels were further increased, resistivity rose again until, for the most heavily doped samples (1.8 at%Ho), room temperature resistivity reached ~$10^3\Omega$cm. The magnitude of the resistivity anomaly of the PTCR characteristic was also affected by donor concentration: in samples doped with <0.2 at%Ho, a steep negative coefficient of resistivity (NTCR) preceeded a relatively short resistivity increase at T_c of ~2 orders of magnitude. As doping levels were increased between 0.2 and 1.4 at%Ho, resistivity below the transition was approximately constant with temperature and rose by 3 - 4 orders of magnitude above T_c. More heavily doped samples (containing >1.4 at%Ho) were again observed to have a steep NTCR below T_c and diminished resistivity increases at the transition, of 2 orders of magnitude.

The PTCR effect is, however, believed to be a grain boundary effect (chapter 2.3) and therefore the number of grain boundaries in a sample will affect its resis-

tivity, possibly masking any direct effect of donor concentration on grain boundary resistance. In order to correct for the grain size effect of donor concentration, it was necessary to normalise the resistance measurements. This was carried out as follows: since the grain bulk may be considered conductive, the sample resistance may be considered to be the sum of sheets of resistive grain boundary layers, arranged in parallel between the electrodes. The area, A, of each sheet is equal to the contacted area of the sample and the number, n, of such sheets is equal to the number of grains between the electrodes. Each sheet is made of two back-to-back grain boundary layers. The sample resistance is then

$$R_{sample} = R_{sheet} \times 2n. \tag{4.1}$$

Assuming cubic grains having length d, the resistance of each face of a grain boundary, R_{gb}, is given in the following,

$$R_{sheet} = R_{gb} \times \frac{d^2}{A} \tag{4.2}$$

From equations (4.1) and (4.2) and putting $R_{gb} \times d^2 = \rho_L$, where ρ_L is the specific resistance of a unit area of grain boundary, the relation

$$\rho_L = \frac{R_{sample} \times A}{2n} \tag{4.3}$$

is obtained. Because the thickness of the grain boundary layer is unknown, the normalization of resistance data can only take into account the grain boundary area, hence specific resistance of a unit area of grain boundary, ρ_L, is used. The units of ρ_L are Ωcm^2.

Figure 4.5 shows typical normalised resistance - temperature curves for samples containing 0.05, 0.4 and 1.8 at%Ho and demonstrates the modifications to the PTCR characteristic upon increasing the donor concentration. Samples containing the lowest addition of holmium (0.05 at%) may be described as resistive, having normalised room temperature resistance, $\rho_{L(RT)}$, $\sim 10^3 \Omega cm^2$. This sample

also showed a large negative temperature coefficient of resistance as temperature was raised towards T_c, with ρ_L $\sim 10^2 \Omega cm^2$ at temperatures close to 130°C, demonstrating typical n-type semiconducting behaviour. Above the transition, ρ_L rose by just less than 2 orders of magnitude, to $\sim 10^4 \Omega cm^2$. Samples with doping levels between 0.4 and 1.4 at%Ho had much lower values of $\rho_{L(RT)}$, of the order $10^{-2} \Omega cm$ and maximum normalised resistance, $\rho_{L(max)}$, 4 orders of magnitude higher. In the most heavily doped samples (containing 1.6 and 1.8 at%Ho) $\rho_{L(RT)}$ increased towards $10^{-1} \Omega cm^2$ and there was a reduced resistivity jump, with $\rho_{L(max)}$ approaching $10^2 \Omega cm^2$. These observations follow the same pattern as the unormalised results, but show accurately the effect of donor concentration on grain boundary resistance. Figure 4.6 shows the dependence of both $\rho_{L(RT)}$ and $\rho_{L(max)}$ on donor concentration, where a broad minimum in both is observed between donor concentrations of 0.4 and 1.2 at%Ho. Where doping is less than 0.4 at%Ho, $\rho_{L(RT)}$ and $\rho_{L(max)}$ are seen to increase by up to 4 orders of magnitude towards 0.05 at%Ho concentration and at the highest doping levels (>1.6 at%Ho) the normalised resistance values are also seen to rise, but to a lesser extent, by $\sim$1 order of magnitude.

In contrast to the behaviour of the resistance characteristics, the temperature, T_{max}, at which $\rho_{L(max)}$ takes place, was observed to rise initially with increasing donor concentration, as seen in figure 4.7. It reached a broad maximum between 0.4 and $\sim$1.2 at%Ho, at $\sim$220°C and then decreased towards 185°C for samples containing 1.8 at%Ho. The most lightly doped samples (with <0.3 at%Ho) had comparatively low T_{max}, between 180°C for those containing 0.05 at%Ho and 200°C for those with with 0.3 at%Ho concentration. The broad maximum in the values of T_{max} between 0.4 and 1.2 at%Ho can be seen to correspond with the broad minima in the values of $\rho_{L(RT)}$ and $\rho_{L(max)}$ of figure 4.6.

4.2.3. Dielectric behaviour

The capacitance measurements were used to calculate apparent permittivity, ϵ'_{app}, of samples of each composition between room temperature and ~200°C. A series of typical plots of ϵ'_{app} versus temperature are shown in figure 4.8, for samples containing 0.1, 0.5 and 1.6 at%Ho, in comparison with an undoped sample, prepared in an identical manner. The undoped sample had permittivity typical of $BaTiO_3$ (chapter 1.2), with approximately constant ϵ'_{app} below T_c, of ~10^3, which rose sharply by an order of magnitude at the transition temperature. Above T_c it fell away, quickly at first, to 2×10^3 at 180°C, then more slowly above this temperature, reaching 10^3 above ~250°C. The addition of even a small amount of donor dopant (0.1 at%Ho) caused a large rise in ϵ'_{app} of more than an order of magnitude, to 5×10^4 at room temperature. Increasing the doping level towards 0.6 at%Ho resulted in a further increase in apparent permittivity to above 10^5 at room temperature. At the highest donor concentrations (> 0.8 at%Ho), ϵ'_{app} at room temperature began to decrease, falling to ~10^4 with 1.8 at%Ho concentration. The temperature at which the maximum took place was found to be shifted by ~5°, to 135°C for all donor doped samples and the height of the peak was affected strongly by the presence of the donor ions. The highest values of ϵ'_{app} below the transition were found for samples doped with intermediate concentrations of holmium (0.4 - 0.8 at%) and, for these samples, the peak at the transition was barely noticable. In addition, ϵ'_{app} for these samples was higher below T_c than above and at T_c it increased by a factor of ~2 compared with an order of magnitude increase for the undoped ceramic. Samples containing <0.4 and >1.2 at%Ho had definite peaks in the value of ϵ'_{app} at the transition temperature, although they were still were also much smaller than for the undoped $BaTiO_3$.

The effect of donor concentration below and above the transition is shown in figure 4.9, where ϵ'_{app} at 40°C can be seen to rise rapidly from 10^3 to 10^5 below 0.2 at%Ho doping and more slowly, to ~2×10^5 between 0.4 and 0.8 at%Ho

concentration. Above 0.8 at%Ho doping, ϵ'_{app} fell gradually, towards 2×10^4 for the sample containing 1.8 at%Ho. Apparent permittivity above the transition temperature was seen to have a similar effect, with a maximum value of $\sim 8 \times 10^4$ between 0.4 and 0.8 at%Ho concentration.

4.2.4. A.c. impedance plots

Room temperature a.c. impedance plots within the audio and radio frequency ranges were carried out on samples containing donor concentrations of 0.05, 0.1, 1.4 and 1.8 at%Ho. These were chosen since their normalised resistances lie on either side of the $\rho_{L(RT)}$ - donor concentration minimum (figure 4.6). The real (R_s) and imaginary (X_s) parts of the impedance were calculated and plotted in the form of a complex impedance diagram (R_s versus X_s). As described earlier (section 3.5.2), these plots enable the separation of the grain boundary resistance, R_{gb}, and the grain bulk resistance, R_{bulk} from the positions of the low and high frequency intercepts on the R_s axis. Figures 4.10 to 4.13 show complex impedance diagrams for samples containing 0.05, 0.1, 1.4 and 1.8 at%Ho, respectively. The high frequency intercept of the curve on the R_s axis, for all four samples, was found to be at a value of $R_s \simeq 2\Omega$, showing that the grain bulk resistance is unaffected by donor concentration. Grain boundary resistance, given by the difference between the low and high frequency intercepts, on the other hand, was found to reflect d.c. sample resistance. The most lightly doped sample (having 0.05 at%Ho concentration) had $R_{gb} \simeq 20k\Omega$, in agreement with a d.c. sample resistance of approximately the same. The sample doped with 0.1 at%Ho had d.c. resistance of 188Ω and $R_{gb} \simeq 185\Omega$. The more heavily doped samples revealed results in agreement: with 1.4 at%Ho, d.c. sample resistance was $\sim 50\Omega$ and R_{gb} was 45Ω and where the doping level was 1.8 at%Ho, d.c. sample resistance was $\sim 500\Omega$ and grain boundary resistance was 500Ω. Thus the trends observed in the a.c. measurements (high values of R_{gb} with 0.05 and 1.8 at%Ho and lower R_{gb}

at 0.1 and 1.4 at%Ho) corresponded well with the dependence $\rho_{L(RT)}$ on donor concentration (figure 4.6).

4.2.5. Current - Voltage measurements

The current through each sample was used to calculate the sample resistance as applied voltage was increased. The number of grain boundaries within the sample enabled the applied voltage per grain boundary, U, to be obtained. In accordance with the previous resistance measurements (section 4.2.1), these resistance values were normalised to give the specific resistance of a unit area of grain boundary, ρ_L. Every sample was observed to have non-ohmic behaviour: figure 4.14 shows typical plots of $\ln\rho_L$ versus U, for samples doped with 0.1, 0.5, 0.6 and 1.8 at%Ho. These plots can be seen to be approximately linear at low applied voltages, becoming sublinear as U was increased beyond a threshold value, U_{limit}. The range of linearity was least for samples doped with between 0.3 and 0.55 at%Ho, where U_{limit} was $\simeq$ 330mV. Below 0.3 at%Ho concentration U_{limit} was in the range of 400 - 500mV and between 0.6 and 1.2 at%Ho concentration linearity of ρ_L versus U was lost at ~450mV. Above 1.4 at%Ho donor doping, however, U_{limit} was approximately constant, at 300 - 350mV. The plots shown in figure 4.14 demonstrate this, with ρ_L for the sample containing 0.1 at%Ho remaining linear until 400mV, whereas ρ_L with 0.5 at%Ho doping became sublinear at 300mV. Samples containing 0.6 and 1.2 at%Ho, on the other hand, had values of U_{limit} closer to 450mV.

4.3. DISCUSSION OF EXPERIMENTAL RESULTS

4.3.1. Morphology and structure

The change in colour of the samples with increasing donor concentration, as well as the reduction in grain size, is in agreement with the observations of previous workers[4.1–4.4]. The blue colour was shown in chapter 1.3 to be due

to the reduction of some of the Ti^{4+} ions to Ti^{3+} within the bulk, to maintain electrical neutrality.

4.3.2. Resistive behaviour

The impedance plots showed that the effect of donor concentration on resistive behaviour, figures 4.10-4.13, is entirely due to the resistance of the grain boundaries, contrary to the predictions of some workers[4.2,4.3,4.5,4.6], where the grain bulk resistance was assumed also to increase at high doping levels.

The initial reduction in normalised resistance at low donor concentrations <0.5 at%Ho), figure 4.6, may be attributed to an increase in the value of N_d in equation 2.5 ($\phi_o = eN_a^2/8\epsilon_o\epsilon' N_d$), causing ϕ_o to be lowered, assuming ϵ' and N_a remain constant with donor concentration. According to the Heywang model[4.7] (equation 2.6), reduction in the value of ϕ_o causes the temperature at which the resistance maximum takes place to be increased as a result of the increased temperature at which E_a approaches the Fermi level (chapter 2.2.3). Depopulation of the acceptor traps therefore takes place at a higher temperature, corresponding to a higher value of T_{max}. Figure 4.7 shows the increase of T_{max} with donor doping, until the donor concentration is ~0.5 at%Ho.

Above ~1.5 at%Ho, room temperature and maximum values of normalised resistance can be seen to increase (figure 4.6), in agreement with the findings of many other workers[4.3,4.5–4.13]. Daniels and co-workers[4.3,4.13] explained the increase in $\rho_{L(RT)}$ and $\rho_{L(max)}$ in terms of the increased width of the insulating barium vacancy-rich zone (~3μm) relative to the grain size. The impedance plots showed that the high resistivity of samples containing 1.8 at%Ho, with grains 4μm in size and therefore similar in size to Daniels' proposed depletion zone width, was entirely due to the grain boundaries, not the grain bulk. The Heywang model, on the other hand, may be used to propose an enhancement of the grain boundary potential barrier over and above the opposing effect of the increased donor

concentration above ~1.5 at%Ho. Such an enhancement might be expected due to an increase in the grain boundary acceptor state density, N_a, as a result of the formation of cation vacancies at high dopant concentrations[4.5]. According to equation 2.6, an increase in the value of N_a, which would cause ϕ_o to be raised, would lead to the depopulation of the acceptor traps taking place at lower temperatures, thus reducing T_{max}. Figure 4.7 also shows just such a decrease in T_{max} at higher donor concentrations, in agreement with the predictions of the Heywang model. It may be concluded, therefore, that the broad minima in the values of $\rho_{L(RT)}$ and $\rho_{L(max)}$ and the maximum in T_{max} may tentatively be attributed to the compensating effects of increased N_d and N_a as donor concentration is increased.

4.3.3. Dielectric behaviour

The large increase in the value of apparent relative permittivity, ϵ'_{app}, resulting from the addition of donor ions, is consistent with the results of previous workers[4.7,4.10,4.14]. Heywang[4.10] attributed this to the presence of thin grain boundary layers in the donor doped material, an assumption which may be substantiated by the following argument: if the small dielectric contribution of the grain bulk is ignored and the low grain bulk resistance assumed to be equal to zero in comparison with the grain boundaries, the donor doped material may be described in terms of an equivalent circuit. Each grain boundary layer may be represented by a parallel combination of resistance and capacitance, of which there are 2l/d in series between the electrodes, where l is the sample thickness and d is the grain size. Assuming cubic grains, there are A/d^2 such series connections throughout the sample, all connected in parallel, where A is the sample area. This equivalent circuit is shown schematically in figure 4.15. Thus a three-dimensional array of R-C parallel combinations is modelled, representing the electrical relationship between the grain boundary layers throughout the sample. The impedance,

Z_L, of each R-C combination is given by

$$Z_L = \frac{R_L}{1 + j\omega C_L R_L} \tag{4.4}$$

where R_L and C_L are the grain boundary resistance and capacitance, respectively.

The impedance, Z_s, of each series of grain boundary layers, is given by

$$Z_s = Z_L \times 2l/d. \tag{4.5}$$

The sample, or apparent, impedance is thus

$$Z_{app} = Z_s \div A/d^2 \tag{4.6}$$

or

$$Z_{app} = Z_L \times 2ld/A. \tag{4.7}$$

Substituting equation 4.4 into equation 4.7 and writing Z_{app} in terms of R_{app} and C_{app}, apparent parallel resistance and capacitance, gives

$$\frac{R_{app}}{1 + j\omega C_{app} R_{app}} = \frac{R_L}{1 + j\omega C_L R_L} \times \frac{2ld}{A}, \tag{4.8}$$

which, upon simplification and equating imaginary parts, gives

$$C_L = C_{app} \times \frac{2ld}{A}. \tag{4.9}$$

Since, by definition, $C_{app} = \epsilon_o \epsilon'_{app} \mathrm{A/l}$, equation 4.9 may be rewritten

$$C_L = \epsilon_o \epsilon'_{app} \times 2d \tag{4.10}$$

or

$$\epsilon'_{app} = \frac{C_L}{2\epsilon_o d}, \tag{4.11}$$

showing ϵ'_{app} to be a function of grain boundary capacitance and grain size. The barrier layer capacitance may be made equivalent to a parallel plate capacitor having area d^2 and thickness b, the width of the depletion layer, so

$$C_L = \epsilon_o \epsilon' \times d^2/b. \tag{4.12}$$

Substituting equation 2.4 into equation 4.12 gives

$$C_L = \epsilon_o \epsilon' \times d^2 \times \frac{2N_d}{N_a}. \tag{4.13}$$

Grain boundary capacitance, normalised per unit area of grain boundary, C'_L (= C_L/d^2), is thus given by

$$C'_L = 2\epsilon_o \epsilon' N_d / N_a. \tag{4.14}$$

As can be seen from equation 4.11, ϵ'_{app} is affected by the reduction in grain size with increasing donor concentration. Consequently, the behaviour of ϵ'_{app} with donor concentration (figure 4.9) does not correspond accurately with any changes in the dielectric properties of the material. On the other hand, C'_L, while showing direct relationships with N_a and N_d, is independent of grain size (equation 4.14) and may be considered instead. C_L was calculated using equation 4.9 and the experimental results of figure 4.8, hence values of C'_L were obtained. Plots of C'_L, calculated below and above T_c, versus donor concentration, are shown in figure 4.16, where they can be seen to be qualitatively similar. For Ho concentrations upto ~0.55 at%, the experimental points lie on straight lines passing through the origin, in agreement with the prediction of equation 4.14 for constant values of ϵ' and N_a or N_d. The reduction in the value of C'_L at high donor concentrations at both temperatures implies a reduction in the value of ϵ'/N_a, a possible explanation for which is an increase in the value of N_a. The increased resistance of samples containing high donor concentrations appears to agree with Jonker's hypothesis[4.5] of an increase in acceptor trap density as a result of the formation of cation vacancies. The colour change from dark blue to blue-grey at high concentrations may be attributed to the formation of additional acceptor traps at the grain boundaries.

Figure 4.16 shows that, since the values of C'_L lie on a straight line up to a donor concentration of ~0.55 at%Ho, evidently the permittivity is independent of donor concentration and is equal to ϵ' of a sample containing 0.0 at%Ho, i.e.

the permittivity of the material within the grain boundary layer is equal to that of pure, undoped barium titanate. Although it is unlikely that the permittivity will be affected by donor concentration above ~0.55 at%, the possibility of this occurring can be ruled out by the following analysis. Expressing equation 4.9 in terms of the relative permittivity gives

$$\epsilon' = \epsilon'_{app} \times 2b/d. \tag{4.15}$$

Since b = $N_a/2N_d$, equation 4.15 may be rewritten,

$$\epsilon' = \epsilon'_{app} \times N_a/dN_d, \tag{4.16}$$

or

$$\epsilon'_{app} = \epsilon' \times dN_d/N_a. \tag{4.17}$$

Up to donor concentrations of ~0.55 at%Ho, it has been shown (figure 4.16) that the permittivity of the material within the grain boundary layers is equal to that of pure, undoped barium titanate. So, above T_c,

$$\epsilon' = \frac{C}{T-\theta}, \tag{4.18}$$

where C is the Curie constant and θ is the Curie point, a few degrees below T_c. Therefore, $1/\epsilon'$ is directly proportional to temperature above T_c. Assuming that the donor concentration has no effect on the value of ϵ', equation 4.17 shows that a plot of $1/\epsilon'_{app}$ versus temperature above T_c will be linear until the temperature at which depopulation of the acceptor traps takes place, since the gradient of this plot is dependent on the value of N_a/N_d. Linearity, therefore, is lost only when the ionized acceptor state density, N_a, starts to fall. Figure 4.17 shows plots of $1/\epsilon'_{app}$ versus temperature for samples containing 0.1, 0.6, 1.0 and 1.8 at%Ho, where it can be seen that they are all linear until temperatures just below those of T_{max} for each composition and at temperatures similar to those at which the normalised resistance values begin to turn towards their maximum values (figure 4.5). In addition, the slope of the linear portion can be used to obtain N_{ao}/N_d.

Rearranging equation 4.14 gives a relationship between ϵ' and C'_L:

$$\epsilon' = \frac{C'_L}{2\epsilon_o} \times \frac{N_a}{N_d}. \tag{4.19}$$

Using the values of C'_L previously obtained and the ratio of N_a/N_d from the plots of figure 4.17, ϵ' was calculated at 160°C for every composition. The results are listed in table 4.1, where they can be seen to agree well, within a reasonable experimental error, with the theoretical value of $\epsilon'(160°)$ of 3333, as calculated from the Curie-Weiss law, showing the permittivity of the material within the grain boundary layers to be equal to that of pure barium titanate at all compositions.

The values of N_{ao}/N_d, obtained above and listed in table 4.1, can be seen to reduce initially with increasing donor concentration, until ~0.5 at%Ho, where it remains approximately constant. At higher doping levels, >1.4 at%Ho, N_{ao}/N_d starts to rise again, describing approximately a broad minimum and suggesting that, above 0.5 at%Ho, either N_a increases or N_d decreases in value.

The impedance measurements showed that grain bulk resistance is constant, at ~2Ω for all compositions and, according to equation 2.10, it is inversely proportional to the charge carrier concentration, showing N_d to be constant for all donor concentrations. Hence the variation in the value of N_{ao}/N_d as donor concentration was increased is due only to the density of the electron traps at the grain boundaries. This is in conflict with the previous models for the broad minima observed in normalised resistance values, which were based on the assumption that resistance was affected by the combined effects of higher values of N_d and N_a, as donor concentration was increased. It is also in apparent contradiction with the results of figure 4.16, which imply that N_d is increased in line with the donor concentration upto 0.55 at%Ho doping. The present results, however, show that N_d is constant at all donor concentrations and that a broad minimum in the value of N_{ao} is obtained.

/eject

4.3.4. Current - voltage measurements

According to the Heywang model[4.7], when a voltage, U, is applied across the grain boundary layer, the space-charge region is shifted, resulting in a reduced effective potential barrier, as desribed fully in section 2.2.3.:

$$\phi(U) = \phi_o(1 - \frac{U}{4\phi_o})^2 \tag{2.18}$$

and resistance is thus,

$$\rho_L(U) = \rho_o exp(\frac{e}{kT} \times \phi(U)). \tag{2.19}$$

This relationship is only valid if U << 4 ϕ_o, hence this equation may be simplified to

$$\rho_L(U) = \rho_o exp(\frac{e\phi_o}{kT} - \frac{eU}{2kT}). \tag{4.20}$$

A plot of $\ln\rho_L$ versus U, therefore, can be expected to be linear until U $\simeq 4\phi_o$. Figure 4.14 shows values of normalised resistance, plotted on a logarithmic scale, versus applied voltage per grain boundary for samples containing different donor concentrations. The value of U_L, the voltage at which linearity, and hence agreement with the Heywang model, is lost, was obtained for samples of each composition and is displayed in table 4.2. It can be seen that, until donor concentrations of ~1.2 at%Ho, a shallow minimum around 0.4 at%, is obtained. Above 1.2 at%Ho doping level, it is thought that depopulation of the grain boundary acceptor traps has already taken place, since the normalised resistance for these samples is close to the maximum value at 170°C (figure 4.5). Consequently these samples may not be expected to reflect the trend observed in the other samples containing lower dopant concentrations. These findings are in agreement with those of previous workers[4.7,4.8,4.10,4.14–4.16].

These results also demonstrate the modification to the grain boundary potential barrier by donor concentration as a result of the effects of doping levels on the density of grain boundary acceptor traps: upto ~0.4 at%Ho, ϕ_o (given by

$U_{limit}/4$) becomes lower as a result of the small value of N_a and above this level the barrier is raised further, as a result of the increased density of grain boundary acceptor traps.

4.4. ANALYSIS OF EXPERIMENTAL RESULTS

In the previous section it was shown that the broad minima observed in normalised resistance, both at room temperature and at the maximum, as donor concentration is increased, is due entirely to the density of the grain boundary acceptor traps causing the grain boundary resistance to be raised. This is in contradiction with previously reported hypotheses, where the grain bulk has been assumed to become insulating[4.2,4.3,4.5,4.6] or where an insulating second phase, rich in undissolved donor ions, has been proposed to exist[4.14,4.17]. The latter was shown to be an unsuitable explanation when the solubility of donor ions in the barium titanate lattice was found to be high[4.18,4.19].

The Heywang model may be utilized to analyse the experimental results further. Combining equations 2.5 and 2.9 gives

$$\rho_L = \rho_o exp(\frac{e^2 N_a^2}{8\epsilon_o \epsilon' N_d kT}). \tag{4.21}$$

The permittivity, ϵ', of the material within the grain boundary layers has been shown to be unaffected by donor concentration and to obey the Curie-Weiss law above T_c. Equation 4.21 may now be rewritten,

$$\rho_L = \rho_o exp(\frac{e^2 N_a^2 (T-\theta)}{8\epsilon_o C k N_d T}). \tag{4.22}$$

Close to the Curie temperature all of the acceptor traps can be assumed to be fully ionized, i.e. N_a is constant and equal to N_{ao} (equation 2.6), since E_a is a long way below the Fermi level. In the temperature range in which N_a is constant, equation 4.22 may be simplified to

$$\rho_L = \rho_o exp(\frac{A(T-\theta)}{T}) \tag{4.23}$$

where A is a temperature independent constant, given by

$$A = \frac{e^2 N_{ao}^2}{8\epsilon_o C k N_d}. \tag{4.24}$$

According to equation 4.23 an Arrhenius plot of $\ln\rho_L$ versus (T - θ)/T can be expected to be linear between T_c and the temperature at which depopulation of the acceptor traps takes place (a few degrees below T_{max}, figures 4.5 and 4.17). Figure 4.18 shows Arrhenius plots of $\ln\rho_L$ versus (T - θ)/T, measured every 5°C above T_c on the normalized resistance plots of figure 4.5, for samples containing donor concentrations of 0.1, 0.6 and 1.8 at%Ho, where it can be seen that linearity is lost at temperatures similar to those at which it is lost in figure 4.17.

The slope of each plot is equal to A, and was found to be similar for Ho concentrations between 0.2 and 1.2 at% (A ~70). Samples containing smaller or greater amounts of donor had steeper plots, with A ~144. The exact values of A obtained for samples of each composition are listed in table 4.3. Arrhenius plots for samples containing 0.05 at%Ho were linear over a short range of temperatures, since the PTCR jump of these samples was very small. Consequently the accuracy of the value of A for this composition cannot be guaranteed.

From equations 2.5 and 4.24, ϕ_o is given by

$$\phi_o = A \times k/e \times (T - \theta). \tag{4.25}$$

Thus, using this equation, estimates of the height of the grain boundary potential barrier may be obtained, until depopulation of the acceptor traps takes place. From figures 4.17 and 4.18 it can be seen that, above ~160°C, the linear behaviour has ceased, indicating that depopulation of the acceptor states has started and that N_a cannot be assumed independent of temperature for all donor concentrations. Values of A from table 4.3 were substituted into equation 4.25 to obtain estimated values of ϕ_o at 150°C, where N_a can be assumed constant for all compositions. Figure 4.19 shows ϕ_o as a function of donor concentration, where it

can be seen to be similar for samples containing between 0.2 and 1.2 at%Ho, at ~0.2eV. Samples containing <0.2 and >1.2 at%Ho had higher ϕ_o, of ~0.4eV.

These estimated values of ϕ_o correspond well with the observations of normalised resistance, both at room temperature and at the maximum since ϕ_o also describes a broad minimum between ~0.3 and 1.4 at%Ho. In addition, they compare well with values of ϕ_o estimated in the literature: Heywang[4.7] thought that ϕ_o at the resistivity maximum is 0.55eV and Ihrig and Puschert[4.15] suggested a range of values between 0.5 and 1.0eV.

Having obtained quantative values for ϕ_o using the slope of the Arrhenius plots of $\ln\rho_L$ versus (T - θ)/T, the values of N_{ao} and N_d may also be found, to confirm the observations of the effect of donor concentration on grain boundary acceptor trap density.

According to Heywang[4.7] and equation 2.10, the charge carrier concentration, N_d, is given by

$$N_d = \frac{1}{e \times \mu \times \rho_{bulk}}, \tag{4.26}$$

where ρ_{bulk} is the resistivity of the grain bulk and μ is the mobility of the charge carriers, estimated by Jonker[4.5] to be $0.5 cm^2 V^{-1} s^{-1}$. The room temperature impedance plots have been used to obtain R_{bulk}, the resistance of the grain bulk. Assuming the volume of the grain boundaries to be negligible in comparison with the bulk, grain bulk resistivity may be calculated from R_{bulk} and the sample dimensions. ρ_{bulk} was found to be ~8Ωcm for all donor concentrations measured and hence N_d was calculated to be $1.5 \times 10^{18} cm^{-3}$. This value is significantly lower than the nominal donor concentration, which ranges from 6.1×10^{18} to $2.2 \times 10^{20} cm^{-3}$, corresponding to holmium additions of 0.05 to 1.8 at%. This finding is in agreement with that of Ihrig and Puschert[4.15], who suggested it to be due to compensation of the donor ions within the bulk by cation (barium) vacancies. It may also be due to the relative size of the holmium and barium ions:

Ho^{3+} is intermediate in size between the Ba^{2+} and Ti^{4+} ions, hence a proportion of the donor dopant may be expected to sit on titanium sites, leading to self-compensation[20].

The acceptor trap density before depopulation may now be calculated at each donor concentration from the slope of the Arrhenius plots of $\ln\rho_L$ versus (T - θ)/T, since

$$N_{ao} = \sqrt{\frac{8\epsilon_o C k N_d A}{e^2}}. \tag{4.27}$$

In addition to this method, N_{ao} may be calculated from the ratio N_a/N_d, obtained earlier, from the slopes of the plots of $1/\epsilon'_{app}$ versus temperature (figure 4.17). Values of N_{ao}, estimated using both methods, are listed in table 4.4 and N_{ao} is plotted in figure 4.20 as a function of donor concentration for the Arrhenius method. Despite some discrepancy between the numerical values, particularly at the lowest donor concentrations, the two methods can be seen to be in general agreement, with each demonstrating a minimum in N_{ao} approximately corresponding to the normalised resistance minima observed in figure 4.5 and confirming the earlier suggestion that the normalised resistance values were affected only by the acceptor trap density at the grain boundaries.

4.4.1. Discussion of analysis

Having determined that N_{ao} describes a broad minimum as donor concentration is increased between 0.05 and 1.8 at%Ho, the question is now raised of how the nature of the acceptor traps is affected. This has remained unclear in the literature, despite a number of proposals put forward: Heywang[4.21] and Brauer[4.22] both suggested the acceptor traps to be impurity ions segregated to the grain boundaries, whereas Jonker[4.23] attributed them to gaseous atoms adsorbed during sintering (e.g. oxygen atoms, when sintering in air). Daniels et al[4.3] and Koshech and Kubalek[4.24], on the other hand, have suggested that the acceptor states are doubly ionized barium vacancies. Clearly, however, it is possible that

all three species are present within the grain boundary layers, collectively making the total number of acceptor traps. Each species is associated with a unique ionization energy, i.e. particular traps are situated at unique energies within the band gap, and hence have their own values of E_a below the bottom of the conduction band (figure 2.4). Hewyang[4.7] and Jonker[4.5] estimated E_a between 0.7 and 1.0eV. Ihrig and Puschert[4.15], on the other hand, evaluated it to be higher, at 1.22eV, although they obtained best fit with experimental resistivity - temperature curves when they considered E_a to range within $\pm$0.5eV of this value. Daniels and Hardtl[4.25] obtained the energy of the doubly ionized barium vacancies from their high temperature diffusion calculations, from which the value of E_a for this species was found to be 1.3eV in the bulk of the grain. Ihrig and Puschert[4.15] proposed the smearing of E_a on account of the different environment of barium vacancies at the grain boundaries compared with the bulk.

According to the Heywang model, E_a may be obtained from equation 2.6, providing N_a, N_{ao}, ϕ_o and E_F are known. N_{ao} is now known, from the present results and E_F may be calculated from equation 2.7 at the desired temperature. Unfortunately, it is not possible to find N_a until ϕ_o is known, but above the temperature of depopulation, ϕ_o cannot be obtained until N_a is found and a stalemate situation is reached.

Above T_{max}, however, ϕ_o is constant at its maximum value, $\phi_{o(max)}$, as a result of the equilibrium between the reduction in N_a and the increase in the value of (T - θ) as temperature is raised. Consequently, NTCR behaviour is obtained above T_{max} and

$$\rho_L = R_o exp(\frac{e\phi_{o(max)}}{kT}) \qquad (4.28)$$

An Arrhenius plot of lnρ_L versus 1/T above the maximum can be expected to be linear, with a slope equal to e$\phi_{o(max)}$/k. Figure 4.21 shows ρ_L, plotted on a logarithmic scale, versus 1/T between the maximum and ~340°C for samples containing 0.1, 0.3, 1.2 and 1.8 at%Ho. The gradients of plots containing between

~0.6 and 1.2 at%Ho were found to be lower than the gradients belonging to samples containing lower and higher donor concentrations, in agreement with the normalised resistance minima (figure 4.5). $\phi_{o(max)}$ was calculated for samples of each composition, from which the value of N_a at an arbitrary temperature above T_{max} (250°C) was calculated by rearranging the Hewyang equation,

$$N_a(T) = \sqrt{\frac{8\epsilon_o C N_d \phi_{o(max)}}{e^2(T-\theta)}}. \tag{4.29}$$

According to equation 2.6,

$$\frac{N_a(T)}{N_{ao}} = \frac{1}{1 + exp(\phi_o(T) + E_F(T) - E_a)/kT} \tag{4.30}$$

which may be rearranged to give

$$\frac{\phi_o(T) + E_F(T) - E_a}{kT} = ln(\frac{N_{ao}}{N_a(T)} - 1), \tag{4.31}$$

hence

$$E_a = \phi_o(T) + E_F(T) - kTln(\frac{N_{ao}}{N_a(T)} - 1). \tag{4.32}$$

Choosing a convenient temperature above T_{max} at which samples of all compositions display the NTCR characteristic (equation 4.28), both ϕ_o and $N_a(T)$ in equation 4.32 are known. Having obtained both values at 250°C, E_a was calculated for all compositions. Table 4.5 shows values of $\phi_{o(max)}$, $N_a(250°)$ and E_a for all donor concentrations above 0.1 at%Ho, together with the value of E_F at 250°C. E_a was found to be unchanged, at 0.9eV ±0.1eV, for all concentrations of Ho donor dopant, showing that, in contrast to the above theories[4.3,4.5,4.25], the nature of the donor is unaffected by the quantity of dopant ions incorporated. The discrepancy between these values and the estimated value of the energy below the conduction band of barium vacancies (1.3eV) appears to suggest that the acceptor traps are not dominated by barium vacancies but are, instead, more shallow traps, e.g. adsorbed gaseous (oxygen) atoms or impurity ions, or that there is a range of values of E_a, where only the lower energies are detectable. The hypothesis that

barium vacancies are largely unimportant is supported by the reported observations of steep PTCR characteristics exhibited by BaO-rich donor doped barium titanate ceramics[4.26,4.27], which clearly may be expected not to contain barium vacancies (although the presence of titanium vacancies acting as acceptors cannot be ruled out in these cases).

Jonker[4.5] proposed that donor ions are electronically compensated at low concentrations but that transition to vacancy compensation takes place at high donor concentrations. In other words, at low dopant levels, each donor ion donates an electron into the conduction band but at high concentrations, metal ion (typically barium) vacancies are formed which act as acceptors, trapping the donor electrons and increasing resistivity by effectively reducing N_d in equation 2.5. The impedance results suggest that these must be segregated to the grain boundaries since the value of N_d is unaffected by donor concentration. Heywang[4.21] suggested that the donor ions, at high concentrations, were incorporated with different valencies at equivalent lattice sites and Murakami et al[4.6] proposed incorporation of the donors with the same valency but at different lattice sites, both cases leading to self-compensation within the grain bulk as well as the grain boundary. The present results, showing that grain bulk resistance as well as N_d are constant at all donor concentrations, are in conflict with both ideas. Having failed to observe the PTCR characteristic in ultra-pure donor doped barium titanate ceramics, Heywang[4.21] suggested the grain boundary acceptor traps to be segregated impurity ions. Although it is possible that N_{ao} is affected by impurities in the present samples, it is unlikely that the broad minimum in this value is due to impurity ions. This is because all of the samples were prepared in an identical manner and therefore all can be assumed to contain the same number of unintentional impurities. In contrast, Daniels et al[4.3] and Wernicke[4.2] concluded that the high resistance observed at high donor concentrations was due to the complete penetration of the grain boundary insulating zone into the bulk of the grain. The

impedance results and the above analysis disagree with this conclusion since, even at the greatest level of donor doping, the high resistance has been shown to be entirely due to the grain boundaries.

The minimum in the value of N_{ao} with donor concentration, together with the finding that the acceptor traps do not change in nature, leads to the question regarding the reason for this behaviour and how it takes place. An explanation may be found in the results of Drofenik[4.28,4.29], who observed the expulsion of oxygen during sintering of donor doped barium titanate ceramics in a vacuum. From these observations he proposed the following equation regarding the incorporation of trivalent Sb ions into the lattice[4.28]:

$$BaO_{latt} + \frac{1}{2}Sb_2O_3 \rightarrow (SbO)_{iatt} + \frac{1}{4}O_2 + e. \tag{4.33}$$

In other words, the donor ions are incorporated onto the barium sites together with the release of an electron into the conduction band and a small amount of oxygen. At high concentrations the donor ions were considered not to be incorporated if the change in surface energy during grain growth was balanced by the change in free surface energy upon release of the oxygen. This condition was found to be satisfied above a certain dopant level, showing that electronic compensation was no longer possible and that grain growth during sintering was suppressed. The positively charged $(SbO)^{\cdot}$ entity within the lattice still needs to be compensated and it is at this point that the grain boundary acceptor states may be considered to be effective as compensating media. At low donor concentrations the oxygen released during incorporation may be assumed to become adsorbed onto the grain surfaces as atomic oxygen, acting as acceptor traps to obtain a full outer shell of electrons (i.e. they become negatively charged). As donor incorporation is gradually suppressed at increasing donor concentration, less oxygen is released and less is available for adsorption onto the grain boundaries, so N_{ao} is reduced. As grain growth is also suppressed, however, more grain boundary area is created, onto

which atmospheric oxygen may be adsorbed and N_{ao} is increased. At intermediate compositions, an equilibrium is established between donor incorporation and grain boundary area, giving a broad minimum in the value of N_{ao}.

This suggests that the total charge on the grain surfaces is dependent on the total amount of grain surface available and that steeper and higher PTCR characteristics may be obtained from samples having smaller grains. Such observations have been reported[4.26,4.30] in porous samples and found to exhibit superior PTCR characteristics when compared with fully dense samples of the same composition. This was explained in terms of the increased amount of available grain surface. In order to investigate the effect of donor concentration on N_{ao}, the total surface charge on any one grain ($6N_{ao} \times d^2$) may be compared with the total amount of grain surface, $6d^2$. Plotting $N_{ao}d^2$ versus d^2 would, therefore, be expected to result in linear behaviour. This is, indeed, seen in figure 4.22, where a straight line passing through the origin has been obtained. Least - squares analysis of the points reveal the gradient of the line to be $\sim 10^{14}$ and the correlation coefficient equal to 0.999. These results confirm the dependence of the total surface charge per grain on grain area, which in turn is dependent on donor concentration (figure 4.1). Since the amount of gaseous atoms adsorbed onto the grain surfaces is additionally dependent on the grain area, it may be concluded that the total surface charge per grain is dependent on the ability of such species to become adsorbed onto the surface.

If, however, acceptor states, dependent on donor ion concentration for their existence (e.g. barium vacancies), at the grain boundaries have any effect on the overall acceptor trap density, the results of Drofenik may also be applicable. As the surface area of the grains increases with increasing donor concentration, as a result of the suppression of grain growth, the number of these states will become progressively larger. Consequently, as donor concentration is increased, the number of these acceptor traps at the grain boundaries is also raised. The total

surface charge per grain would then be dependent on the donor ion concentration per grain, the latter being given by $N_{Ho} \times d^3$, where N_{Ho} is the nominal holmium ion concentration. Figure 4.23 shows a plot of $N_{ao}d^2$ versus $N_{Ho}d^3$, where linear behaviour is obtained until $N_{Ho}d^3 \simeq 12 \times 10^7$ (corresponding to $\geq$0.4 at%Ho concentration), with least - squares gradient $\sim 10^{14}$ and correlation coefficient 0.93. This plot demonstrates that, although the total surface charge is dependent on the grain area (figure 4.22), above 0.4 at%Ho doping it is also dependent on the donor ion concentration per grain, suggesting that the acceptor states are induced by the presence of the impurity ions, in agreement with the hypothesis of Heywang[4.10]. At donor concentrations <0.4 at%Ho, $N_{ao}d^2$ is larger than expected and so, therefore, will the surface charge density. The potential barrier height and resistivity, consequently, will also be higher for these samples than for the more heavily doped samples, as observed in figures 4.19 and 4.6. According to Daniels[4.3,4.25], barium vacancies are created at the grain boundaries to compensate the incorporated donor ions, hence the total surface charge arising from these acceptor states is dependent on donor concentration. The increase in the value of N_{ao} at the highest donor concentrations (>1.4 at%Ho) may be attributed to the increase in both the adsorbed species and the created barium vacancies or other acceptor states, dependent on the presence of donor ions for their existance.

Ihrig and Puschert's proposal[4.15] that, at the grain boundary, the acceptor states exist within a range of energies instead of one discrete energy, is very plausible. They also suggested that the compensating acceptors have energy levels in the bulk of the grain different from those at the boundary because of the different environments at each region. Hence, the value of E_a for barium vacancies, calculated by Daniels and Härdtl[4.25] for the grain bulk, cannot be guaranteed to be the same as E_a at the grain boundaries. As a result, it is very possible that all three acceptor trap species: impurity ions, adsorbed gaseous atoms and barium vacancies, are present at the grain boundaries, the density of the latter two types

being also affected by donor concentration, within an average energy level of 0.9eV below the conduction band.

4.5. EXAMINATION OF THE CONDUCTION MECHANISM

Heywang[4.10] assumed that the current through the grain boundary layer was limited by thermionic emission and hence the current density, J(U), across the grain boundary layer upon application of a voltage, U, per grain boundary, was proposed to be approximately equal to

$$J(U) = J_o exp(-\frac{e\phi(U)}{kT}) \tag{4.34}$$

where J_o is the saturation current density. For U << $4\phi_o$ as before, equation 4.34 can be simplified to

$$J(U) = J_o exp(-\frac{e\phi_o}{kT} + \frac{eU}{2kT}). \tag{4.35}$$

Plotting ln(J(U)) versus U, therefore, can be expected to show linear behaviour until U $\simeq 4\phi_o$. Figure 4.24 shows such plots for samples containing 0.1, 0.5, 0.6 and 1.2 at%Ho. Although the plots appear to be linear over short, intermediate ranges of U, it is clear that the characteristic trend of these plots is not linear. In other words, current transport does not take place by thermionic emission.

Recently, Ihrig and Puschert[4.15] suggested that the current transport mechansim was limited by diffusion, giving

$$J(U) = A[1 - exp(\frac{-eU}{kT})] \times exp(-\frac{e\phi_o}{kT} + \frac{eU}{2kT}) \tag{4.36}$$

where A is a constant. This equation is also only valid for U < $4\phi_o$ and, for very small values of U ($\leq$2kT/e), the extra term in equation 4.36 cannot be ignored. Clearly, however, the dependence of ln(J(U)/[1 - exp(-eU/kT)]) on U can be expected to be linear. The results obtained for figure 4.24 were then replotted and are shown in figure 4.25, where the points can be seen to follow straight lines for low values of U. Linearity is found to be lost in a similar fashion to the

normalised resistance plots, having a shallow minimum in U_{limit} at ~0.4 at%Ho and a saturation of this value at dopant concentrations >1.2 at%Ho. In general, U_{limit} was ~100mV lower, measured from the plots of J(U)/[1 - exp(-eU/kT)] versus U, compared with the values obtained from plots of ρ_L versus U (figure 4.14).

The slope of the linear portions of the plots of lnJ(U)/[1 - exp(eU/kT)] versus U can be expected to be equal to e/2kT. The slope of the graph for each donor concentration was measured and compared with the theoretical value, where agreement within 20% was obtained for the majority of the samples. The error from e/2kT of the experimental values may be compared with typical ideality functions in semiconductor physics which measure the deviation from perfect behaviour of semiconductor junctions. Common values are 1.1 - 1.4, with more perfect behaviour being found towards 1.0, and are in agreement with the present results.

The mechanism of current conduction in donor doped barium titanate ceramics is clearly most accurately described by a simple diffusion theory. Deviations from the ideal diffusion process, in particular at higher applied voltages, may be due to the influence of instantaneous Joule heating at the grain boundaries, leading to increased grain boundary resistance[4.16]. This may contribute to an explanation why U_{limit} was lower in figure 4.23 than in figure 4.14 and why there was occasionally poor agreement between the theoretical and experimental values of e/2kT.

4.6. CONCLUSION

The investigation of the effect of donor dopant concentration, described in this chapter, have shown that the modifications to the PTCR characteristic obtained are due entirely to the density of grain boundary acceptor traps. These traps, which do not change in nature as donor concentration is raised, have been tentatively proposed to be made of segregated impurity ions, adsorbed oxygen

atoms and doubly ionized barium vacancies. The total surface charge per grain was found to be dependent on the total surface area per grain for all compositions and, for doping levels >0.4 at%Ho, dependent on the donor ion concentration per grain. The suppression of grain growth which takes place as donor concentration increased may be used to explain why the total number of adsorbed oxygen atoms and barium vacancies is increased at high dopant levels. High values of N_{ao} at low donor concentrations were considered to be due to the ease of incorporation of the donors into the lattice, together with the expulsion of oxygen and the creation of barium vacancies at the grain boundaries for the purposes of electrical neutrality.

Finally, the mechanism of current transport in donor doped barium titanate has been shown, using current - voltage measurements, to be one of diffusion. Deviation from the ideal process was considered to be due to the difficulty in obtaining accurate results from highly resistive grain boundaries, particularly where high voltages were applied, leading to Joule heating.

REFERENCES

4.1 Eror N.G. and Smyth D.M., in *The Chemistry of Extended Defects in Non-metallic Solids*, Ed. Le Roy Eyring and M. O'Keeffe (North-Holland, Amsterdam, 1970), p.658.

4.2 Wernicke R., Phys. Stat. Sol. (a), **47**, 139, 1978.

4.3 Daniels J., Härdtl K.H. and Wernicke R., Philips Tech. Rev., **38**, 73, 1978/79.

4.4 Zajc I. and Drofenik M.H., Br. Ceram. Trans. J., **88**, 223, 1989.

4.5 Jonker G.H., Sol. Stat. electron., **7**, 895, 1964.

4.6 Murakami T., Nakahara M., Miyashita T. and Sekina E., J. Am. Ceram. Soc., **56**, 294, 1973.

4.7 Heywang W., Sol. Stat. Electron., **3**, 51, 1961.

4.8 Saburi O., J. Phys., Soc., Jpn., **14**, 1159, 1959.

4.9 Tennery V.J. and Cook R.L., J. Am. Ceram. Soc., **44**, 187, 1961.

4.10 Heywang W., J. Am. Ceram. Soc., **47**, 484, 1964.

4.11 Kahn M., J. Am. Ceram. Soc., **54**, 452, 1971.

4.12 Fukami T. and Tsuchiya H., Jpn. J. Appl. Phys., **18**, 735, 1979.

4.13 Basu R.N. and Maiti H.S., in *Proceedings of the 6th IEEE International Symposium on the Applications of Ferroelectrics*, Ed. E. Wood (IEEE, New York, 1986), p.658.

4.14 Murugaraj P. and Kutty T.R.N., Mater. Res. Bull., **20**, 1473, 1984.

4.15 Ihrig H. and Puschert W., J. Appl. Phys., **48**, 3081, 1977.

4.16 Mader G., Meixner H. and Kleinschmidt P., J. Appl. Phys., **56**, 2832, 1984.

4.17 Mololkhia N.M., Issa M.A.A. and Nasser S.A., J. Am. Ceram. Soc., **67**, 289, 1984.

4.18 Ueda I. and Ikegami S., J. Phys. Soc. Jpn., **20**, 546, 1964.

4.19 Jonker G.H., Havinga E.E., Mater. Res. Bull., **17**, 345, 1982.

4.20 Xue L.A., Chen Y. and Brook R.J., Mater. Sci. Eng., **B1**, 193, 1988.

4.21 Heywang W., J. Mater. Sci., **6**, 1214, 1971.

4.22 Brauer H., Z. Angew. Phys., **23**, 373, 1976.

4.23 Jonker G.H., Mater. Res. Bull., **2**, 401, 1967.

4.24 Koshech G. and Kubalek E., J. Am. Ceram. Soc., **68**, 582, 1984.

4.25 Daniels J. and Härtdl K.H., Philips Res. Rep., **31**, 489, 1976.

4.26 Kuwabara M., J. Am. Ceram. Soc., **64**, C170, 1981.

4.27 Tseng T.Y and Lu Y.Y., J. Mater. Sci., **7**, 182. 1988.

4.28 Drofenik M.H., J. Am. Ceram. Soc., **69**, C8, 1986.

4.29 Drofenik M.H., J. Am. Ceram. Soc., **70**, 311, 1987.

4.30 Kuwabara M., Jpn. J. Appl. Phys., **20** (Suppl 20-4), 131, 1981.

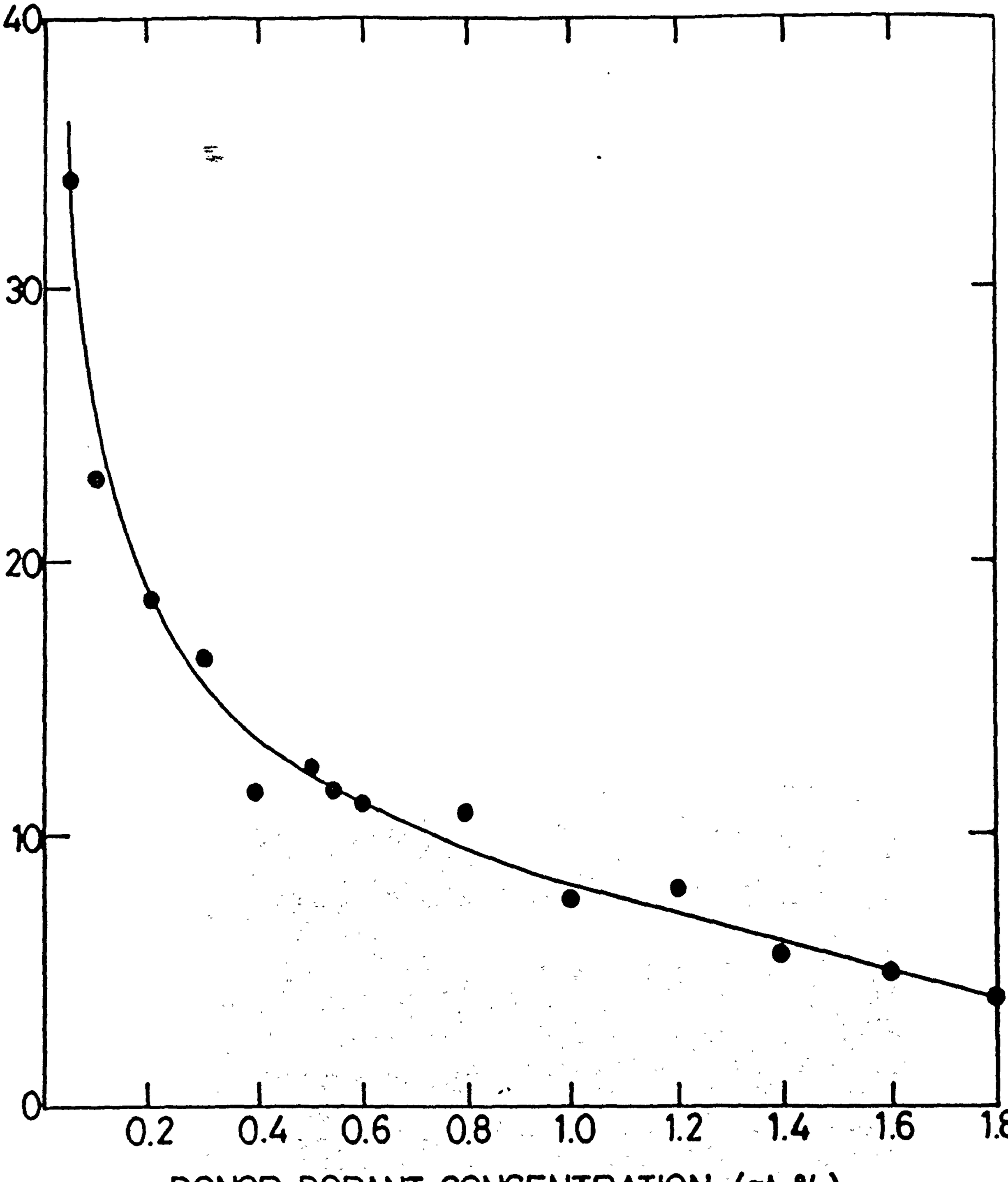

Figure 4.1 Variation of grain size with donor concentration.

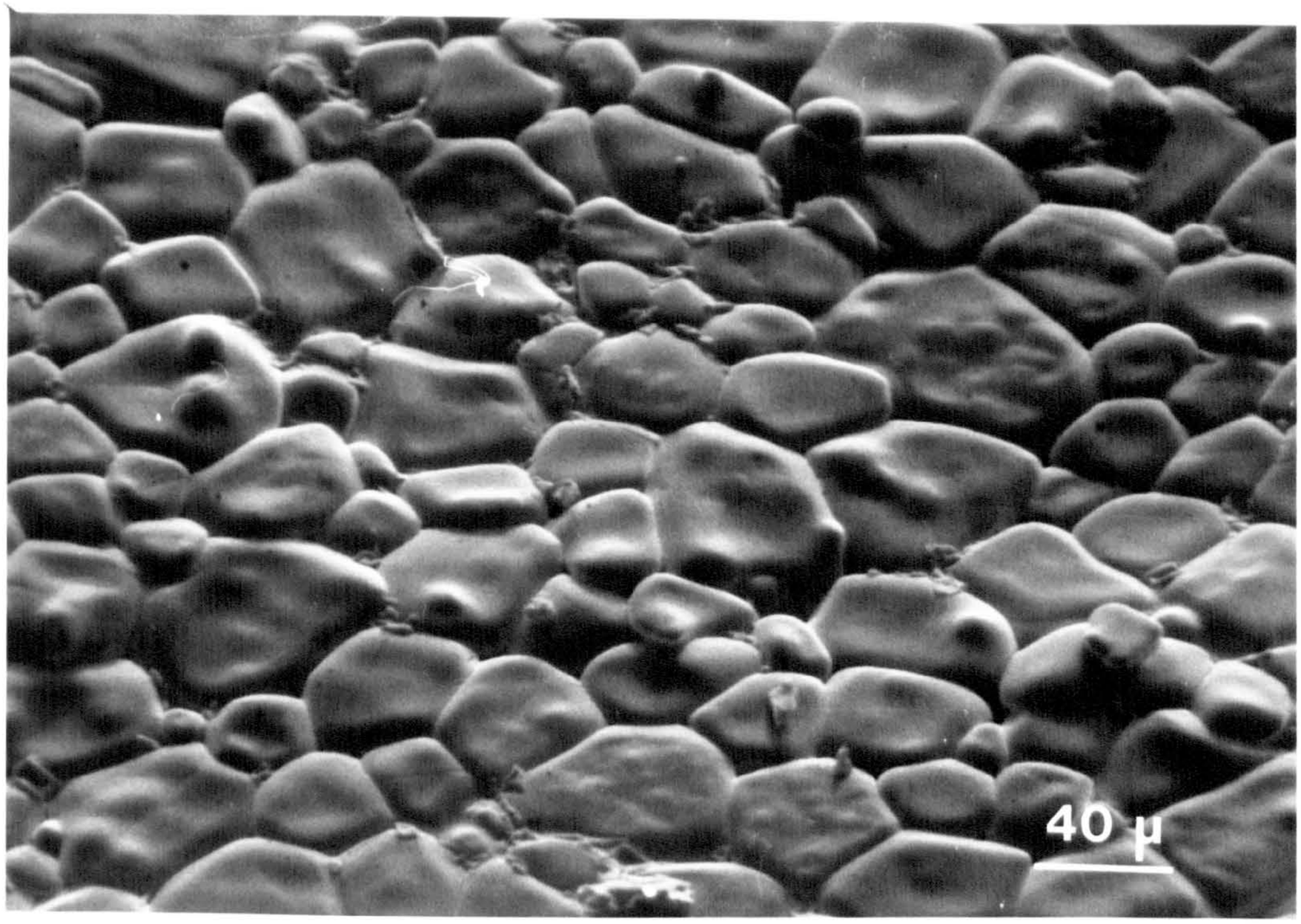

Figure 4.2 Scanning Electron Micrograph of the as-fired surface of a sample containing 0.05 at%Ho (bar = 40μm).

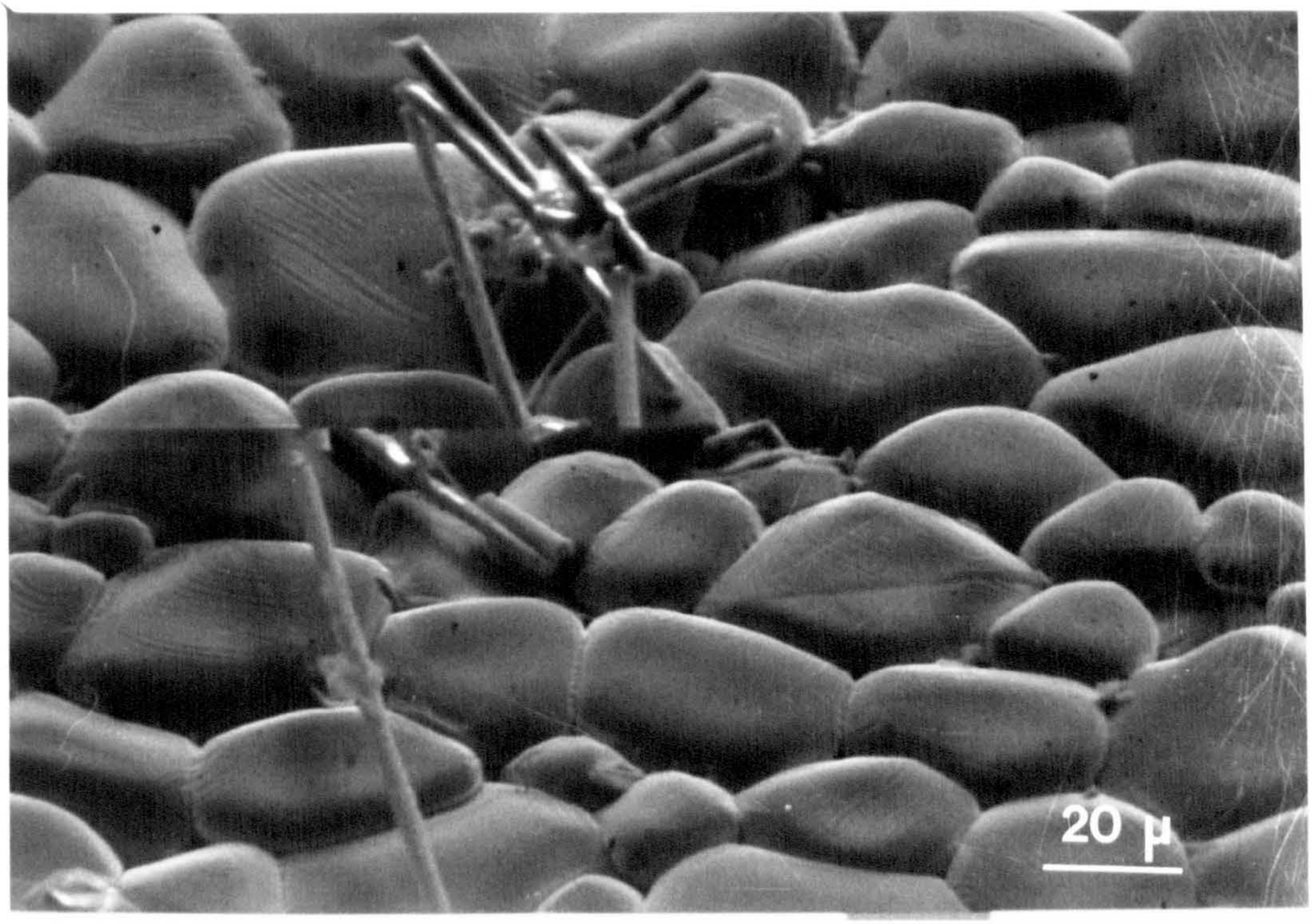

Figure 4.3 Scanning Electron Micrograph of second phase features on the surface of a sample with 0.1 at%Ho concentration (bar = 20μm).

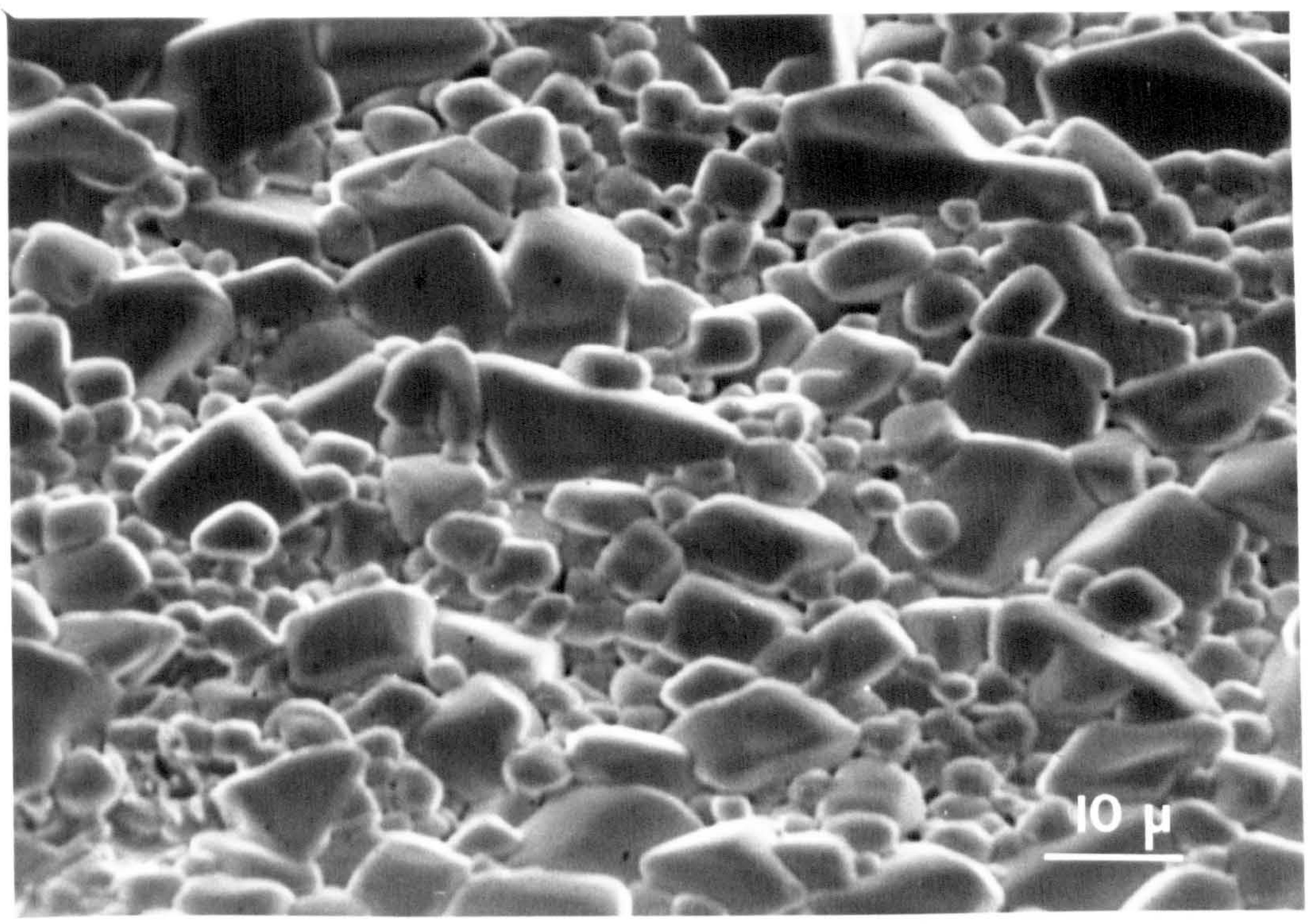

Figure 4.4 Scanning Electron Micrograph of sample doped with 1.4 at%Ho.

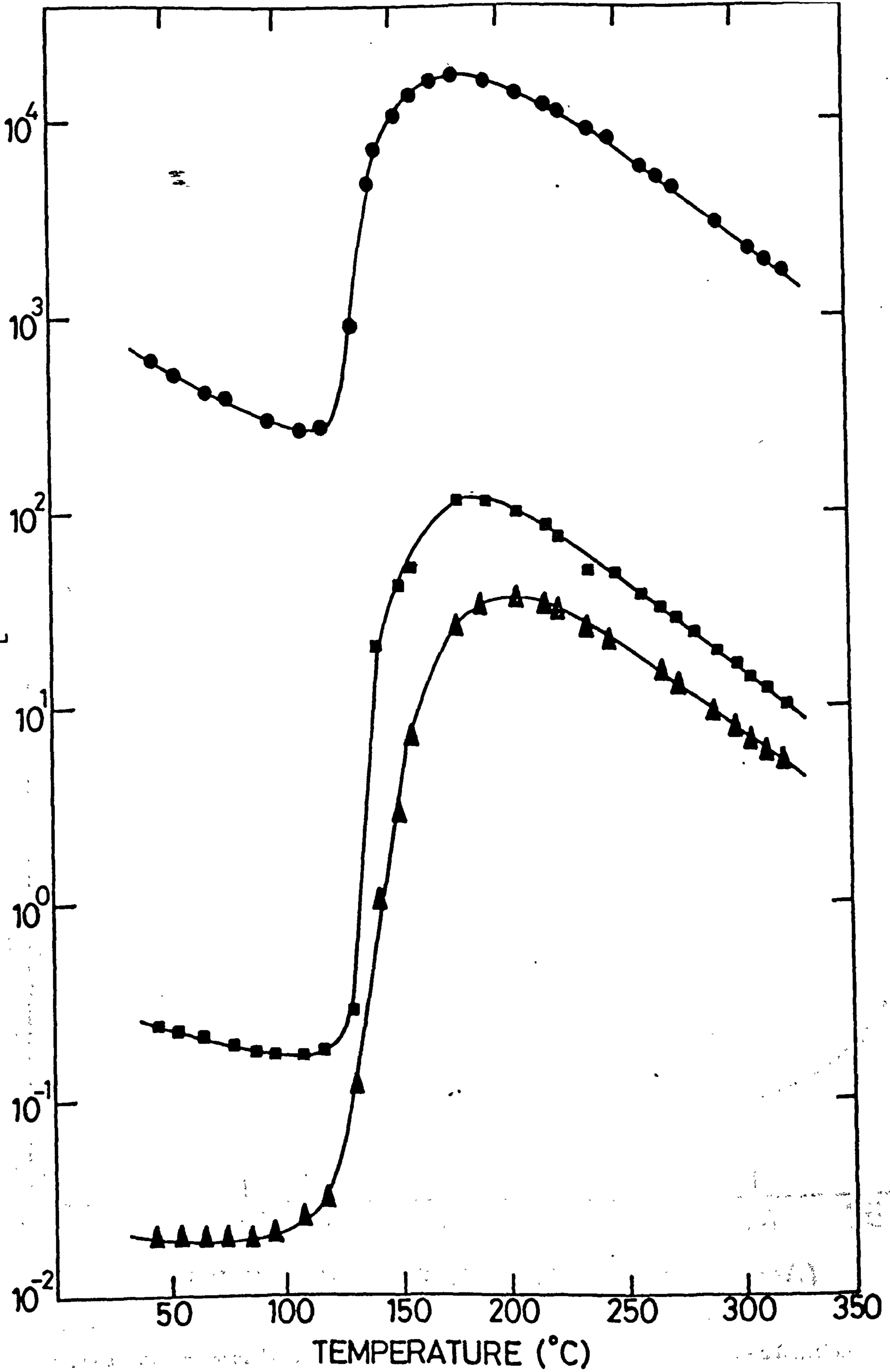

Figure 4.5 Normalised resistance of samples containing 0.05 (•), 0.4 (▲) and 1.8 (■) at%Ho donor concentration, between 50 and 320°C.

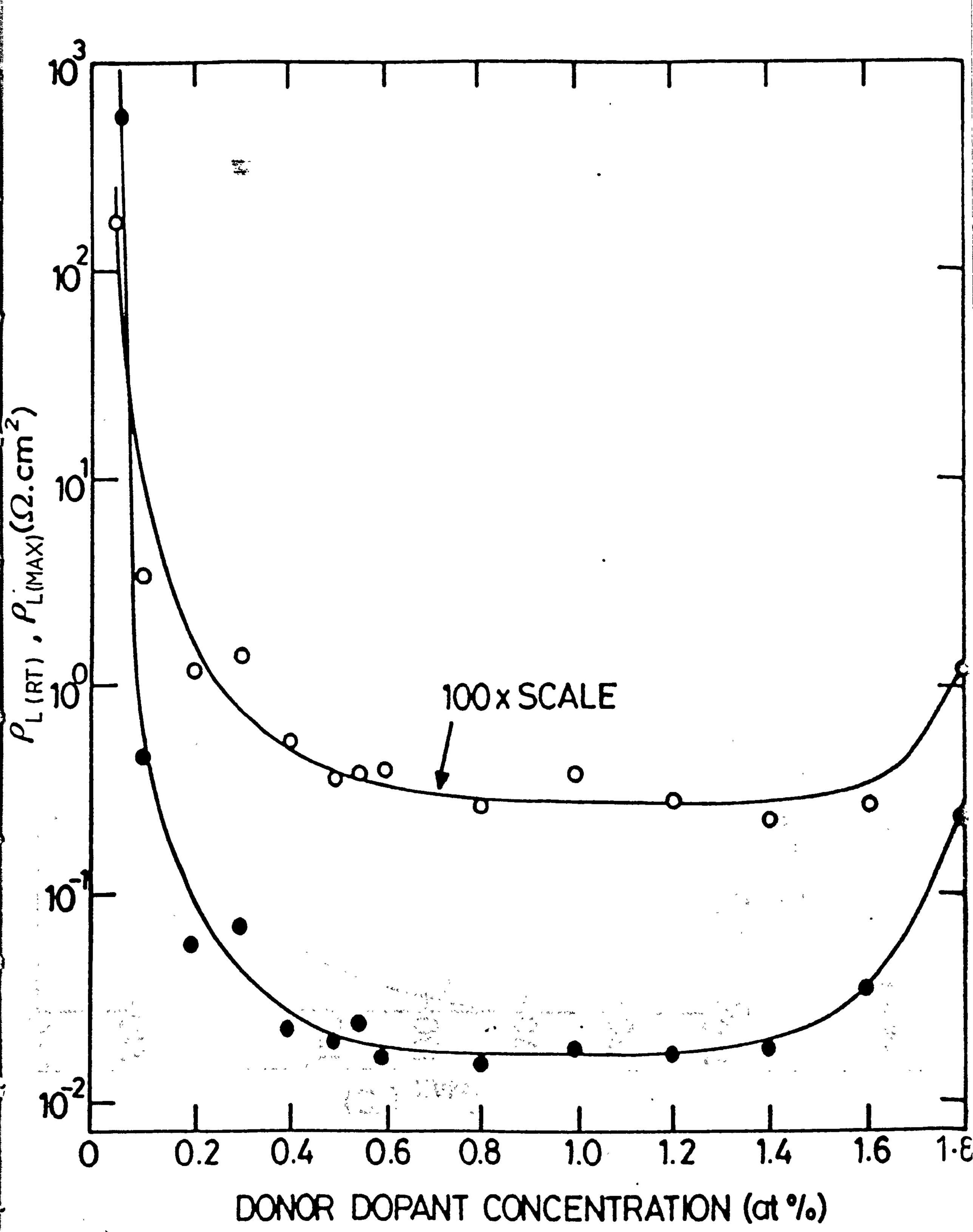

Figure 4.6 Maximum and room temperature values of normalised resistance, as a function of donor concentration.

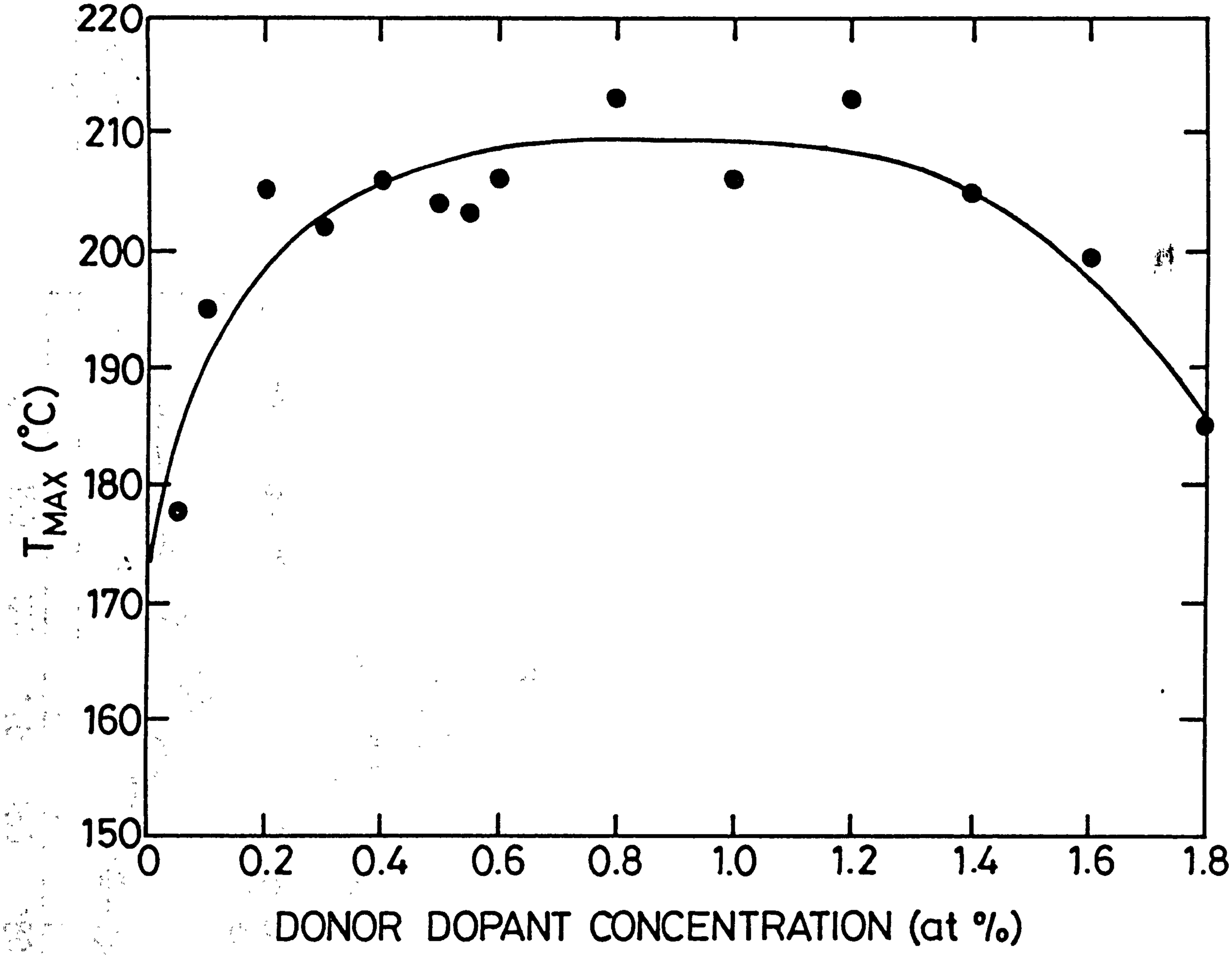

Figure 4.7 Temperature at which the resistance maximum takes place, versus donor concentration.

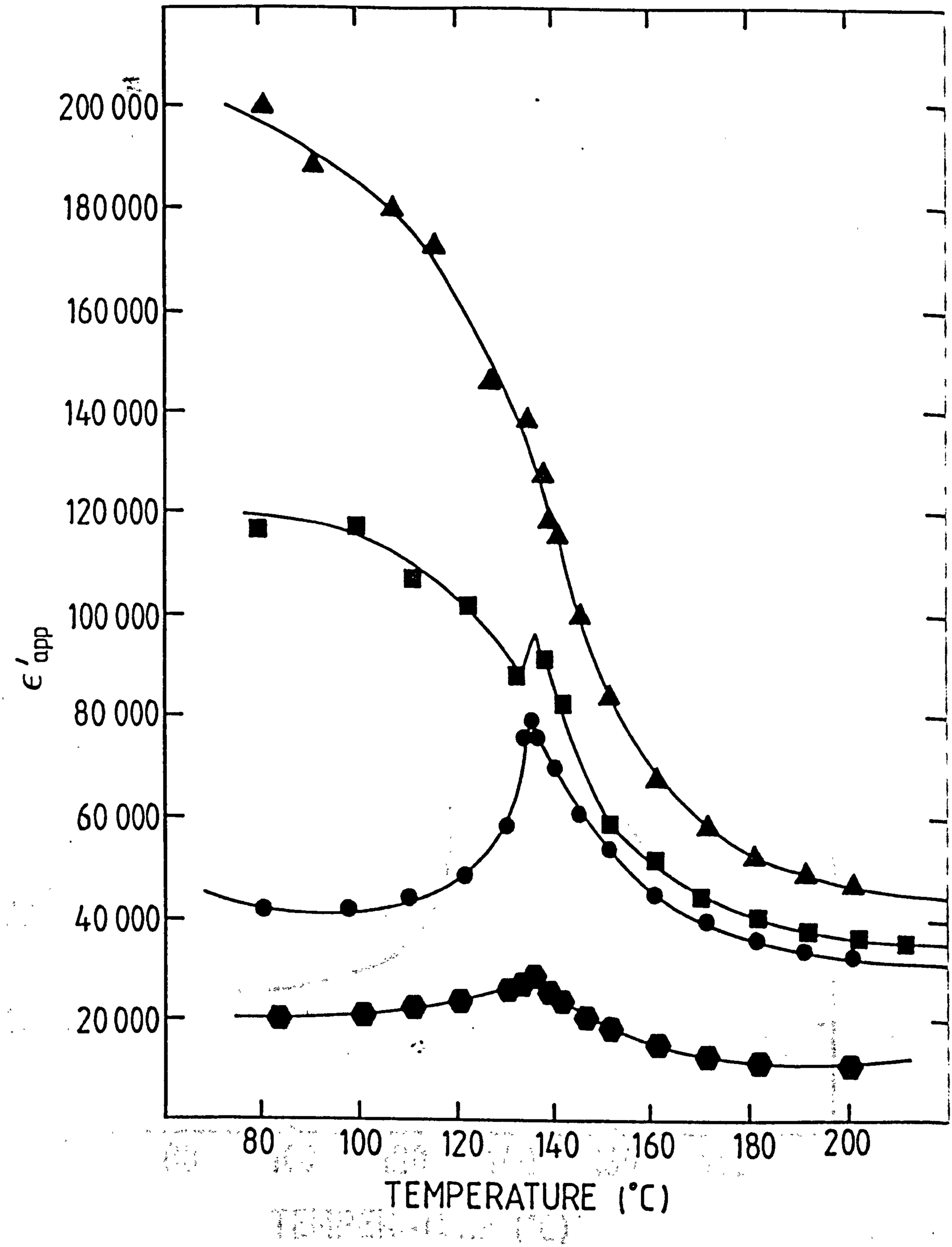

Figure 4.8a Apparent permittivity versus temperature for samples containing 0.1 (●), 0.5 (▲), 1.0 (■) and 1.8 (⬣) at%Ho dopant concentration.

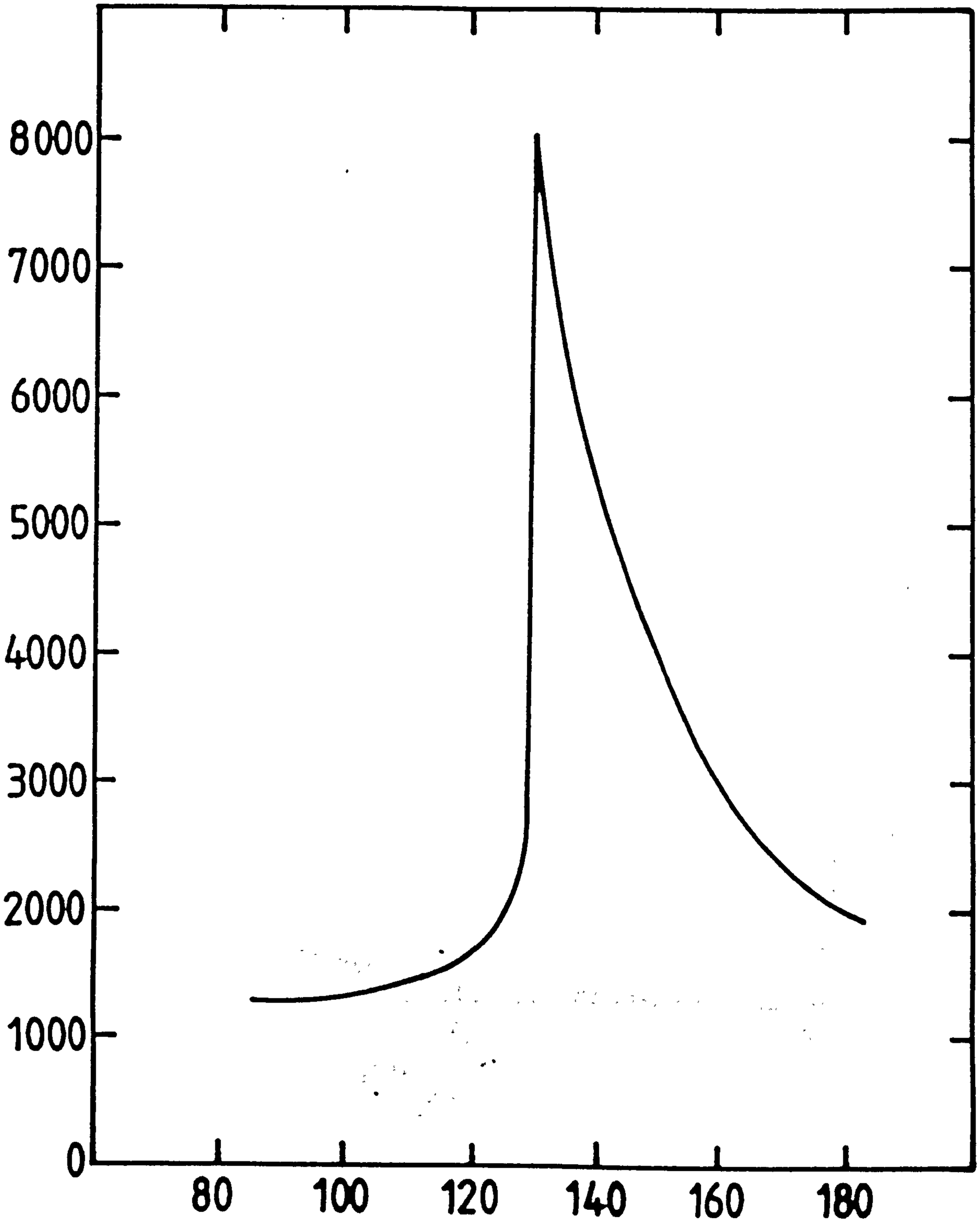

Figure 4.8b Apparent permittivity versus temperature of an undoped sample of barium titanate.

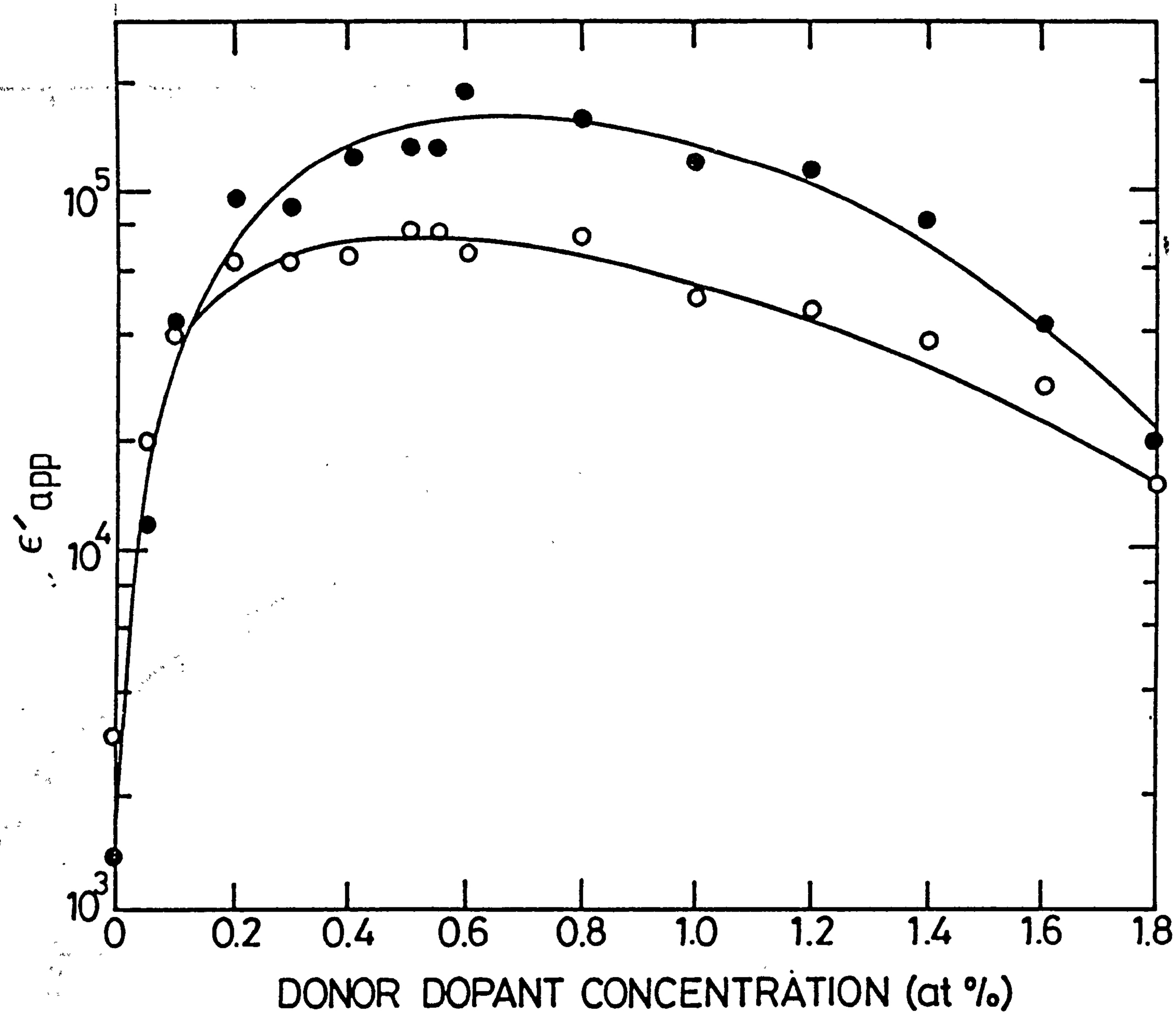

Figure 4.9 Apparent permittivity below (•) and above (o) T_c versus donor concentration.

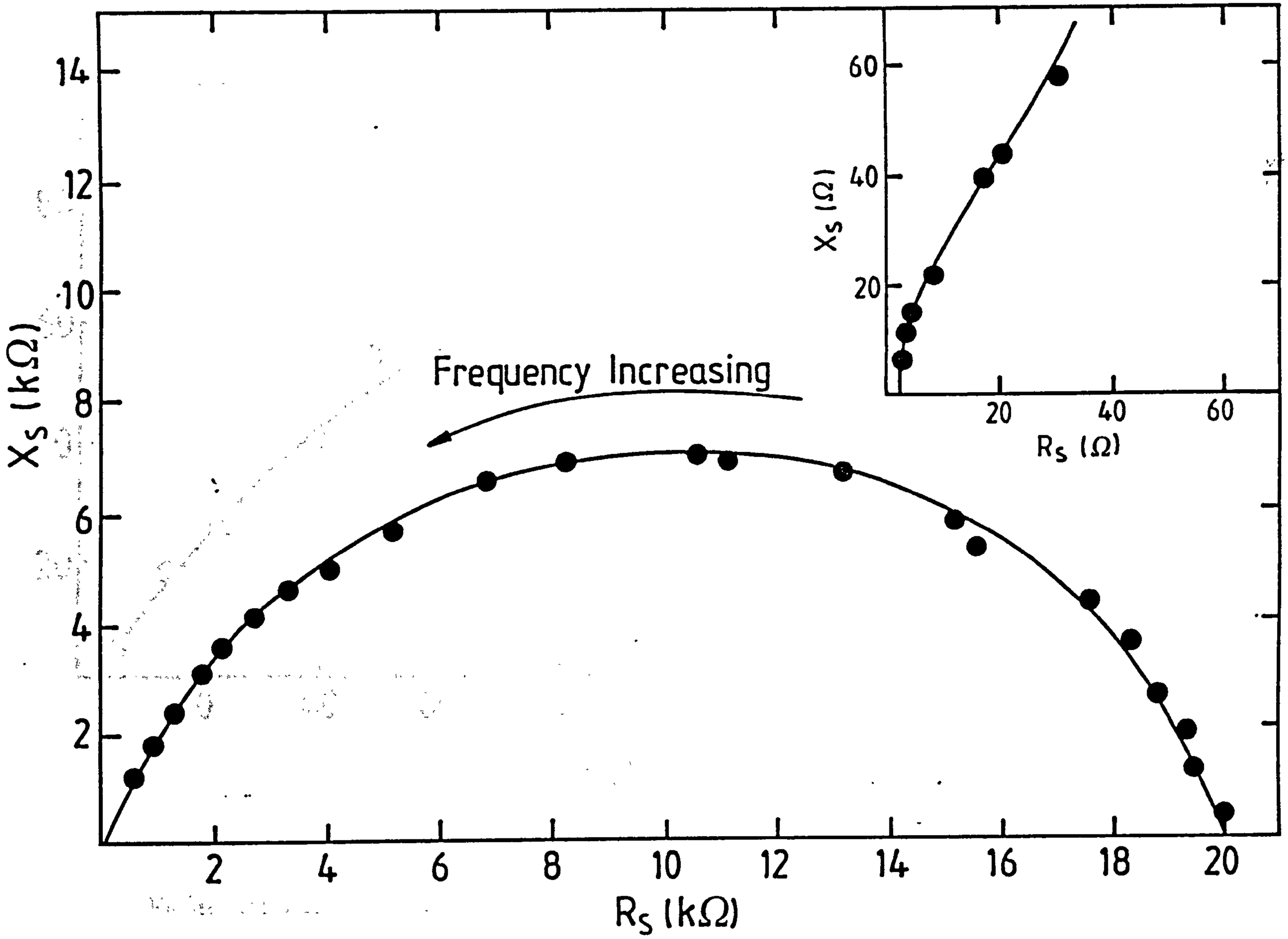

Figure 4.10 Room temperature impedance plot for a sample containing 0.05 at%Ho concentration.

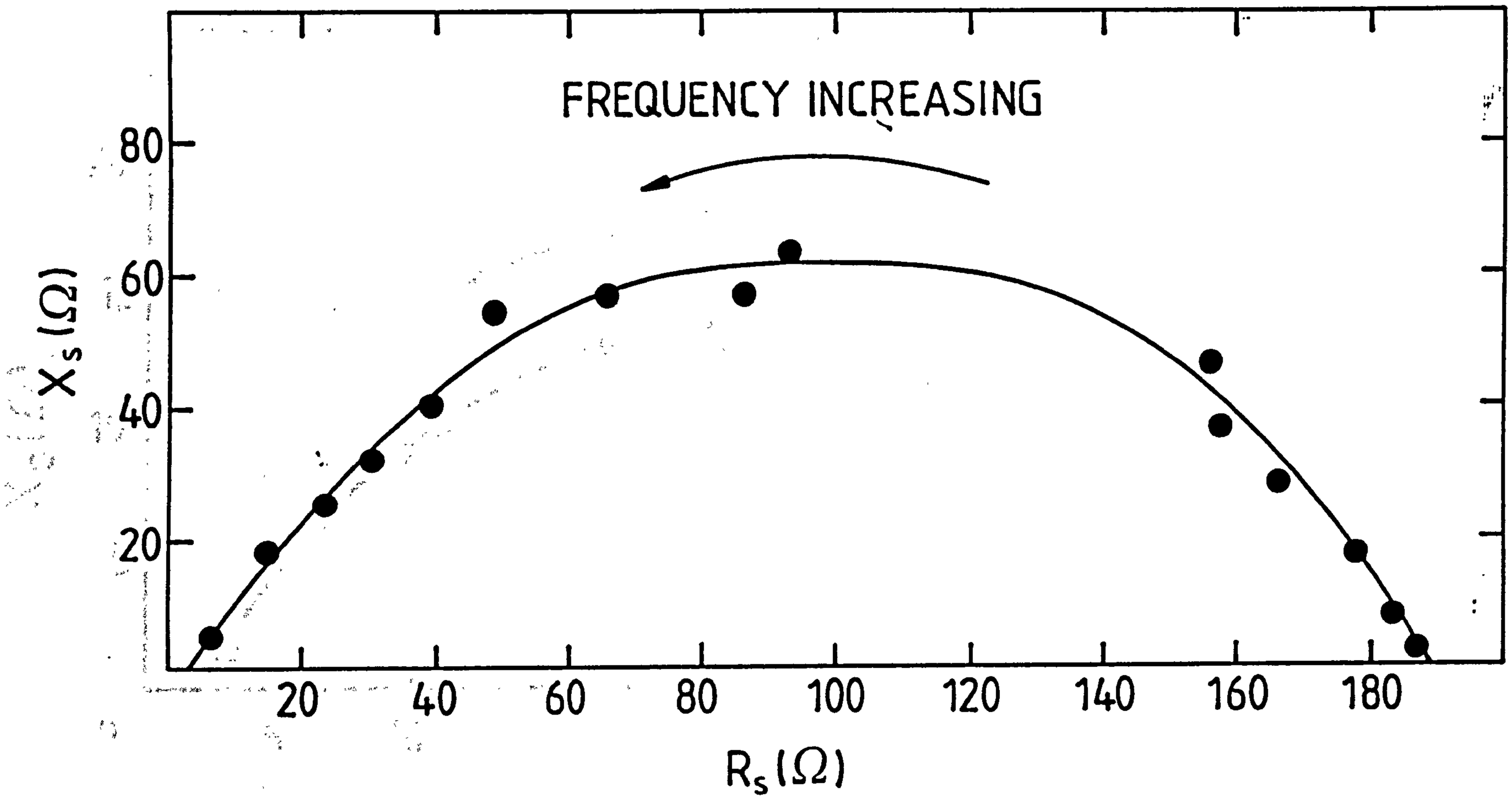

Figure 4.11 Room temperature impedance plot for a sample containing 0.1 at%Ho.

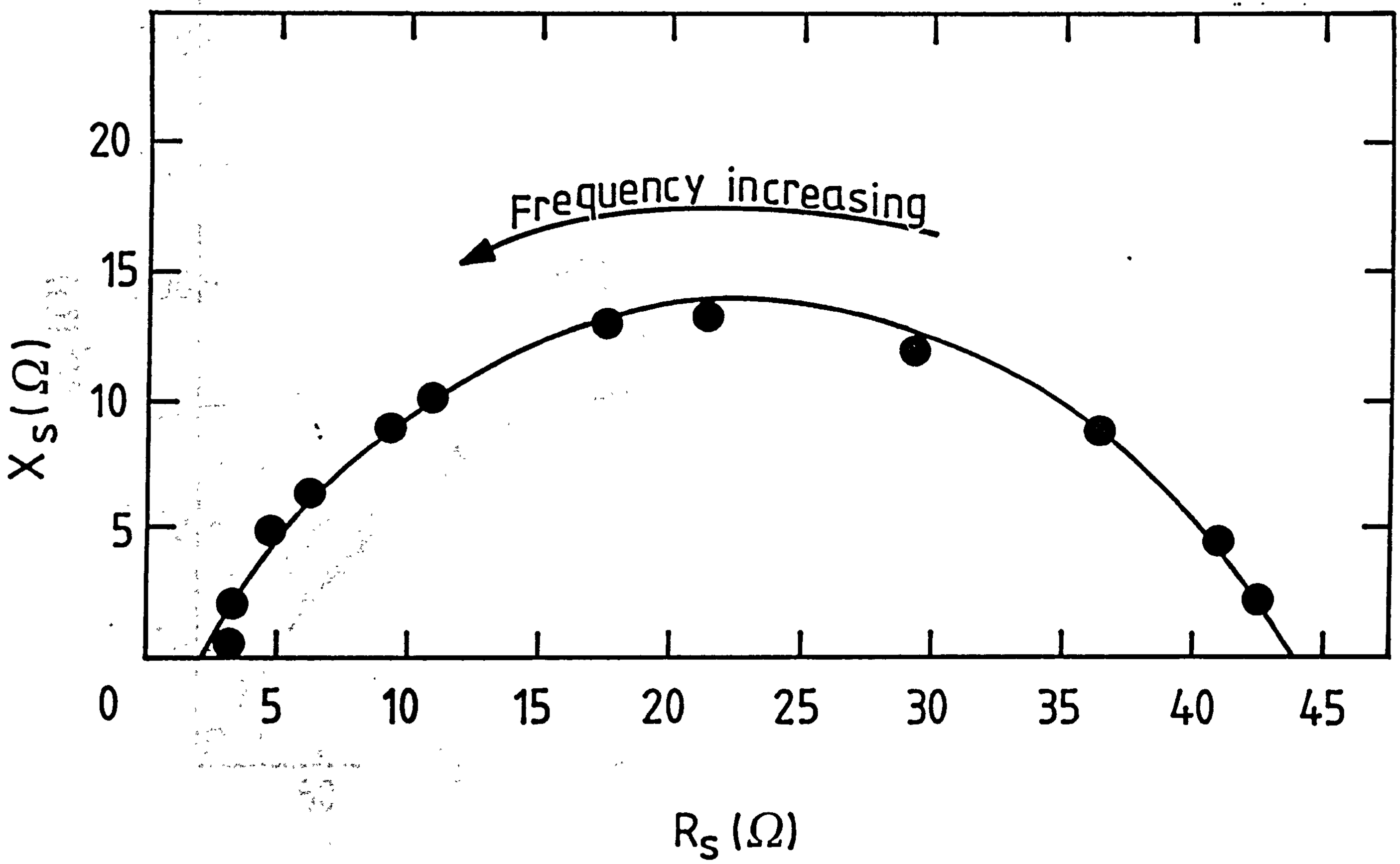

Figure 4.12 Room temperature impedance plot for a sample doped with 1.4 at%Ho.

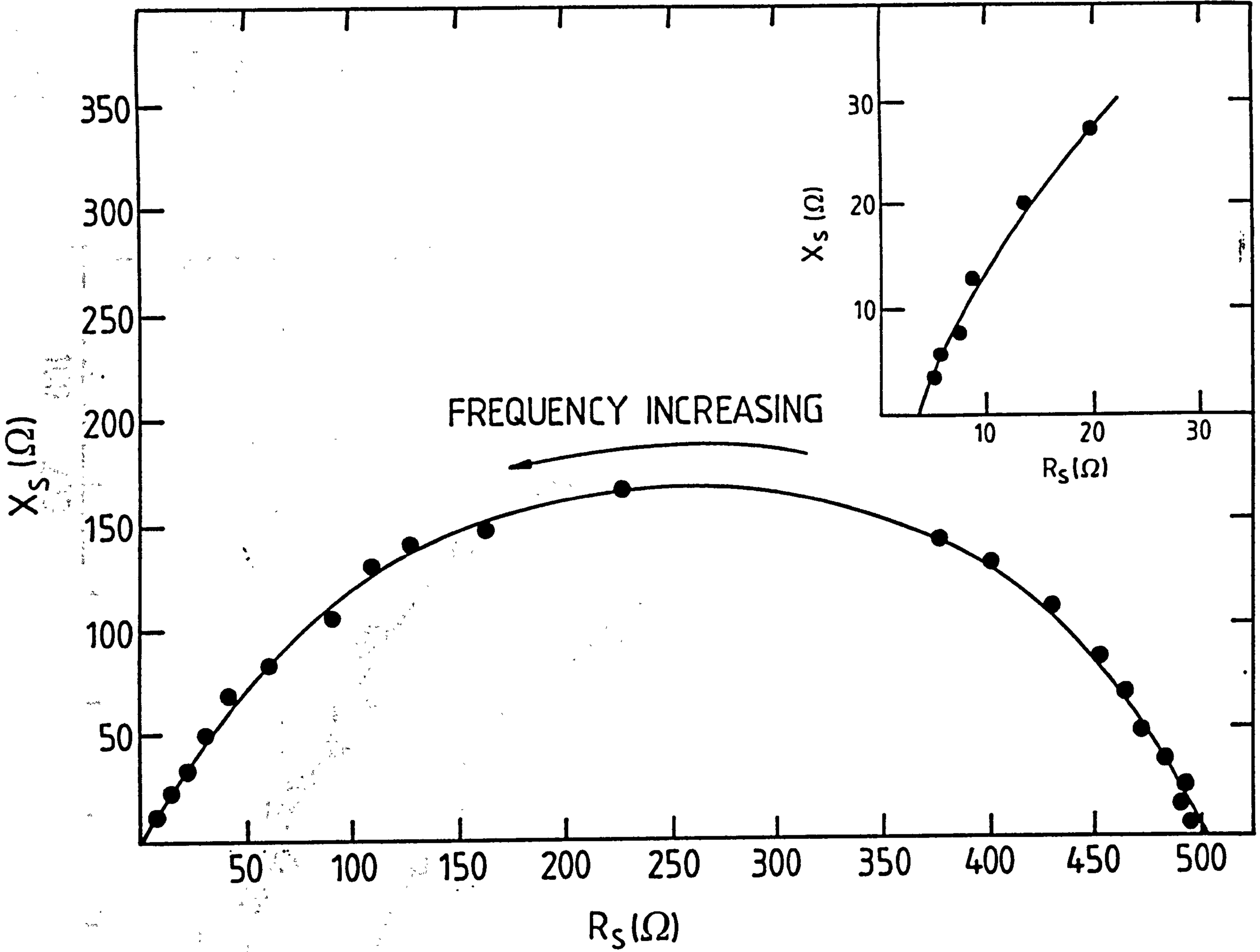

Figure 4.13 Room temperature impedance plot for a sample doped with 1.8 at%Ho concentration.

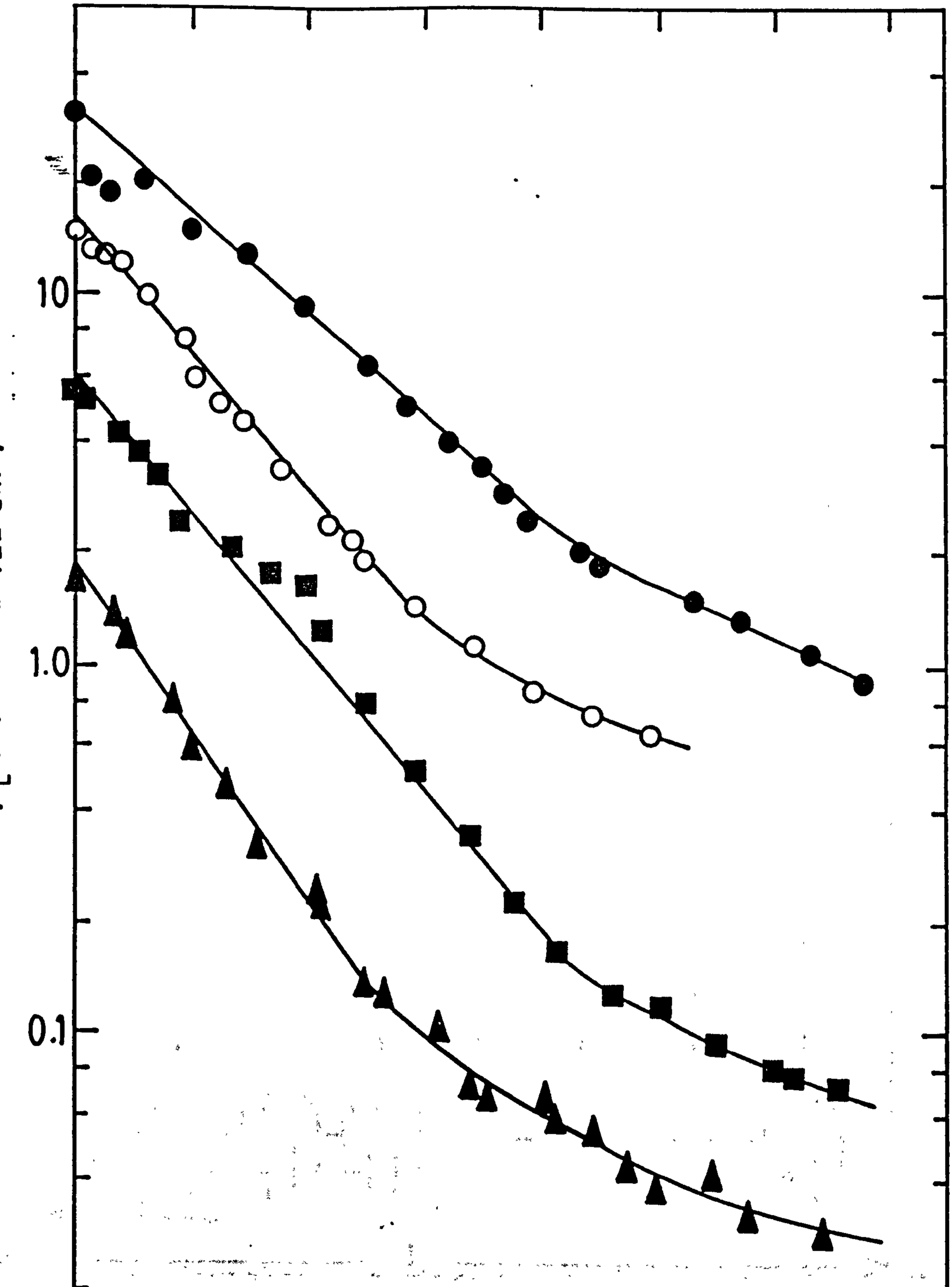

Figure 4.14 Normalised resistance at 170°C versus applied voltage per grain boundary for samples doped with 0.1 (•), 0.5 (▲), 0.6 (■) and 1.8 (o) at%Ho.

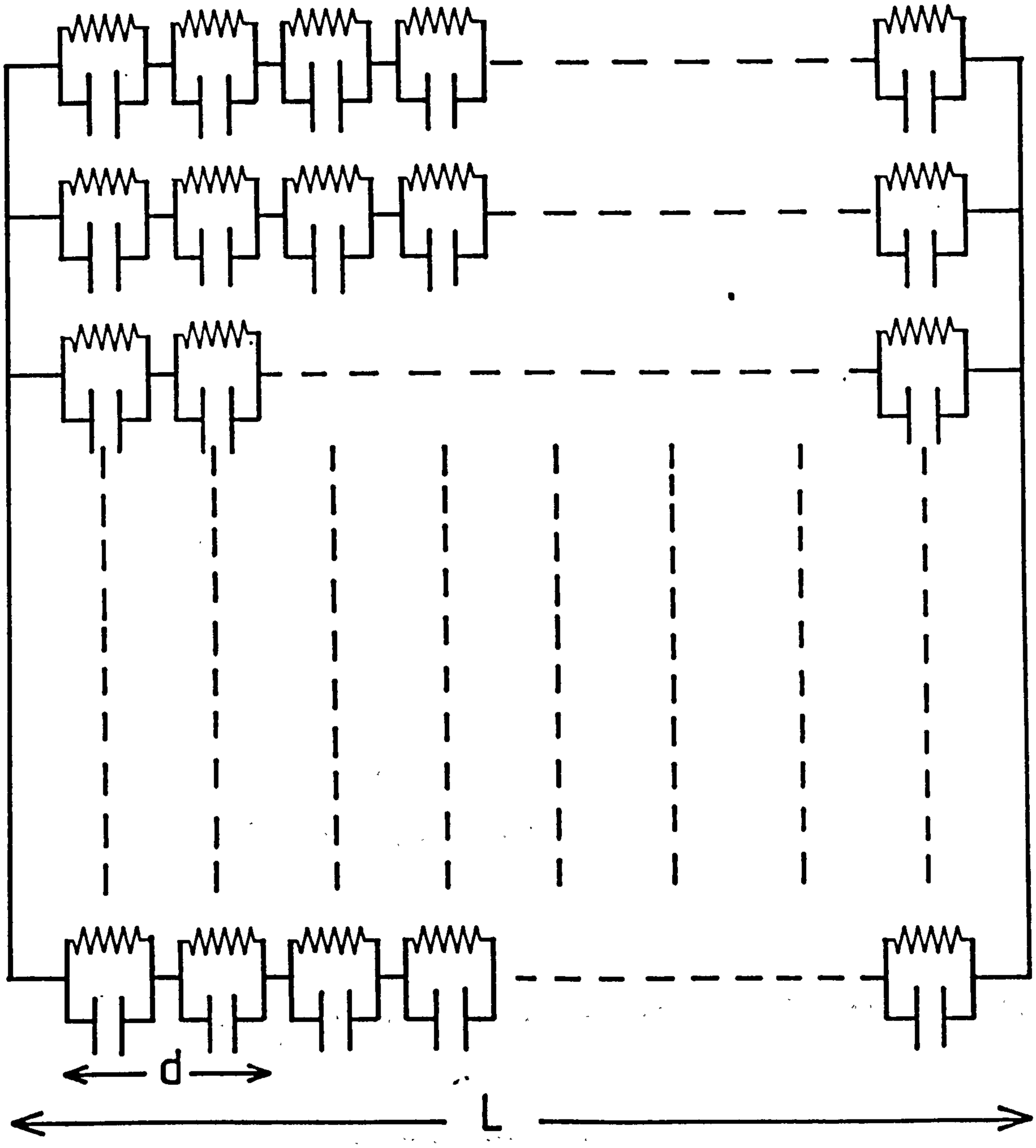

Figure 4.15 Schematic equivalent circuit for donor doped barium titanate sample.

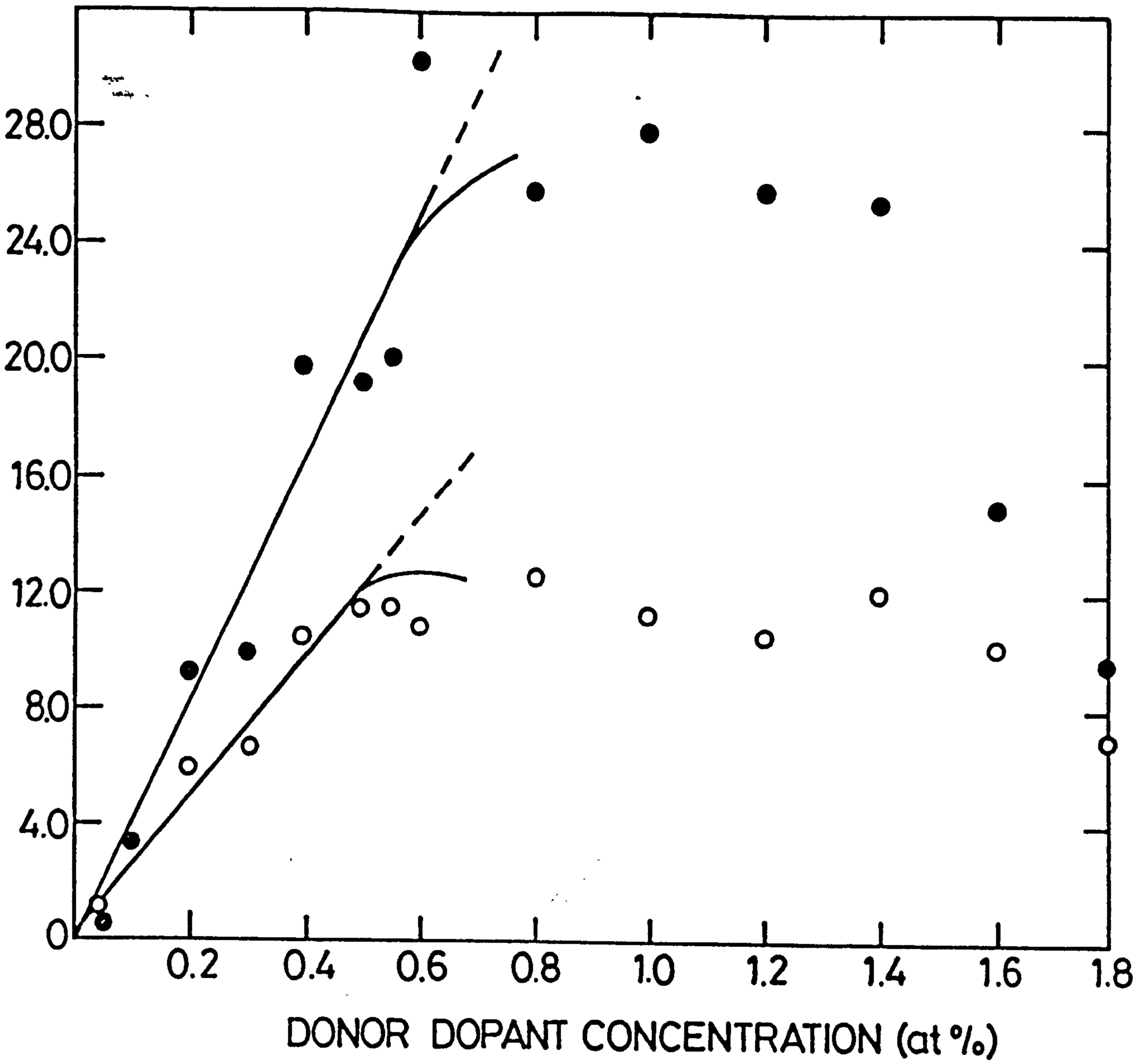

Figure 4.16 Normalised capacitance versus donor concentration, below (•) and above (o) T_c.

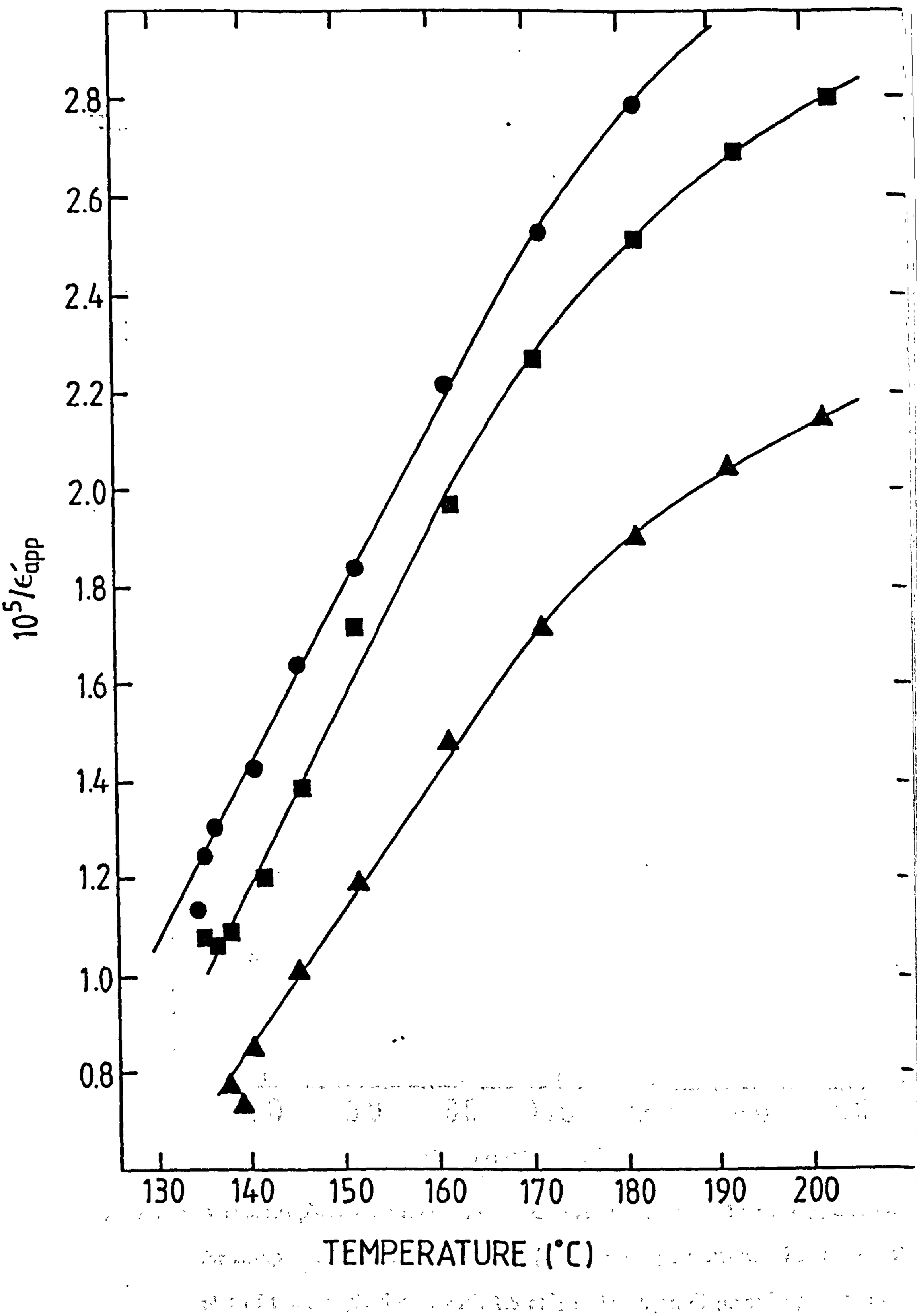

Figure 4.17 $1/\epsilon'_{app}$ versus temperature for samples containing 0.1 (●), 0.6 (▲) and 1.0 (■) at%Ho.

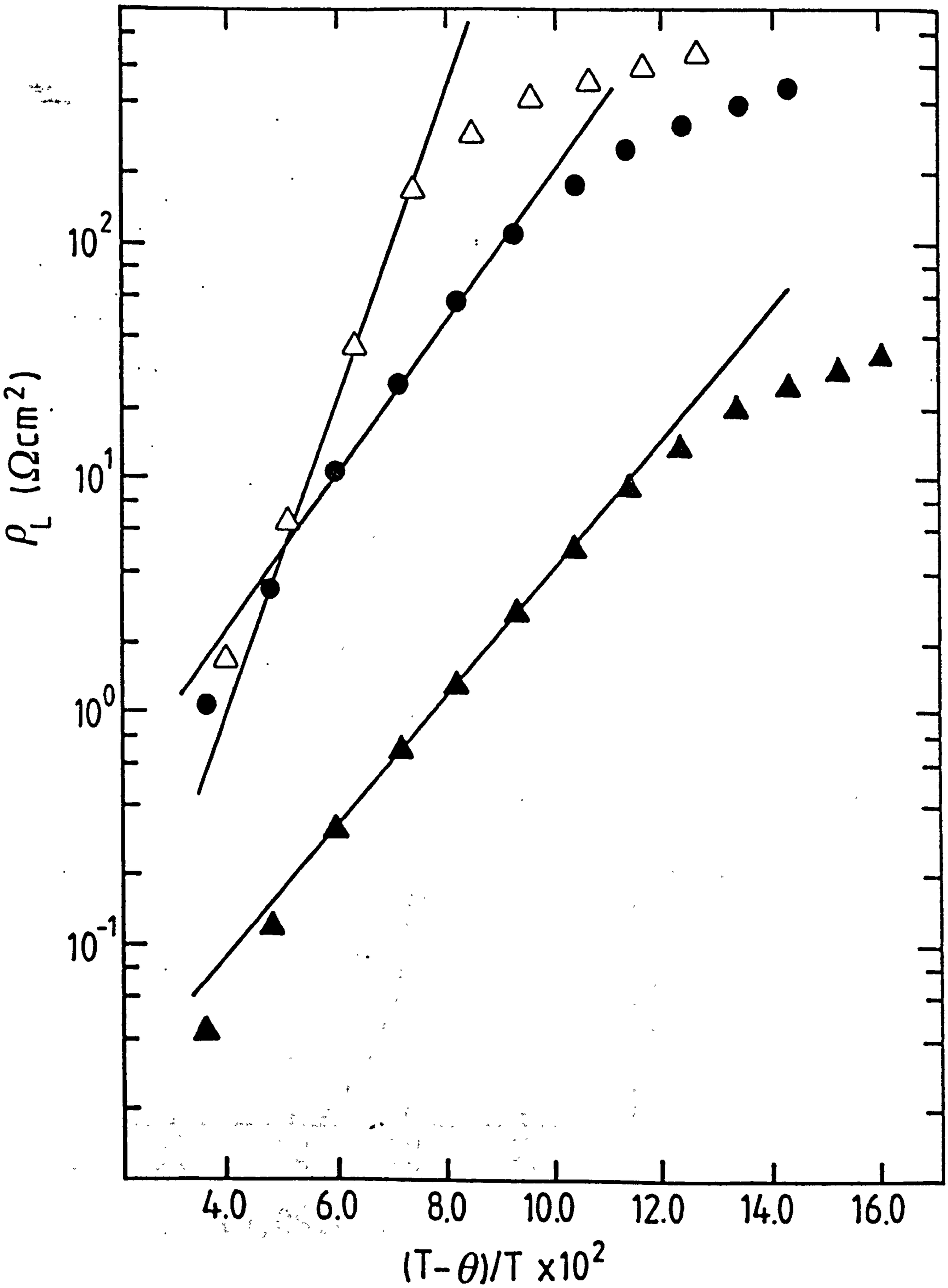

Figure 4.18 Arrhenius plots of normalised resistance versus (T - θ)/T between T_c and T_{max} for samples containing 0.1 (•), 0.6 (▲) and 1.8 (△) at%Ho. For clarity the plot of the sample doped with 1.8 at%Ho has been displaced upwards by an order of magnitude.

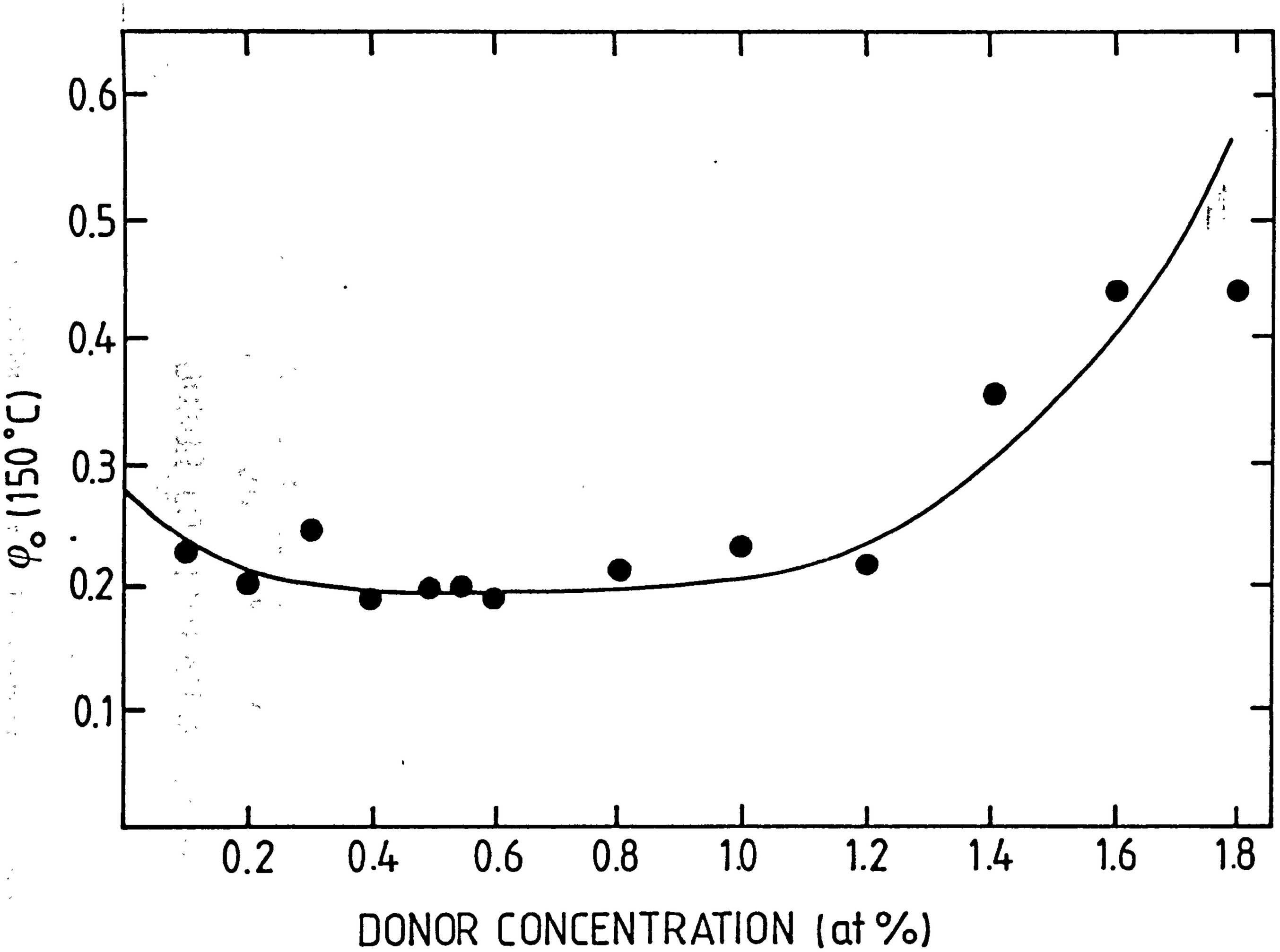

Figure 4.19 Potential barrier height at 150°C versus donor concentration.

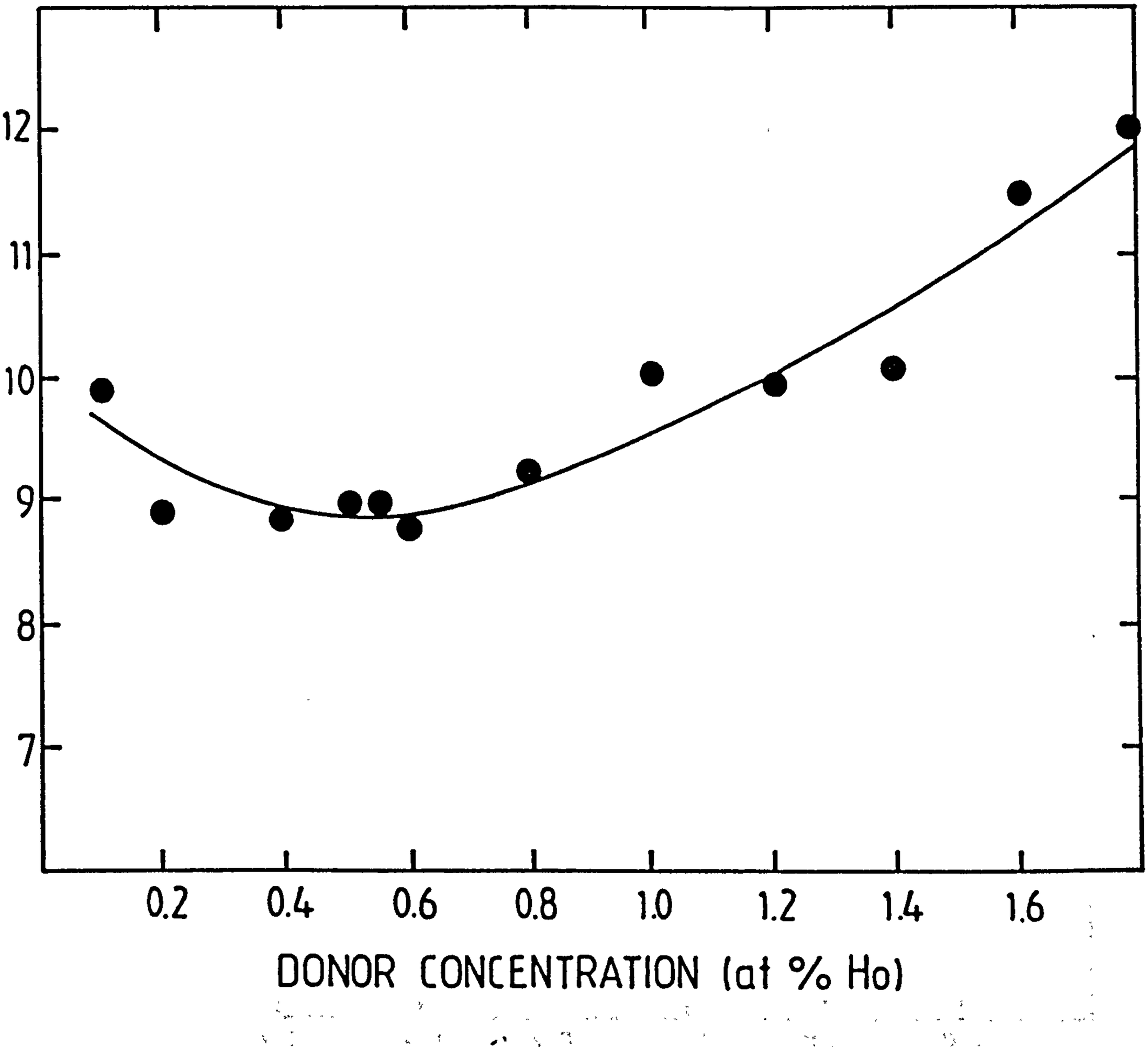

Figure 4.20 Total ionized acceptor density calculated from the slope of the plots of figure 4.18.

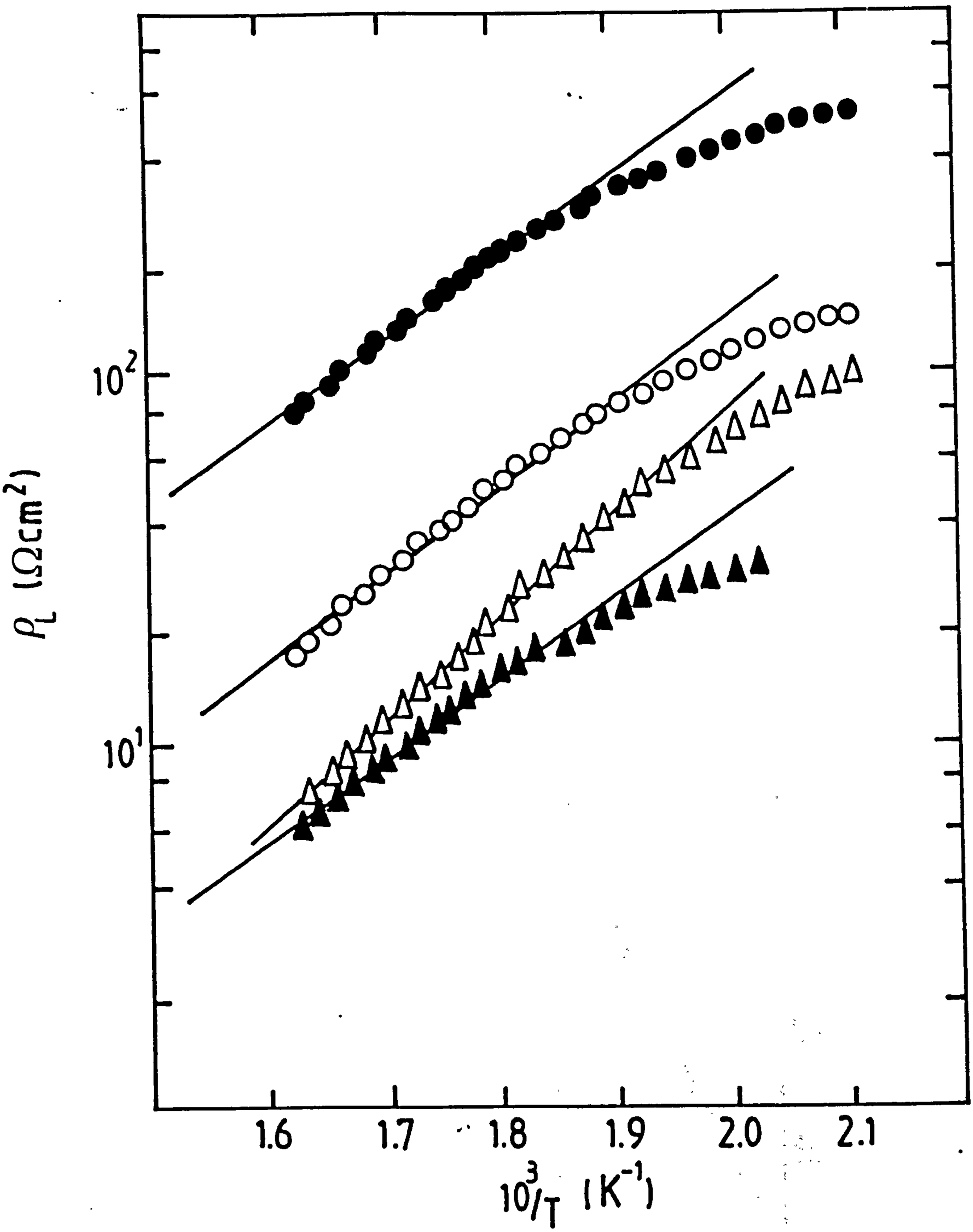

Figure 4.21 Arrhenius plots of normalised resistance versus 1/T above T_{max} for 0.1 (•), 0.3 (o), 1.2 (▲) and 1.8 (△) at%Ho.

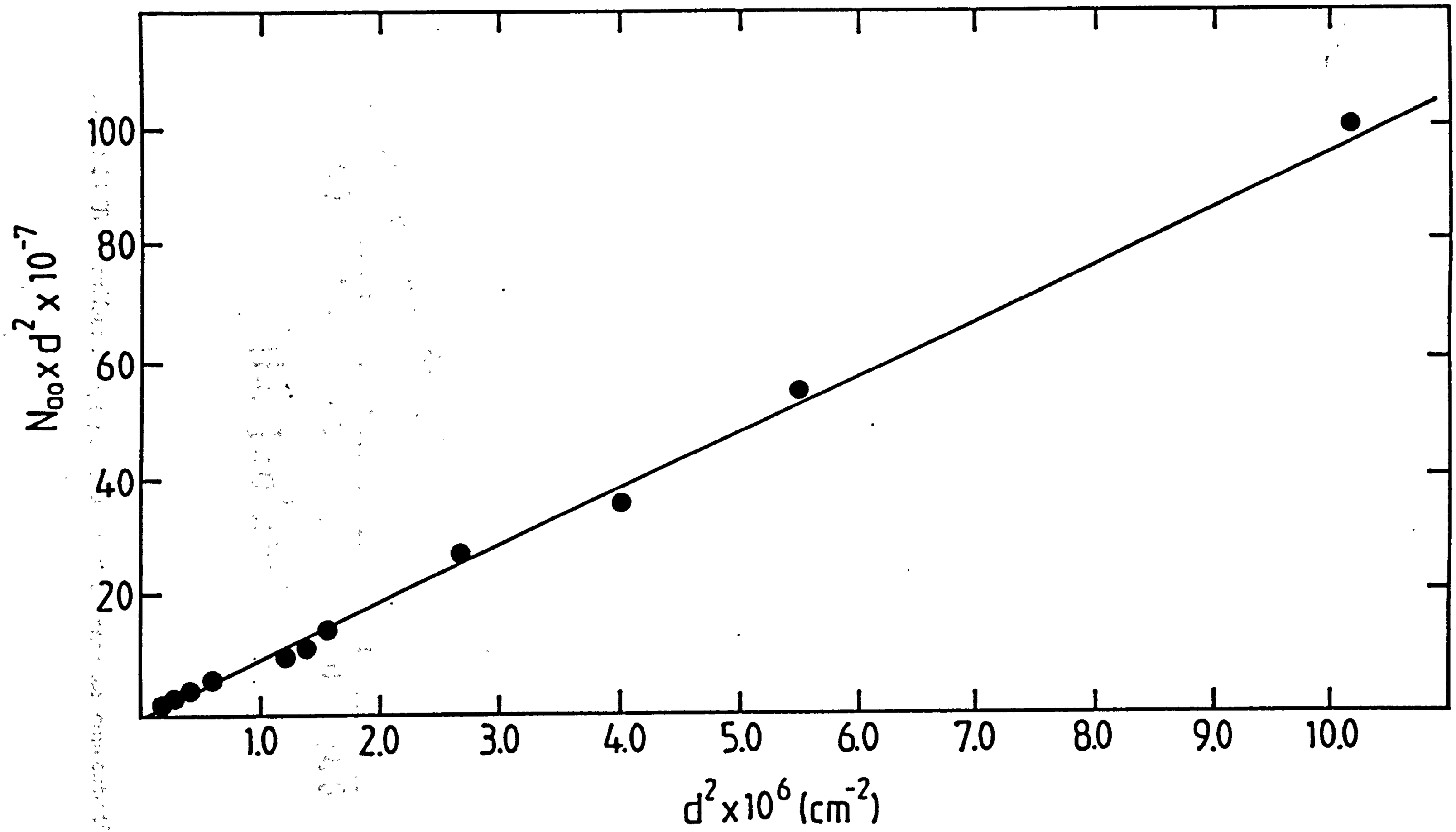

Figure 4.22 Total surface charge per grain versus grain surface area.

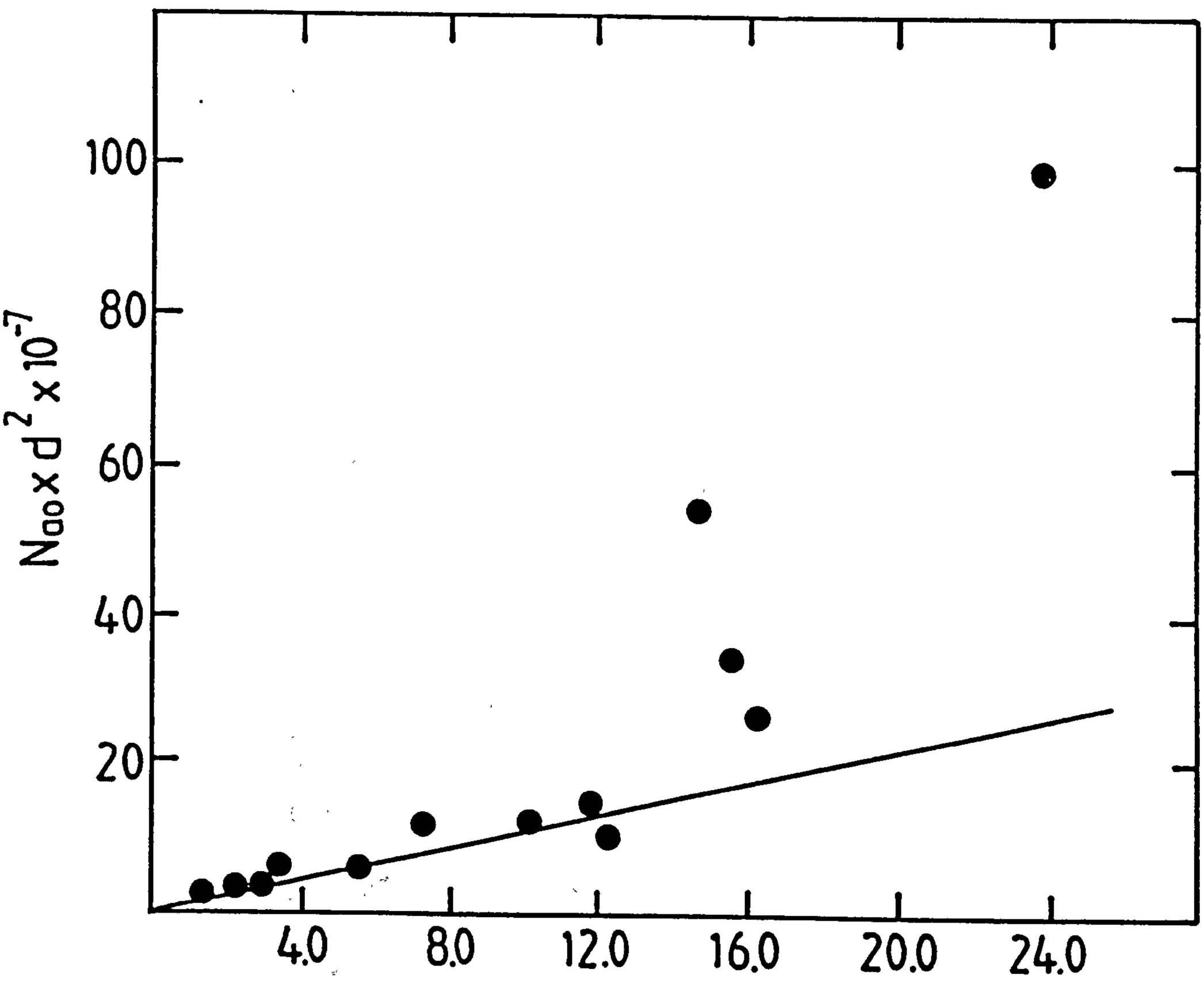

Figure 4.23 Total surface charge per grain versus donor ion concentration per grain.

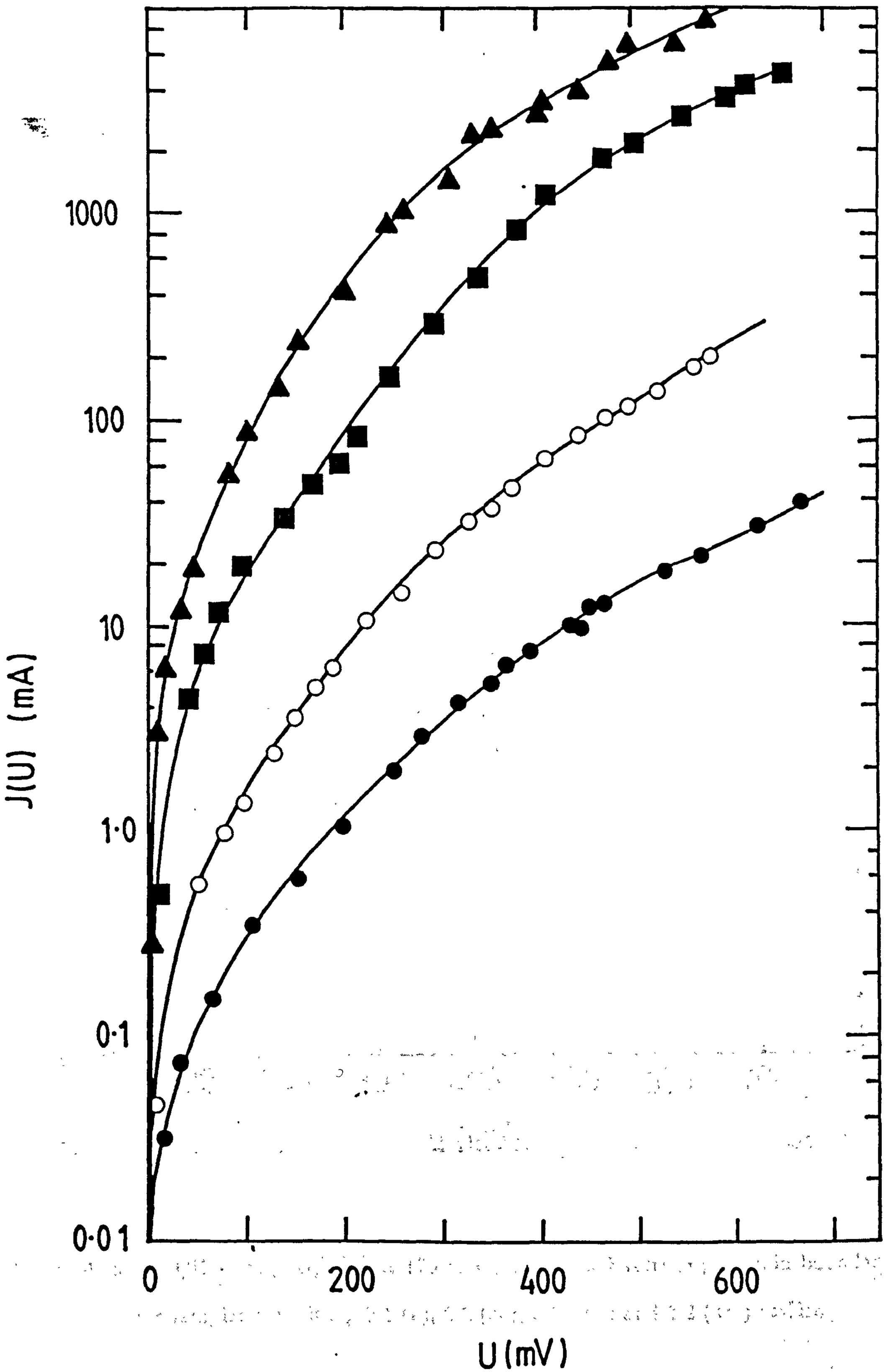

Figure 4.24 Current density at 170°C versus applied voltage per grain boundary for samples containing 0.1 (●), 0.5 (o), 0.6 (▲) and 1.2 (■) at%Ho.

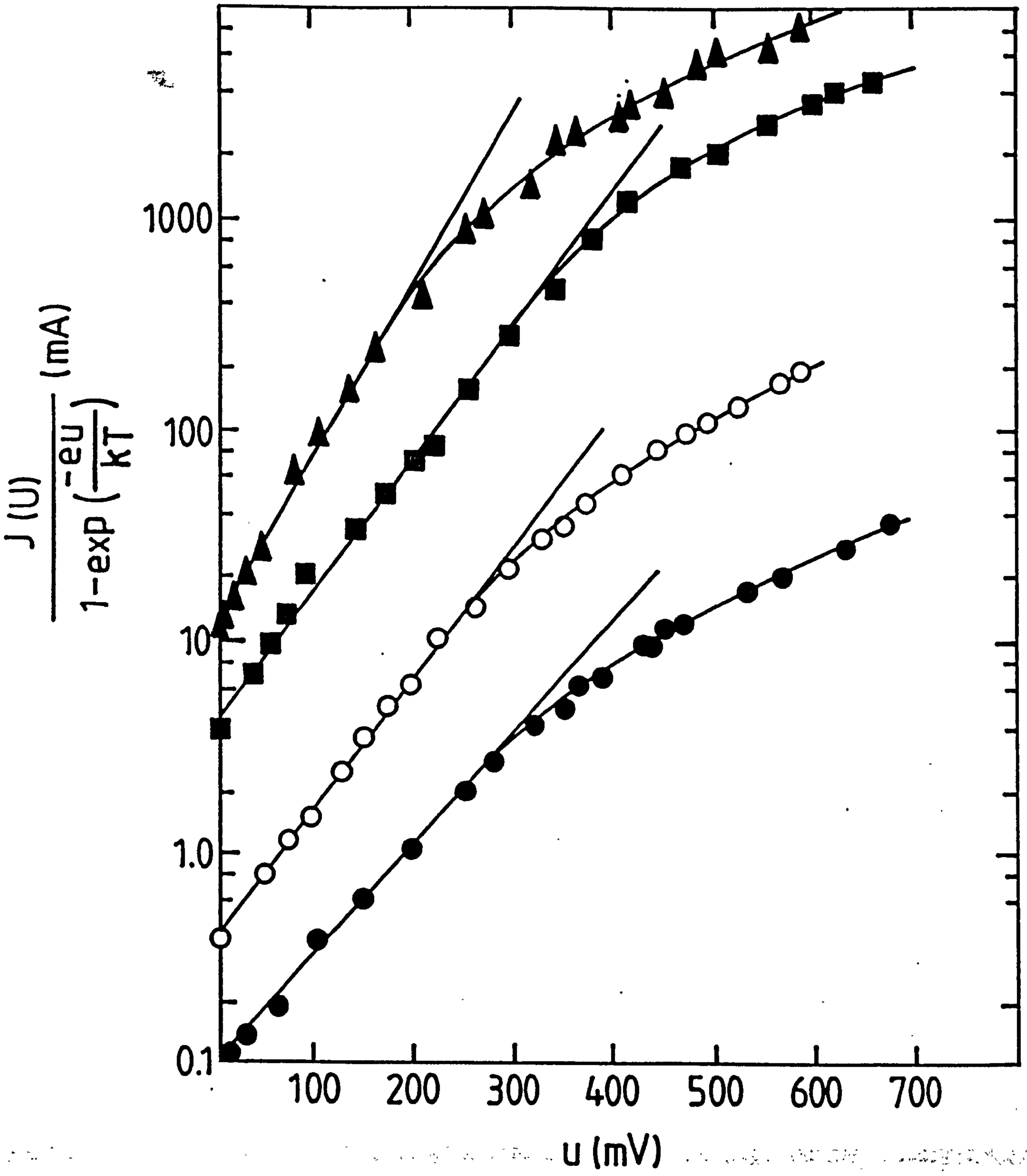

Figure 4.25 J(U)/[1 - exp(-eU/kT)] at 170°C versus applied voltage per grain boundary for samples containing 0.1 (•), 0.5 (o), 0.6 (▲) and 1.2 (■) at%Ho.

Donor Concentration (at % Ho)	Estimated ε' at 160°C	% error from 3333
0.05	2664	20
0.1	2362	29
0.2	2341	30
0.3	2639	21
0.4	2817	15
0.5	2911	13
0.55	2621	21
0.6	2796	16
0.8	2473	26
1.0	2917	12
1.2	2875	14
1.4	2936	12
1.6	2677	20
1.8	2710	19

TABLE 4.1

Estimated values of grain boundary permittivity at 160°C compared with the theoretical value of 3333, for all samples.

Donor Concentration (at % Ho)	U (mV)	Estimated ϕ_o (mV)
0.1	500	125
0.2	450	113
0.3	325	81
0.4	100	25
0.5	275	69
0.55	275	65
0.6	450	113
0.8	375	94
1.0	450	113
1.2	425	113
1.4	325	81
1.6	325	81
1.8	300	75

TABLE 4.2

Voltage at which normalized resistance no longer obeys the Heywang model and corresponding estimated potential barrier height.

Donor Concentration (at % Ho)	A
0.05	83.7
0.1	75.5
0.2	68.0
0.3	83.4
0.4	63.7
0.5	66.1
0.55	65.8
0.6	63.4
0.8	70.9
1.0	102.3
1.2	94.3
1.4	118.1
1.6	147.0
1.8	154.4

TABLE 4.3

Slope of the Arrhenius plots of $\ln\rho_L$ versus $(T - \theta)/T$ for all samples

Donor Concentration (at % Ho)	N_{ao} Arrhenius Method (cm^{-2})	N_{ao} From $1/\varepsilon'_{app}$ versus T (cm^{-2})
0.05	8.5×10^{13}	5.8×10^{14}
0.1	8.1×10^{13}	1.8×10^{14}
0.2	7.6×10^{13}	1.0×10^{14}
0.3	8.5×10^{13}	1.0×10^{14}
0.4	7.4×10^{13}	6.9×10^{13}
0.5	7.5×10^{13}	6.9×10^{13}
0.55	7.5×10^{13}	6.2×10^{13}
0.6	7.4×10^{13}	6.8×10^{13}
0.8	7.8×10^{13}	5.3×10^{13}
1.0	9.4×10^{13}	6.6×10^{13}
1.2	9.0×10^{13}	7.2×10^{13}
1.4	1.0×10^{14}	6.5×10^{13}
1.6	1.1×10^{14}	6.9×10^{13}
1.8	1.2×10^{14}	1.1×10^{14}

TABLE 4.4

Fully ionized values of grain boundary acceptor state density, obtained from the Arrhenius method and from apparent permittivities, for samples of all compositions.

Donor Concentration (at %)	ϕ_o (max) (eV)	N_a (250°C) (cm^{-2})	N_a/N_{ao}	E_a (eV)
0.1	0.434	6.69×10^{13}	0.67	0.89
0.2	0.398	6.41×10^{13}	0.72	0.86
0.3	0.466	6.94×10^{13}	0.69	0.92
0.4	0.434	6.69×10^{13}	0.76	0.90
0.5	0.561	7.61×10^{13}	0.85	1.05
0.55	0.465	6.93×10^{13}	0.77	0.93
0.6	0.430	6.66×10^{13}	0.76	0.90
0.8	0.341	5.93×10^{13}	0.64	0.79
1.0	0.378	6.25×10^{13}	0.61	0.82
1.2	0.412	6.52×10^{13}	0.66	0.86
1.4	0.420	6.59×10^{13}	0.61	0.86
1.6	0.530	7.40×10^{13}	0.64	0.98
1.8	0.568	7.66×10^{13}	0.64	1.02

TABLE 4.5

Maximum grain boundary potential barrier height, acceptor state density at 250°C and acceptor energy, for samples containing between 0.1 and 1.8 at % Ho.

CHAPTER FIVE

INVESTIGATION OF DONOR CONCENTRATION, WITH SAMPLES SINTERED AT A LOWER TEMPERATURE

The previous chapter described the effect of donor dopant concentration of between 0.05 and 1.8 at%Ho on aspects of the PTCR characteristics. The presence of broad minima in the normalised resistance data ($\rho_{L(RT)}$ and $\rho_{L(max)}$), together with a maximum in T_{max}, between ~0.4 and 1.4 at%Ho was finally attributed to changes in the grain boundary acceptor state density, N_{ao}. Analysis using the Heywang model[5.1,5.2] of the experimental data enabled both N_{ao} and the acceptor energy, E_a, to be estimated. Contrary to predictions of other workers[5.3,5.4], E_a remained constant, showing that the nature of the grain boundary acceptor states was not affected by donor concentration.

According to the Daniels model[5.3,5.4], the concentration of acceptor - like doubly ionized barium vacancies depends on the equilibrium temperature in such a way that, as temperature is reduced, the concentration of barium vacancies is increased. Below ~1100°C, however, their diffusivity is very low and they essentially freeze into position at the grain boundaries. To sinter samples prepared in an identical manner to those of the previous chapter but at a lower temperature may be expected to result, according to Daniels, in both an increase in the acceptor state density and the acceptor energy, as a result of the increased number of barium vacancies.

5.1. SAMPLE PREPARATION

The samples used were identical to those of the previous chapter: $BaTiO_3$, Ho_2O_3, SiO_2 and TiO_2 were ball milled together in the required proportions for 12 hours using the polyethylene mill, agate media and deionized water. The concentration range of donor dopant was more narrow for this investigation, in anticipation of the resistivity results (section 5.2.2), the exact holmium concen-

trations being 0.05, 0.1, 0.2, 0.3, 0.4, 0.5, 0.55, 0.6 and 0.8 at%. Approximately ten samples of each composition were sintered together in the tube furnace, under flowing gas of composition 20%O_2/80%N_2 (air), at 1420°C for 60 minutes, followed by slow cooling (300°C/hour) to 800° and thereafter at the natural cooling rate of the furnace, to room temperature.

Scanning electron microscopy and energy dispersive x-ray analysis enabled the microstructure and any surface features to be examined. Average grain sizes were determined as usual, with the area count method of between 200 and 300 grains to obtain sufficient statistical accuracy. Simple density measurements were performed to ensure full densification of samples of each composition.

Samples were polished slightly to give flat surfaces for the electrical measurements. Resistivity - temperature characteristics were obtained between 50 and ~450°C for five samples of each composition to ensure reproducibility and to enable average resistivites to be calculated.

Thin samples (~0.7mm thick) were prepared, by further polishing the above samples, and used for dielectric, a.c. impedance and current-voltage measurements. The capacitance was obtained between room temperature and ~300°C at a constant frequency of 30kHz and a.c. impedance measurements were made at room temperature in the audio and radio frequency ranges.

5.2. EXPERIMENTAL RESULTS

5.2.1. Microstructure and morphology

The samples were qualitatively similar in appearance to those of the previous chapter: the colour and grain morphology changed as donor concentration was increased from 0.05 to 0.8 at%Ho. Samples doped with the lowest amounts of Ho ions (<0.2 at%) were blue-grey in colour and had shiny surfaces. In particular, the corners where the flat surfaces met the edges of samples doped with 0.05 at%Ho were translucent in appearance. Those doped with >0.3 at%Ho were dark blue

and matt, the blue colour gradually being replaced by blue-grey as doping was increased above 0.55 at%Ho.

The trend observed in the microstructure of these samples was also found to be qualitatively the same as that of the previous chapter. Samples containing the lowest amounts of donor dopant (<0.1at%Ho) had large, flat grains which fitted very closely together. Surface features, rich in Ti and Si, the second phase additives, were observed between and across grains of these samples. Twinning and growth terracing were also seen clearly in the larger grains of these samples, as shown in figure 5.1, a scanning electron micrograph of a large grain belonging to the sample doped with 0.05 at%Ho. The average size of the grains of this sample was 32μm, although the grain shown in figure 5.1 is ~50μm across. As donor concentration was increased, the average size of the grains was reduced in a similar manner to the previous samples (chapter 4), from ~20μm in samples containing 0.1 at%Ho concentration, to approximately 10μm where there was 0.4 at%Ho and finally to 2μm with 0.8 at%Ho doping. Typical grains of a sample doped with 0.6 at%Ho are shown in the scanning electron micrograph of figure 5.2, where they can be seen to be very small, less than the scale marker of 4μm in size. Plotting average grain size versus donor concentration in figure 5.3 demonstrates the large reduction in grain size with increasing donor concentration from 0.05 to 0.4 at%Ho and the less dramatic reduction between 0.4 and 0.8 at%Ho.

The shape of the grains was also changed with increasing donor concentration. With the lowest doping levels (0.05 - 0.2 at%Ho) the grains were flat and elongated in shape and fitted very closely together with little intergranular space. Samples containing intermediate quantities of dopant (0.3 - 0.5 at%Ho) had irregularly sized and shaped grains, with large, slab-like grains in excess of 20μm in size among rounded grains which were much smaller, giving an average grain size of ~10μm. Figure 5.4 is a scanning electron micrograph of a sample doped with 0.4 at%Ho, where such grains can be seen. As donor concentration was increased

further, towards 0.8 at%Ho, the grains all became rounded in shape and had a small distribution of sizes. These latter samples had many intergranular spaces which could accommodate the second phase, unlike the lightly doped ones which expelled this material to the surface. Consequently these samples were matt in appearance, in contrast to those doped with <0.2 at%Ho.

5.2.2. Resistance - temperature characteristics

The reduction in average grain size with increasing donor concentration meant that it was necessary to normalize the resistance data to eliminate the effect of grain size. This was carried out as described previously (chapter 4.2.2), using equation 4.3 to obtain values of specific resistance of a unit area of grain boundary, ρ_L. Five nominally identical samples of each composition were measured, from which the average variation between samples of each batch was found to be ~6%.

A typical series of plots of normalised resistance versus temperature is shown in figure 5.5, for samples containing 0.05, 0.4 and 0.55 at%Ho concentration, where it can be seen that donor concentration affects normalised resistance at room temperature and the maximum, as well as the temperature of the maximum (indicated by arrows). Samples containing the lowest donor concentrations (0.05, 0.1 at%Ho) had high normalised resistance at room temperature, $\rho_{L(RT)}$: the sample doped with 0.05 at%Ho had $\rho_{L(RT)}$ of the order of $1\Omega cm^2$ and where there was 0.1 at%Ho concentration, $\rho_{L(RT)}$ was $\sim 10^{-1}\Omega cm^2$. Normalised resistance was lowest in samples containing 0.3 and 0.4 at%Ho, of the order of $10^{-3}\Omega cm^2$, and increased sharply above these doping levels, towards $10^3\Omega cm^2$ with 0.8 at%Ho. The maximum normalised resistance, $\rho_{L(max)}$, was affected in a similar way, reducing in value from $\sim 10^2\Omega cm^2$ with the samples containing 0.05 at%Ho towards $1\Omega cm^2$ when doping was increased to 0.4 at%Ho. Increasing donor concentration further resulted in an increase in $\rho_{L(max)}$, close to $10\Omega cm^2$ with 0.6 at%Ho. Figure 5.6 shows the behaviour of $\rho_{L(RT)}$ and $\rho_{L(max)}$ with donor concentration, where each

can be seen to describe a narrow minimum around 0.3 - 0.4 at%Ho doping, in qualitative agreement with the results of the previous chapter. The temperature, T_{max}, at which $\rho_{L(max)}$ takes place, was found to describe a narrow maximum in value between 0.3 and 0.4 at%Ho concentration, as shown in figure 5.7. It increased initially from ~235°C with 0.05 at%Ho doping, to 260°C in samples containing 0.3 at%Ho and then fell more quickly towards 204°C after doping with 0.6 at%Ho.

Samples containing 0.8 at%Ho, on the other hand, exhibited a completely different temperature characteristic. They did not show any PTCR effect at all, having instead a negative temperature coefficient of resistance at all temperatures, with a plateau between approximately 110 and 150°C. ρ_L was of the order of $10^3\Omega cm^2$ at room temperature and fell towards $10^2\Omega cm^2$ at T_c. It then continued to fall above 150°C, towards $10\Omega cm^2$ at temperatures close to that of T_{max} for the samples containing 0.6 at%Ho (~200°C). The normalised resistance - temperature plot of this sample is shown in figure 5.8.

5.2.3. Capacitance Measurements

Apparent permittivity, ϵ'_{app}, was calculated from the capacitance measurements of samples of each composition, between room temperature and ~320°C (see chapter 3.3). Figure 5.9 shows a typical series of plots of ϵ'_{app} versus temperature for samples containing 0.1, 0.4, 0.5 and 0.6 at%Ho. It can clearly be seen, with reference to the permittivity of pure barium titanate in figure 4.8, that the addition of the donor dopant causes the permittivity of the ceramic to be increased by at least one order of magnitude. Apparent permittivity of the least doped samples (containing 0.05 at%Ho) was $\sim 2 \times 10^4$ at room temperature and increased sharply to 4×10^5 with 0.4 at%Ho. Increasing the donor concentration further resulted in a reduction in the value of ϵ'_{app} at room temperature, towards 8×10^4 in samples containing 0.6 at%Ho. The effect of donor concentration

on ϵ'_{app} at room temperature is shown in figure 5.10, where it describes a sharp maximum around 0.4 at%Ho concentration. Samples doped with 0.05, 0.1 and 0.6 at%Ho had ϵ'_{app} similar in characteristic to that of pure barium titanate, i.e. it was approximately constant below T_c and increased sharply at the transition, above which it fell in accordance with Curie-Weiss behaviour. Those containing between 0.2 and 0.5 at%Ho, on the other hand, had high values of ϵ'_{app} below T_c which then fell as temperature was increased through the transition. Above T_c, ϵ'_{app} followed Curie-Weiss behaviour in a similar manner to the other samples.

5.2.4. A.C. impedance plots

Specimens doped with 0.05, 0.1 and 0.6 at%Ho were chosen for these measurements since their normalized resistances lay on either side of the $\rho_{L(RT)}$ - donor concentration minimum (figure 5.6). Complex impedance plots of X_s (imaginary impedance) versus R_s (real impedance) were drawn for each sample, from which grain bulk resistance was separated from the grain boundary resistance, as described in the previous two chapters (sections 4.2.4. and 3.5.2.). The grain bulk resistance, R_{bulk} and grain boundary resistance, R_{gb}, were thus obtained from the high frequency intercept and the difference between this and the d.c. intercept of the curve on the R_s axis, respectively. Figures 5.11, 5.12 and 5.13 show X_s versus R_s for doping levels of 0.05, 0.1 and 0.6 at%, respectively, where it can be seen that, although sample resistance varies enormously, R_{bulk} remains the same, at $\sim 2\Omega$. In contrast, R_{gb} is affected, decreasing from 350Ω to 70Ω upon increasing the donor concentration from 0.05 to 0.1 at%Ho, and then increasing sharply to $\sim 9k\Omega$ in the sample containing 0.6 at%Ho.

5.3. DISCUSSION OF EXPERIMENTAL RESULTS

5.3.1. Microstructure

The reduction in grain size and the change of colour of the samples as donor

concentration was increased are in agreement with the observations of previous workers[5.5–5.7] and with the results of the previous chapter (chapter 4.2.1.). The presence of the second phase features on samples containing the lowest amounts of donor dopant (<0.2 at%Ho) and their absence on the remainder of the specimens also agrees with the findings of the previous chapter and is indicative of the amount of intergranular space available in the different samples.

With reference to figures 4.3 and 5.3, it can be seen that the grains of the present samples are smaller in size than those belonging to the previous chapter. This observation lends weight to the argument (chapter 3.2.) that the average grain size of donor doped barium titanate ceramics is dependent most on the sintering temperature[5.7–5.11] According to Kingery[5.8], this is due to the presence of an activation energy for the grain growth process, whereas Zajc and Drofenik[5.7] explain it in terms of the relationship between nucleation and growth rates of the grains. They have proposed that a fine grained microstructure is produced by controlling a high nucleation rate and a low growth rate (vice-versa for a large grained structure), suggesting that, as donor concentration is increased, so is the nucleation rate of new grains, but the growth rate of these grains is lowered.

5.3.2. A.C. impedance measurements

It is apparent from the ac impedance plots of X_s versus R_s that the effect of donor concentration on normalized resistance is entirely due to the grain boundary resistance, in agreement with the results presented earlier (chapter 4.2.4.) and contrary to the predictions of proposals in the literature[5.3,5.4,5.12–5.14], which suggest the presence of compensating acceptors within the grain bulk. Grain bulk resistivity, ρ_{bulk}, was calculated from the values of R_{bulk}, assuming the volume of the grain boundaries to be negligible in comparison with that of the grain bulk, from which N_d, the charge carrier concentration, was obtained (equation 4.26),

$$N_d = \frac{1}{e \times \mu \times \rho_{bulk}}$$

where e is the electronic charge and μ is the mobility of the electrons within the bulk. Average grain bulk resisitivity was found to be 4Ωcm and N_d determined to be $3.1 \times 10^{18}cm^{-3}$. This value, which is similar to that found previously ($1.5 \times 10^{18}cm^{-3}$), is also significantly lower than the nominal charge carrier concentration (the holmium ion concentration). The small change in the value of N_d after sintering at the lower temperature may be attributed to less autocompensation of the donor ions within the bulk. Ihrig and Puschert[5.15] proposed that autocompensation took place by the presence of cation (barium) vacancies within the grain bulk, whereas Xue et al[5.6] suggested that the Ho^{3+} ion, being intermediate in size between Ba^{2+} and Ti^{4+}, can reside at either site, although for size and coordination reasons mostly occupies Ba^{2+} sites. Although creating more barium vacancies at the grain boundaries[5.3,5.4], sintering at lower temperatures reduced barium vacancy diffusivity since there is less thermal energy available. Consequently there are fewer cation vacancies within the grain bulk, implying from the work of Ihrig & Puschert[5.15], that N_d will be correspondingly higher. The sintering temperature may not be expected to affect the solubility of holmium in barium titanate, particularly when this reaction is known to take place at temperatures as low as 1240°C[5.7], but the reduced thermal energy of the system at lower sintering temperatures may cause fewer Ho^{3+} ions to find places in the less stable Ti^{4+} sites.

5.3.3. Resistive behaviour

The present results are in agreement, both with the results of the previous chapter and the observations of other workers[5.1,5.13,5.16,5.17] and demonstrate the effect of donor concentration on the grain boundary layer characteristics. It was shown in the previous chapter (sections 4.3, 4.4) that the initial reduction in room temperature and maximum normalized resistance with increasing donor concentration is due, not to an increase in the value of N_d, as originally thought, but to

a reduction in the value of N_{ao}, the total ionized grain boundary acceptor state density. This reduction causes ϕ_o and hence resistivity to be lowered. Above ~0.4 at%Ho doping N_{ao} is increased which, in turn, raises ϕ_o and the normalised resistance. It is likely, therefore, that this is also the case for the present samples.

The behaviour of T_{max} (figure 5.7), describing a maximum with donor concentration, substantiates this hypothesis since, when ϕ_o is reduced, the temperature at which depopulation of the grain boundary acceptor states can take place (equation 2.6) is increased and hence T_{max} is high. On the other hand, high ϕ_o is reflected by low T_{max} as a result of the lower temperatures at which depopulation of the grain boundary acceptor states takes place.

The a.c. impedance plots, in particular for the sample doped with 0.6 at%Ho (figure 5.13), emphasise the insufficiency of the explanation of Daniels and co-workers[5.3,5.4] for the increase in normalized resistance at the higher doping levels. This sample had grains of an average size of 2μm, smaller than Daniels' proposed grain boundary barium vacancy - rich depletion zone, yet showed the presence of separate grain boundary and grain bulk resistances common to all samples. According to the Daniels model, the entire sample would have been insulating and the a.c. impedance plot would have given a high frequency intercept on the R_s axis at the origin.

The behaviour of the sample containing 0.8 at%Ho (figure 5.8), although continuing the trend in $\rho_{L(RT)}$ (figure 5.6), is highly unexpected. Explanations in the literature which may apply to this result mostly regard the formation of insulating intergranular layers[5.18–5.20] which have been put forward as reasons for the increase in normalized resistance above 0.4 at%Ho doping. Such insulating layers, however, are unlikely to be present because of the non-ohmic behaviour of highly doped samples (figure 4.14)[5.17]. In addition, an intergranular (third) layer would be expected to be represented in the ac impedance plots as a third peak (chapter 3.3). No such peak is present (figure 5.13). It is more likely that a large number

of acceptor states is present at the grain boundaries so that, even with the compensating effects of the spontaneous polarization, the residual potential barrier below T_c is very high. Such a high potential barrier may be expected to result in steep NTCR (negative temperature coefficent of resistance) behaviour below the transition, as observed in figure 5.8. As temperature is raised through T_c the PTCR effect may be considered to take place but is superimposed onto the steep NTCR effect, giving the plateau effect observed. This anomalous behaviour may be seen to a lesser extent in the samples containing 0.55 and 0.6 at%Ho, which also have steep NTCRs below T_c (figure 5.6). The PTCR effect, superimposed onto the NTCR characteristic, however, is sufficiently high in comparison with the normalised room temperature resistance to be seen over about an order of magnitude. A shift in the value of $\rho_{L(RT)}$ towards $10^3\Omega cm^2$ can therefore be seen to mask much of the PTCR effect at T_c and to give a resistance - temperature characteristic as seen for the sample doped with 0.8 at%Ho.

The residual potential barrier below T_c and the maximum value of ϕ_o above T_{max} for samples doped with 0.6 and 0.8 at%Ho were obtained from plots of $\ln\rho_L$ versus 1/T throughout the temperature range. The gradients of these plots (equation 2.9) are equal to ϕ_o/k, where k is the Boltzmann constant, and therefore enable constant values of the grain boundary potential barrier to be estimated. Figure 5.14 shows ρ_L, plotted on a logarithmic scale, versus 1/T between ~40 and 450°C, for both samples. The gradients of each plot below T_c were measured and found to correspond to activation energies of 0.2eV for the sample containing 0.6 at%Ho and 0.5eV for the more heavily doped sample. Above the resistivity maximum, the gradients of both plots were similar, representing activation energies of ~0.4eV. Below the transition, therefore, the sample doped with 0.8 at%Ho has a residual potential barrier higher than the maximum potential barrier of other samples (see tables 4.5 and 5.3) and consequently any PTCR effect taking place is hidden.

5.3.4. Dielectric behaviour

The large increase in apparent permittivity associated with donor doping can be seen, with reference to figure 4.8, to agree with the previous results and with other workers' observations[5.1,5.2,5.5,21]. Having shown in the last chapter (4.3.4.) that the permittivity, ϵ', of the material within the grain boundary layers is unaffected by donor concentration, equation 4.17 was used to show that the gradient of a plot of $1/\epsilon'_{app}$ versus temperature above T_c is given by dN_d/CN_a, where d is the average grain size and C is the Curie constant. Such a plot is also linear at temperatures below that at which depopulation of the acceptor states takes place and hence N_{ao}, the total ionized acceptor state density, can be estimated.

Plots of $1/\epsilon'_{app}$ versus temperature above T_c were drawn for all donor concentrations, a typical series of which are shown in figure 5.15 for samples doped with 0.2, 0.4 and 0.6 at%Ho. Each plot is linear between T_c and a few degrees below T_{max}, as expected, and the gradient is steeper for the samples containing 0.2 and 0.6 at%Ho, which have higher values of normalized resistance (figure 5.6). The gradient of the linear portions of each plot was measured, from which values of N_{ao} were obtained. The values of gradient, d and N_{ao} are listed in table 5.1, where N_{ao} can be seen to reach a minimum value between 0.3 and 0.4 at%Ho.

5.4. ANALYSIS OF EXPERIMENTAL RESULTS

5.4.1. Calculation of acceptor state density

The normalized resistance - temperature characteristics, as shown in the previous chapter, may be utlilized to calculate the total ionized grain boundary acceptor state density, N_{ao}, through a rearrangement of the Heywang equations. Equations 4.23,

$$\rho_L = \rho_o exp(\frac{A(T-\theta)}{T})$$

and 4.24,

$$A = \frac{e^2 N_{ao}^2}{8\epsilon_o C k N_d}$$

were derived and used to draw Arrhenius plots of $\ln\rho_L$ versus (T - θ)/T between T_c and T_{max}. Within the range for which $N_a = N_{ao}$, i.e. below the temperature of depopulation of the acceptor states, these plots were expected to be linear, with the gradient, A, dependent on the values of N_{ao} and N_d.

Arrhenius plots of $\ln\rho_L$ versus (T - θ)/T were thus drawn for the present samples containing between 0.05 and 0.6 at%Ho, since the sample doped with 0.8 at%Ho did not exhibit any PTCR properties at all. Figure 5.16 shows plots of ρ_L, on a logarithmic scale, versus (T - θ)/T for samples with 0.1 and 0.4 at%Ho concentration, where the gradient for the 0.1 at%Ho sample can be seen to be steeper than that belonging to the sample doped with 0.4 at%Ho. The plots for samples containing >0.5 at%Ho were linear over a short range of temperatures because of their relatively small PTCR resistance jumps, particularly in the sample doped with 0.6 at%Ho.

The gradient, A, of the linear portions of the Arrhenius plots was estimated using a least - squares analysis, from which N_{ao} was obtained for each composition using equation 4.27,

$$N_{ao} = \sqrt{\frac{8\epsilon_o C k N_d A}{e^2}}.$$

Table 5.2 contains A and N_{ao} for every donor concentration between 0.05 and 0.6 at%Ho. For clarity, the effect of donor concentration on N_{ao}, calculated using the gradient of the plots of $1/\epsilon'_{app}$ versus T above T_c, is shown in figure 5.17. The curve can be seen to describe a minumum around ~0.5 at%Ho, although estimates of N_{ao} for the samples doped with 0.05 and 0.1 at%Ho are very high in comparison with those from the Arrhenius plots (table 5.2), as was the case in the previous chapter. Comparison of figure 5.17 with the results listed in table 4.4 and figure 4.20 for the previous chapter's samples show good qualitative agreement, with the present samples having slightly higher values than the previous ones. This

suggests that a greater number of acceptor - like barium vacancies are present at the grain boundaries than in the previous samples, since the precursor powders and all other sintering conditions (except temperature) were identical.

5.4.2. Calculation of acceptor energy

Having obtained the values of N_{ao} for each donor concentration it is now possible to analyse more fully the normalized resistance characteristics of samples of each composition at temperatures above the resistance maximum. Arrhenius plots of $\ln\rho_L$ versus 1/T above T_{max} were shown, in the previous chapter, to have a gradient equal to $\phi_{o(max)}$/k, where k is the Boltzmann constant since, above T_{max}, (equation 4.28)

$$\rho_L = \rho_o exp\frac{e\phi_{o(max)}}{kT}.$$

Such plots were drawn for samples of all compositions except those doped with 0.05 and 0.55 at%Ho because the resistivity - temperature measurements for these samples failed to give good straight lines above T_{max} due to the high temperatures required for these measurements and which led to difficulties with melting of the In/Ga contacts. A typical series of plots of ρ_L, drawn on a logarithmic scale, versus 1/T above T_{max} is shown in figure 5.18 for samples containing 0.1, 0.4 and 0.6 at%Ho, where the gradients can be seen to decrease initially with dopant concentration between 0.1 and 0.4 at%Ho and then to increase again as doping was increased above 0.4 at%Ho, in agreement with the minimum observed in the values of $\rho_{L(max)}$ (figure 5.6). Least - squares analysis was employed to calculate the gradient of each line, from which $\phi_{o(max)}$ was obtained. From equation 4.29,

$$N_a(T) = \sqrt{\frac{8\epsilon_o C N_d \phi_{o(max)}}{e^2(T-\theta)}},$$

the acceptor state density at a convenient temperature above T_{max} was found for all samples. This temperature was chosen to be 280°C, just above the maximum value of T_{max} for the present samples and close to the temperature chosen

previously. These values of $N_a(280°)$ were then substituted into equation 4.31,

$$E_a = \phi_{o(max)} + E_F(T) - kTln(\frac{N_{ao}}{N_a(T)} - 1),$$

to obtain $\bar{E_a}$ between 0.1 and 0.6 at%Ho doping. Table 5.3 shows $\phi_{o(max)}$, $N_a(280°)$ and E_a for the donor concentrations used. The acceptor energy can be seen to be approximately the same, at ~0.85 ±0.05eV. This value is in agreement with that found for the previous samples, 0.9eV, showing no significant change to take place in the nature of the grain boundary acceptor traps, despite their slightly larger number, upon sintering at a lower temperature.

These results are clearly in contrast to what may be derived from the work of Daniels and co-workers[5.3,5.4] who determined the energy of the doubly ionsized acceptor - like barium vacancies to be 1.3eV. Although this value may not be entirely relevant, having been calculated for the grain bulk, it seems that the presumed increase in the density of this type of grain boundary acceptor state has not had any effect on the effective acceptor state energy. If the barium vacancies had been the most dominant acceptors, the energy would have been expected to increase towards 1.3eV rather than remaining the same. These results suggest that the more effective grain boundary acceptor states are segregated impurity ions and adsorbed oxygen atoms. The oxygen atoms, in particular, have more opportunity for adsorption in greater numbers since the total grain boundary surface area is larger than in the previous chapter's samples.

5.5. CONCLUSION

Sintering samples containing different donor concentrations at a lower temperature has resulted in the following observations: average grain sizes were smaller in agreement with the predictions of Kingery[5.8], the minima in the values of normalized room temperature and maximum resistance and the maximum in the value of T_{max} are less broad and have been shifted towards lower donor concentrations. Analysis of the experimental results revealed that, although the total ionized acceptor state density for these samples was slightly higher than that for samples sintered at a higher temperature, the acceptor energy was the same for both sets of samples. It also suggests that the adsorption of oxygen atoms is important for the creation of effective grain boundary electron traps. All of the experimental results and analysis was in qualitative agreement with the results of the previous chapter, showing a degree of reproducibility and consistency in the analytical methods.

UNIV DUNELM

REFERENCES

5.1 Heywang W., Sol. Stat. Electron., **3**, 51, 1961.

5.2 Heywang W., J. Am. Ceram. Soc., **47**, 484, 1964.

5.3 Daniels J. and Hardtl K.H., Phil. Res. Rep., **31**, 489, 1976.

5.4 Daniels J., Hardtl K.H. and Wernicke R., Phil. Tech. Rev., **38**, 73, 1978/79.

5.5 Daniels J. and Wernicke R., Phil. Res. Rep., **31**, 544, 1976.

5.6 Xue L.A., Chan Y. and Brook R.J., Mater. Sci. Eng., **B1**, 193, 1988.

5.7 Zajc I. and Drofenik M., Br. Ceram. Trans. J., **88**, 223, 1989.

5.8 Kingery W.D., Bowen H.K. and Uhlmann D.R., *Introduction to Ceramics*, (John Wiley & Sons, New York, 2^{nd} Edition, 1976), 452.

5.9 Yoneda Y., Kato H. and Sasaki H., J. Am. Ceram. Soc., **59**, 531, 1976.

5.10 Basu R.N. and Maiti H.S., Mater. Lett., **5**, 99, 1987.

5.11 Chiou B.S., Koh C.M. and Duh J.C., J. Mater. Sci., **22**, 2893, 1987.

5.12 Jonker G.H., Sol. Stat. Electron., **7**, 895, 1964.

5.13 Murakami T., Nakahara M, Miyashita T. and Ueda S., J. Am. Ceram. Soc., **56**, 294, 1973.

5.14 Wernicke R., Phys. Stat. Sol. (a), **47**, 139, 1978.

5.15 Ihrig H. and Puschert W., J. Appl. Phys., **48**, 3081, 1977.

5.16 Fukami T. and Tsuchiya H., Jpn. J. Appl. Phys., **18**, 735, 1979.

5.17 Al-Allak H.M., Brinkman A.W., Russell G.J., Roberts A.W. and Woods J., J. Phys. D.: Appl. Phys., **21**, 1226, 1988.

5.18 Sauer H.A. and Fisher J.R., J. Am. Ceram. Soc., **43**, 297, 1960.

5.19 Tennery V.J. and Cook R.L., J. Am. Ceram. Soc., **44**, 187, 1961.

5.20 Basu R.N. and Maiti H.S., *Procecdings of the IEEE International Symposium on the Applications of Ferroelectrics, Lehigh University, USA*, Ed. Wood V.A. (IEEE New York, 1986), 685.

5.21 Murugaraj P. and Kutty T.R.N., Mater. Res. Bull., **20**, 1473, 1985.

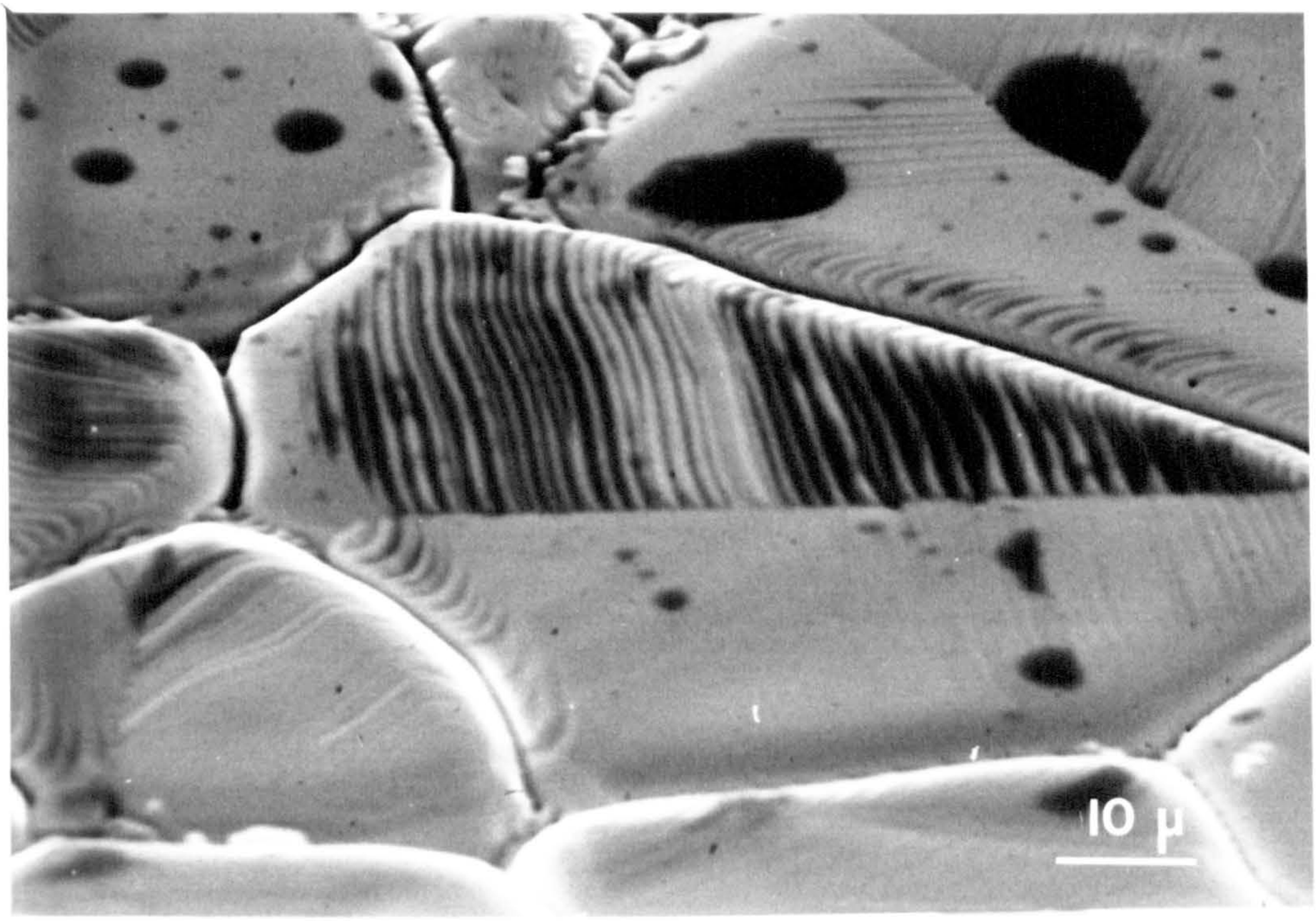

Figure 5.1 Scanning Electron Micrograph of large grains within a sample doped with 0.05 at%Ho (bar = 10μm).

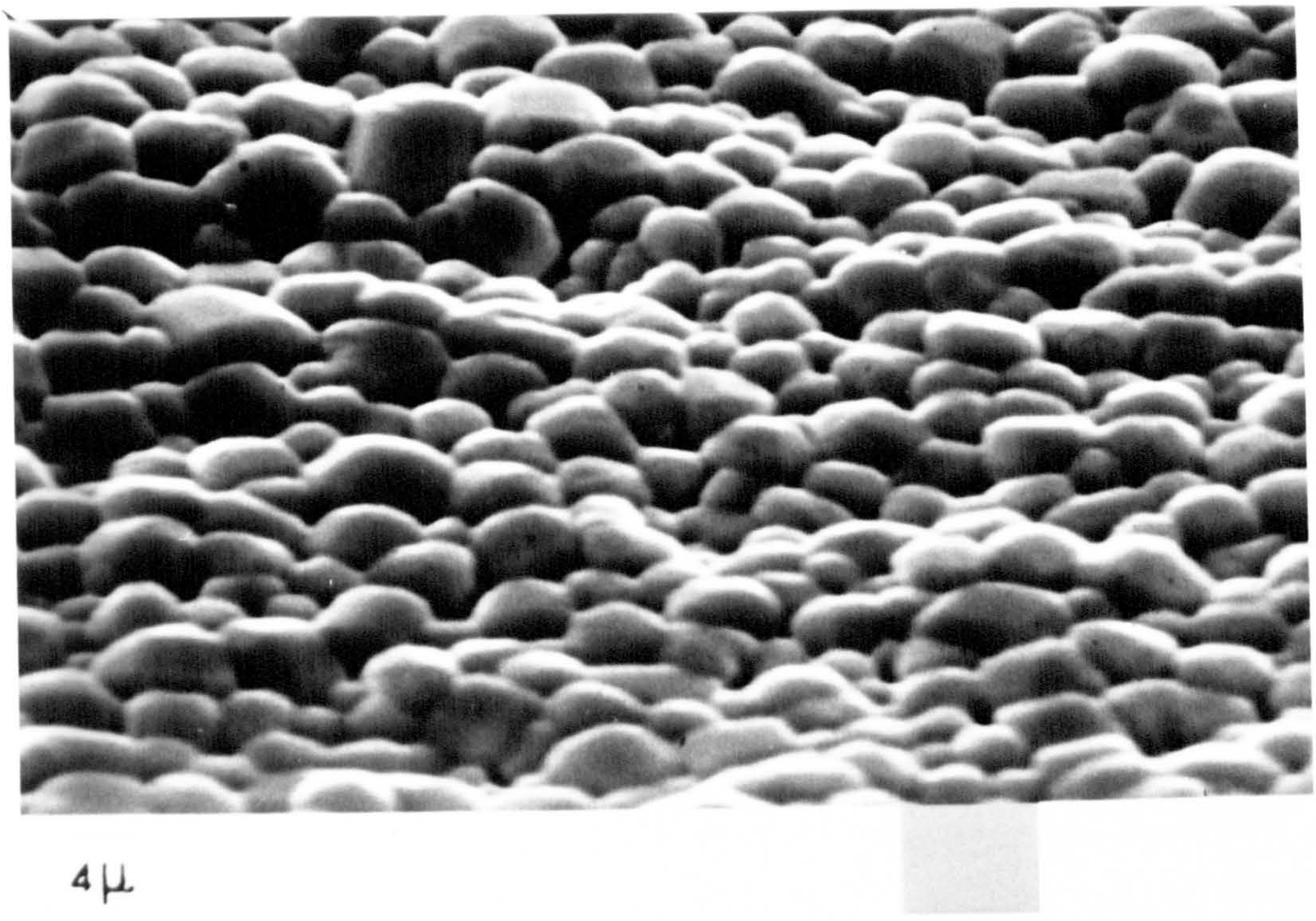

Figure 5.2 Scanning Electron Micrograph of a typical area of a sample containing 0.0 at%Ho concentration (bar = $4\,\mu$m).

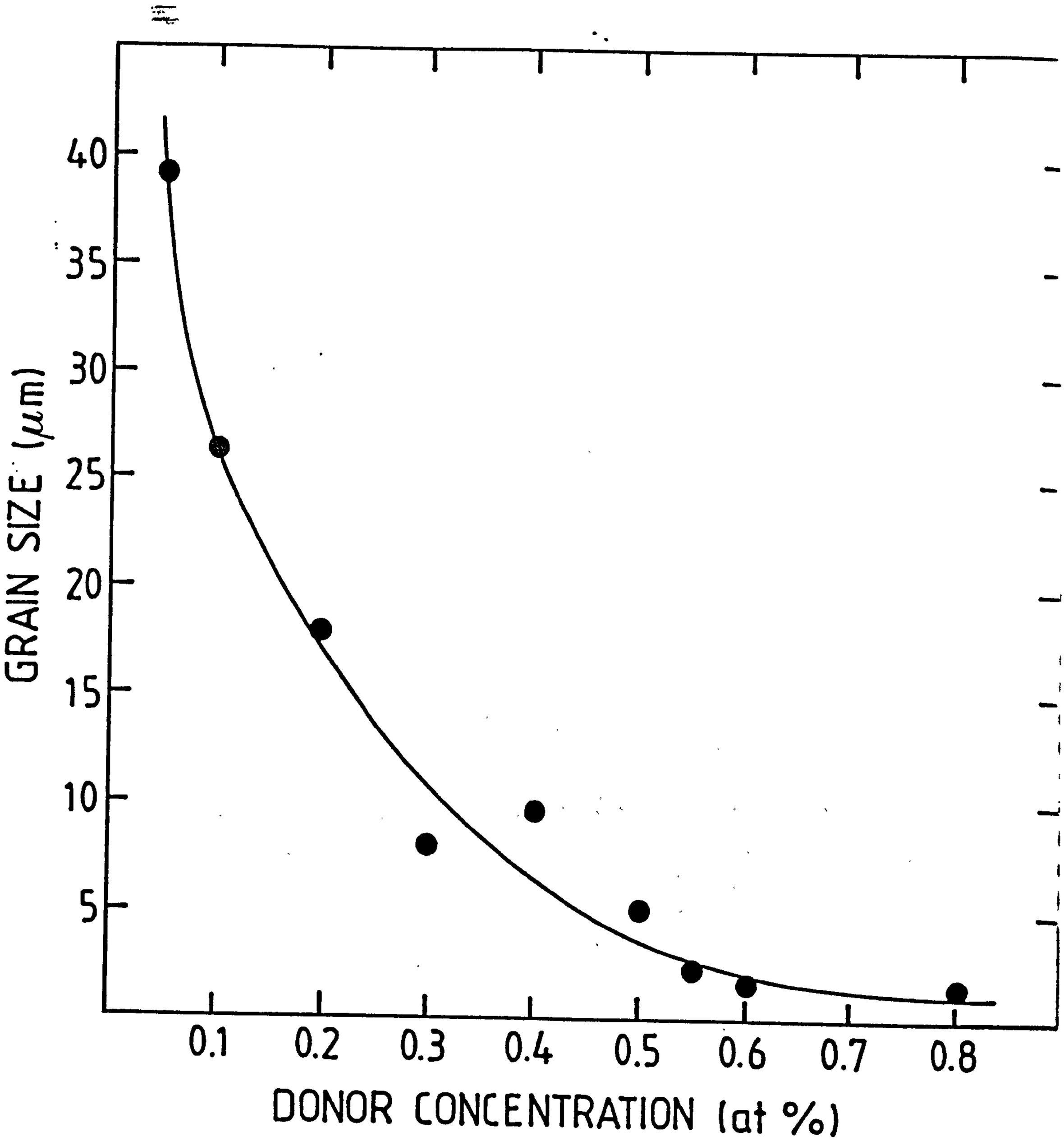

Figure 5.3 Average grain size versus donor concentration.

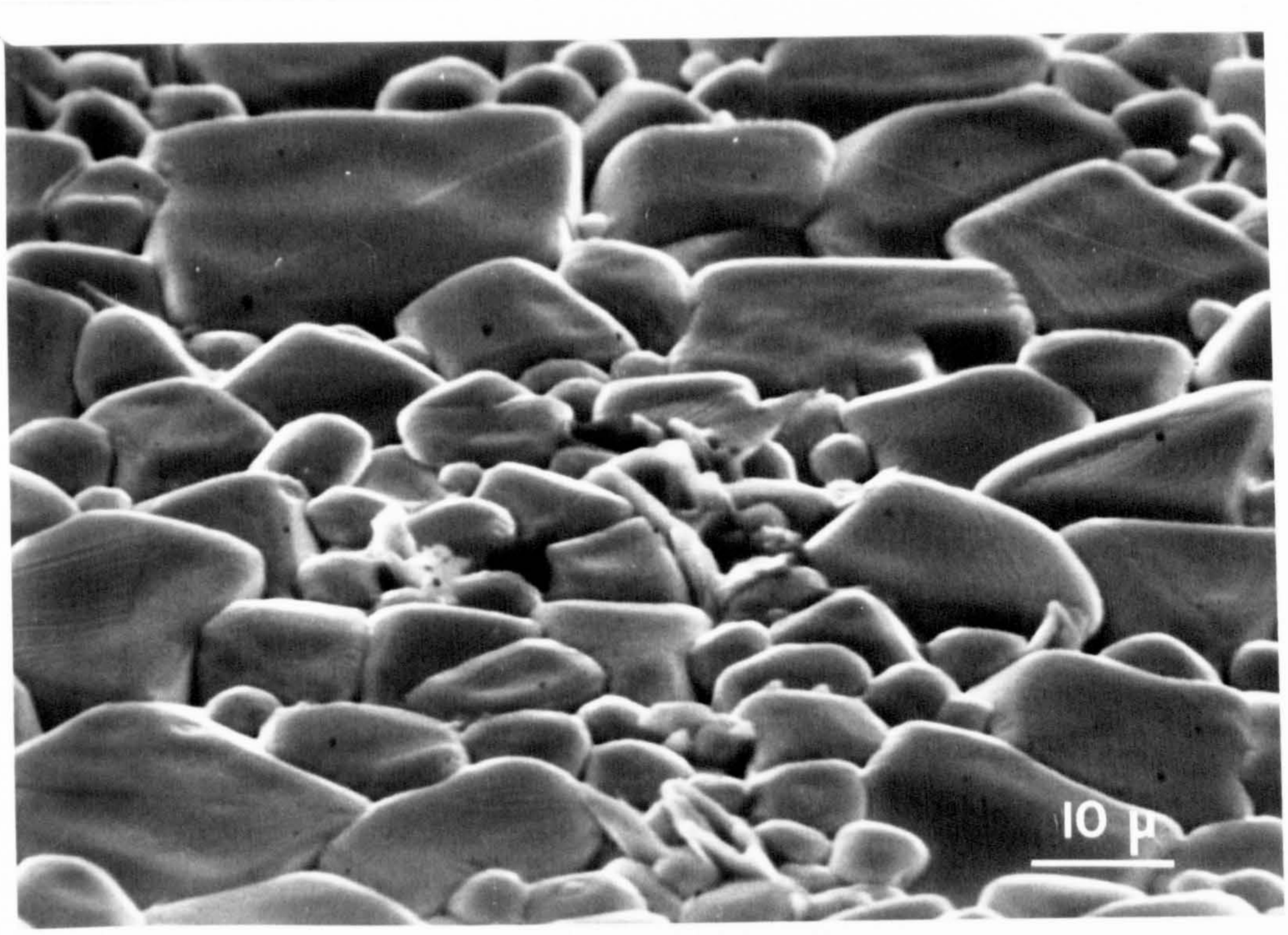

Figure 5.4 Scanning Electron Micrograph of an area of a sample doped with 0.4 at%Ho (bar = 10μm).

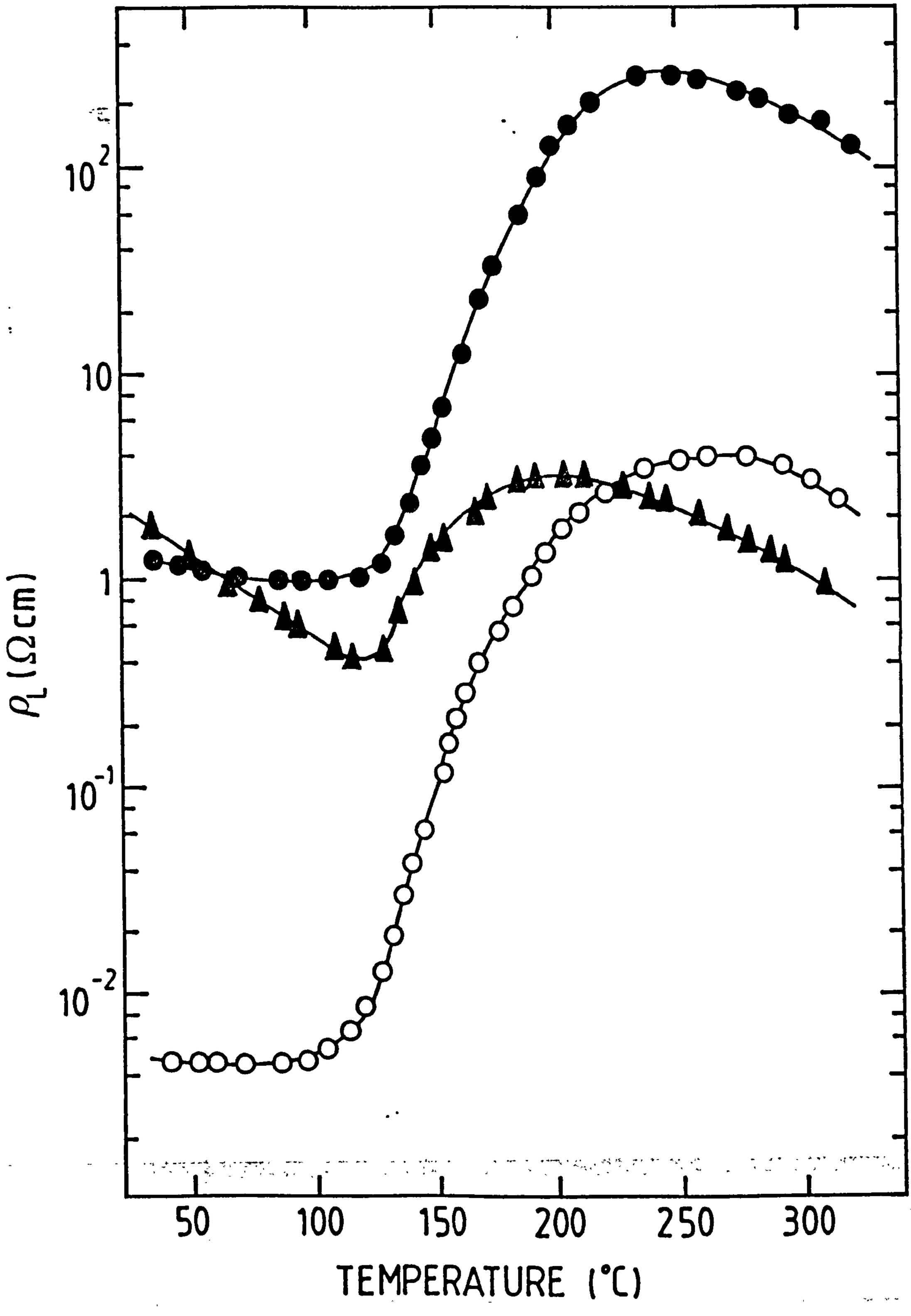

Figure 5.5 Normalised resistance versus temperature characteristics for samples containing 0.05 (•), 0.4 (o) and 0.55 (▲) at%Ho concentration.

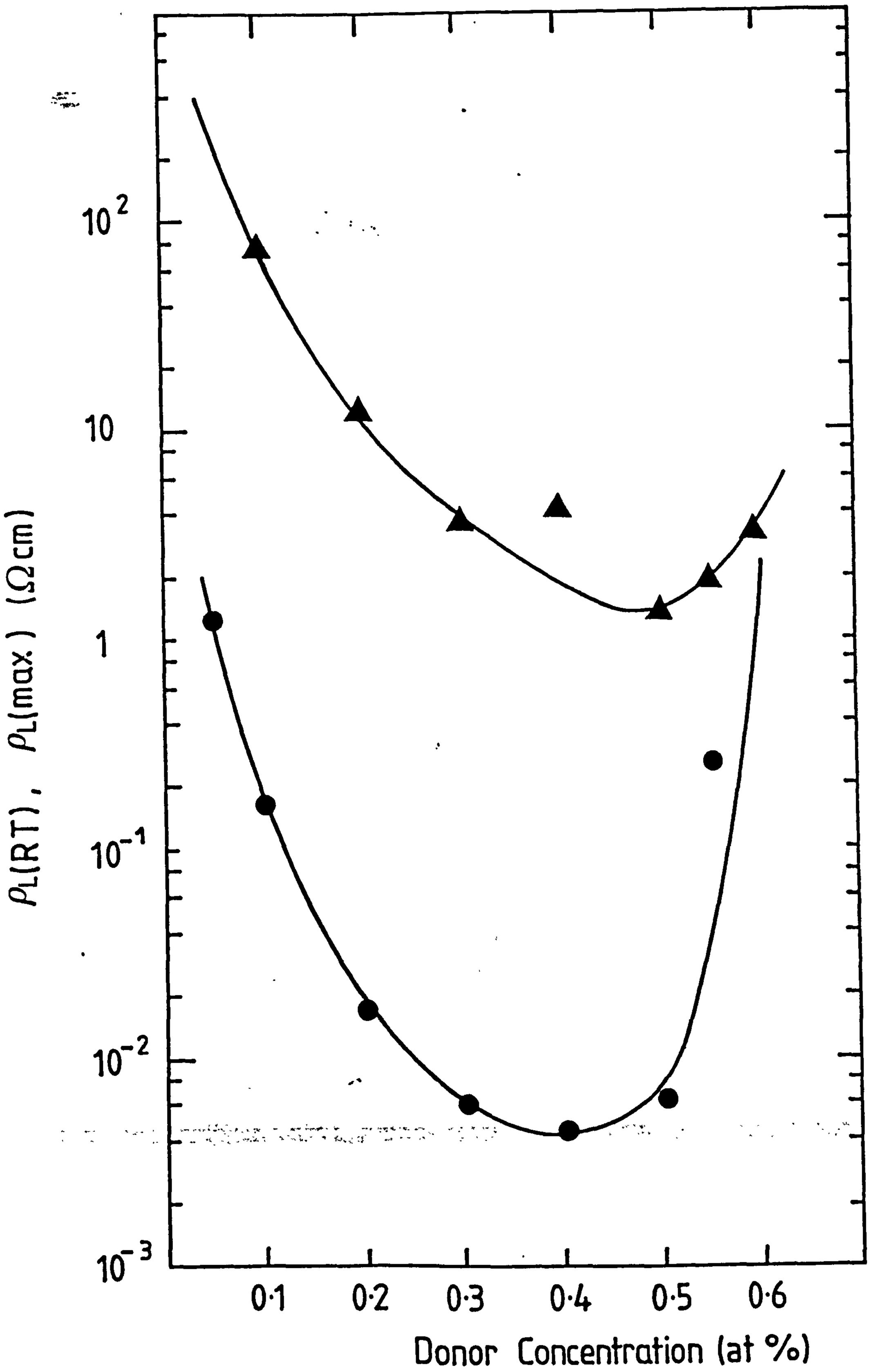

Figure 5.6 Room temperature and maximum normalised resistance ($\rho_{L(RT)}$ and $\rho_{L(max}$ versus donor concentration.

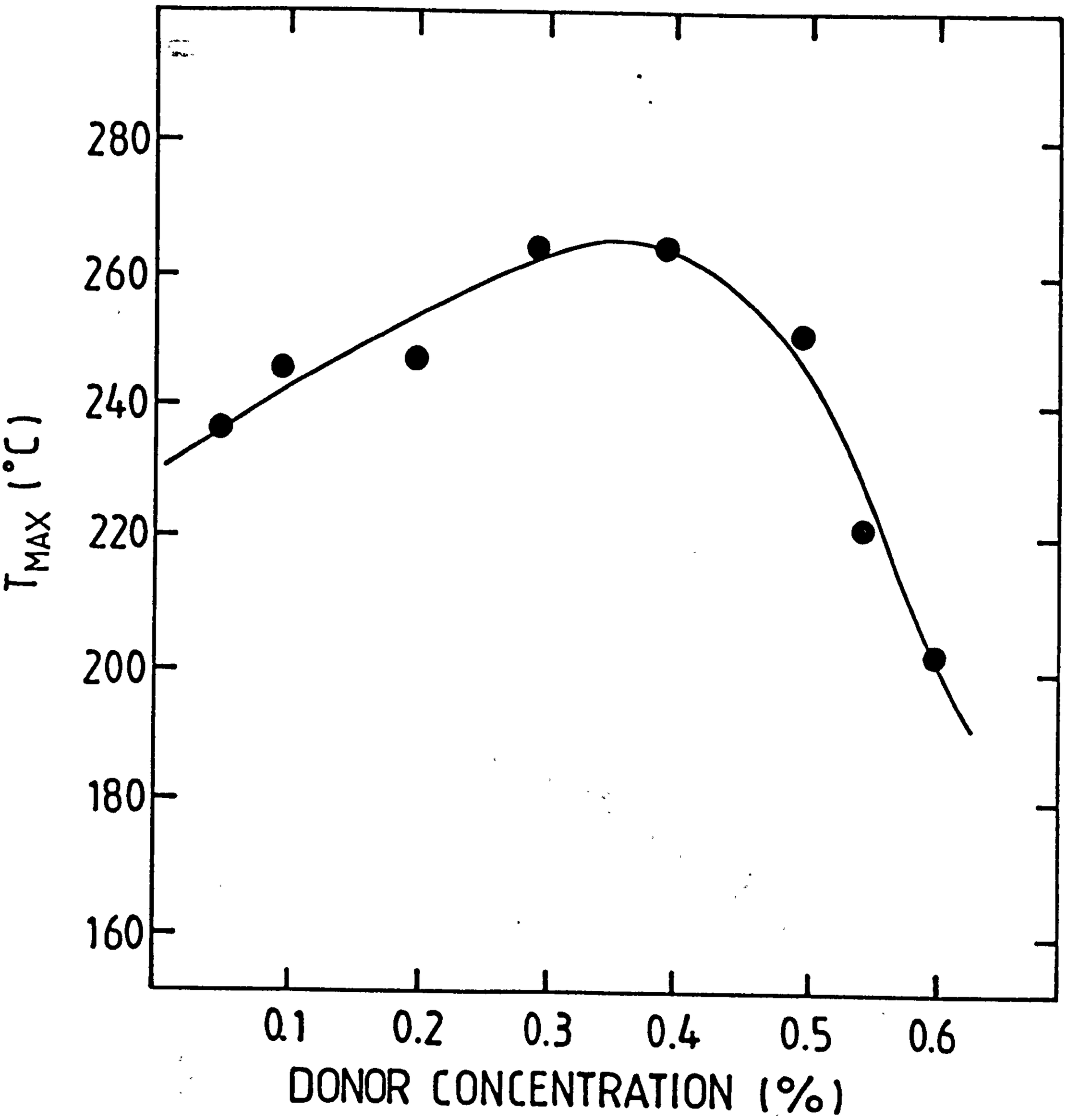

Figure 5.7 T_{max} **versus donor concentration.**

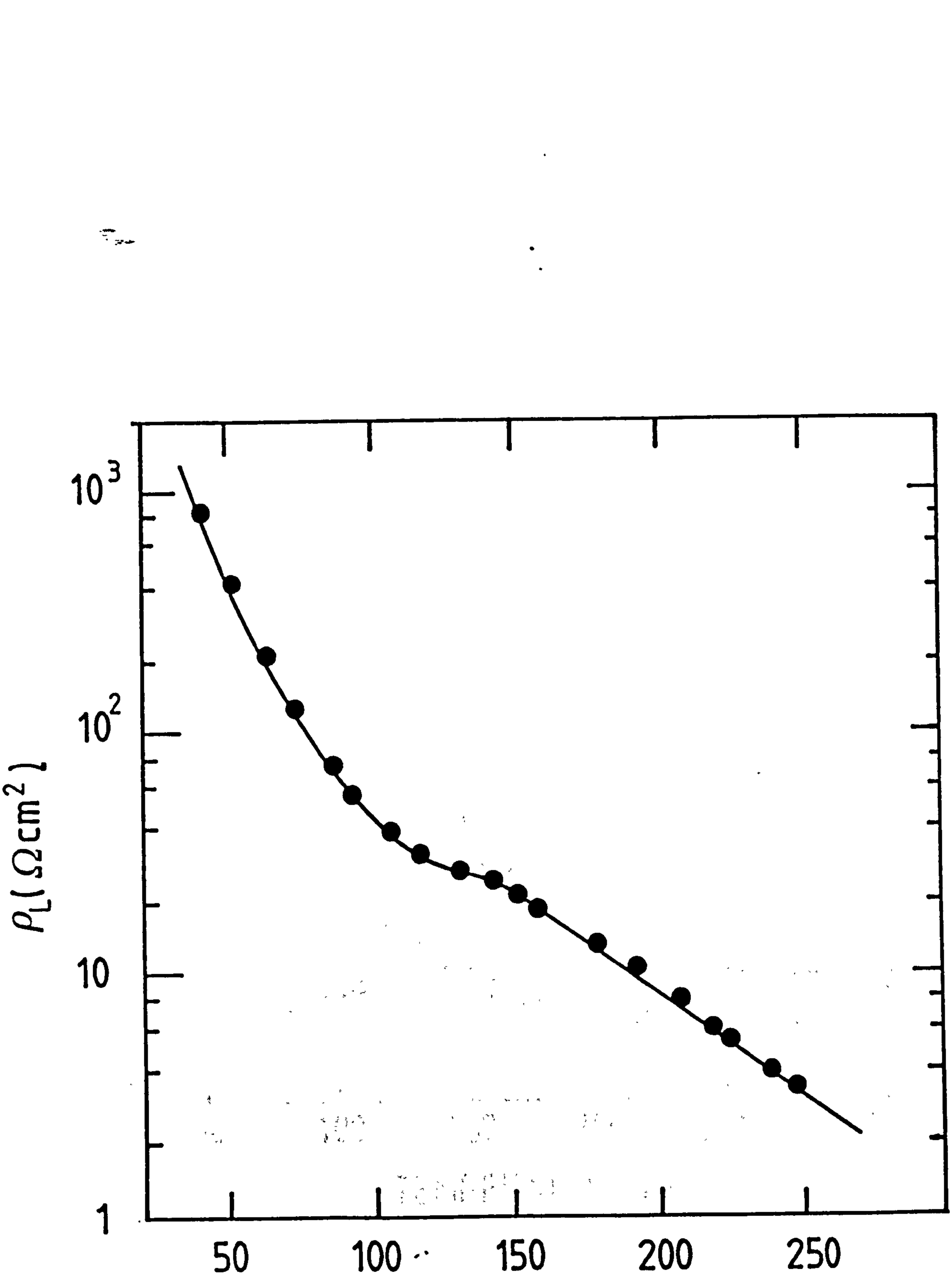

Figure 5.8 Normalised resistance versus temperature for samples doped with 0.8 at%Ho.

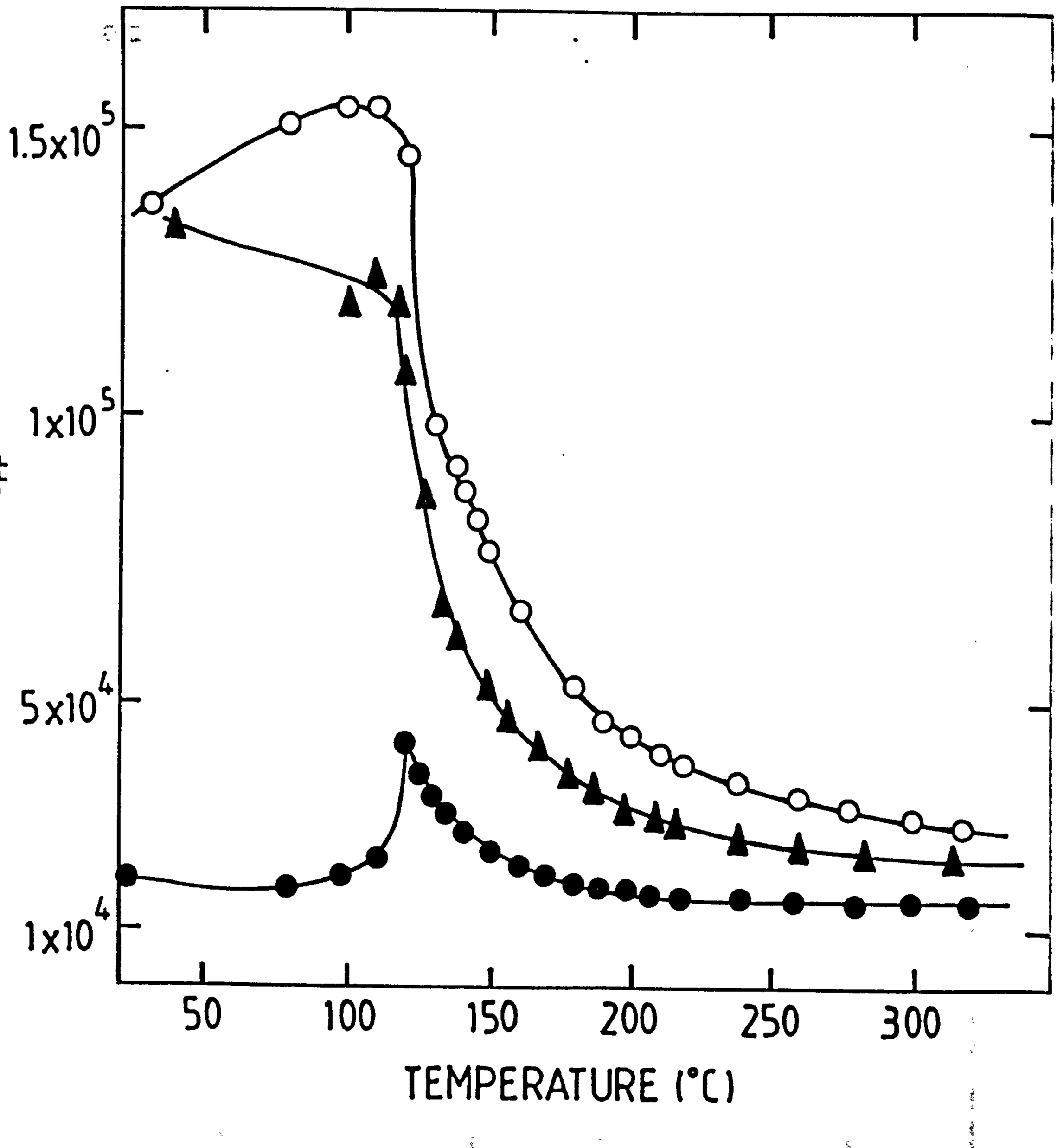

Figure 5.9 Apparent permittivity versus temperature characteristics for samples doped with 0.1 (•), 0.3 (o) and 0.5 (▲) at%Ho.

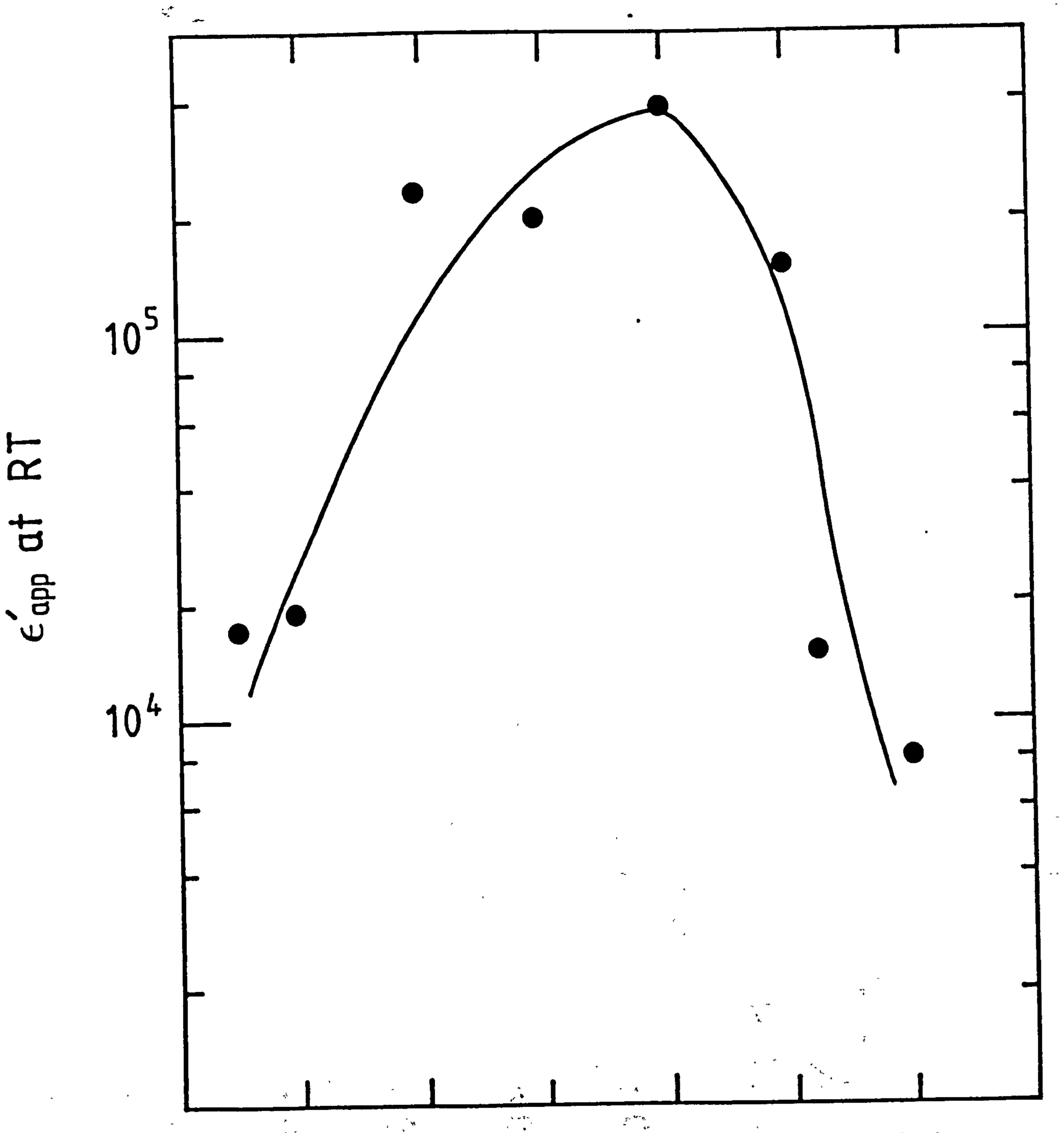

Figure 5.10 Apparent permittivity at room temperature versus donor concentration.

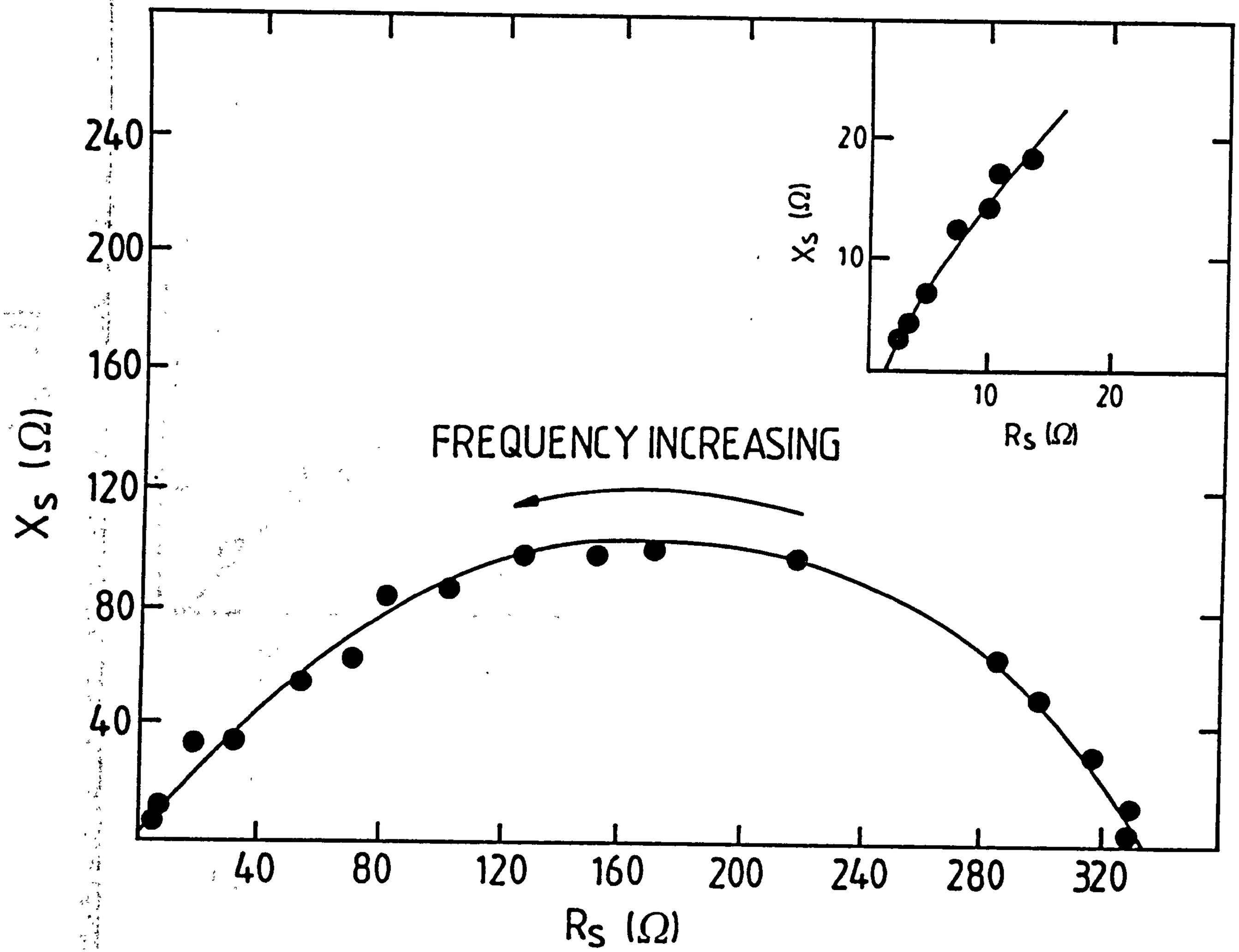

Figure 5.11 A.c. impedance plot for sample containing 0.05 at%Ho concentration.

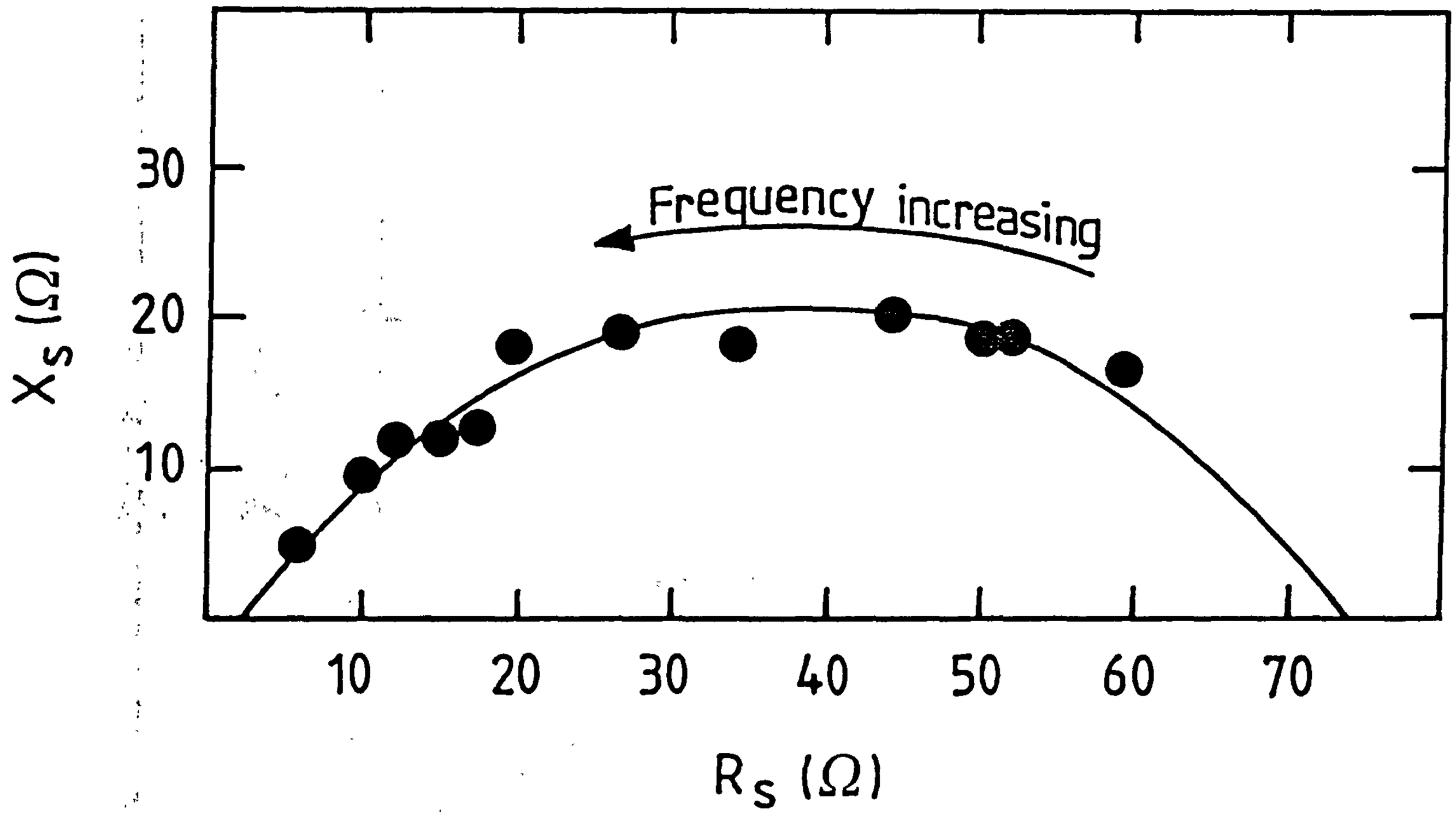

Figure 5.12 A.c. impedance plot for sample doped with 0.1 at%Ho.

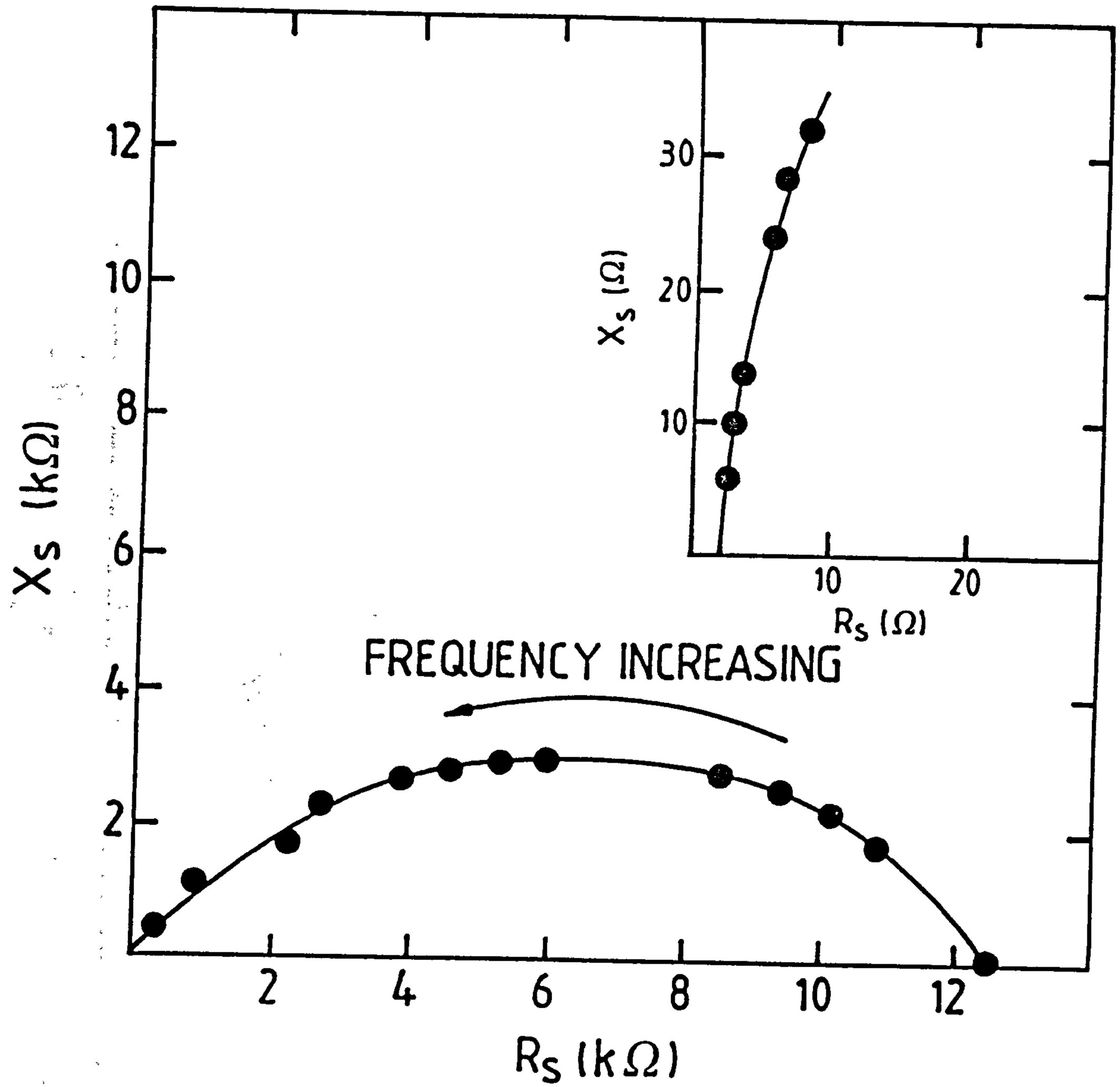

Figure 5.13 A.c. impedance plot for sample with 0.6 at%Ho concentration.

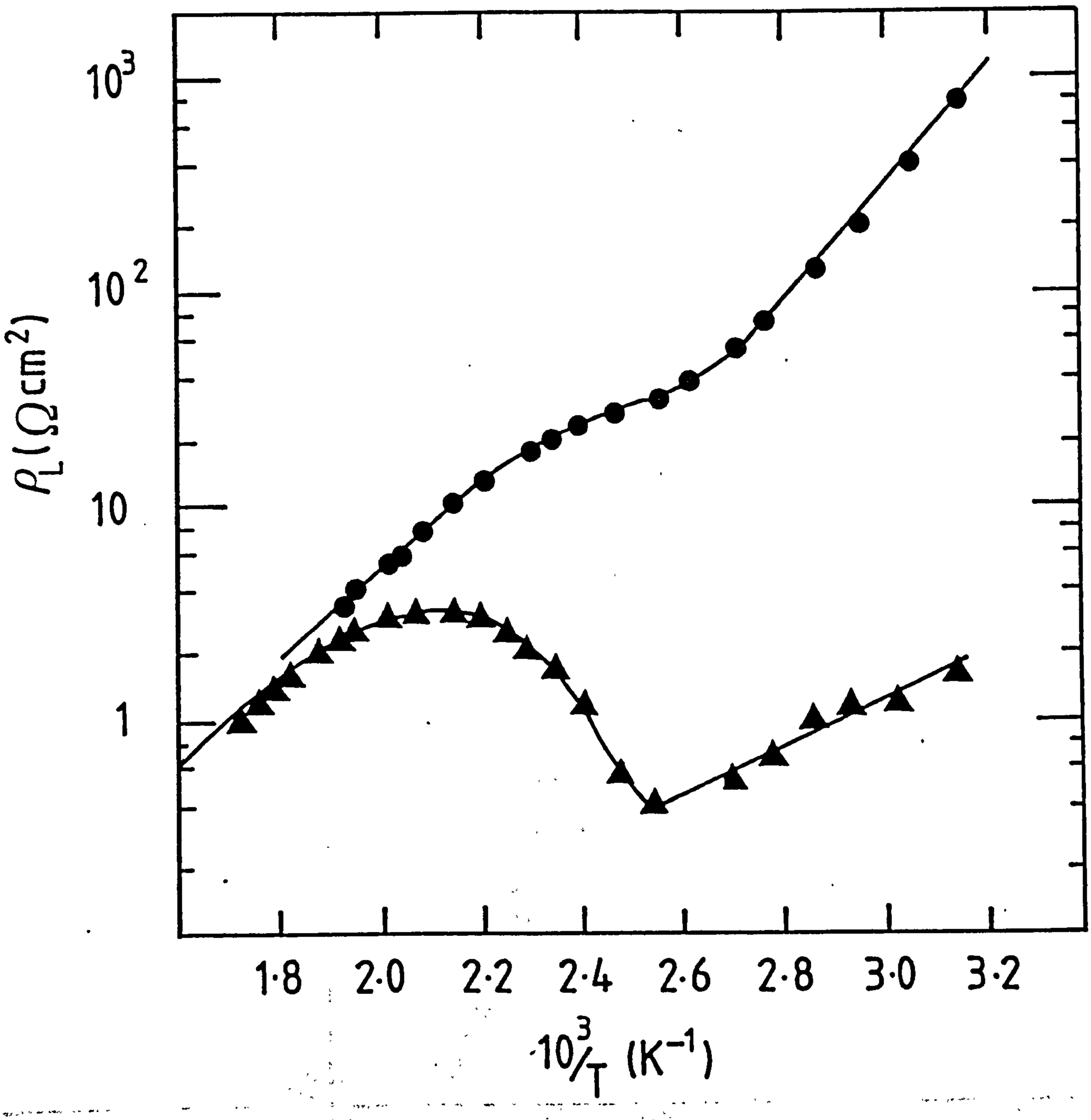

Figure 5.14 Normalised resistance versus 1/T for samples containing 0.6 (•) and 0.8 (△ at%Ho concentration.

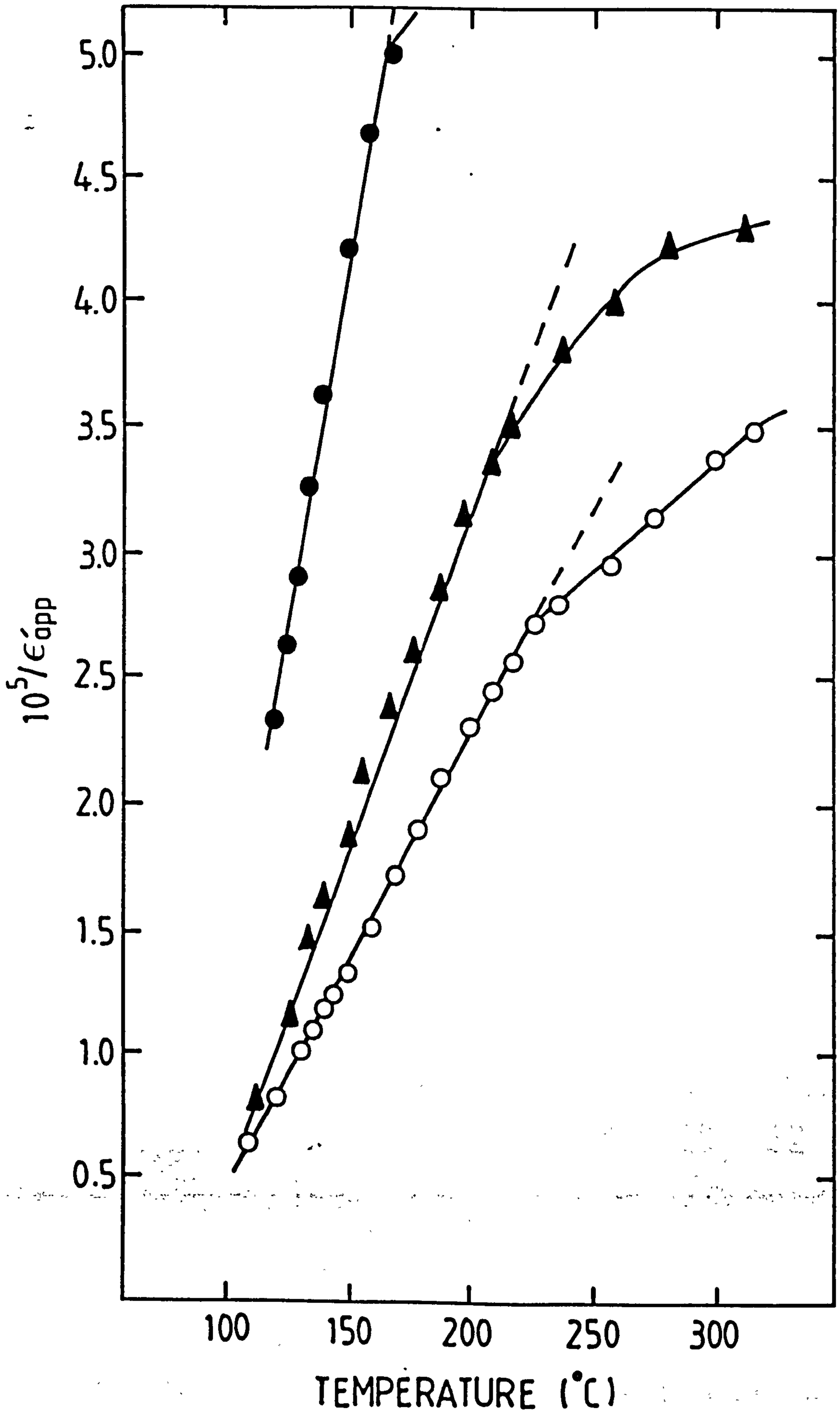

Figure 5.15 $1/\epsilon'_{app}$ versus temperature above T_c for samples doped with 0.1 (•), 0.3 (○ and 0.5 (▲) at%Ho.

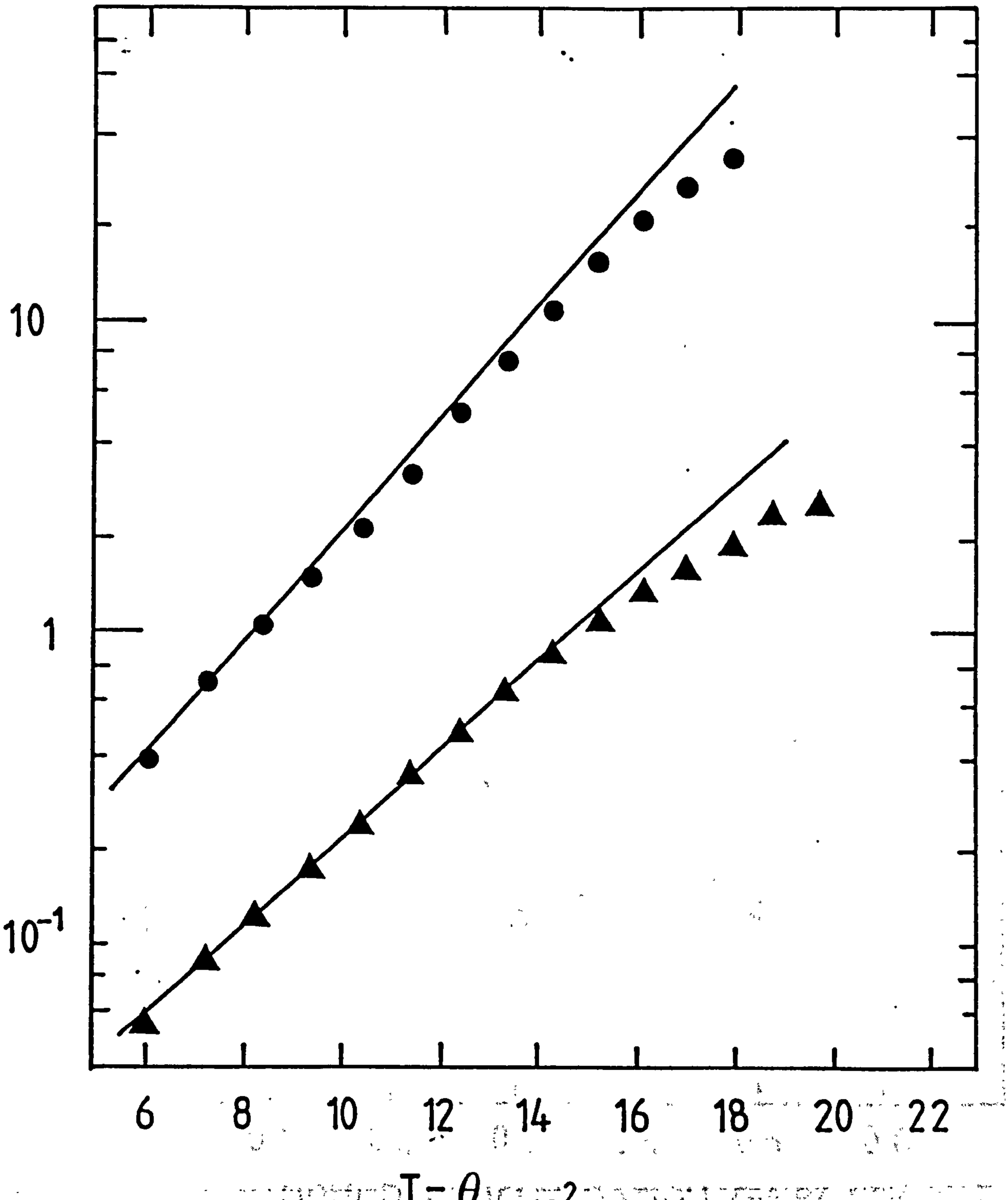

Figure 5.16 Lnρ_L versus (T - θ)/T for 0.1 (•) and 0.4 (▲) at%Ho concentrations.

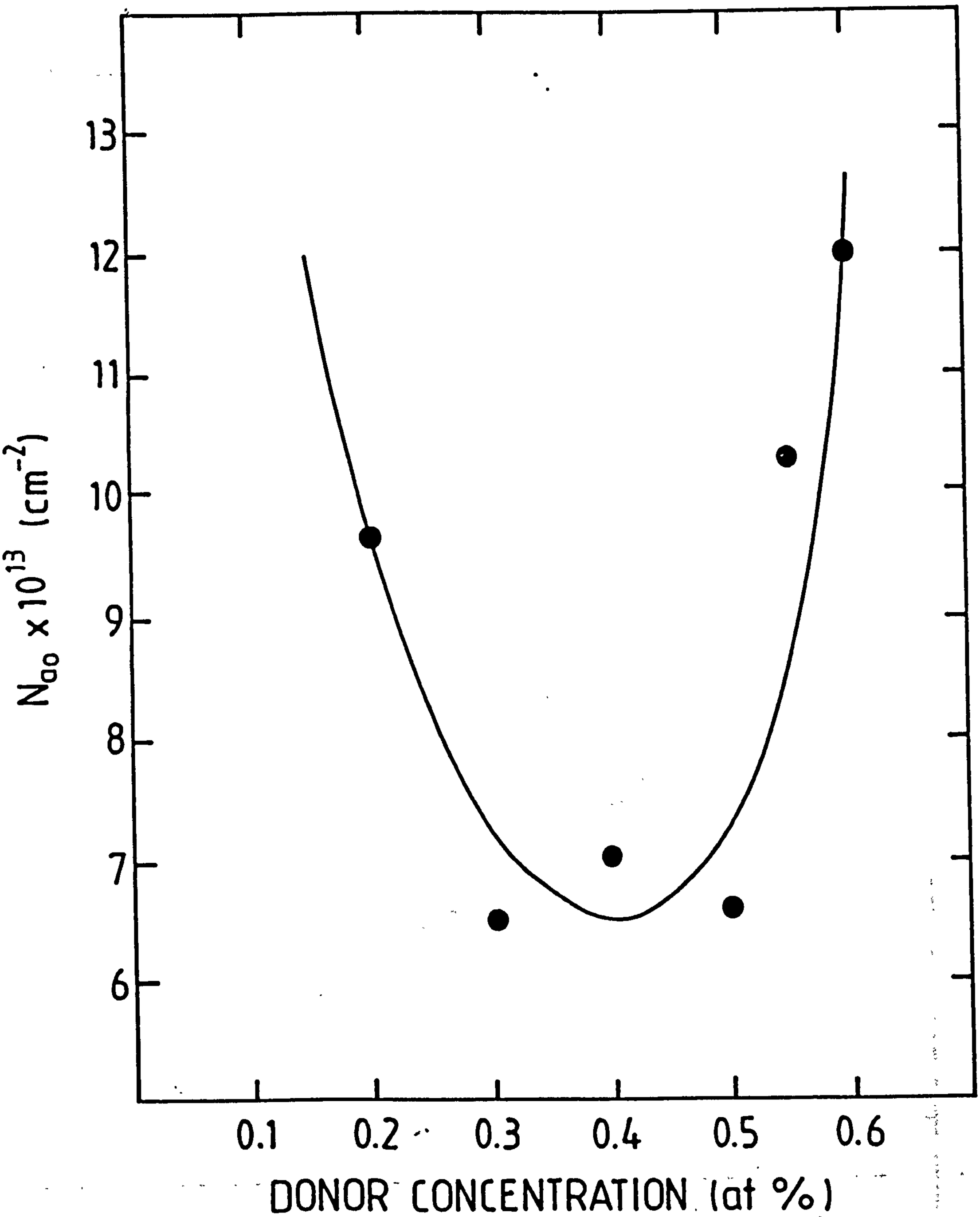

Figure 5.17 Grain boundary acceptor state density, calculated from the gradient of figure 5.15, versus donor concentration.

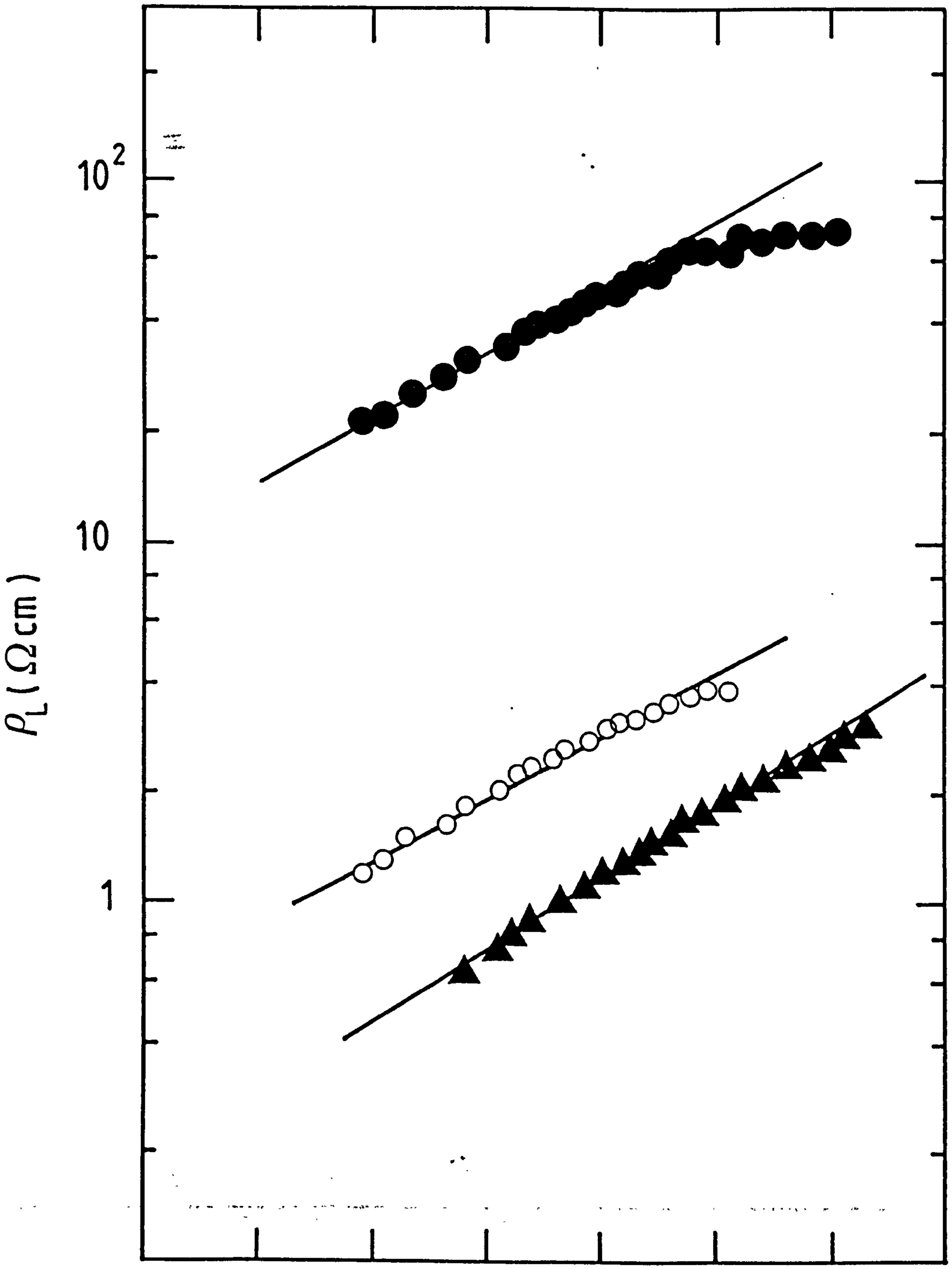

Figure 5.18 Lnρ_L versus 1/T above T_{max} for samples doped with 0.1 (•), 0.4 (o) and 0.6 (▲) at%Ho.

Donor Concentration (at %)	m	d (μm)	N_{ao} (cm^{-2})
0.1	5.62×10^7	26.5	69.0×10^{13}
0.2	1.16×10^7	17.9	9.7×10^{13}
0.3	1.77×10^7	7.9	6.5×10^{13}
0.4	1.67×10^7	9.0	7.0×10^{13}
0.5	2.66×10^7	5.3	6.6×10^{13}
0.55	8.50×10^7	2.6	10.3×10^{13}
0.6	13.90×10^7	1.9	12.0×10^{13}

TABLE 5.1

Gradient of plot of $1/\varepsilon'_{app}$ versus temperature, grain size and total ionized grain boundary acceptor state density, for samples containing 0.1-0.6 at % Ho.

Donor Concentration (at %)	A	N_{ao} (cm^{-2})
0.05	36.40	8.03×10^{13}
0.1	39.03	8.32×10^{13}
0.2	37.70	8.17×10^{13}
0.3	35.42	7.92×10^{13}
0.4	32.66	7.61×10^{13}
0.5	29.33	7.91×10^{13}
0.55	25.30	6.92×10^{13}
0.6	26.74	6.98×10^{13}

TABLE 5.2

Slope of Arrhenius plots of $\ln\rho_L$ versus $(T - \theta)/T$ and total ionized acceptor state density, for all samples containing less than 0.8 at% Ho.

Donor Concentration (at %)	ϕ_o (max) (eV)	N_a(280°C) (cm^{-2})	N_a/N_{ao}	E_a (eV)
0.05	0.56	7.17×10^{13}	0.89	1.08
0.1	0.34	6.47×10^{13}	0.78	0.81
0.2	0.37	6.81×10^{13}	0.83	0.86
0.3	0.35	6.62×10^{13}	0.84	0.84
0.4	0.34	6.50×10^{13}	0.85	0.84
0.5	0.36	6.72×10^{13}	0.93	0.90
0.55	0.36	6.72×10^{13}	0.97	0.94
0.6	0.36	6.73×10^{13}	0.96	0.92

TABLE 5.3

Maximum grain boundary potential barrier height, acceptor state density at 280°C and acceptor energy, for samples containing less than 0.8% Ho.

CHAPTER SIX

THE EFFECT OF THE ADDITION OF ACCEPTOR IONS TO DONOR DOPED BARIUM TITANATE CERAMICS

It has long been recognised that small additions of 3d transition metal elements to the donor doped barium titanate composition result in an enhancement of the PTCR effect. The exact way in which these elements modify the PTCR behaviour, in particular because they are added in very small quantities (typically <0.1 at%), has not yet been thoroughly understood. The literature contains a number of often contradictory proposals about the mechanics of incorporation of these acceptor ions and the way in which they enhance the PTCR characteristic. This investigation was carried out to examine the effect of the addition of a small amount of manganese to a standard PTCR composition, through a comparative study of Mn-doped and Mn-free samples.

6.1. SAMPLE PREPARATION

Samples with formulations $Ba_{1-n}Ho_nTiO_3$ and $Ba_{1-n}Ho_nTi_{1-p}Mn_pO_3$ were prepared in the usual manner, where $n = 0.004$ and $p = 0.0004$. $BaCO_3$ and TiO_2 in the correct stoichiometric proportions, were used as the precursor, with the donor and acceptor dopants added in the form of Ho_2O_3 and $MnCO_3$, respectively. As usual, the sintering aids Si_3N_4 (0.9 mol%) and excess TiO_2 (0.5 mol%) were also added. $BaCO_3$ and TiO_2 were used instead of $BaTiO_3$ because of their superior purity: it was most important to control purity as much as possible since the acceptor dopant was added in similar quantities to the known impurity level of the available $BaTiO_3$ powder. Each composition was prepared identically, by the two-stage method described in chapter 3.1, with calcining taking place at 1100°C for 12 hours to ensure complete reaction between the $BaCO_3$ and the TiO_2. The

samples themselves were sintered in the muffle furnace at 1400°C for 60 minutes, followed by slow cooling at 300°C/hour to 1200°C where they were annealed for 5 hours. They were then cooled slowly to 800°C and thereafter at the natural cooling rate of the furnace, to room temperature.

As-fired surfaces of each composition were examined using the Scanning Electron Microscope (SEM) in order to determine the grain size and shapes and to observe any second phase segregated to the sample surface. The chemical composition of any such second phase was found using Energy Dispersive X-ray (EDX) analysis. Average grain sizes were found using the area count method of ~300 grains in order to obtain an accurate statistical mean. Polished and etched cross-sections of each type of sample were also examined to observe any effects of the Mn addition on the internal microstructure.

The resistivity of four samples of each composition was measured using the R-T system, between 50 and ~320°C. The samples were prepared in the usual manner and ohmic contacts were obtained with the In/Ga amalgam.

Thin samples were prepared for the capacitance-temperature measurements and room temperature impedance plots. The capacitance of the samples was obtained between room temperature and ~250°C at a constant frequency of 30kHz. The impedance measurements, from which the complex-plane plots of R_s versus X_s were obtained, were made at room temperature in the audio and radio frequency ranges.

6.2. EXPERIMENTAL RESULTS

6.2.1. Microstructure and morphology

Samples of both compositions were dark blue in colour, with the Mn-doped ones being shaded slightly green-grey in comparison with the Mn-free material. The as-fired surfaces of samples of each composition were very similar, having pebble-shaped grains ranging from 20-30μm to <5μm in size.

The most obvious difference between the samples was the presence of slightly more second (glassy) phase segregated to the surface of the Mn-free sample, appearing mostly between the grains in the form of an intergranular phase. Elemental analysis of the second phase material with EDX revealed it to be rich in silicon and titanium, i.e. composed of the glassy sintering aids. Figure 6.1 shows a scanning electron micrograph of a sample of the Mn-free formulation which may be compared with the micrograph of figure 6.2 of a Mn-doped sample. It can be seen that they are virtually identical, with the possible exception of a greater number of the larger, flat grains in the Mn-doped sample. This material, however, also contains more of the smaller, <5μm grains, as well as more intergranular second phase. The polished and etched surfaces of each sample were very similar, although the grains of the Mn-doped sample were observed to be more closely arranged and there appeared to be pockets of glassy material in some intergranular spaces of the Mn-free sample.

The average grain size was obtained in the usual way, where an equivalent cubic grain length was calculated. Both types of sample were found to have an average grain size of 10μm, showing that the addition of the Mn acceptor had little effect on microstructure.

Few intergranular pores are visible on the micrographs of figures 6.1 and 6.2 and very few were seen on the polished surfaces, suggesting that the samples were fully dense. Simple density measurements verified this: each sample was found to have acheived ~95% of the theoretical density (6.01g/cm^3).

6.2.2. Resistive Behaviour

Resistivity - temperature characteristics of samples of both compositions are shown in figure 6.3, where the effect of the added acceptor ions on the PTCR effect is clear. Since the grains of samples of each composition were found to be the same size, no normalisation of the resistance data was necessary. The Mn-

free sample has room temperature resistivity, ρ_{RT}, of 100Ωcm and a resistivity increase above 130°C of approximately 3 orders of magnitude, with the resistivity maximum, ρ_{max}, equal to 1.5×10^5Ωcm. In contrast, Mn doping has caused ρ_{RT} to be approximately doubled, to 220Ωcm and the resistivity increase above the transition to give $\rho_{max} = 5 \times 10^6$Ωcm, 30 times higher than that of the Mn-free material. The temperature of the resistivity maximum, T_{max}, was also affected by Mn doing: the Mn-free sample has $T_{max} = 214$°C whereas T_{max} was increased by ~40°, to 256°C for the Mn-doped material. Figure 6.3 shows that, above the maximum, the resistivity of the Mn-doped sample fell more rapidly with temperature than that of the Mn-free material, i.e. the high temperature NTCR behaviour of resistivity was steeper in the Mn-doped sample. This suggests that the maximum grain boundary potential barrier height was larger in the Mn-doped material.

6.2.3. Capacitance Measurements

The capacitance of each sample was used to calculate apparent permittivity, ϵ'_{app}, as temperature was raised through T_c. The temperature dependence of ϵ'_{app} for both compositions is shown in figure 6.4, where it can be seen that, above T_c, the values are very similar. The apparent permittivity of the Mn-free sample can be seen to fall rapidly between 135° and ~170°C and appears approximately constant at higher temperatures. The Mn-doped sample, on the other hand, has ϵ'_{app} falling more smoothly, in a similar manner to that of the pure $BaTiO_3$ sample in figure 4.8, above T_c. Below the transition ϵ'_{app} is very different for the two compositions. The Mn-free sample has ϵ'_{app} close to 6×10^4, whereas the Mn-doped material has ϵ'_{app} approximately half this value, $\sim 3 \times 10^4$. In addition, the Mn-free sample has temperature - dependent permittivity below T_c, similar to the samples of the donor concentration investigation containing 0.6 at%Ho (figure 4.8), where ϵ'_{app} increases as temperature is lowered below T_c. The Mn-

doped sample, on the other hand, has approximately constant ϵ'_{app} below T_c. Each sample, however, has ϵ'_{app} more than an order of magnitude higher than that of pure barium titanate (figure 4.8b), demonstrating the presence of grain boundary layers.

6.2.4. Impedance plots

As shown earlier (section 3.5.2, 4.2.4), complex impedance diagrams of imaginary impedance (X_s) versus real impedance (R_s) can be used to separate grain boundary and grain bulk resistance. Such plots were made for samples of both compositions and are shown in figure 6.5. It is clear from this that the grain bulk resistance, given by the high frequency intercept of the curve on the R_s axis, is unchanged by the addition of the Mn acceptor, at ~3Ω. The grain boundary resistance, on the other hand, was found to be 58Ω for the Mn-free sample and 108Ω for the Mn-doped material. Sample resistance in the absence of Mn was 61Ω and, in the presence of the acceptors, 106Ω. The values of R_{gb}, being increased by approximately 2 times upon Mn doping, corresponds very well with the approximate doubling of sample resistivity below T_c, observed in figure 6.3.

6.3. DISCUSSION OF EXPERIMENTAL RESULTS

6.3.1. Microstructure

The similarity of microstructure of both types of sample is in agreement with the observations of previous studies[6.1] and demonstrates that the addition of the Mn acceptor has no significant effect on grain size. The presence of slightly larger amounts of second phase on the surface of the Mn-doped sample indicates a minor change in grain shape within the bulk of the sample, as seen on the polished surfaces, leading to the presence of smaller intergranular spaces into which the liquid phase can fit during cooling and hence more is expelled to the surface.

6.3.2. Impedance measurements

It is clear from figure 6.3 that the addition of Mn has caused a large increase in the magnitude of the PTCR characteristic. The impedance plots (figure 6.5) show that the increase in room temperature resisivity is due entirely to the grain boundaries and that the grain bulk resistance is constant, at between 3 and 4Ω. Allowing for a small error in the accuracy of measurement of R_{bulk} and making the assumption that the volume of the grain boundary layers is negligible in comparison with that of the grain bulk, the grain bulk resistivity, ρ_{bulk} was calculated to be 6.6Ωcm and the effective charge carrier concentrations, N_d, found to be 1.9 $\times$ 10^{18}cm^{-3}. This value compares very well with N_d calculated in the previous chapters (1.8 and 3.1 $\times$ 10^{18}cm^{-3}), despite the different starting materials and sintering process involved in this investigation. N_d found for the present samples is much less than the nominal donor density, 6.1 $\times$ 10^{19}cm^{-3}, corresponding to the amount of Ho ions added, again as found in the previous chapter. This reinforces the suggestions of Ihrig and Puschert[6.2] and Xue et al[6.3] that a form of autocompensation takes place, either by barium vacancy formation or by incorporation of some donor ions onto Ti^{4+} sites, within the grain bulk.

The consistency of R_{bulk} shows that the acceptor ions are not effective within the grain bulk and therefore suggests that they are not present in these regions. Electron probe microanalysis and scanning transmission electron microscopy have been reported[6.4] to show the segregation of acceptor ions at the grain boundaries of doped barium titanate ceramics, although conflicting evidence by other workers[6.5] suggested that this does not take place. The present results, however, support the experimental observations of the former[6.3] rather than the analytical observations of the latter[6.5].

6.3.3. Resistive behaviour

The approximate doubling of room temperature resistivity and the increased

magnitude of the PTCR characteristic (figure 6.5) with the addition of the Mn acceptor are in agreement with results reported by other workers[6.1,6.2,6.6–6.13]. The large rises in ρ_{max} and T_{max} with the addition of the Mn dopant suggest an increase in the value of N_{ao} and E_a in the Heywang model (equations 2.5 and 2.6). Increasing N_{ao} results in a corresponding increase in the grain boundary potential barrier so that resistivity rises more rapidly with temperature. A larger value of E_a has the effect of raising the temperature at which the acceptor traps reach the Fermi level, i.e. the temperature at which depopulation of the acceptor traps takes place, which in turn raises T_{max}. The combination of larger values of both N_{ao} and E_a thus increases both the magnitude of the PTCR characteristic and the temperature range over which it takes place.

6.3.4. Capacitance measurements

The higher value of ϵ'_{app} for the Mn-free sample below T_c in comparison with that measured for the Mn-doped material may be explained with reference to equation 4.17,

$$\epsilon'_{app} = \epsilon' \times \frac{dN_d}{N_a}.$$

In chapter four it was shown that the donor concentration has no effect on the the value of ϵ', the permittivity of the material within the grain boundary layer, which is given by the Curie-Weiss law above T_c. It will be assumed, therefore, that the incorporation of Mn also has no effect on ϵ', particularly because such a small quantity has been added in comparison withe the amount of donor dopant. Below T_c the permittivity of pure barium titanate is comparatively low (figure 4.8) at $\sim 10^3$, and it is now recognised that the high apparent permittivity of donor doped barium titanate is due to the presence of the thin grain boundary layers. Clearly, the Mn-free material, having fewer grain boundary acceptor traps than the Mn-doped, i.e. it has lower N_a, will have a higher value of apparent permittivity in accordance with equation 4.17. The higher value of N_a in the Mn-doped material

causes the grain boundary layers to be thicker (equation 4.2), hence ϵ'_{app} of these samples can be expected to be lower.

The behaviour of $1/\epsilon'_{app}$ above T_c follows a linear dependence on temperature until depopulation of the grain boundary acceptor states takes place and N_a is no longer equal to N_{ao}. Figure 6.7 shows $1/\epsilon'_{app}$ versus temperature, plotted between T_c and just below T_{max} for samples of both compositions. It can be seen that linearity of the Mn-doped sample extends to 190°C, whereas the corresponding plot for the Mn-free material is linear only until 170°C. This extension of the linear region in the presence of the Mn acceptor is a direct consequence of the increased depth of the grain boundary acceptor traps, i.e. that E_a has been incre/apparant/e additional acceptor doping.

The slope, m, of the plot of $1/\epsilon'_{app}$ versus temperature, below the depopulation temperature, is given from equation 4.17 as

$$m = C \times N_a/dN_d \tag{6.1}$$

where C is the Curie constant. Figure 6.7, however, shows that the slope of the plot from the Mn-doped material is lower than that from the Mn-free sample, in contradiction to expectation. The slopes of the linear portions of the plots for each composition were measured and found to be 9.52×10^{-7} and $5.94 \times 10^{-7}\mathrm{K}^{-1}$ for the Mn-free and Mn-doped compositions, respectively. Using equation 6.1 and C $= 1.5 \times 10^5$K, d $= 10 \times 10^{-4}$cm and $N_d = 1.9 \times 10^{18}\mathrm{cm}^{-3}$, N_{ao} was estimated for each composition. The Mn-free sample was found to have $N_{ao} = 2.7 \times 10^{14}\mathrm{cm}^{-2}$ and the Mn-doped material had $N_{ao} = 1.6 \times 10^{14}\mathrm{cm}^{-2}$. Comparing these values with those obtained for the samples containing different donor concentrations in the last two chapters suggests that N_{ao} for the Mn-free sample has been calculated to be very high. The present value is about half an order of magnitude higher than N_{ao} for samples containing the same amount of donor dopant (table 4.4 and figure 5.17). N_{ao} for the Mn-doped sample, however, is quite realistic since it is approximately twice the values calculated for the same donor concentration in the

last two chapters. The reason for the high value of N_{ao} calculated for the Mn-free material is unknown.

6.4. ANALYSIS OF EXPERIMENTAL RESULTS

6.4.1. Calculation of grain boundary acceptor state density and potential barrier height

According to the Heywang model[6.14,6.15], normalised grain bounday resistance, ρ_L, is given by equation 4.21. Rewriting this equation in terms of sample resistivity, since normalisation of the present results was not necessary, gives

$$\rho = C_o exp(\frac{e^2 N_a^2}{8\epsilon_o \epsilon' N_d kT}) \tag{6.1}$$

where C_o is a constant. In the last two chapters it was shown that donor concentration has no effect on the permittivity of the material within the grain boundary layer. Assuming that the addition of the acceptor dopant also has no effect on ϵ', equation 6.1 may therefore be rewritten,

$$\rho = C_o exp(\frac{e^2 N_a^2 (T-\theta)}{8\epsilon_o C N_d kT}). \tag{6.2}$$

Analysis in the same way as described in the previous chapter was then possible, where

$$\rho = C_o exp(\frac{A(T-\theta)}{T}), \tag{6.3}$$

with, as before (equation 4.24),

$$A = \frac{e^2 N_{ao}^2}{8\epsilon_o C N_d k}.$$

Arrhenius plots of lnρ versus (T - θ)/T may be expected to follow straight lines until depopulation of the acceptor traps begins to take place and N_a is no longer equal to N_{ao}. The slope of the plot is given by A which is proportional to the square of the total acceptor trap density. Figure 6.8 shows ρ, plotted on a logarithmic scale, versus (T - θ)/T for samples of each composition. Both plots follow

straight lines until temperatures close to those of T_{max}, in agreement with the observations of the plots of $1/\epsilon'_{app}$ versus temperature (figure 6.7). The slope, A, of the plots was determined by drawing the best-fit straight line through the points, as well as performing least-squares and regression analysis. The statistical analyses revealed that the Mn-free samples had A = 51.4 and those doped with the acceptor had A = 71.8, with correlation coefficients of >0.99. From equation 4.27, N_{ao} was calculated to be 7.47×10^{13} and $8.83 \times 10^{13}\text{cm}^{-2}$ for the two compositions, respectively. This corresponds to an increase in the value of ~20% upon the addition of the Mn acceptor dopant. The value of N_{ao} for the Mn-doped sample can be seen to agree with N_{ao} found from the capacitance measurements, but those for the Mn-free material do not agree at all. The reason for this discrepancy is not known, but suggests that the capacitance measurements may have been in error.

From equations 2.5 and 4.24, equation 4.25 has been shown to be

$$\phi_o = A \times k/e \times (T - \theta).$$

ϕ_o was thus calculated between T_c and the depopulation temperature for both types of specimens and the results are shown in figure 6.9. It is apparent that the addition of the Mn acceptor has led to an increase of ~40% in the value of ϕ_o throughout the temperature range for which N_a is constant. At higher temperatures, close to T_{max}, ϕ_o starts to saturate towards its maximum value as a result of the depopulation of the acceptor traps.

6.4.2. Calculation of acceptor energy

Having determined values of N_{ao} for both compositions, below the depopulation temperature, it becomes possible to estimate the value of the acceptor energy, E_a. Following the same method as described in the last two chapters, $\ln\rho$ was plotted against 1/T, for each composition, above T_{max}. Least-squares analysis was performed to calculate the gradient of the plots, from which values of $\phi_{o(max)}$

of 0.49eV for the Mn-free composition and 0.81eV for the Mn-doped samples were obtained. Correlation coefficients for these plots were in excess of 0.95, showing agreement between the points and the least-squares best-fit line. The temperature was again chosen to be 250°C, above T_{max} for both sets of sample. Corresponding values of N_a were calculated using equation 2.5 to give 6.76 × 10^{13} and 8.70 × 10^{13}cm^{-2} for the Mn-free and Mn-doped compositions, respectively. Equation 4.31 was then used to obtain E_a of 1.00eV for the Mn-free samples and 1.40eV for the Mn-doped material. Any inaccuracies in the measurement of N_d (section 6.3.2) made insignificant effects to the value of E_a for both compositions, with maximum deviations of <0.01eV. The literature cites estimates of E_a ranging from 0.5eV - 1.22eV, depending on the nature of the acceptor states[6.1,6.2.6.14–6.18], in agreement with the present results.

To verify these calculations, theoretical predictions of the values of ρ_{max} and T_{max} for both compositions, were made using a computer program to solve equations 2.5 and 2.6 numerically. For the purpose of this problem, values of N_{ao}, E_a, N_d, d and μ must be supplied. The experimentally obtained values of N_d and d were used but N_{ao} and E_a were estimated ($\mu = 0.5\text{cm}^2\text{V}^{-1}\text{s}^{-1}$). The purpose was to obtain the same values of T_{max} and ρ_{max} as found from the resistivity - temperature plots and hence to have predicted N_{ao} and E_a. From experiment, ρ_{max} and T_{max} of the Mn-free material were 1.5 × $10^5\Omega$cm and 214°C, respectively. Mn-doping increased these values to 5.6 × $10^6\Omega$cm and 254°C, respectively. The computer model predicted the same results with $N_{ao} = 1.0 \times 10^{14}$ cm^{-2} and $E_a = 1.2$eV for the Mn-free composition and $N_{ao} = 1.0 \times 10^{13}$ cm^{-2} and E_a = 1.48eV for the Mn-doped material, showing a measure of agreement with the experimentally obtained values.

6.5. CONCLUSION

In summary, the addition of impurity ions which, upon incorporation into the $BaTiO_3$ lattice do so onto Ti^{4+} sites with valency less than +4, act as acceptors. The most obvious effect of these ions is to increase both the maximum resistivity and the temperature at which the maximum takes place. It has been suggested that these ions tend to segregate at the grain boundary regions, thereby having no effect on the overall charge carrier concentration, but increasing the density of grain boundary acceptor states. In turn, the grain boundary potential barrier is raised to higher levels at temperatures above T_c and, consequently, resistivity increases rapidly with temperature above the transition. In addition, the nature of the electron traps is affected by additional acceptor doping, since the PTCR effect was observed to extend over a longer temperature range in the Mn-doped sample. Calculation of estimates of acceptor energy revealed that the addition of 0.04at% Mn to a standard composition of PTCR sample containing 0.5 at%Ho caused acceptor energy to be increased by 0.4eV, from 1.0eV for the Mn-free sample to 1.4eV for the Mn-doped material. Clearly, the Mn ions were responsible for this effect, which was also verified by means of theoretical calculations of the PTCR effect using numerical solution of equations 2.5 and 2.6 (the Heywang model).

REFERENCES

6.1 Al-Allak H.M., Brinkman A.W., Russell G.J. and Woods J., J. Appl. Phys., **63**, 4530, 1988.

6.2 Ihrig H. and Puschert W., J. Appl. Phys., **48**, 3081, 1977.

6.3 Xue L.A., Chen Y. and Brook R.J., Mater. Sci. Eng., **B1**, 193, 1988.

6.4 Xue L.A., PhD Thesis, University of Leeds, 1987.

6.5 Kutty T.R.N. and Murugaraj P., Mater. Lett., **3**, 1951, 1985.

6.6 Brauer H., Z. Angew. Phys., **23**, 373, 1967.

6.7 Rheme H., Phys. Stat. Sol., **26**, K1, 1968.

6.8 Hewyang W., J. Mater. Sci., **6**, 1214, 1971.

6.9 Matsuoka T., Matsuo Y., Sasaki H. and Hayakawa S., J. Am. Ceram. Soc., **55**, 108, 1972.

6.10 Ihrig H., J. Am. Ceram. Soc., **64**, 617, 1981.

6.11 Ueoka H., Ferroelectrics, **7**, 351, 1974.

6.12 Cipollini N.E., Sowa J.M., Forbes C.E. and Lynch J.F., *Proceedings of the 6th IEEE International Symposium on Applications of Ferroelectrics*, Ed. Wood V.E. (IEEE, New York, 1986), 665.

6.13 Murugaraj P. and Kutty T.R.N., J. Mater. Sci. Lett., **5**, 171, 1986.

6.14 Hewyang W., Sol. Stat. Electron., **3**, 51, 1961.

6.15 Heywang W., J. Am. Ceram. Soc., **47**, 484, 1964.

6.16 Jonker G.H., Sol. Stat. Electron., **7**, 895, 1964.

6.17 Daniels J. and Härdtl K.H., Phil. Res. Rep., **31**, 489, 1976.

6.18 Daniels J., Härdtl K.H. and Wernicke R., Phil. Tech. Rev., **38**, 73, 1978/79.

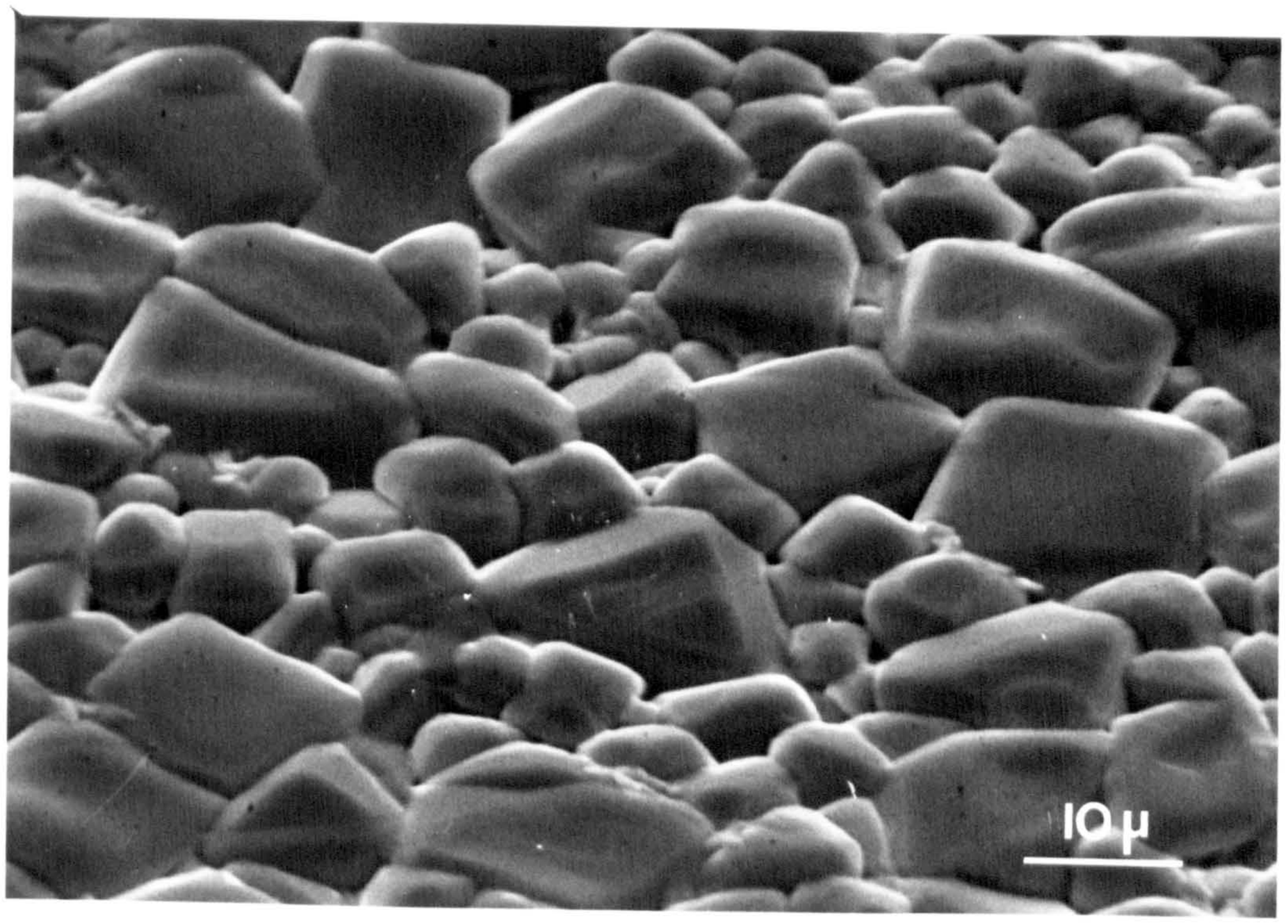

Figure 6.1 Scanning Electron Micrograph of a typical Mn-free sample (bar = 10μm).

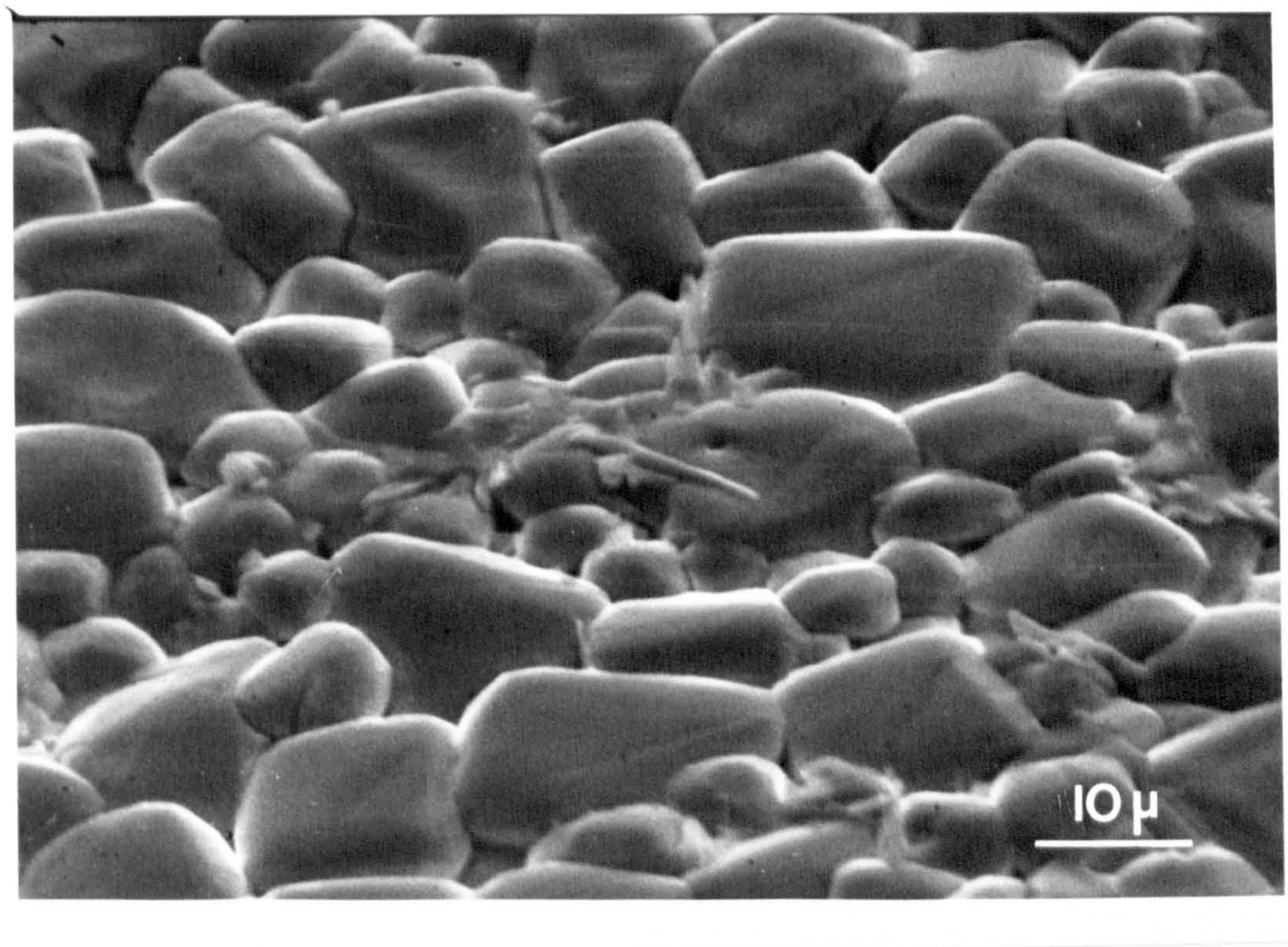

Figure 6.2 Scanning Electron Micrograph of an area of a Mn-doped sample (bar = 10μm).

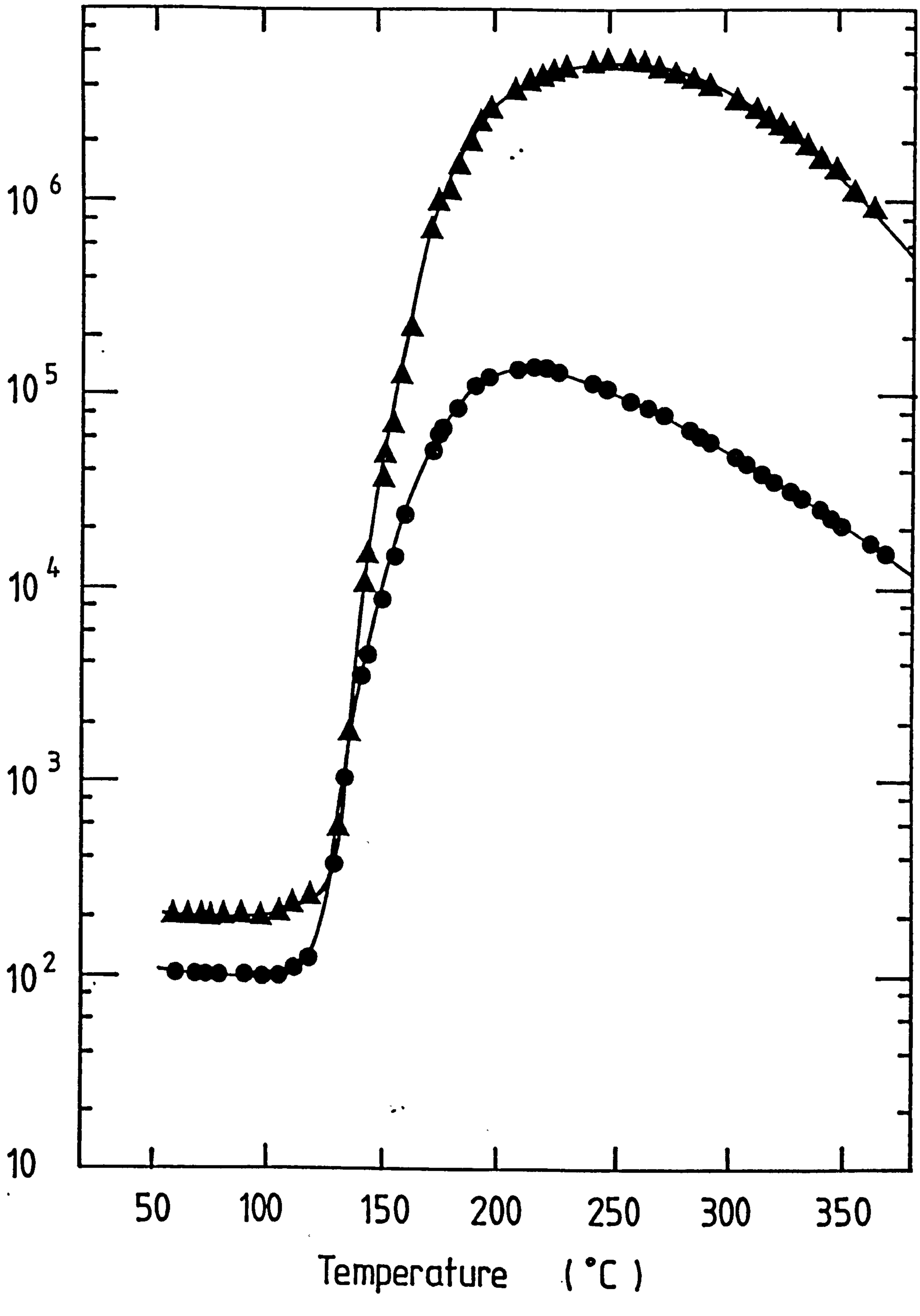

Figure 6.3 Resistivity versus temperature characteristics of Mn-free (•) and Mn-doped (▲) samples.

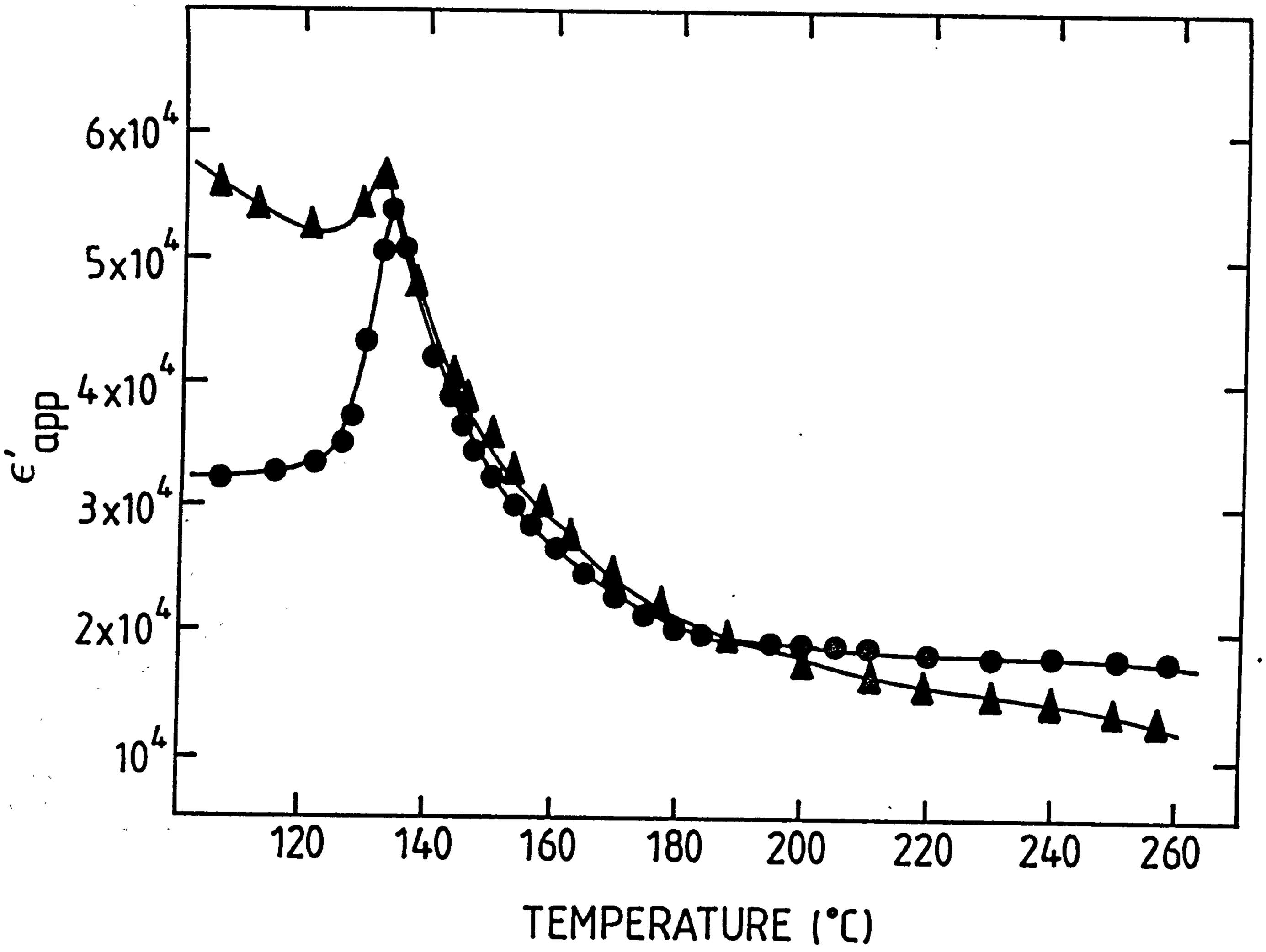

Figure 6.4 Apparent permittivity versus temperature for Mn-free samples (•) and Mn-doped (▲) material.

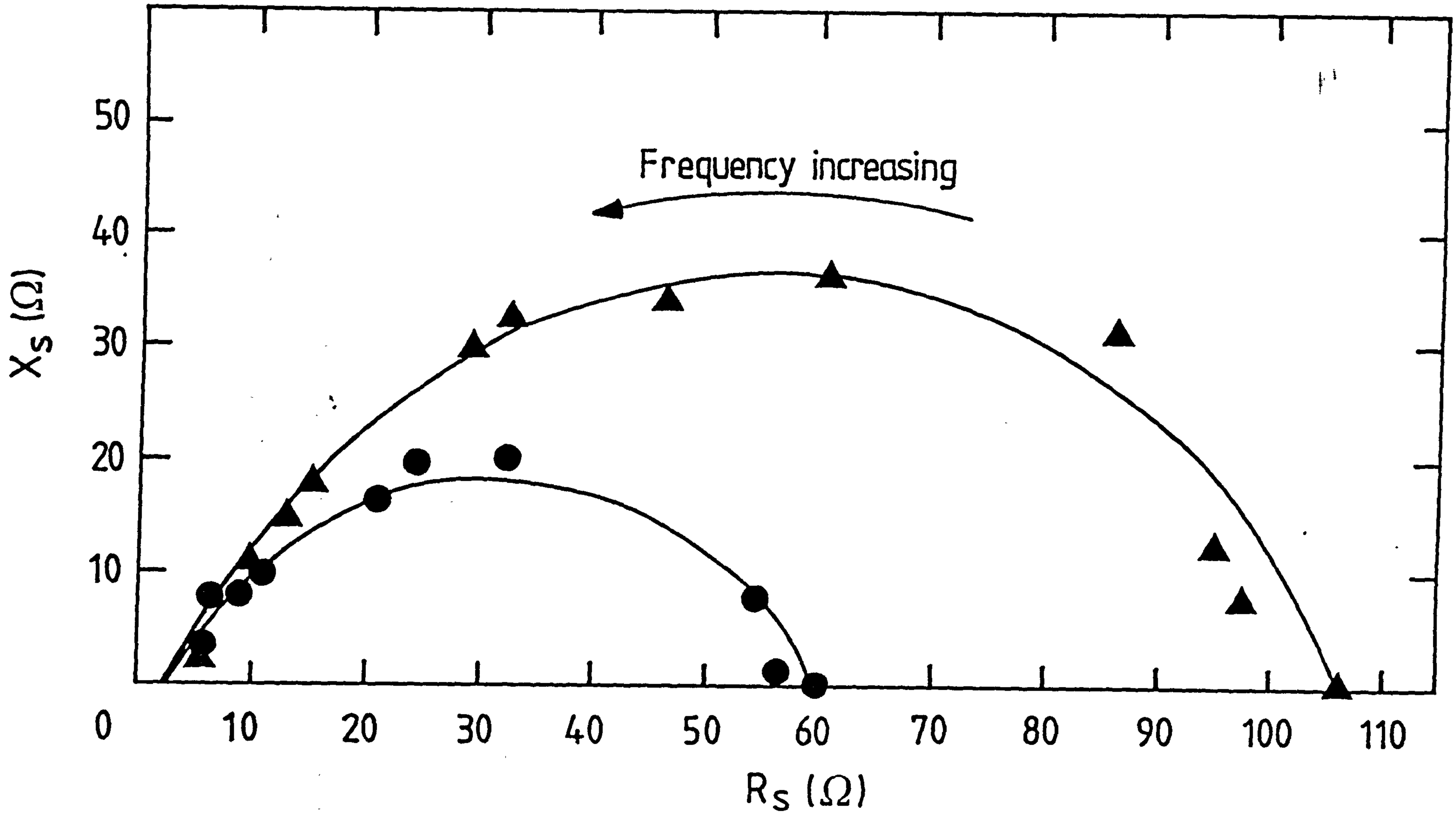

Figure 6.5 A.c. impedance plots at room temperature for Mn-free (•) and Mn-doped (▲) samples.

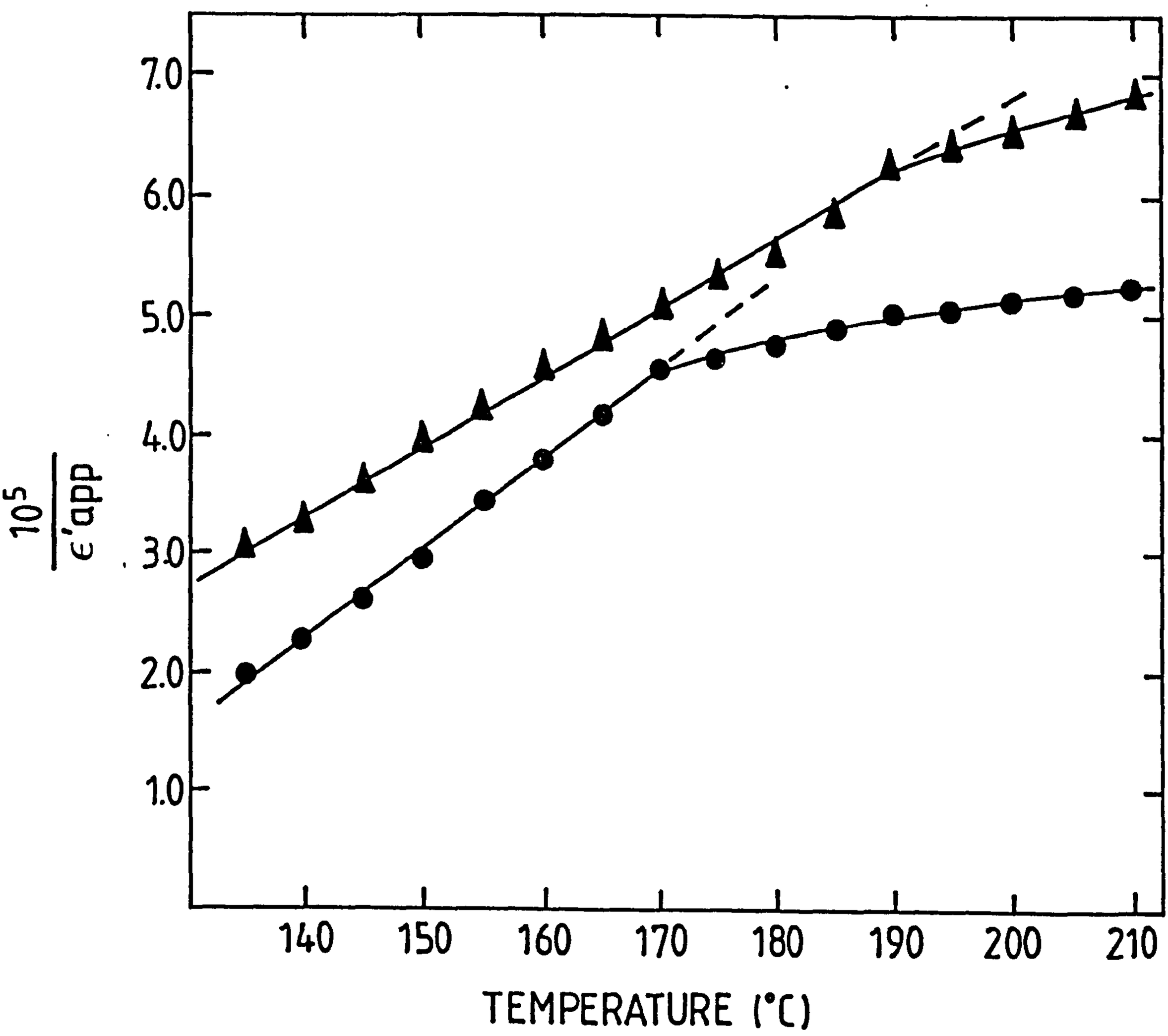

Figure 6.6 $1/\epsilon'_{app}$ versus temperature above T_c for Mn-free (●) and Mn-doped (▲) compositions.

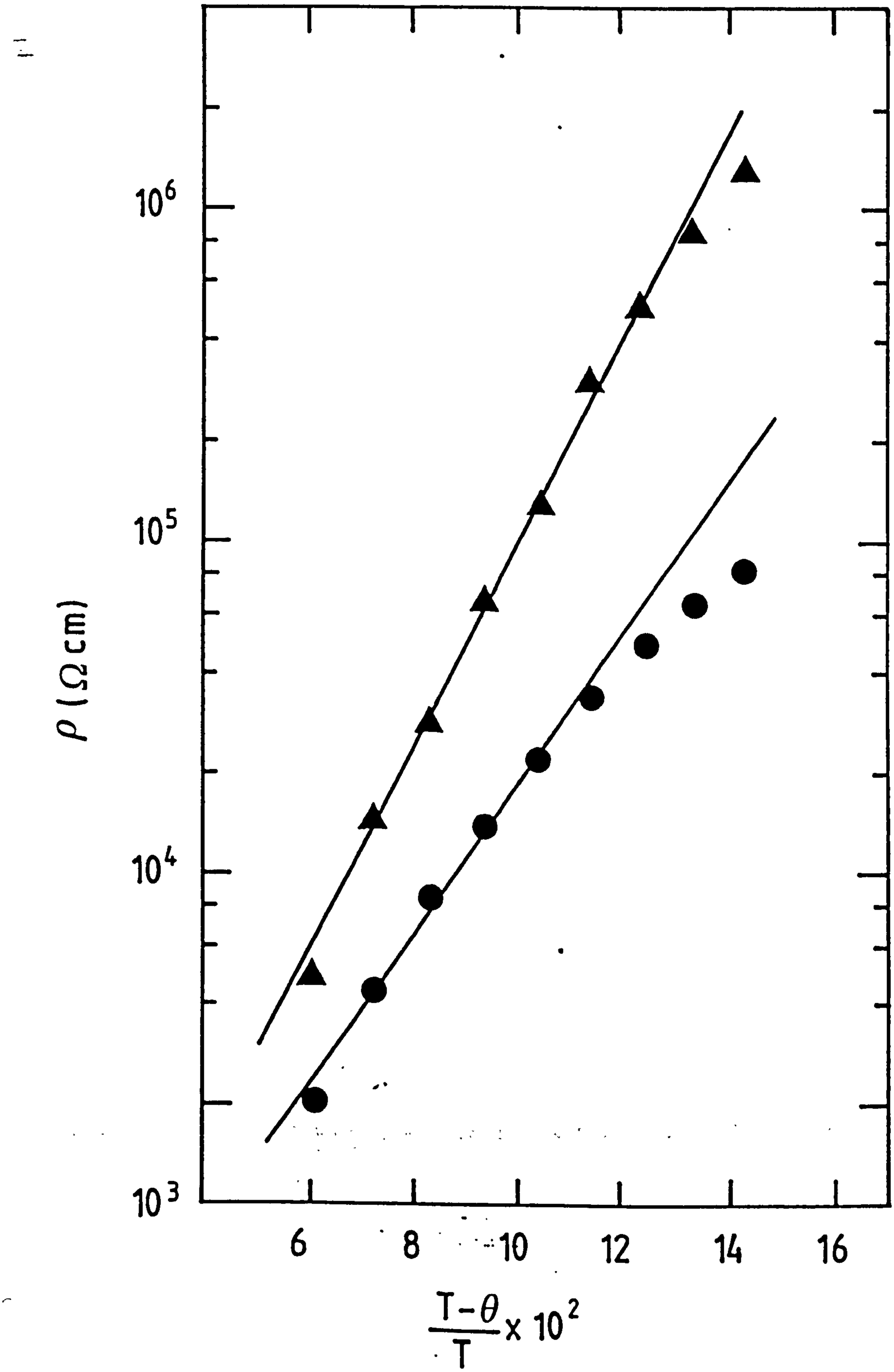

Figure 6.7 Arrhenius plots of lnρ versus (T - θ)/T for Mn-free (•) and Mn-doped (▲) samples.

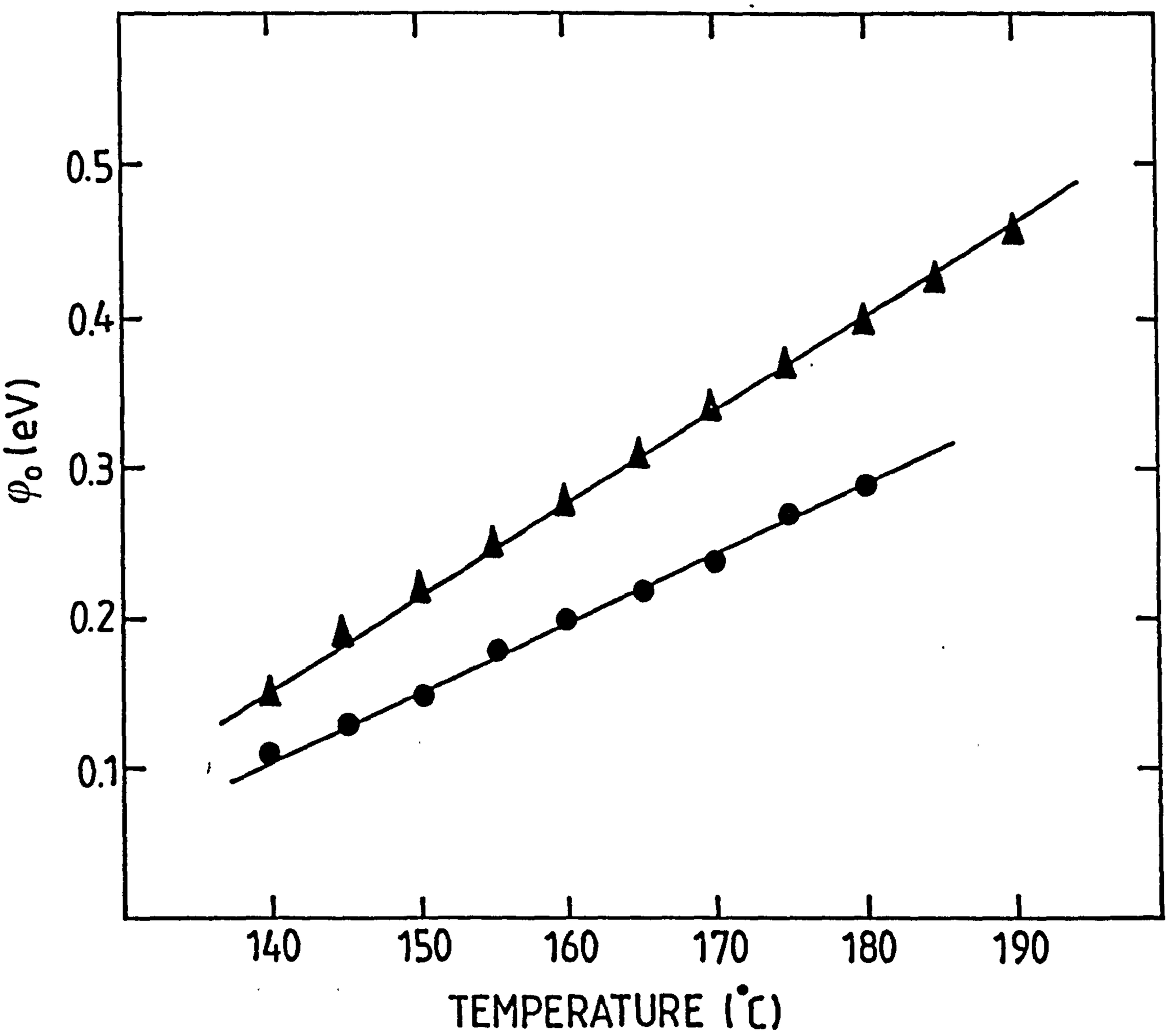

Figure 6.8 Potential barrier height versus temperature above T_c for Mn-free material (•) and Mn-doped samples (▲).

CHAPTER SEVEN

EFFECT OF SINTERING ATMOSPHERE ON THE PTCR CHARACTERISTIC

In the last chapter it was shown that the addition of small quantities of ions which substitute with a lower valency onto metallic lattice sites act as grain boundary acceptors. They segregate towards the grain boundaries, increasing the total ionized acceptor state density and the energy of the electron traps. The resulting effect of acceptor doping on the PTCR characteristic was to increase the magnitude of the resistivity jump and its temperature range. Chapters 4 and 5 concentrated on the effect of donor concentration on the PTCR characteristic, demonstrating that the minima observed in room temperature and maximum normalised resistance was entirely attributed to changes in the acceptor trap density at the grain boundaries. The acceptor energy was unique for each species and was found, for all of the donor doped samples, to be the same, showing no change in the nature of the acceptor traps with donor concentration. The results were unable to confirm the exact nature of the acceptor states, although adsorbed oxygen atoms and doubly ionized barium vacancies were implicated. It is possible to control the quantity of adsorbed oxygen on the grain boundaries by sintering samples in a controlled atmosphere, hence it is possible to investigate the effect of grain boundary oxygen acceptors. The acceptor energy of the oxygen acceptors may then be calculated and compared with that of the donor concentration study to show whether the majority grain boundary acceptor traps in the previous investigation were barium vacancies or other acceptors. The purpose of the work described in this chapter was to examine the effect of oxygen content in the sintering atmosphere on the PTCR characteristic.

7.1. SAMPLE PREPARATION

One standard composition was chosen, $Ba_{0.996}Ho_{0.004}TiO_3$, to which 0.3mol% Si_3N_4 and 0.5 mol% TiO_2 were added as sintering aids. Commercial grade $BaTiO_3$ powder was used as the precursor and samples were prepared in the usual way, where $BaTiO_3$, Ho_2O_3, Si_3N_4 and TiO_2 were ball milled together for 12 hours. Small pellets were pressed from this mixture and sintered in the tube furnace at 1400°C for 60 minutes, followed by slow cooling to 800°C and thereafter at the natural rate of the furnace to room temperature. The sintering atmosphere was regulated between 0.18 and 100%O_2 by volume, the remainder being made up by O_2-free N_2. Samples were also sintered in 100%N_2 for comparison. The gas flowed through the furnace at a rate of 1 l/min.

As-fired surfaces were examined in the SEM, with compositional analysis of any surface features being carried out by EDX. Average grain sizes were calculated by the usual method of an area count of >200 grains. Simple measurements were performed to ensure the samples were dense.

The samples were polished slightly to ensure flat surfaces for the resistivity - temperature measurements, which were carried out between 40 and ~450°C. They were then thinned to ~0.5mm for the purpose of the room temperature ac impedance and dielectric measurements between room temperature and ~250°C. Ohmic contacts were obtained as usual with the In/Ga amalgam.

7.2. EXPERIMENTAL RESULTS

7.2.1. Microstructure

The samples sintered to a dense, dark blue ceramic material, achieving >90% density in all cases. Average grain sizes were determined and found to be approximately the same size for all sintering atmospheres. The mean of the average grain sizes was 8.4μm, with a typical variation of $\pm$2μm between samples sintered in different oxygen contents. Those sintered in 100%N_2 had large, flat grains 14μm

across, in contrast. The morphology of the grains changed with oxygen content of the sintering atmosphere: at higher partial pressures of oxygen the grains were rounded and unevenly sized, ranging between ~25μm and 8μm. Figure 7.1 is a scanning electron micrograph of a sample sintered in 80%O_2, where regions of the two differently sized grains are apparent. Sintering in oxygen concentrations less than ~20% resulted in a more evenly sized microstructure, with most grains between 5 and 15μm in size: figure 7.2 shows a micrograph of a sample sintered in 0.25%O_2. The shape of the grains changed from being rounded at high oxygen concentrations towards the very flat shape of the sample sintered in 100%N_2, of which a micrograph is shown in figure 7.3. The sample of figure 7.2 can be seen to contain more surface glassy phase features than that of figure 7.1, suggesting the presence of flatter grains within the bulk which fit together well, leaving very little intergranular space. The sintering aids, which form the glassy second phase, are then expelled to the surface and appear as the needle-shaped features or the odd shaped features between grains.

7.2.2. Resistive behaviour

Since the samples all had comparable average grain sizes, normalisation of the resistance data was not necessary. Samples sintered in air (20%O_2) had resistivity - temperature characteristics similar to those of the Mn-free samples of the last chapter: room temperature resistivity, $\rho_{(RT)}$, was ~10Ωcm and the maximum resistivity, ρ_{max}, was approaching $10^4\Omega$cm, representing a PTCR characteristic of 3 orders of magnitude. Increasing the oxygen content of the sintering atmosphere to 60% resulted in a gradual rise in ρ_{max} to $\sim 1.5 \times 10^4\Omega$cm, with $\rho_{(RT)}$ remaining approximately constant. The samples sintered in 100%O_2, however, had a smaller PTCR characteristic, with $\rho_{(RT)}$ ~10Ωcm and ρ_{max} only $2\frac{1}{2}$ orders of magnitude higher. The same results were obtained when these measurements were repeated using either the same or freshly sintered samples.

Reduction of the oxygen content during sintering, below 20%, resulted in diminished PTCR characteristics: as the partial pressure of oxygen decreased, the magnitude of the PTCR characteristic (i.e. the value of ρ_{max}) was reduced. Room temperature resistivity remained approximately constant at ~10Ωcm but ρ_{max} was progressively reduced from 5×10^3Ωcm for the sample sintered in 10%O_2 to <500Ωcm after sintering in 0.25%O_2. Figure 7.4 shows resistivity - temperature characteristics belonging to typical samples sintered between 0.25 and 60%O_2, where the steady reduction in the PTCR characteristic can be seen. This figure also shows, for comparison, the resistivity - temperature plot of a sample sintered in 100%N_2, where it is apparent that there is no PTCR effect.

Figure 7.4 also demonstrates the effect of oxygen content on the temperature, T_{max}, at which the resistivity maximum takes place. As oxygen partial pressure during sintering was reduced, T_{max} can be seen to increase, with the result being that, since ρ_{max} decreased, the PTCR characteristic became gradually less steep. For the two samples sintered in the lowest oxygen concentrations (0.18, 0.25%), accurate values of T_{max} and ρ_{max} were unobtainable since their resistivity increased very slowly with temperature and reached the maximum over a large range of temperatures. The resistivity increase above T_c for these samples was only about an order of magnitude so that the PTCR effect may be described as minimal.

The effect of oxygen concentration during sintering on ρ_{max} and T_{max} is summarised in figures 7.5 and 7.6, respectively. ρ_{max} can be seen to decrease quickly with oxygen partial pressure, particularly below 40%O_2. T_{max} has an approximately linear relationship with oxygen concentration, increasing from ~240°C at 100%O_2 to 350°C after sintering in 1%O_2.

7.2.3. Dielectric behaviour

Apparant permittivity, ϵ'_{app}, was calculated from the capacitance measure-

ments, between room temperature and ~240°C. A series of typical plots of ϵ'_{app} versus temperature are shown in figure 7.7 for samples sintered in 0.5, 5 and 30%O_2 where it can be seen that, despite the high values, apparent permittivity below T_c falls with increasing oxygen content during sintering. The samples sintered in 0.5 at%O_2 have ϵ'_{app} at ~100°C of 2.65×10^5 in comparison with those sintered in 30%O_2 which have ϵ'_{app} ~2.1×10^5. Above 60%O_2 sintering atmosphere it was found to be very high, with samples sintered in 100%O_2 having ϵ'_{app} ~3.7×10^5. In comparison, the samples sintered in 100%N_2 had even higher ϵ'_{app}, ~5.2×10^5 at 100°C. The high values of permittivity of these samples in comparison with ϵ' of pure, undoped $BaTiO_3$ (figure 4.8) indicate the presence of thin grain boundary layers, in the same manner as the samples discussed in previous chapters.

7.2.4. A.c. impedance plots

Room temperature ac impedance plots within the audio and radio frequency ranges were carried out on samples sintered in 80%, 10%, 5%, 2%, 1% and 0.5% O_2. The real (R_s) and imaginary (X_s) parts of the impedance were calculated and plotted in the form of a complex impedance diagram. Figure 7.8 shows plots of X_s versus R_s for samples sintered in 80%, 10% and 1%O_2 and demonstrates the dominant effect of the grain boundaries on sample resistance. R_{bulk}, given by the intercept of the curve on the R_s axis at the high frequency end, can be seen to be approximately 1.5Ω for the samples sintered in the higher oxygen contents (10%, 80%) but is lower for the sample sintered in 1%O_2. As oxygen content was reduced, so did sample resistance, as apparent in figure 7.8, and hence very few points were available for impedance plots in samples sintered in <5%O_2. These samples appeared to have R_{bulk} of ~1Ω. In common with other a.c. impedance plots, the value of R_{gb} fell with sample resistance, as the oxygen concentration during sintering was reduced.

7.3. DISCUSSION OF EXPERIMENTAL RESULTS

7.3.1. Morphology and microstructure

According to the work of Drofenik and colleagues[7.1–7.5], substitution of the donor dopant ion into the relevant lattice site is accompanied by the release of some oxygen (equation 4.35):

$$BaO_{latt} + \frac{1}{2}Ho_2O_3 \rightarrow (HoO)_{iatt} + \frac{1}{4}O_2 + e^-.$$

In other words, a local partial pressure of oxygen is created, which is higher than that of the atmosphere. At high oxygen partial pressures the reaction may be driven backwards, preventing the efficient incorporation of the donor ions. At low oxygen atmospheres, on the other hand, the reaction is driven forwards and donor incorporation proceeds rapidly. Drofenik[7.4] sintered samples in a vacuum and observed much larger grains than those of identical samples sintered in air. He explained his results in terms of the above equation, where the partial pressure of oxygen determines the process of donor incorporation.

In apparent contrast to the results of Drofenik, the present samples all contain grains of similar average size, $\sim 8\mu$m, regardless of oxygen partial pressure during sintering. Those sintered in 100%N_2, on the other hand, having grains much larger than the rest, are in agreement with Drofenik's results.

During sintering the donor ions are incorporated into the $BaTiO_3$ lattice with the accompanying release of oxygen as well as grain growth. The energy required for these processses is made up of the energy required for dissolution of the dopant ions and the energy needed for grain growth. Clearly, the former takes priority, with only the remaining energy being available for the grain growth process. Thus grain size is dependent on the sintering temperature (chapter 3.2). In chapters 4 and 5 the grain size was used as an indicator of the donor concentration (figures 4.1 and 5.3). At low oxygen partial pressures the oxygen released during donor incorporation (equation 4.35) can diffuse quickly to the grain surfaces and into the atmosphere, permitting rapid incorporation of all of the donors. The grains of

such samples (<20%O_2 concentration) were evenly sized and flat in shape, fitting together well. The microstructure indicates that homogeneous donor incorporation took place, a process which would be expected to result in evenly sized grains. It is likely, in the present case, that proportionally less energy remained after this for the purpose of grain growth, since sintering took place at 1400°C, compared with 1420 and 1460°C for the donor concentration investigations. The reason for this hypothesis is that additional grain growth took place to a limited extent, since the grains are closely packed together and flat, suggesting that further grain growth would have taken place had the temperature been raised an extra 20-40°C.

At high oxygen concentrations (>20%), donor incorporation may be impeded as a result of the higher partial pressure of O_2 in the atmosphere, driving the incorporation reaction backwards. Clearly, the hindrance could not be very great since the maximum pressure used was 1 atmosphere, less than an order of magnitude higher than the partial pressure of oxygen in air. The presence of unevenly sized and shaped grains suggests that donor incorporation experienced local variation, so that some regions contained larger concentrations of donor dopant and hence have smaller, more rounded grains than other regions.

7.3.2. Resistive and dielectric behaviour

The steady rise in the magnitude of the PTCR characteristic as oxygen partial pressure was increased towards 80% from 0.18%O_2 is in agreement with the results of Jonker[7.6]. He heat-treated samples in atmospheres of various gases for different lengths of time and observed similar increases in the magnitude of the resistivity characteristic, particularly as treatment time was increased.

The reduction in values of ρ_{RT} and ρ_{max} as oxygen partial pressure was decreased indicates a reduction in the grain boundary potential barrier height, probably as a result of the grain boundary acceptor state density, N_{ao} becoming progressively smaller[7.7–7.9]. The steadily increasing values of T_{max} are consistent

with this indication, since correspondingly higher temperatures are necessary to initiate depopulation of the grain boundary acceptor traps where the potential barrier is low. Also commensurate with this idea were the measurements of apparent permittivity of samples sintered between 0.5 and 40%O_2. Figure 7.9 shows ϵ'_{app} below T_c (~100°C) versus partial pressure of oxygen, where, below 40%O_2, the permittivity can be seen to fall with increasing oxygen content. (Least - squares analysis of these points revealed correlation to the solid line of 0.93.)

Such a reduction in ϵ'_{app} indicates an increase in the density of grain boundary acceptor states, N_a, in accordance with equation 4.17,

$$\epsilon'_{app} = \epsilon' \times \frac{dN_d}{N_a}$$

If, as suggested in the previous chapters, the grain boundary acceptor states consist of adsorbed oxygen atoms, then N_a would be dependent on the partial pressure of oxygen during sintering. Clearly, as this (and hence the amount of available oxygen, ignoring the oxygen released during donor incorporation) was reduced below 40%, the number of adsorbed oxygen atoms within the grain boundary regions would be smaller, leading to an increase in ϵ'_{app}.

The behaviour of samples sintered in the higher oxygen atmospheres (>60%O_2) is contradictory to the expectations of the theory that the grain boundary acceptor traps consist mostly of adsorbed oxygen atoms. Above 60%O_2 ϵ'_{app} at ~100°C is higher than expected from the apparent trend, at 3.7×10^5 at 100%O_2 (figures 7.7 and 7.9) but ρ_{max} remains approximately constant at ~$10^4\Omega$cm (figure 7.5). Anticipated results for these samples would give values of ϵ'_{app} below T_c of ~1.7×10^5 (i.e. about half of that measured) after sintering in 100%O_2 and ρ_{max}, for the same material, twice its actual value. There is less contradiction in the values of T_{max}, which all lie on a good straight line between 1 and 100%O_2 (figure 7.6). Such unexpected results may arise from three possible effects: the density of the adsorbed oxygen atoms saturates at ~40%O_2; there is an increase in the charge carrier concentration for some reason; or that the higher concentrations of oxygen

affect the permittivity of the material within the grain boundary layer. These possibilities will be discussed further in later sections, when more information will have been obtained about these samples.

In the previous chapters, plots of $1/\epsilon'_{app}$ versus temperature between T_c and T_{max} were used to find the temperature at which depopulation of the acceptor states started to take place and to estimate values of N_{ao}. Such plots were drawn for the current investigation, a typical series of which are shown in figure 7.10 for samples sintered in 0.5, 5 and 80%O_2. Both the gradients of the plots and the temperatures at which linearity is no longer observed (the depopulation temperature) were affected by oxygen content in the sintering atmosphere. The depopulation temperature for the sample sintered in 5%O_2 was ~240°C, which was reduced to 200°C after sintering in 80%O_2. It appears to be very low for the sample sintered in 0.5%O_2, at ~170°C, in contrast to what may be expected. Depopulation for the samples sintered in >60%O_2 took place very rapidly with temperature, with the slope of the plot of $1/\epsilon'_{app}$ versus temperature changing suddenly at ~200°C. In addition, the slopes of the plots, for all samples, were increased as oxygen content was raised, highlighting the increase in the value of N_{ao} with partial pressure of oxygen.

The ac impedance plots, at first examination, appear to suggest a small reduction in the value of R_{bulk} at the lowest oxygen partial pressures and hence an increase in the concentration of charge carriers. The actual change in the position at which the curve meets the R_s axis at high frequency changes very little, by 0.5Ω. In addition, the analysis described in chapter 3.5.2. emphasises the need for great care with the measurements. As described fully in chapter 3, R_s and X_s are determined in the following way, having measured the capacitance and Q of the circuit without the sample and then with the sample incorporated in series:

$$R_s = \frac{(C_1/C_2)Q_1 - Q_2}{\omega C_1 Q_1 Q_2} \tag{3.15}$$

$$X_s = Q \times R_s \tag{3.13}$$

where

$$Q = \frac{Q_1 Q_2 (C_1 - C_2)}{C_1 Q_1 - C_2 Q_2}. \tag{3.14}$$

The exact value of X_s, therefore, depends on the accurate measurement of C_1 and C_2. When the sample is conducting (resistance typically <100Ω) C_1 and C_2 are often very close together and an accurate value of C_1 - C_2 is difficult to obtain. Hence Q is subject to larger experimental error. In addition, R_s is dependent on the careful measurement of Q_1 and Q_2, the former of which, especially when the sample is conducting, is difficult to obtain accurately. It is reasonable, therefore, only to consider the results of the samples sintered in low oxygen concentrations to be indicative of the difference between grain bulk and grain boundary resistance, i.e. to be qualitative. Hence the small variation in R_{bulk} may be ignored and the value assumed to be given by the more resistive samples sintered in higher oxygen contents as 1.5Ω. Equation 4.26 thus enabled N_d to be calculated to be 2.8 × $10^{18}cm^{-3}$, which can be seen to agree with N_d values of the previous chapters. It is to be noted that R_{bulk} for the samples sintered in 10% and 80%O_2 are identical, indicating no change in N_d at the highest oxygen concentrations during sintering. This can be verified since the average size of the grains of all samples have been found to be approximately the same, indicating that, overall, the concentration of incorporated donor dopant is the same.

7.4. ANALYSIS OF EXPERIMENTAL RESULTS

7.4.1. Calculation of acceptor state density

In the previous chapter it was shown that, where normalisation of resistance data was not necessary, the resistivity, above T_c and below the temperature of grain boundary acceptor state depopulation, may be written (equation 6.3),

$$\rho = C_o exp\left(\frac{A(T-\theta)}{T}\right)$$

where the slope of the linear portion is given by equation 4.24,

$$A = \frac{e^2 N_{ao}^2}{8\epsilon_o C k N_d}$$

and C_o is a constant. Making the assumption that the permittivity, ϵ', of the material within the grain boundary layers is unaffected by the sintering atmosphere, Arrhenius plots of lnρ versus (T - θ)/T may be drawn to obtain N_{ao} from the gradient A, of the linear portion. It may be anticipated that, as the oxygen content of the sintering atmosphere is reduced, so is the gradient of the Arrhenius plot and hence N_{ao} become smaller.

Such plots were drawn for all samples of the present investigation, a typical series of which are shown in figure 7.11 for samples sintered in 60%, 20%, 5%, 2% and 1%O_2 atmospheres. It can clearly be seen that the gradient becomes smaller as oxygen partial pressure during sintering is reduced, suggesting that N_{ao} also becomes smaller. In addition, the range over which the plots are linear is extended to increasingly higher temperatures as oxygen content is reduced, in agreement with the plots of $1/\epsilon'_{app}$ versus temperature (figure 7.10) and the T_{max} values (figure 7.6). This indicates that depopulation of the acceptor states takes place at increasing temperatures, as a result of the lowering of the grain boundary potential barrier associated with reduced values of N_{ao}. Least - squares analyses of the points lying in straight lines were performed for every sample to obtain the best estimates of the gradients. The correlation coefficient, r, of the points to the solid line for each sample was >0.99, giving statistical confidence in these results. The slope of the Arrhenius plots of lnρ versus (T - θ)/T and N_{ao} values thus obtained are listed in table 7.1, where a gradual increase in the grain boundary acceptor state density can be seen between 0.18 and 60%O_2 sintering atmosphere. N_{ao} was plotted against partial pressure of oxygen to observe any correlation between the parameters, as shown in figure 7.12, where, between 0.18 and ~60%O_2, N_{ao} can be seen to follow approximately a straight line. Above 60%O_2 sintering atmosphere N_{ao} appears to reach a saturation value, remaining

constant at $\sim 7 \times 10^{13} cm^{-2}$. Least - squares analysis was performed on all points to give the solid line drawn on figure 7.11, the gradient of which was $6.08 \times 10^{12} cm^{-2} atm^{-1}$, with excellent correlation (r = 0.96). From simple algebra, an empirical relationship between the oxygen partial pressure compared with total pressure during sintering, p_{O_2}, and the density of grain boundary acceptor states was obtained,

$$N_{ao}(p_{O_2}) = (7.52 + 0.608 ln p_{O_2}) \times 10^{13}. \tag{7.1}$$

This relationship demonstrates the controlling effect on the grain boundary acceptor state density of the partial pressure of oxygen during sintering. It also suggests that there are other electron traps present at the grain boundaries, possibly impurity ions or barium vacancies, which are unaffected by the oxygen partial pressure. The number of oxygen atoms adsorbed onto the grain boundaries, however, determine the effective density of acceptor states in these regions.

The above calculations of N_{ao} from the Arrhenius plots of lnρ versus (T - θ)/T included the assumption that the permittivity of the material within the grain boundary layer, ϵ', is unaffected by the sintering atmosphere. To verify this assumption, the slope of the plots of $1/\epsilon'_{app}$ versus temperature (figure 7.10), together with the experimentally obtained values of A (the gradient of the Arrhenius plots of lnρ versus (T - θ)/T) and N_d, may be used to calculate C, the Curie constant. The slope, m, of the plots of $1/\epsilon'_{app}$ versus temperature above T_c, is given by

$$m = \frac{1}{C} \times \frac{N_{ao}}{dN_d}. \tag{7.2}$$

N_{ao} is obtained from A using equation 4.27, which includes the use of C. Therefore,

$$C = \sqrt{\frac{8\epsilon_o C k N_d}{e}} \times A \times \frac{1}{m} \times \frac{1}{dN_d}. \tag{7.3}$$

Simplification of equation 7.3 gives an expression for C in terms of the gradients of the linear portions of the Arrhenius plots of lnρ versus (T - θ)/T and the plots

of $1/\epsilon'_{app}$ versus T, above T_c,

$$C = \frac{8\epsilon_o k}{ed^2 N_d} \times \frac{A}{m^2}. \tag{7.4}$$

C was thus calculated for samples sintered in all oxygen concentrations and the results listed in table 7.2, together with the experimentally obtained values of A and m. Excellent agreement can be seen to have been achieved between the calculated and actual values of C (1.5×10^5), with an average error of 12%.

These results show that C is not affected by the oxygen atmosphere during sintering. In addition, the shape of the plots of ϵ'_{app} versus temperature are all very similar (figure 7.7), showing that the Curie temperature and therefore θ, the Curie point, are not changed in any way by the sintering atmosphere. θ can also be seen to be unaffected by oxygen partial pressure, by means of the temperature at which the straight lines of figure 7.10 (the plots of $1/\epsilon'_{app}$ versus T) reach the temperature axis: they can all be extrapolated to approximately the same temperature, 100-115°C. It may be concluded, therefore, that the permittivity of the material within the grain boundary layers is not affected by the sintering atmosphere.

7.4.2. Calculation of acceptor energy

The suggestion in the previous section that the amount of oxygen adsorbed onto the grain boundaries during sintering and cooling controls the grain boundary acceptor state density can be verified by calculating the acceptor energy, E_a, in the usual manner. Resistivity above the maximum was analysed using Arrhenius plots of $\ln\rho$ versus 1/T for samples sintered in every atmosphere. The slope of these plots gave $\phi_{o(max)}$, the maximum grain boundary potential barrier height. N_a was calculated at a suitable temperature above the maximum: 400°C was chosen in the present case. It was then substituted into equation 4.31, together with the required value of E_F, the Fermi energy, and E_a was thus obtained. The samples sintered in <1%O_2 had very high values of T_{max} and only a short

temperature range was available over which the resistivity could be measured above the maximum. Consequently, E_a could not be calculated for these samples. Figure 7.13 shows resistivity, plotted on a logarithmic scale, versus 1/T above T_{max} for typical samples sintered in 60%, 20%, 5% and 1%O_2, where the gradient and hence $\phi_{o(max)}$ can be seen to decrease with oxygen content. In addition, the range of temperatures available for this mesurement decreases, particularly below 5%O_2, as the oxygen concentration during sintering was reduced. Values of $N_a(400°\ C)$, $\phi_{o(max)}$ and E_a are listed in table 7.3 for all samples sintered in >1%O_2. Least - squares analysis was performed on the Arrhenius plots of lnρ versus 1/T above the maximum to determine the gradients; correlation of the points to the solid lines drawn was very good, with r ~0.99 for all samples. E_a for all sintering atmospheres was found to be 0.9 ±0.1eV, with the exception of the samples sintered in 1% and 2%O_2. These samples had E_a = 0.7eV, although this difference is probably due to errors in obtaining an accurate value of $\phi_{o(max)}$ from the lnρ versus 1/T plot because of the small number of points, rather than to any change in the nature of the acceptor states.

These values of E_a are in agreement with those obtained for both donor concentration studies and for the Mn-free sample of the previous investigation, as well as with estimates in the literature[7.8–7.13]. It suggests strongly that the oxygen atoms adsorbed onto the grain boundaries during sintering are the dominant factor in controlling the energy and density of acceptor states.

7.5. CONCLUSION

Samples of a standard composition were sintered in oxygen concentrations between 0.18% and 100%O_2. The magnitude of the PTCR characteristic and the values of apparent permittivity below T_c were found to become smaller as the partial pressure of oxygen was reduced, corresponding to a reduction in the density of grain boundary acceptor states. It was also shown that the permittivity

of the material within the grain boundary layers was not changed by the partial pressure of oxygen during sintering, either by means of the Curie constant or the Curie point. An empirical relationship between N_{ao} and oxygen partial pressure during sintering showed that the grain boundary acceptor state density varies logarithmically. In addition, it revealed that there appear to be grain boundary electron traps which are unaffected by oxygen partial pressure, possibly barium vacancies or segregated impurity ions. The acceptor energy was found to remain constant, at 0.9 $\pm$0.1eV for all sintering atmospheres, demonstrating the dominant nature of adsorbed oxygen atoms as grain boundary acceptor traps.

REFERENCES

7.1 Drofenik M., Popovic A., Irmancnik L, Kolar D. and Krasevec V., J. Am. Ceram. Soc., **65**, C203, 1982.

7.2 Drofenik M., Popvic A. and Kolar D., Ceram. Bull., **63**, 702, 1984.

7.3 Drofenik M., J. Am. Ceram. Soc., **69**, C8, 1986.

7.4 Drofenik M., J. Am. Ceram. Soc., **70**, 311, 1987.

7.5 Zajc I. and Drofenik M., Br. Ceram. Trans. J., **88**, 223, 1989.

7.6 Jonker G.H., Mater. Res. Bull., **2**, 401, 1967.

7.7 Hewyang W., Sol. Stat. Electron., **3**, 51, 1961.

7.8 Hewyang W., J. Am. Ceram. Soc., **47**, 484, 1964.

7.9 Heywang W., J. Mater. Sci., **6**, 214, 1971.

7.10 Jonker G.H., Sol. Stat. Electron., **7**, 895, 1964.

7.11 Daniels J. and Härdtl K.H., Phil. Res. Rep., **31**, 489, 1976.

7.12 Ihrig H. and Puschert W., J. Appl. Phys., **48**, 3081, 1977.

7.13 Daniels J., Härdtl K.H. and Wernicke R., Phil. Tech. Rev., **38**, 73, 1978/79.

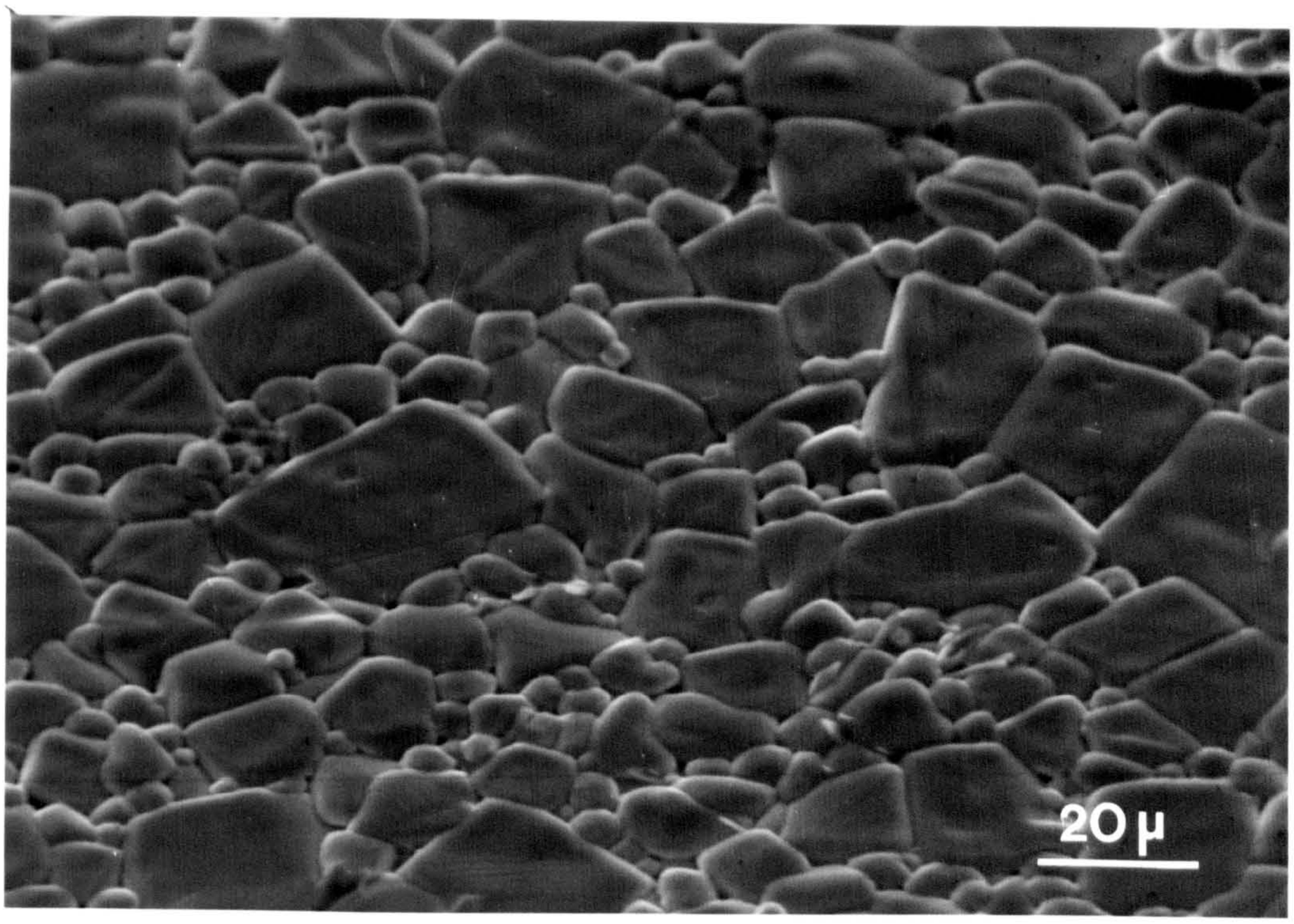

Figure 7.1 Scanning electron micrograph of an area of a sample sintered in 80%O_2 (bar = 20μm).

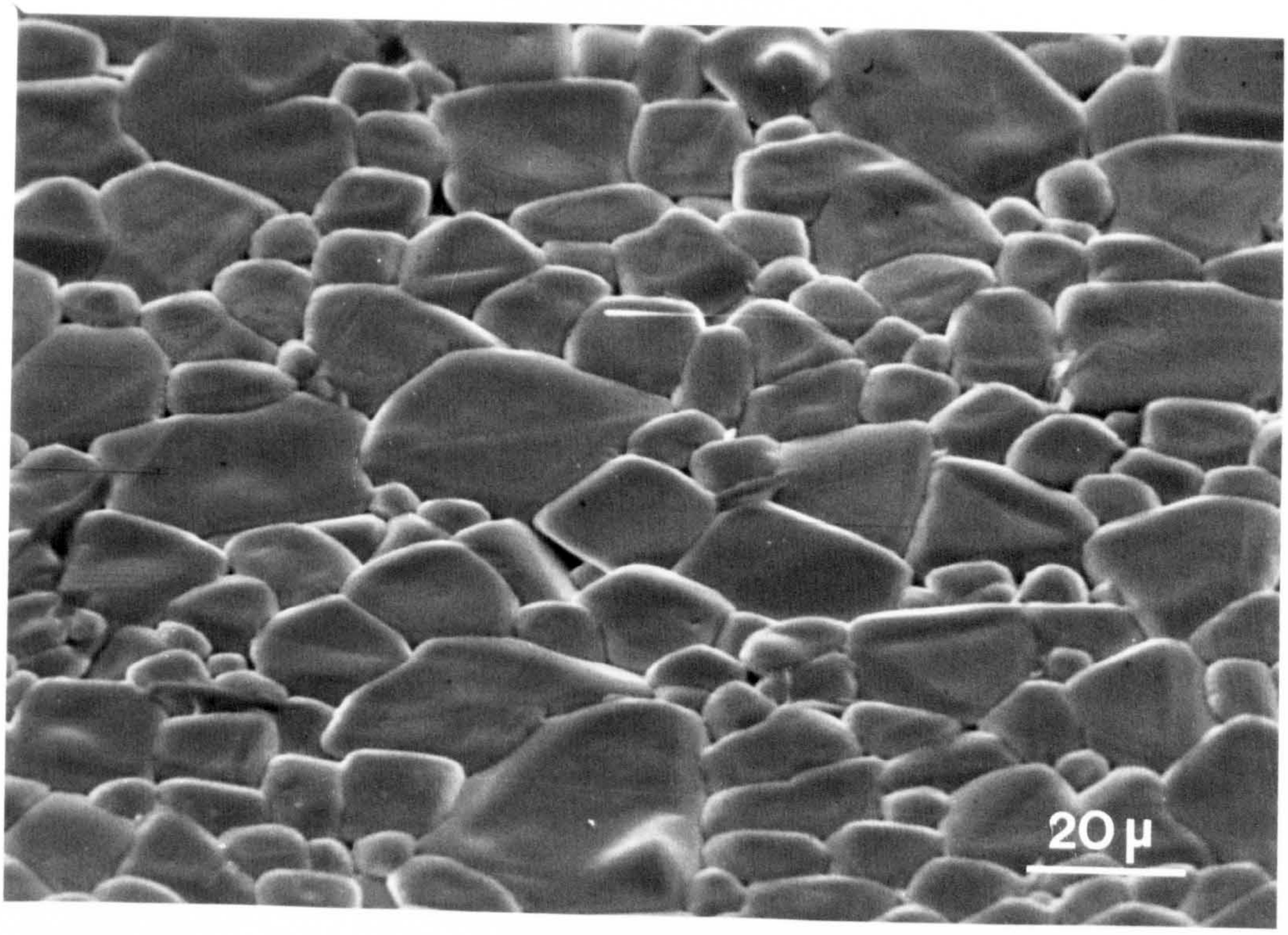

Figure 7.2 Scanning electron micrograph of a sample sintered in 0.25%O_2 (bar = 20μm

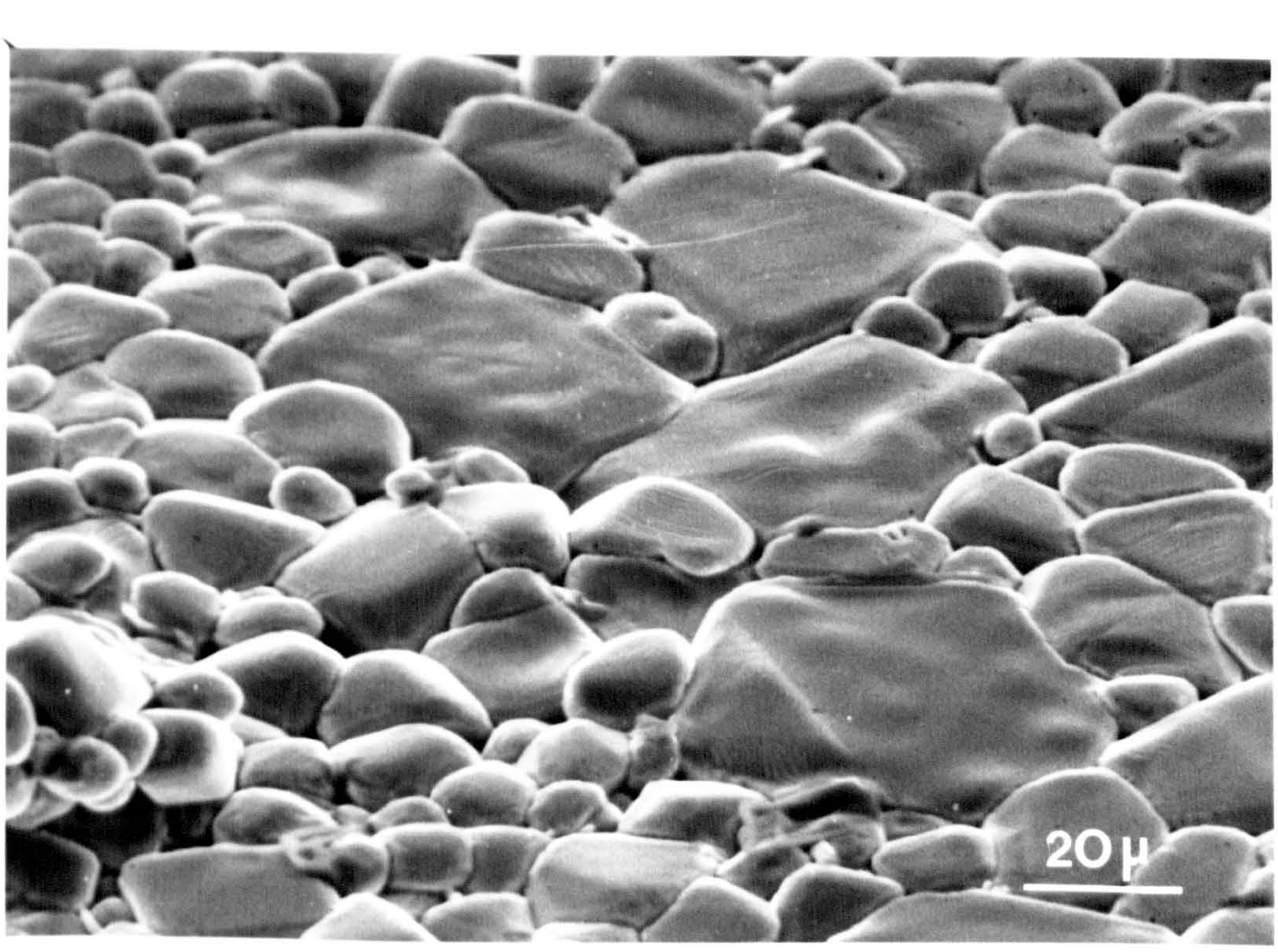

Figure 7.3 Scanning electron micrograph of a typical sample sintered in 100%N_2 (bar = 20μm).

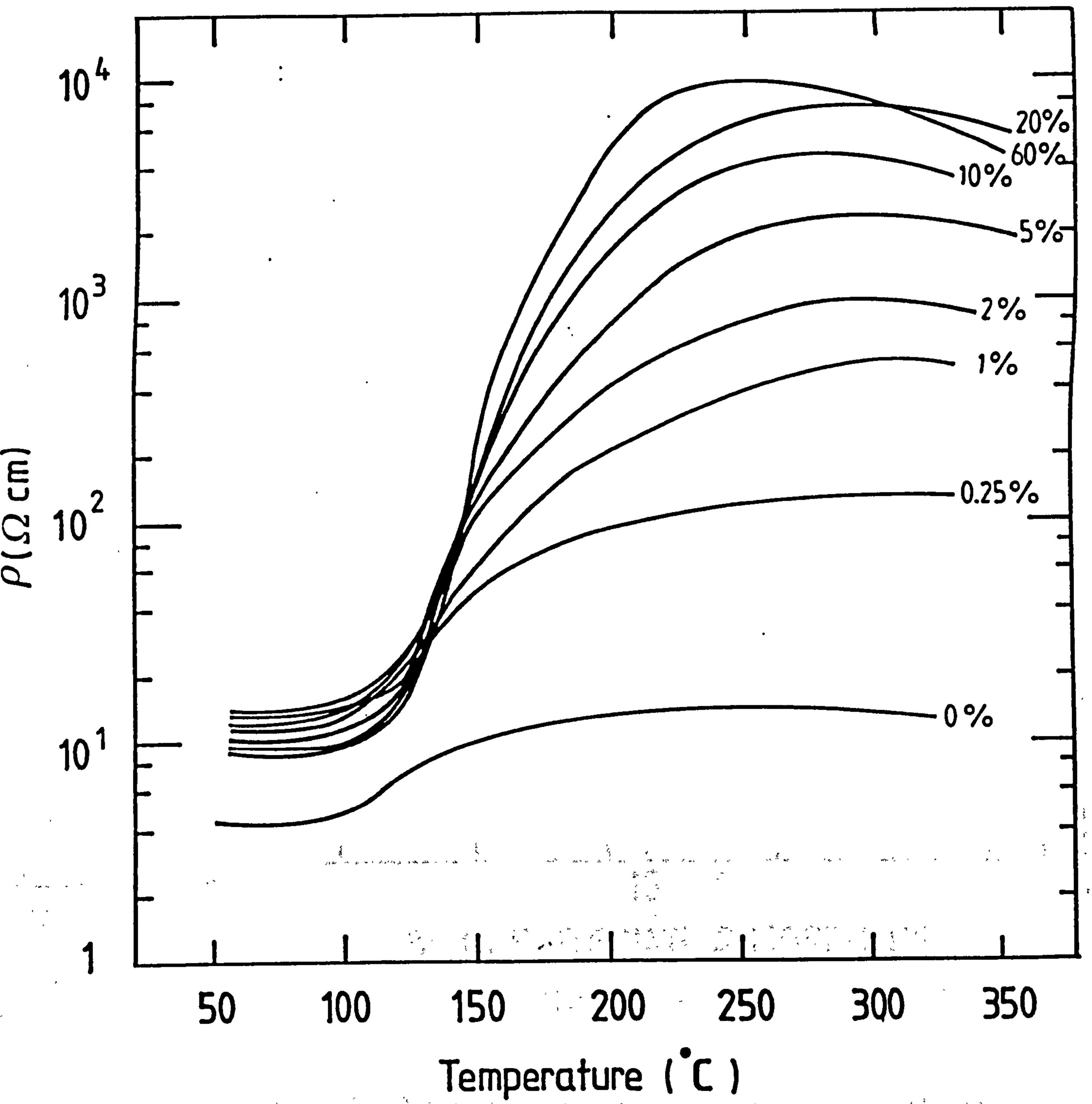

Figure 7.4 Resistivity - temperature characteristics of samples sintered in oxygen atmospheres between 60% and 0% O_2.

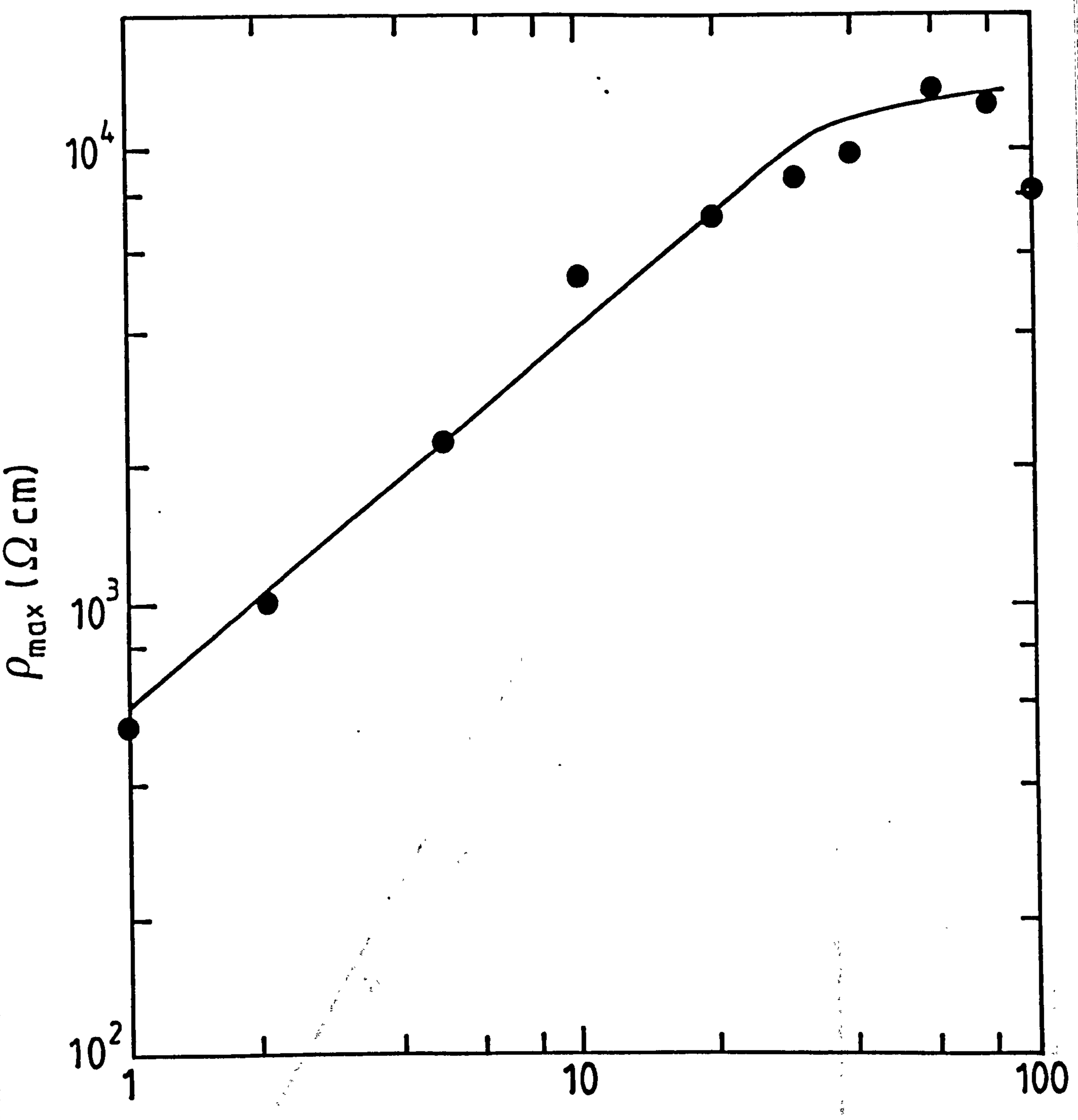

Figure 7.5 Dependence of ρ_{max} on oxygen content during sintering.

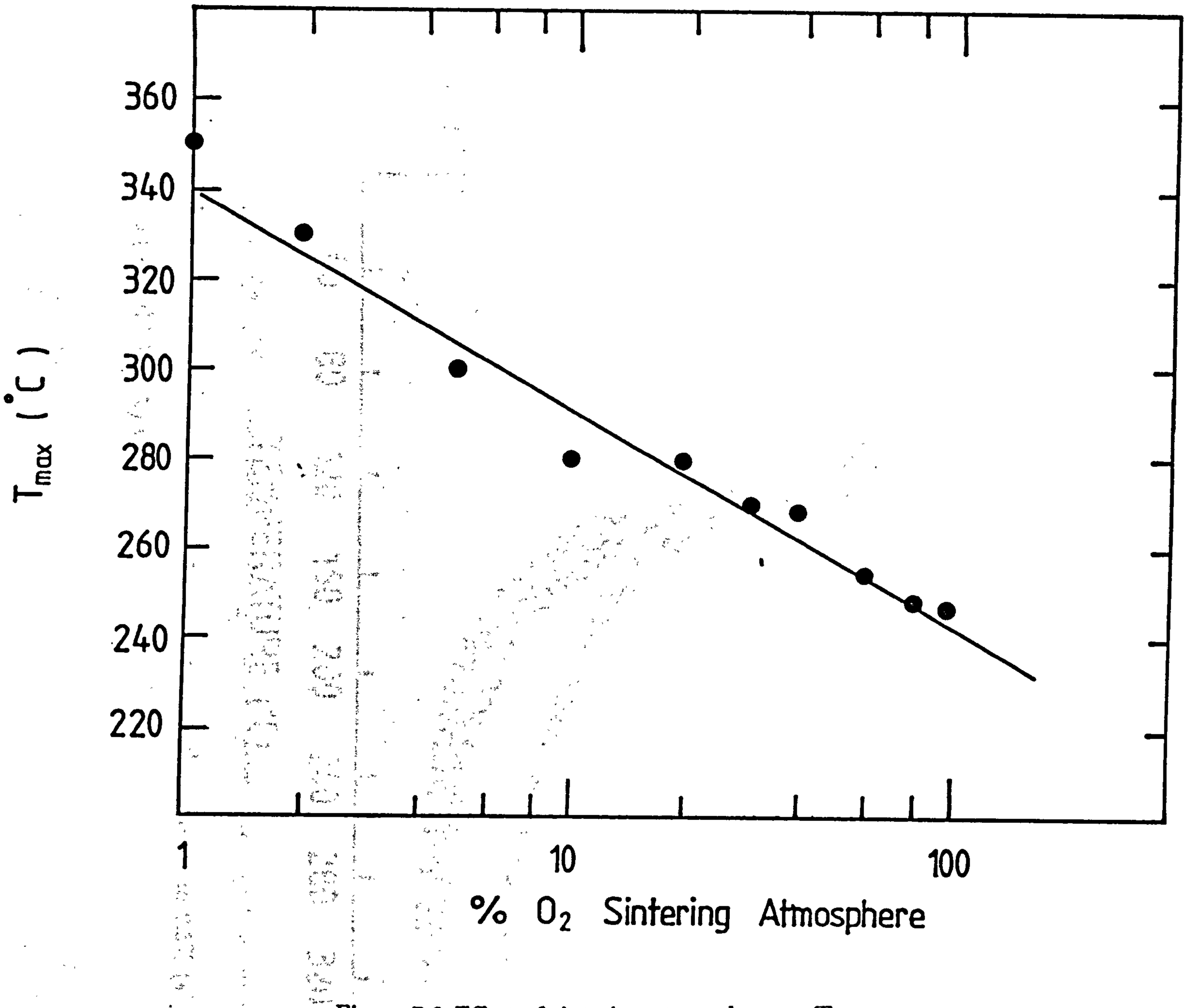

Figure 7.6 Effect of sintering atmosphere on T_{max}.

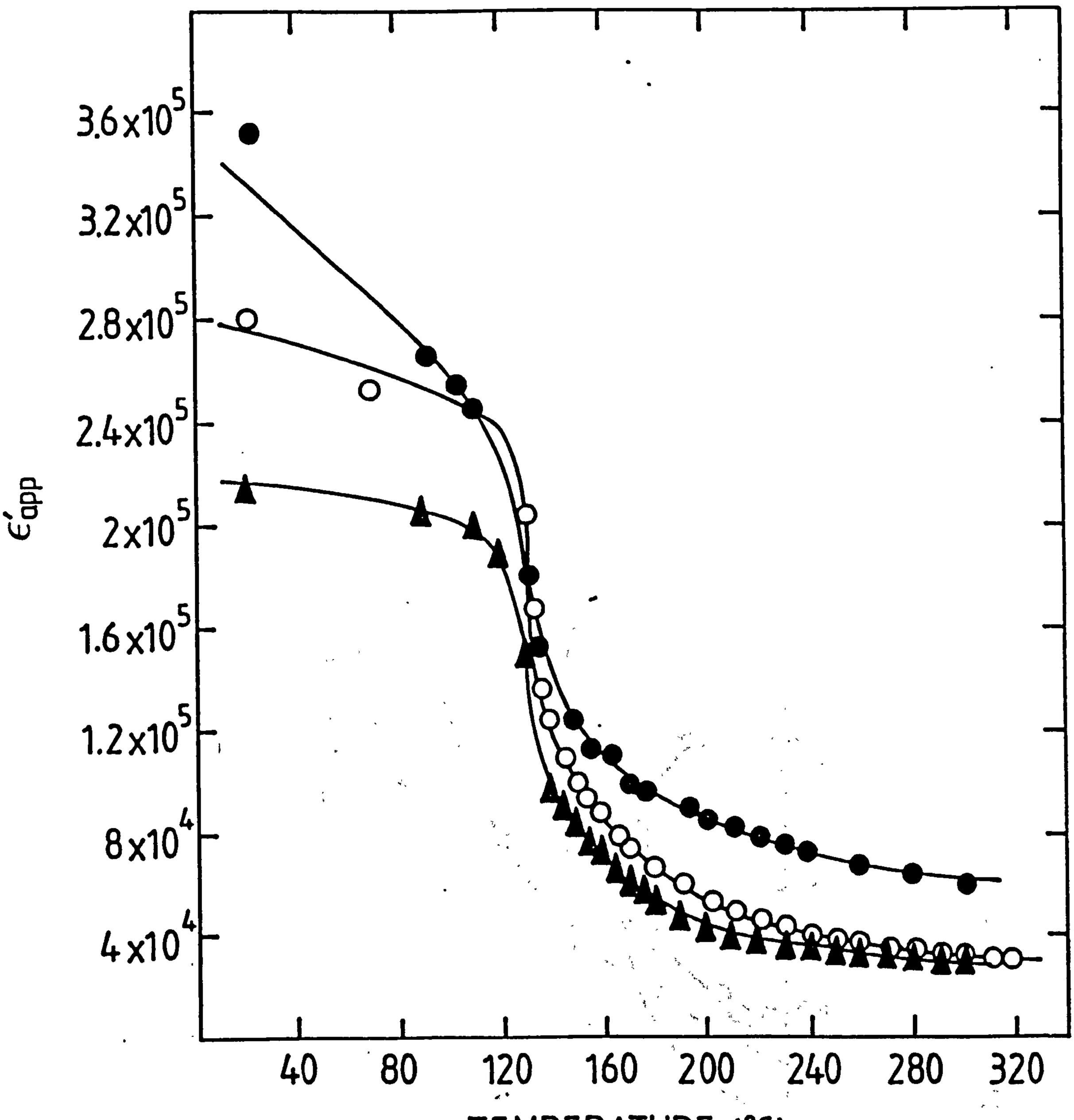

Fgigure 7.7 Apparent permittivity versus temperature for samples sintered in 0.5% (•), 5% (o) and 30% (▲) O_2.

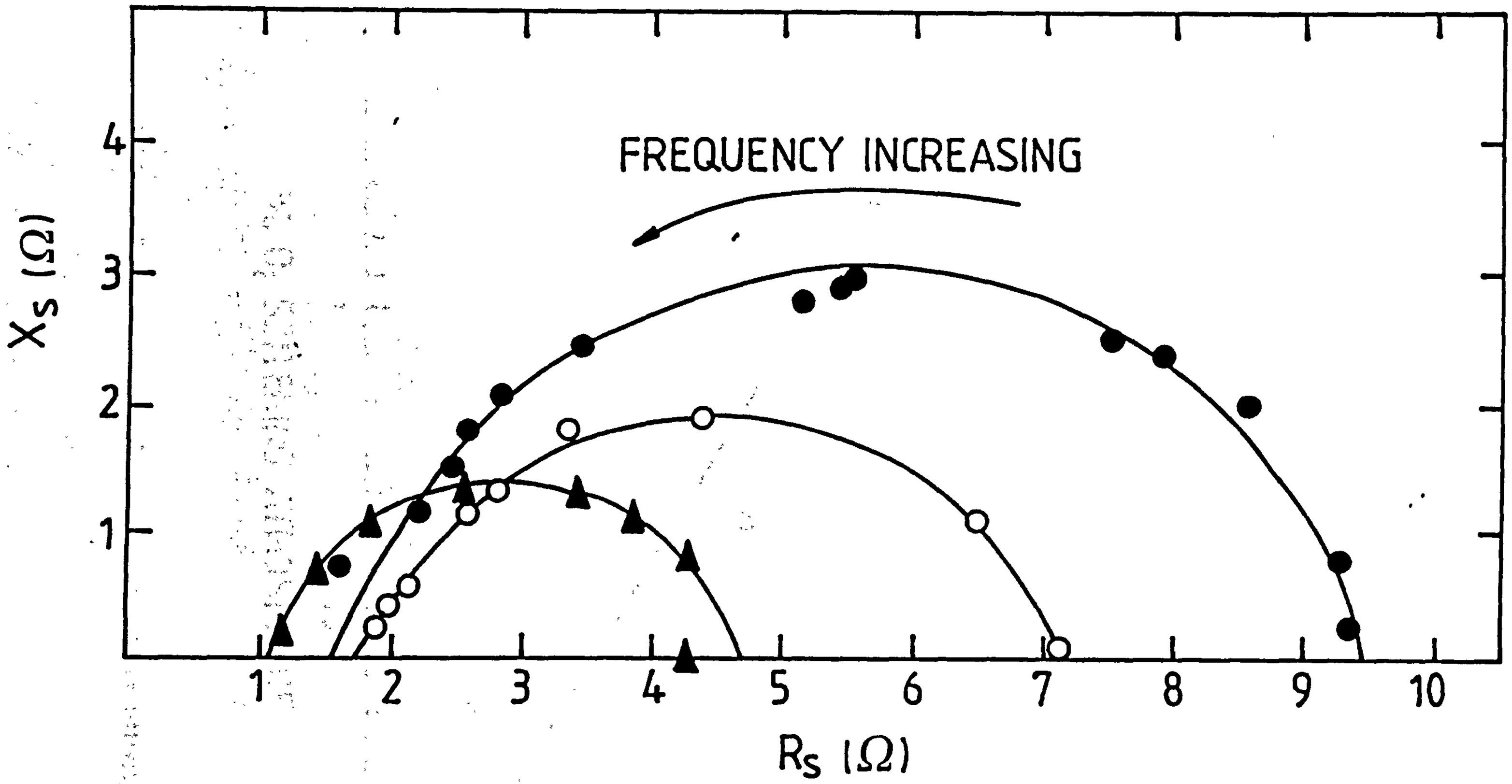

Figure 7.8 A.c. impedance plots for samples sintered in 80% (o), 10% (•) and 1% (▲) O_2.

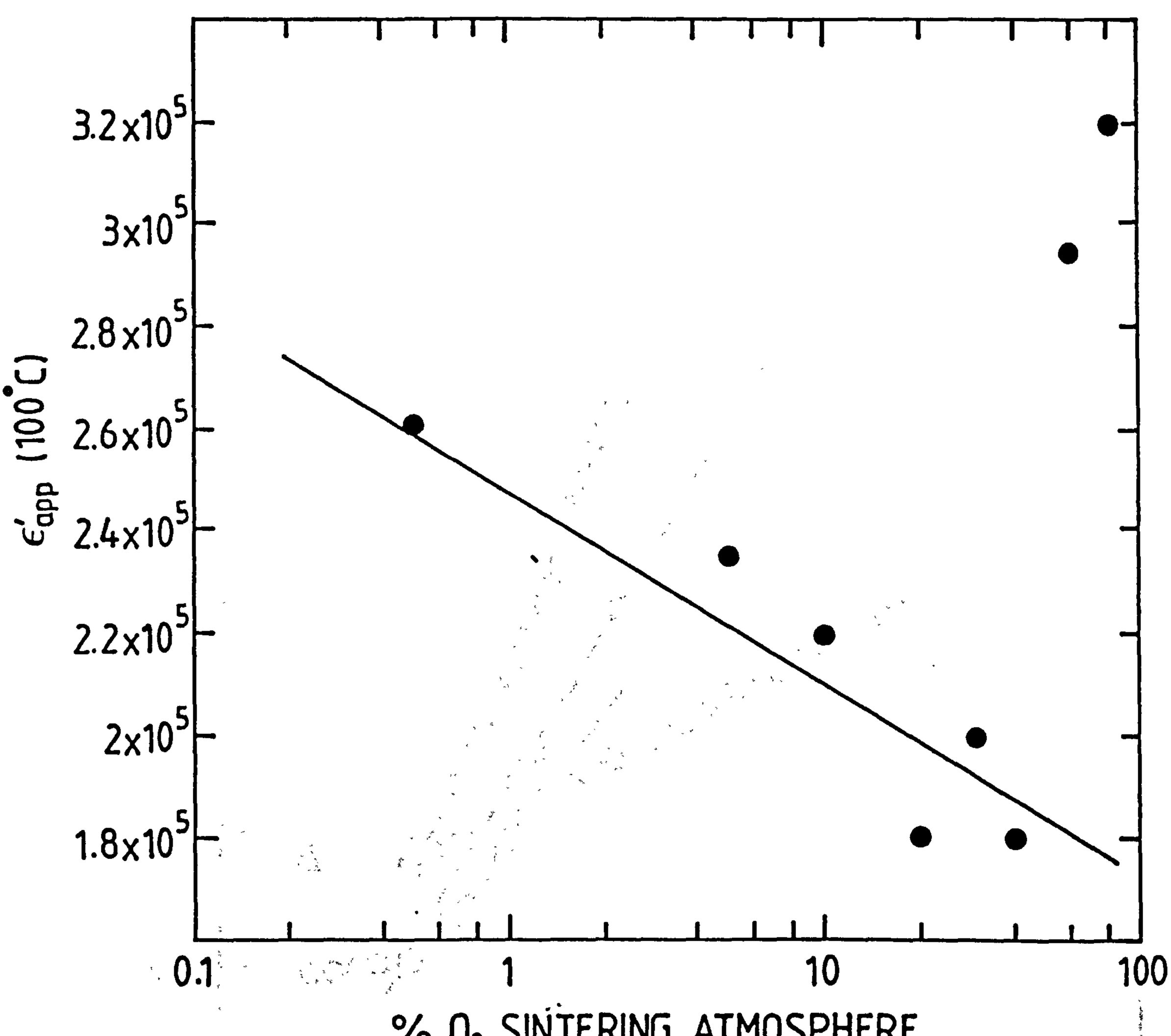

Figure 7.9 Effect of sintering atmosphere on apparent permittivity at 100°C.

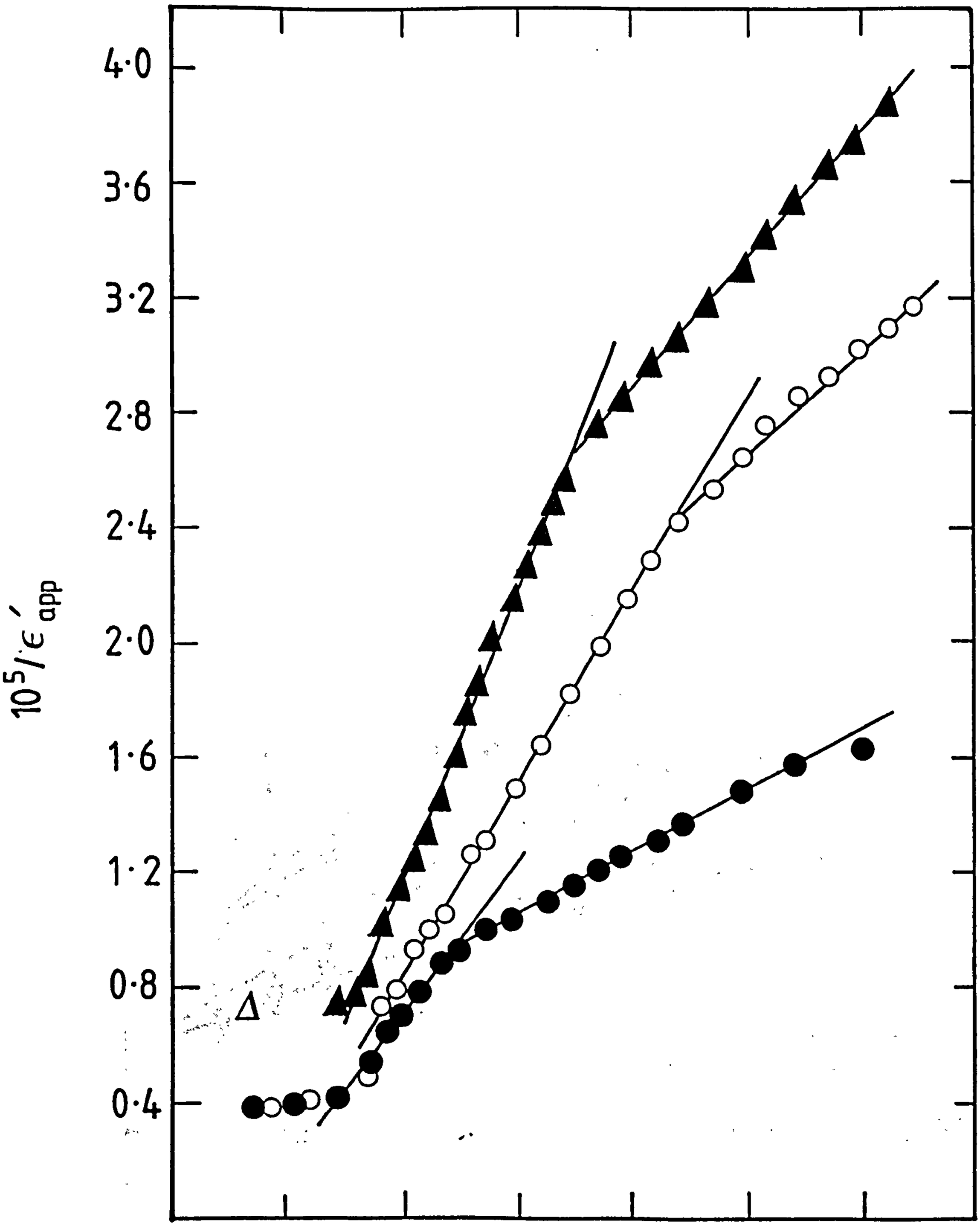

Figure 7.10 $1/\epsilon'_{app}$ versus temperature above T_c for samples sintered in 0.5% (•), 5% (○) and 30% (▲) O_2.

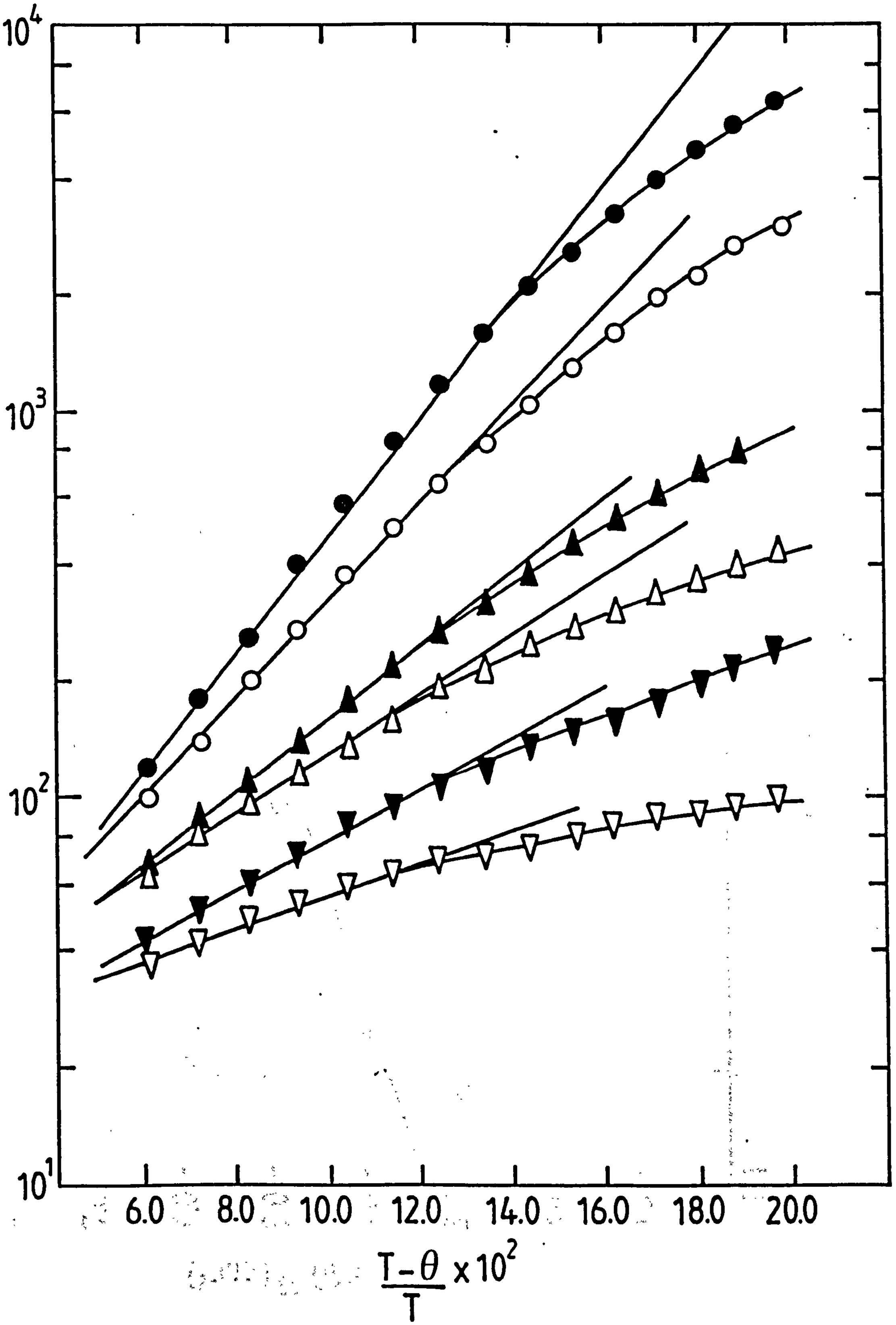

Figure 7.11 Arrhenuis plots of lnρ versus (T - θ)/T for samples sintered in 0.25% (▽), 1% (▼), 2% (△), 5% (▲), 20% (o) and 60% (•) O_2.

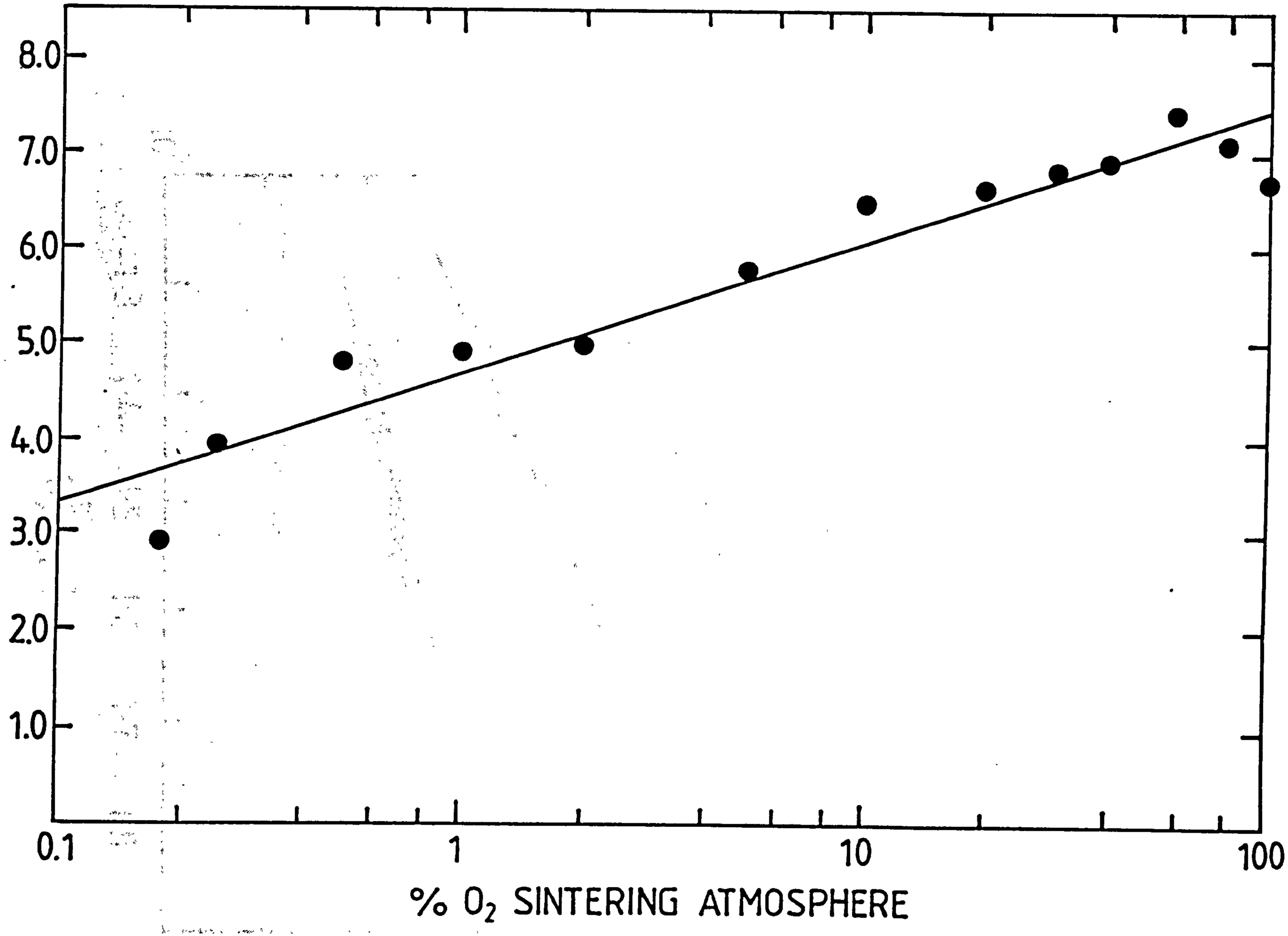

Figure 7.12 Dependence of N_{ao} on oxygen partial pressure during sintering.

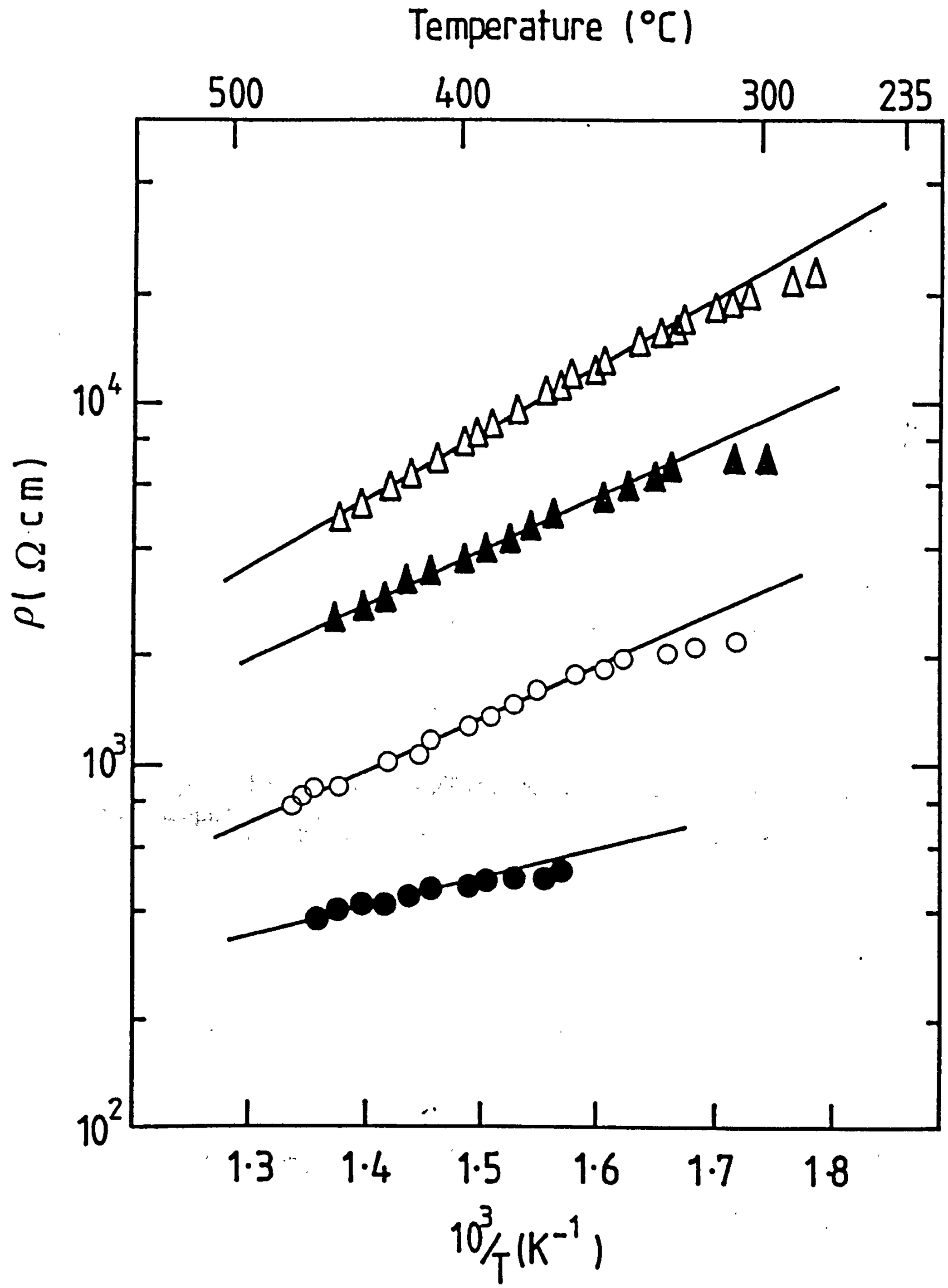

Figure 7.13 Lnρ versus 1/T above T_{max} for samples sintered in 1% (•), 5% (o), 20% (▲) and 60% (△) O_2. For the purposes of clarity, the points belonging to the sample sintered in 60% O_2 have been plotted a factor of two above their actual values.

% O_2 Sintering Atmosphere	A	N_{ao} (cm^{-2})
100	29.2	6.8×10^{13}
80	32.1	7.2×10^{13}
60	34.9	7.5×10^{13}
40	30.4	7.0×10^{13}
30	29.4	6.9×10^{13}
20	28.4	6.7×10^{13}
10	26.4	6.5×10^{13}
5	20.7	5.8×10^{13}
2	15.6	5.0×10^{13}
1	14.8	4.9×10^{13}
0.5	14.4	4.8×10^{13}
0.25	9.3	3.9×10^{13}
0.18	5.4	2.9×10^{13}

TABLE 7.1

Slope of the Arrhenius plots of $\ln\rho$ versus $(T-\theta)/T$ and total ionized grain boundary acceptor state density, for all samples.

% O_2 Sintering Atmosphere	A	m	Estimated C (K)	% error from 1.5×10^5 (K)
100	29.2	2.03×10^{-7}	1.37×10^5	9
80	32.1	2.47×10^{-7}	1.01×10^5	33
60	34.9	2.07×10^{-7}	1.57×10^5	5
40	30.4	2.12×10^{-7}	1.30×10^5	13
30	29.4	2.11×10^{-7}	1.24×10^5	17
20	28.4	2.15×10^{-7}	1.18×10^5	21
10	26.4	1.79×10^{-7}	1.59×10^5	6
5	20.7	1.68×10^{-7}	1.42×10^5	5
0.5	14.4	1.34×10^{-7}	1.54×10^5	3

TABLE 7.2

Slope of the Arrhenius plots of $\ln\rho$ versus $(T-\theta)/T$ and of the plots of $1/\varepsilon'_{app}$ versus T which were used to estimate C, and the error of C from 1.5×10^5, for all samples measured.

% O_2 Sintering Atmosphere	ϕ_o (max) (eV)	N_a (400°C) (cm^{-2})	N_a/N_{ao}	E_a (eV)
100	0.42	5.89×10^{13}	0.87	0.99
80	0.33	4.62×10^{13}	0.64	0.90
60	0.31	4.49×10^{13}	0.60	0.88
40	0.26	4.11×10^{13}	0.59	0.83
30	0.37	4.91×10^{13}	0.72	0.96
20	0.29	4.35×10^{13}	0.65	0.87
10	0.26	4.11×10^{13}	0.60	0.83
5	0.28	4.30×10^{13}	0.74	0.88
2	0.14	3.02×10^{13}	0.60	0.71
1	0.13	2.93×10^{13}	0.60	0.70

TABLE 7.3

Maximum grain boundary potential barrier height, acceptor state density at 400°C and acceptor energy, for samples sintered in >1% O_2.

CHAPTER EIGHT

THE EFFECT OF SINTERING ATMOSPHERE AND ADDITIONAL ACCEPTOR DOPING ON THE PTCR EFFECT

The results of chapter six demonstrated the effect of a small amount of additional acceptor ions on the PTCR characteristc, in particular the increase in its magnitude resulting from the raised values of N_{ao} and E_a, the acceptor state density and energy, respectively. This was explained in terms of segregation of the acceptor ions to the grain boundary regions, there being no difference in the bulk grain charge carrier concentration between Mn-doped and Mn-free samples. In the last chapter the influence of sintering atmosphere on the value of N_{ao} was clearly demonstrated, resulting in the derivation of an empirical relationship between acceptor state density and oxygen partial pressure. There being no discernable change in E_a as oxygen partial pressure was reduced towards 10^{-3} atmospheres, it was concluded that the adsorbed oxygen atoms were the most dominant species of acceptor within that particular material.

The samples employed in the last chapter were of a standard composition, containing 0.4 at%Ho concentration. The exact nature of the dominant acceptor states for these samples cannot be exactly identified, although by speculation of the experimental and analytical results, they were concluded to be grain boundary oxygen. If, on the other hand, the dominant acceptor state is controlled and samples investigated in the same way, the effect of sintering atmosphere will enlighten particularly the effect of the adsorbed oxygen atoms on the values of N_{ao} and E_a. The purpose of the present investigation was to use samples additionally doped with a small amount of acceptor ions (manganese) to increase N_{ao} and E_a artificially and then to observe and analyse the effect of sintering atmosphere on the grain boundary characteristics. These were then able to be compared with the results of the Mn-free samples belonging to the last chapter.

8.1. SAMPLE PREPARATION

Samples having composition $Ba_{0.996}Ho_{0.004}Ti_{0.9996}Mn_{0.0004}O_3$, i.e. $BaTiO_3$ containing 0.4 at%Ho and 0.04 at%Mn, were prepared in the usual manner, together with 0.3 mol%Si_3N_4 and 0.5 mol%TiO_2 sintering aids. Their nominal composition was the same as that of the samples of chapter six, except that $BaTiO_3$ powder was used as the precursor instead of $BaCO_3$ and TiO_2. Following ball-milling and binder addition the small pellets 4mm in diameter were pressed in the standard way. Samples were sintered identically to those of the last chapter, in the tube furnace at 1400°C for 60 minutes, preceeded by binder burn-out at 500°C and followed by slow cooling to 800°C and furnace cooling thereafter to room temperature. The sintering atmosphere was controlled between 0.18 and 100%O_2 and made up to 100% by O_2-free N_2. Samples were also sintered in 100%N_2 for comparison. The gas flowed through the furnace at a steady rate of 1 l/min.

The microstructure of samples from each batch was examined using the SEM and EDX facilities. The average size of 200 - 300 grains was measured using the area count method. Any surface features, particularly of second phase were also studied with EDX to determine their chemical composition.

Resistivity - temperature measurements between 40 and ~450°C were made with four nominally identical samples from each batch to ensure reproducibility and accuracy. Some samples were then thinned for the a.c. impedance measurements at room temperature in the audio and radio frequency ranges. Ohmic contacts were obtained, as usual, by rubbing In/Ga amalgam onto the flat surfaces.

8.2 EXPERIMENTAL RESULTS

8.2.1. Microstructure

All samples sintered to a dark blue-green colour and ≥90% density. Average grain size was measured for each type of sample and found, as for the last chap-

ter, to be ~8μm in all cases, with a similar grain size distribution. The exception was the sample sintered in 100%N_2, which had grains 15μm across. The shape of the grains, however, was affected by sintering atmosphere, with those sintered in the lower oxygen concentrations (<1%) having flat, evenly sized grains, as demonstrated in the micrograph of the sample sintered in 0.5%O_2 in figure 8.1. As oxygen content was increased, the grains became more rounded and less evenly sized, as shown in figure 8.2, which is a micrograph of a sample sintered in 40%O_2. The general trend of grain shape as oxygen concentration was increased towards 100% was towards rounded, boulder - like shapes and the grains themselves became less evenly sized, ranging between ~5μm and 20-30μm.

The surfaces of some of the samples had second phase features, rich in Si and Ti, between and across the grains, demonstrating good densification of the grains within the bulk of the samples. More surface second phase was present on the samples sintered in low oxygen contents (<0.5%), where the grains were more flat and fitted together more tightly.

8.2.2. Resistivity measurements

There being very little difference in average grain size between samples sintered in different atmospheres, normalization of the resistance data was not necessary. Samples sintered in 20%O_2 had resistivity - temperature characteristics qualitatively similar to those of the Mn-doped samples of chapter 6 (figure 6.3), with room temperature resistivity, ρ_{RT}, ~20Ωcm and maximum resitivity, ρ_{max}, 3.5 $\times$ $10^5\Omega$cm. The PTCR characteristic extended over a wide temperature range, with ρ_{max} being found at $T_{max} = 326°C$.

As oxygen concentration was increased above that of air, ρ_{RT} increased slightly to 35Ωcm for the sample sintered in 80%O_2. In a similar manner, ρ_{max} increased, but more dramatically, being close to 3 $\times$ $10^6\Omega$cm for the same sample. Those sintered in 100%O_2 had slighlty reduced PTCR characteristics, with ρ_{RT} ~30Ωcm

and $\rho_{max} = 1.5 \times 10^6 \Omega$cm. This trend can be compared with the observations of resistivity values for the Mn-free samples of the last chapter, where the magnitude of the PTCR characteristic for samples sintered in $\geq 80\%O_2$ appeared to saturate and diminish (figure 7.4).

Reduction of the oxygen concentration below that of air resulted in smaller PTCR characteristics, as expected from the observations of the samples of the last investigation, with ρ_{RT} for samples sintered in $5\%O_2$ $\sim$15Ωcm and decreasing to 10Ωcm for those prepared in $0.5\%O_2$. Maximum resistivity also reduced in accordance with oxygen partial pressure, being $2.2 \times 10^4 \Omega$cm for the samples sintered in $5\%O_2$ and $3 \times 10^3 \Omega$cm after sintering in $0.5\%O_2$. T_{max}, likewise, increased in value, from 330°C when sintering took place in $5\%O_2$ to >400°C at the lowest oxygen concentrations (<$1\%O_2$). When the samples were sintered in $100\%N_2$, no PTCR effect was observed at all.

Typical resistivity - temperature characteristics of samples sintered in 80%, 20%, 10%, 5%, 1%, 0.5% and 0% O_2 are shown in figure 8.3, where the magnitude of the resistivity characteristic can be seen to diminish with oxygen partial pressure. The effect of oxygen atmosphere on ρ_{max} and T_{max} is demonstrated in figures 8.4 and 8.5, respectively, where ρ_{max} falls and T_{max} increases approximately linearly, below $80\%O_2$, with reducing oxygen concentration. Comparison of these data with the results of the last chapter (figures 7.4 and 7.5) show qualitative agreement.

8.2.3. A.c. impedance plots

Room temperature a.c. impedance plots in the audio and radio frequency ranges were carried out on samples sintered in 80%, 10%, 5%, 2% and $0.5\%O_2$. X_s versus R_s was plotted as usual for all samples to observe the effect of sintering atmosphere on the grain boundary and grain bulk resistance of the material. Figure 8.6 shows the a.c. impedance plots for typical samples sintered in 80%,

10% and 2% O_2, where it can be seen that R_{bulk} is constant at $\sim 2\Omega$ for all samples, with the increase in sample resistance with increasing oxygen concentration being entirely due to the grain boundaries. These results show good agreement with those of the last chapter (figure 7.8).

8.3. DISCUSSION

8.3.1. Microstructure and morphology

The samples sintered in 100%N_2 had grains approximately twice the size of the mean grain size of samples sintered in 0.18 - 100%O_2, in agreement with the results of the last chapter and of Drofenik[8.1.8.2], showing grain growth to have proceeded unhindered and in accordance with equation 4.35,

$$BaO_{latt} + \frac{1}{2}Ho_2O_3 \rightarrow (HoO)_{iatt} + \frac{1}{4}O_2 + e^-.$$

The incorporation of oxygen into the sintering atmosphere appears to constrain this reaction so that grain growth is restricted to 8μm. A slight trend in grain size was observed, however, with the average size of grains of samples sintered in <0.5%O_2 found to be $\sim$10μm, compared with $\sim$7μm after sintering in >10%O_2. This suggests that the reaction equation 4.35 above was driven to the right slightly more readily during sintering in the lowest amounts of oxygen, resulting in slightly larger grains.

As the oxygen concentration of the sintering atmosphere was increased above 5%, the homogeneity of the microstructure was reduced, in agreement with the last chapter's results. It was proposed (chapter 7.3.1.) that donor incorporation and grain growth takes place locally during sintering, resulting in regions of large and small grains where there were different quantities of donor dopant incorporated. The present results are consistent with this proposal, where unevenly sized grains between $\geq$20μm and 5μm are apparent in figure 8.2, for the sample sintered in 40%O_2.

8.3.2. Resistivity characteristics

As oxygen content of the sintering atmosphere was increased above 0.18%, the magnitude of the PTCR characteristic, i.e. the value of ρ_{max}, was raised in agreement with the results of Jonker[8.3] and of the last chapter. The effect of the addition of the acceptor ions to the present samples may be observed by comparing the results with those of previous equivalent samples. Such comparison may also be observed to agree with the comparison between the two types of sample of chapter six (figure 6.3). The room temperature resistivity, for any given sintering batch, of the present samples is approximately double that of samples of the last chapter. For example, the Mn-free samples sintered in 20%O_2 had $\rho_{RT} \simeq 10\Omega$cm and the air-sintered samples of the present batch had $\rho_{RT} \simeq 20\Omega$cm. Maximum resistivity, on the other hand, was more affected by sintering atmosphere, being >2 orders of magnitude larger than the Mn-free samples after sintering in 80%O_2 but only approximately twice ρ_{max} of the previous samples, when sintering took place in 1%O_2. These observations indicate that ρ_{max}, and therefore N_{ao}, are dependent on the quantity of adsorbed oxygen atoms as well as the concentration of added acceptor impurity ions and suggests that the two species combine to create the most effective grain boundary electron traps.

The increase in the value of T_{max} as oxygen partial pressure was reduced is also in agreement with the previous chapter's results, as well as the predictions of the Heywang model[8.4–8.6]. As N_{ao} is reduced, the temperature at which the acceptor states start to depopulate is increased, since ϕ_o is also lower, and this is reflected in higher values of T_{max}.

8.3.3. A.c. impedance measurements

The impedance plots of figure 8.6 show clearly that grain bulk resistance is not affected by the sintering atmosphere, remaining at $\sim 2\Omega$ for all samples. As oxygen concentration was raised, the only effect is exhibited by the grain

boundary resistance, which was raised from ~5Ω after sintering in 2%O_2 to >15Ω when sintering took place in 80%O_2. In addition, the incorporation of the Mn acceptor can be seen, with reference to figure 7.8 for the Mn-free samples of the last chapter, to increase only the grain boundary resistance, demonstrating that the Mn ions have been segregated to the grain boundaries[8.7]. The approximate doubling of the d.c. resistivity with Mn-doping, demonstrated in the resistivity - temperature characteristics of figures 7.4 and 8.3 can be seen to be associated with an approximate doubling of R_{gb} from the a.c measurements.

Assuming the volume of the grain boundaries to be negligible in comparison with that of the grain bulk, ρ_{bulk} was calculated as usual from R_{bulk} and the sample dimensions. N_d was then evaluated from equation 4.26 to be $2.3 \times 10^{18}cm^{-3}$. This value is very close to those of the previous chapters and to the results of other workers[8.8–8.10].

8.4. ANALYSIS OF EXPERIMENTAL RESULTS

8.4.1. Calculation of grain boundary acceptor density

At temperatures between T_c and those of depopulation of the grain boundary acceptor states, resistivity has been shown (chapter 6.4.) to be given, in the absence of normalization of the resistance data, by equation 6.3,

$$\rho = C_o exp(\frac{A(T-\theta)}{T})$$

where A is a constant, given by equation 4.24,

$$A = \frac{e^2 N_{ao}^2}{8\epsilon_o C k N_d}$$

and C_o is constant. In the previous chapters it has been shown that the gradient of an Arrhenius plot of lnρ versus (T - θ)/T is equal to A. Since C, the curie constant, has also been shown (chapter 7.4.1) not to be affected by the sintering atmosphere, N_{ao} can be obtained from A. In accordance with the results for the

Mn-free samples, the gradient, and hence N_{ao}, are expected to become smaller as oxygen partial pressure during sintering was reduced.

Figure 8.7 shows a typical series of plots of ρ, on a logarithmic scale, versus (T - θ)/T for samples sintered in 60%, 20%, 5%, 2% and 1%O_2 atmospheres. Samples sintered in <1%O_2 had very small PTCR characteristics which increased slowly, over long temperature ranges, making accurate measurement difficult. From figure 8.7, however, it is clear that the gradient decreases and the temperature range over which linearity is obtained is extended, as the oxygen concentration during sintering was reduced.

Least - squares analysis of the points lying in straight lines was performed to ensure best estimates of A. Corresponding linear correlation coefficients generated from the statistical analysis were >0.99 for all samples. N_{ao} was calculated for each batch of material using equation 4.27,

$$N_{ao} = \sqrt{\frac{8\epsilon_o C k N_d A}{e^2}},$$

the values of which are listed in Table 8.1 together with A for each sintering atmosphere. N_{ao}, after sintering in >60%O_2, was 9.4 $\times$ $10^{13}cm^{-2}$ and fell to approximately half this value (5.1 $\times$ $10^{13}cm^{-2}$) after sintering in 1%O_2. N_{ao} has been plotted against the logarithm of partial pressure of oxygen in figure 8.8, where linear behaviour between acceptor state density and $\ln p_{O_2}$, similar to that of the last investigation (figure 7.11), is obtained until ~60%O_2. Above this concentration, N_{ao} saturates, in agreement with the behaviour of the Mn-free samples, to ~9.5 $\times$ $10^{13}cm^{-2}$. Least - squares analysis of all of the points of figure 8.8 revealed excellent correlation (r = 0.99) to the solid line, the gradient of which was found to be 9.3 $\times$ $10^{12}cm^{-2}$ and the intercept on the N_{ao} axis was 6.84 $\times$ $10^{13}cm^{-2}$. An empirical relationship between grain boundary acceptor state density and sintering atmosphere was thus obtained for Mn-doped samples,

$$N_{ao}(p_{O_2}) = (9.41 + 0.93 ln(p_{O_2})) \times 10^{13}. \qquad (8.1)$$

Comparison of this relation with that of equation 7.1 shows a certain amount of similarity between the values of the constant, being 9:41 presently and 7.52 in the former chapter, having been increased by ~25%, in agreement with the increase in the value of N_{ao} in the samples of chapter 6. The coefficient of the second term, however, is increased for the present samples, being ~50% larger than that of the Mn-free samples (0.93 compared with 0.61). These results demonstrate the controlling effect of both the segregated Mn ions and the adsorbed oxygen atoms, implying that there is some kind of interaction between the two different species, possibly the activation of the Mn ions by oxygen. This is supported by the increase in the value of the second term of equation 8.1 since, were there no interaction, this term would have been expected to remain constant at ~7 × $10^{13}cm^{-2}$. The higher overall impurity concentration is reflected in the value of the first term of the equation, the oxygen-independent term. The introduction of the additional acceptor ions above those present naturally in the material, whether they are unintentional impurities or barium vacancies, can be seen, therefore, to cause N_{ao} to rise more rapidly with oxygen concentration during sintering.

8.4.2. Calculation of acceptor energy

If interaction between the segregated impurity ions and the adsorbed oxygen atoms takes place at the grain boundaries, the acceptor energy may be expected to be affected by oxygen partial pressure during sintering. E_a can be found from equation 4.32,

$$E_a = \phi_{o(max)} + E_F(T) - kTln(\frac{N_{ao}}{N_a(T)} - 1),$$

where $\phi_{o(max)}$ is the maximum potential barrier height at and above the resistivity maximum. Arrhenius plots of lnρ versus 1/T above T_{max} were drawn, the gradient of which has been shown previously (equation 4.28) to give $\phi_{o(max)}$. Samples sintered in <1%O_2 had very high T_{max} and consequently the Arrhenius plots of lnρ versus 1/T were not linear over a sufficiently large temperature range to ensure

accuracy of the value of $\phi_{o(max)}$ and hence were not included in the analysis. A typical series of such plots for samples sintered in 60%, 20%, 5% and 1%O_2 are shown in figure 8.9, where the gradient, and hence $\phi_{o(max)}$ can be seen to become smaller with a reduction in the partial pressure of oxygen. $\phi_{o(max)}$ is assumed constant above T_{max} so that the the acceptor state density, $N_a(T)$, falls as temperature rises, since (equation 4.29)

$$N_a(T) = \sqrt{\frac{8\epsilon_o C N_d \phi_{o(max)}}{e^2(T-\theta)}}.$$

At a convenient temperature above T_{max} for all samples, $N_a(T)$ was evaluated using this equation, from which $N_a(T)/N_{ao}$ was obtained. The Fermi level was then found from equation 2.7 and E_a estimated using the above (equation 4.32). The temperature chosen for this analysis was 400°C, the same temperature that was selected for the analysis of the Mn-free samples (chapter 7.4.2.) and above T_{max} for all of the present batch. Table 8.2 contains $\phi_{o(max)}$, $N_a(400°)$, N_a/N_{ao} and E_a obtained for samples sintered in 1 - 100%O_2. The Fermi level at 400°C was 0.511eV. Firstly, it can be seen that $\phi_{o(max)}$ decreases as oxygen concentration was reduced between 60 and 1%O_2, from 0.86eV to ~0.2eV, reflecting the reduction in N_{ao} (table 8.1 and figure 8.8). Secondly, and more dramatically, however, is the reduction in the value of E_a, from $\geq$1.4eV after sintering in 60%O_2, to ~0.8eV with 1%O_2 concentration. These values are all in agreement with E_a estimated in the literature[8.5,8.6,8.8,8.11,8.12] and suggest that some kind of interaction indeed takes place between the acceptor species such that, where there is a large number of both segregated impurities and adsorbed oxygen atoms, E_a is large. This reduction in E_a at low oxygen concentrations implies that both types of grain boundary acceptor, i.e. oxygen and impurity ions, must be present for the creation of the most effective electron traps, possibly because the Mn ions are activated by oxygen.

E_a may be plotted against oxygen partial pressure to demonstrate the effect of sintering atmosphere on acceptor energy, as shown in figure 8.10. Least - squares

analysis of the points revealed excellent correlation to the solid line, with r = 0.92, and resulted in the derivation of the following empirical relationship,

$$E_a = 1.44 + 0.17 ln p_{O_2}. \tag{8.2}$$

The points, however, may also be considered to follow the broken line, which belongs to least - squares analysis of the intermediate ones, i.e. those representing sintering in 5 - 60%O_2. The relationship thus obtained is,

$$E_a = 1.65 + 0.30 ln p_{O_2}. \tag{8.3}$$

At high values of oxygen partial pressure, i.e during sintering in 80 and 100%O_2, the amount of oxygen required for the formation of effective grain boundary electron traps may be considered to be exceeded, resulting in the saturation of E_a. At very low oxygen partial pressures, on the other hand, E_a is higher than expected, suggesting that either the measurement of $\phi_{o(max)}$ was too inaccurate as a result of the small temperature range available, or that the inherent acceptor states (unintentional impurities and barium vacancies) combine with the segregated Mn ions to form more effective electron traps, similar to those created in the presence of oxygen.

8.5. CONCLUSION

The oxygen partial pressure during sintering has been shown to dominate both the values of acceptor state density and acceptor energy in manganese acceptor doped samples. As p_{O_2} was reduced, ρ_{max} fell and T_{max} increased, in the same way as for the Mn-free samples of the last chapter. Grain bulk resistance and hence N_d were unaffected by the sintering atmosphere, showing only the grain boundary layer characteristics to be modified. Analysis of the experimental results showed that the grain boundary acceptor state density is dependent of the logarithm of oxygen partial pressure during sintering and resulted in the derivation

of an empirical relationship between N_{ao} and $\ln(p_{O_2})$. Calculation of the acceptor energy revealed a dependence on oxygen concentration during sintering, with E_a reducing from 1.4eV after sintering in 60%O_2, to ~0.8eV in 1%O_2. An empirical relationship between E_a and $\ln(p_{O_2})$ was also derived for oxygen atmospheres between 5 and 60% O_2, where it was suggested that the Mn ions are activated by the oxygen atoms to create the most effective electron traps. Deviation from this relationship at low concentrations of oxygen was suggested to be due to the combination of Mn and other acceptor - like impurities and at high amounts of oxygen, to the saturation of the electron traps.

REFERENCES

8.1 Drofenik M., Popvic A., Irmancnik L, Kolar D. and Krasevec V., J. Am. Ceram. Soc., **65**, C203, 1982.

8.2 Drofenik M., J. Am. Ceram. Soc., **69**, C8, 1986.

8.3 Jonker G.H., Mater. Res. Bull., **2**, 401, 1967.

8.4 Heywang W., Sol. Stat. Electron., **3**, 51, 1961.

8.5 Heywang W., J. Am. Ceram. Soc., **47**, 484, 1964.

8.6 Heywang W., J. Mater. Sci., **6**, 214, 1971.

8.7 Xue L.A., PhD Thesis, University of Leeds, 1987.

8.8 Ihrig H. and Puschert W., J. Appl. Phys., **48**, 3081, 1977.

8.9 Al-Allak H.M., Brinkman A.W., Russell G.J. and Woods J., J. Appl. Phys., **63**, 4530, 1988.

8.10 Xue L.A., Chen Y. and Brook R.J., Mater. Sci. Eng., **B1**, 193, 1988.

8.11 Jonker G.H., Sol. Stat. Electron., **7**, 895, 1964.

8.12 Daniels J., Härdtl K.H. and Wernicke R., Phil. Tech. Rev., **38**, 73, 1978/79.

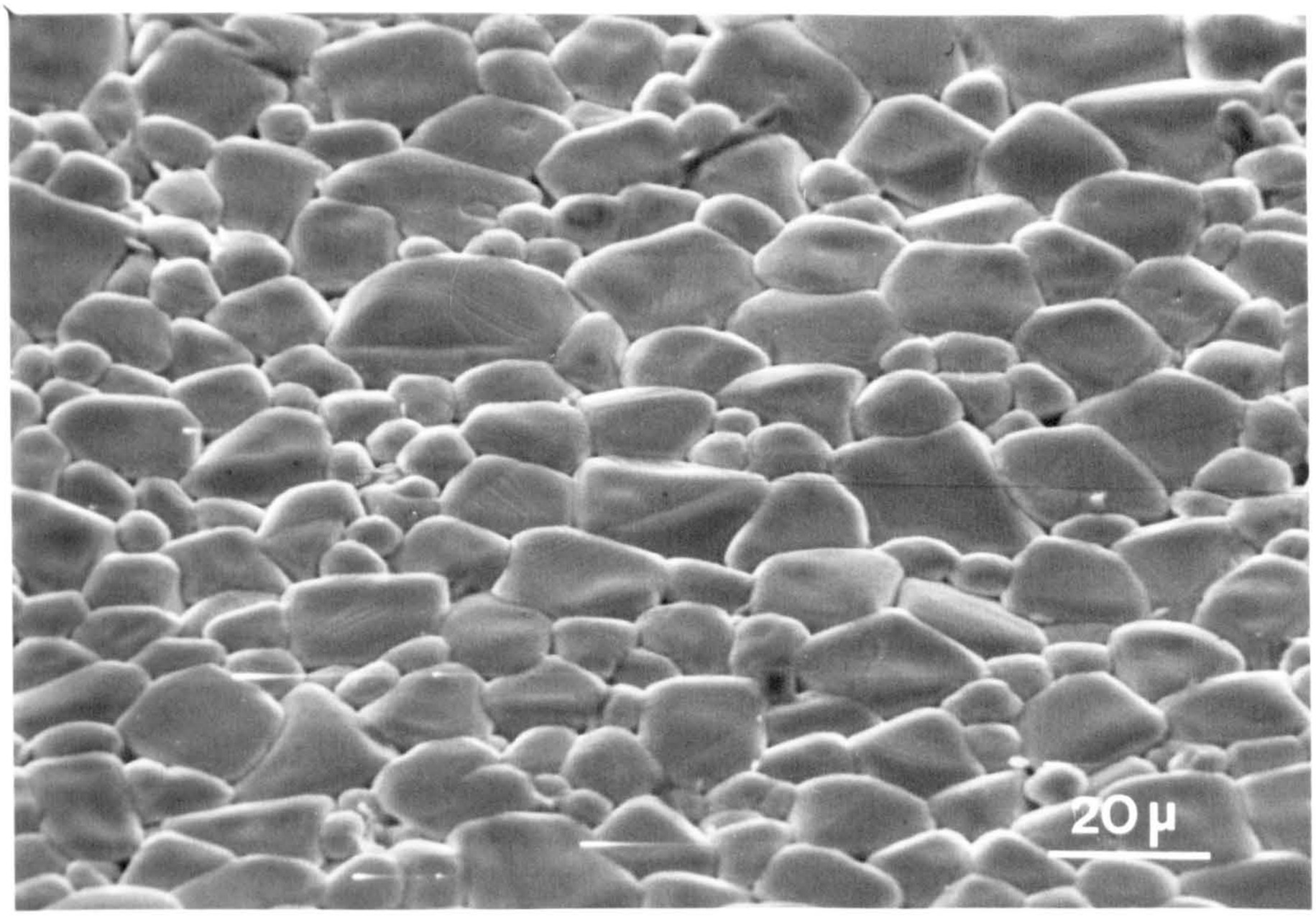

Figure 8.1 Scanning electron micrograph of a typical sample sintered in 0.5% O_2 (bar = 20μm).

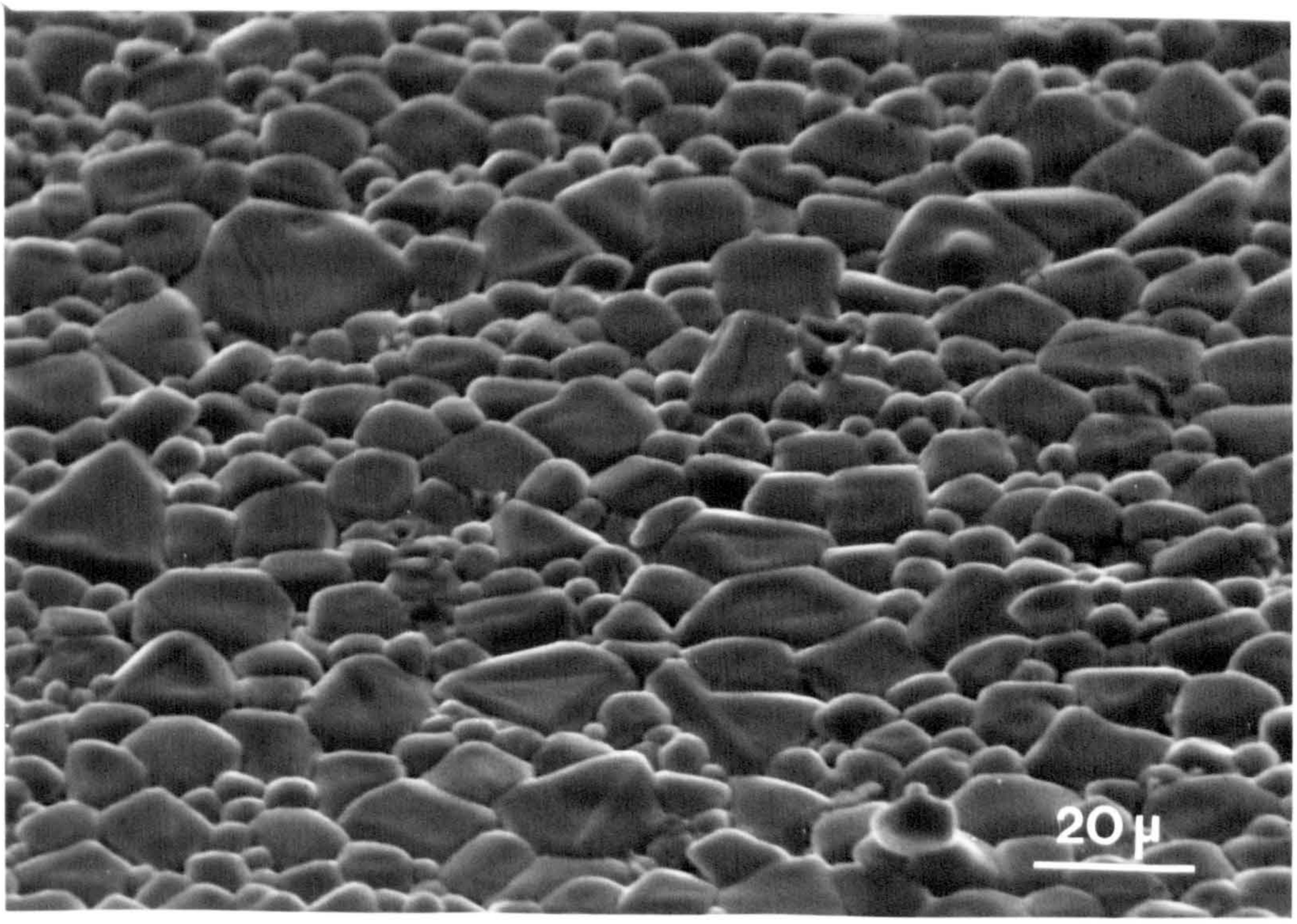

Figure 8.2 Scanning electron micrograph of an area of a sample sintered in 40% O_2 (bar = 20 μm).

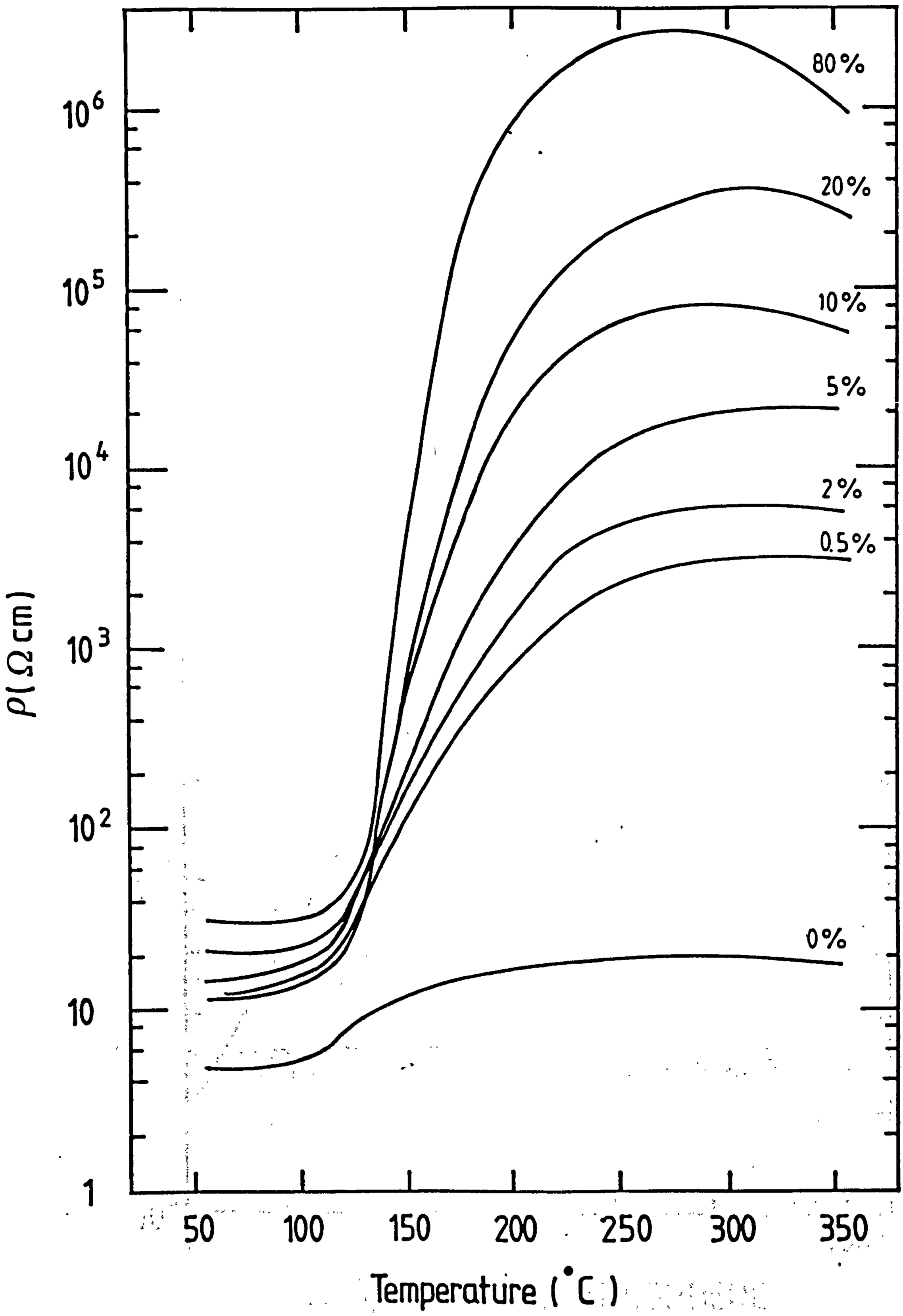

Figure 8.3 Resistivity - temperature characteristics for samples sintered in atmosphere containing between 80% and 0% O_2.

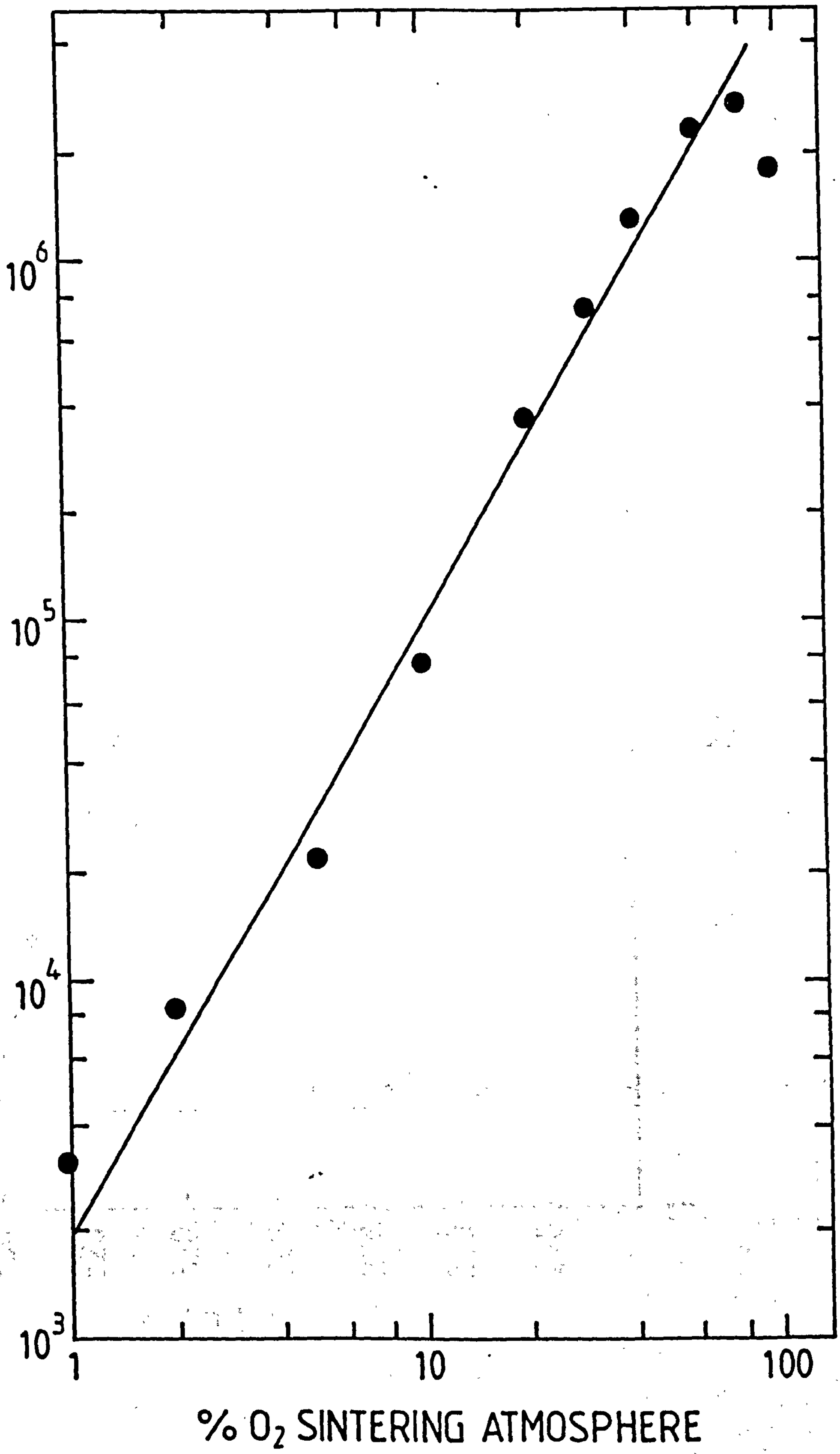

Figure 8.4 Effect of sintering atmopshere on ρ_{max}.

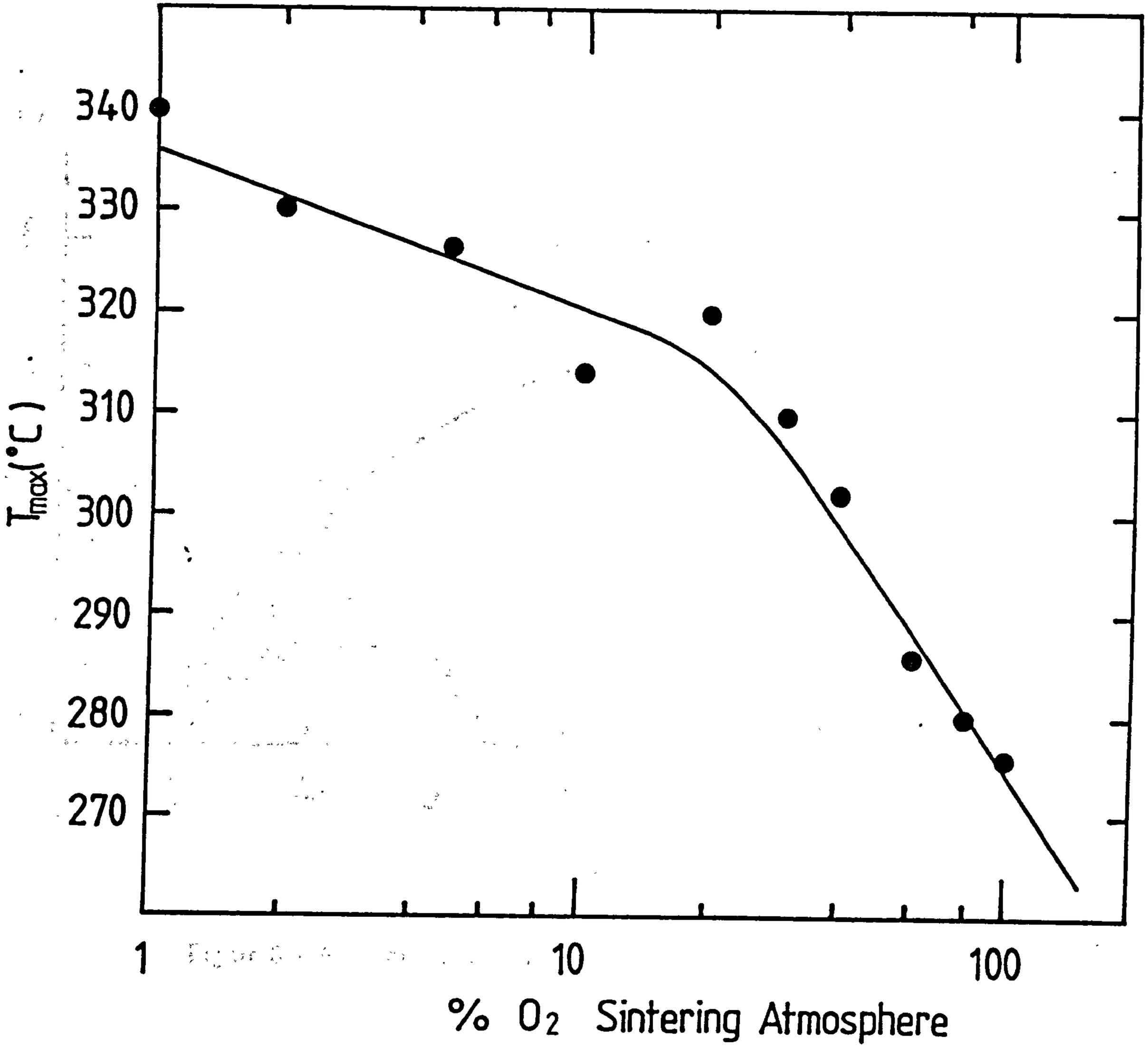

Figure 8.5 Effect of sintering atmosphere on T_{max}.

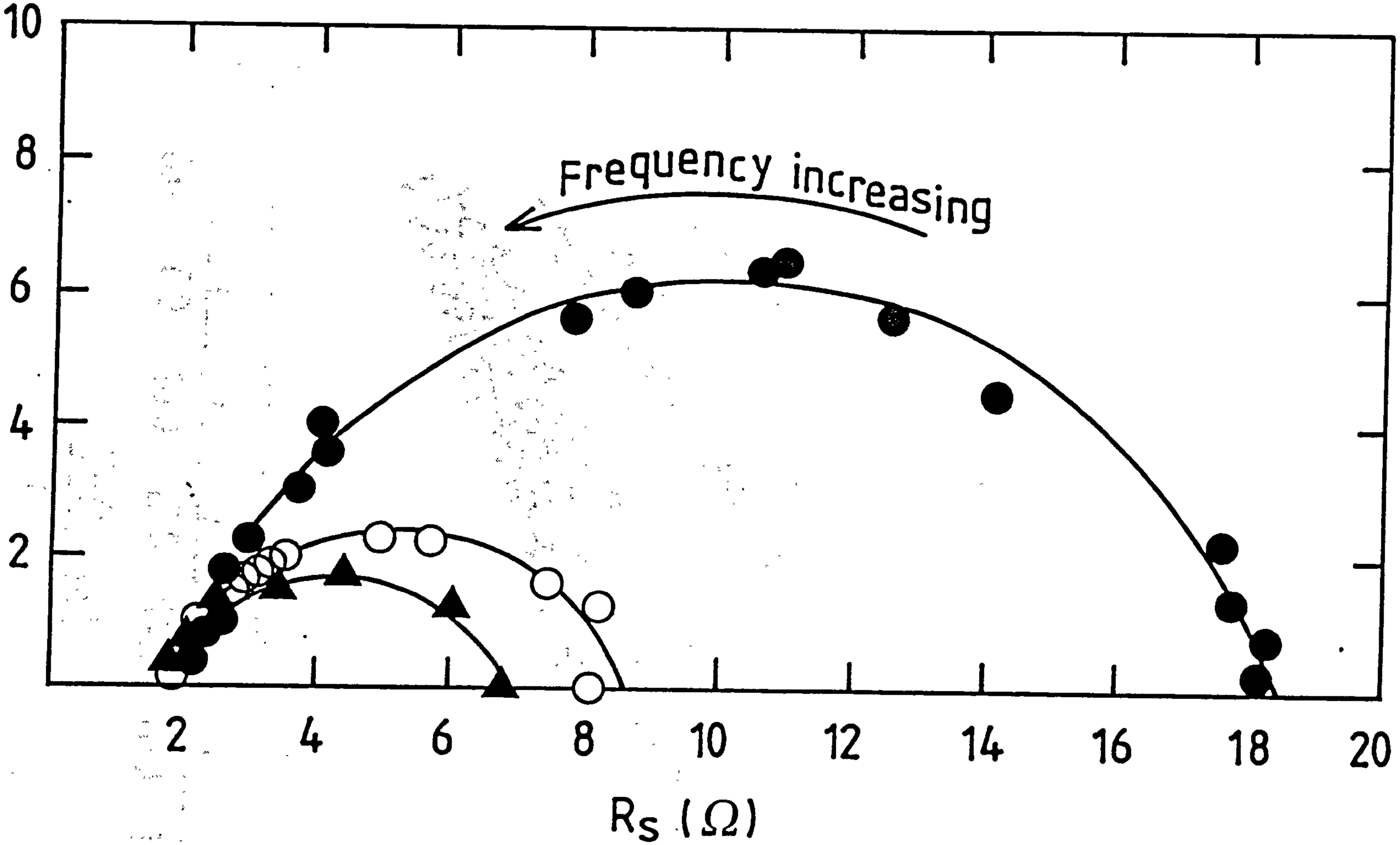

Figure 8.6 A.c. impedance plots for samples sintered in 80% (•), 10% (o) and 2% (△) O_2.

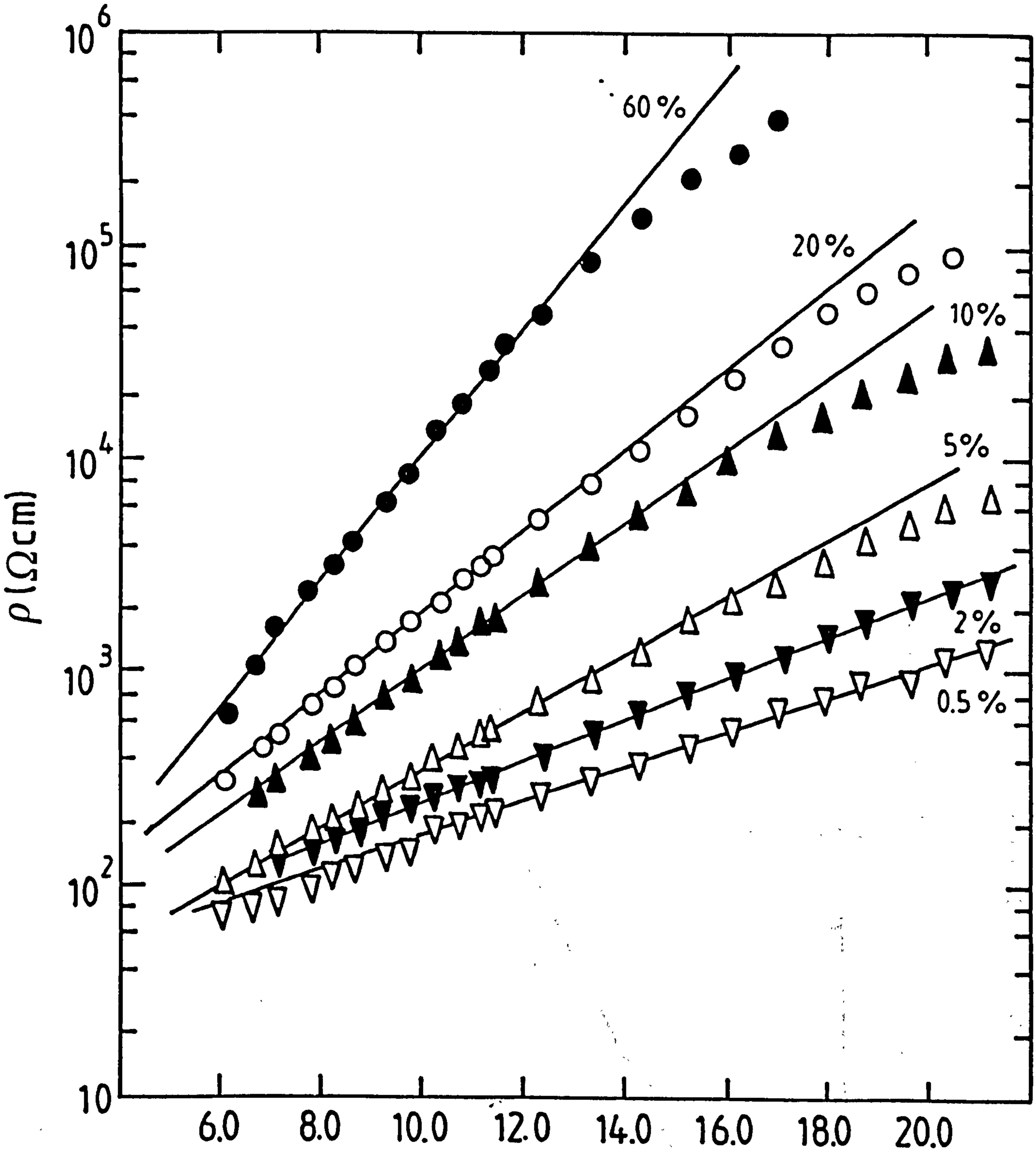

Figure 8.7 Lnρ versus (T - θ)/T for samples sintered in 60% (•), 20% (o), 10% (▲), 5% (△), 2% (▼) and 0.5% (▽) O_2.

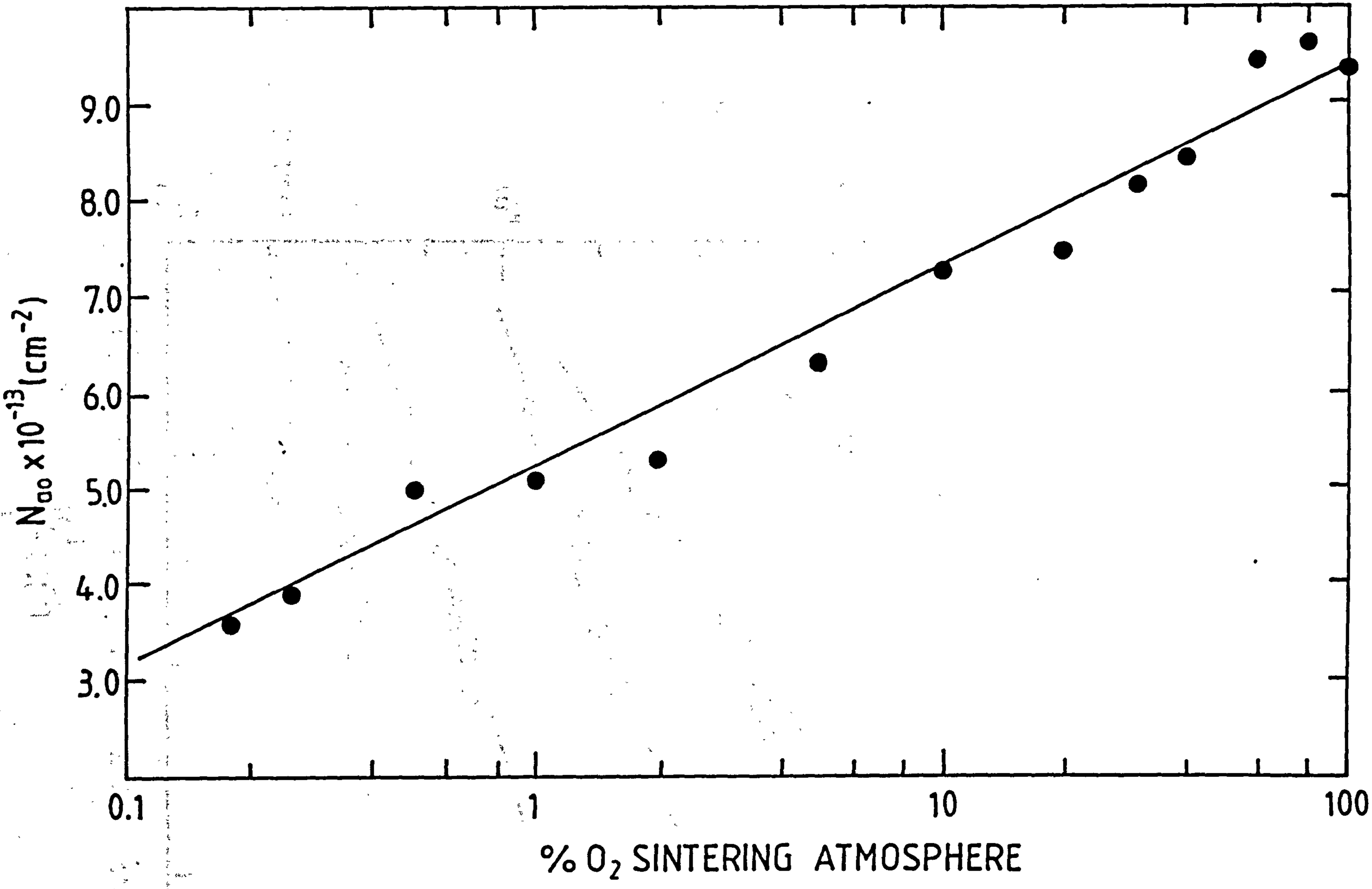

Figure 8.8 Effect of sintering atmosphere on grain boundary acceptor state density.

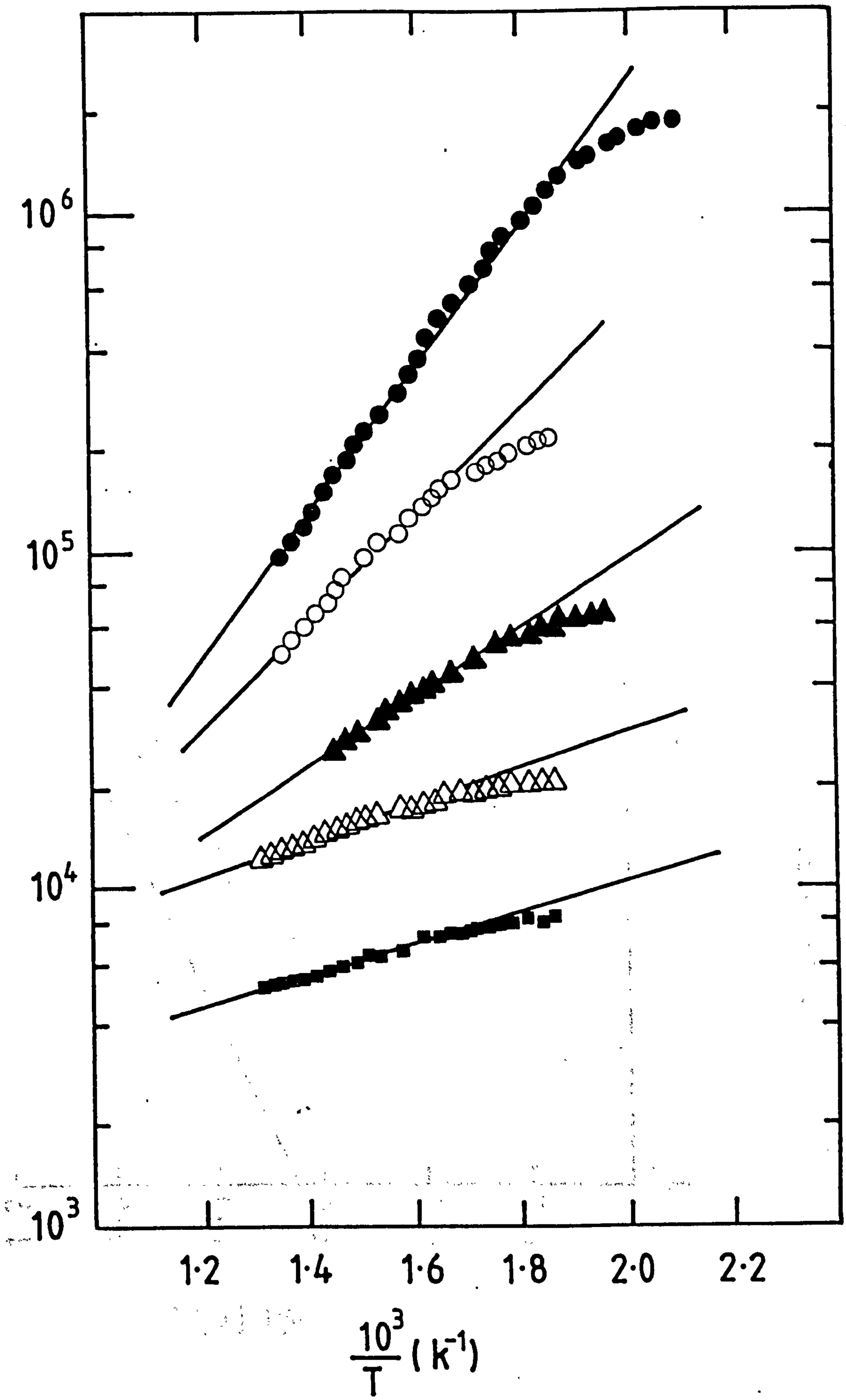

Figure 8.9 Lnρ versus 1/T above T_{max} for samples sintered in 60% (•), 20% (o), 10% (▲), 5% (△) and 2% (■) O_2.

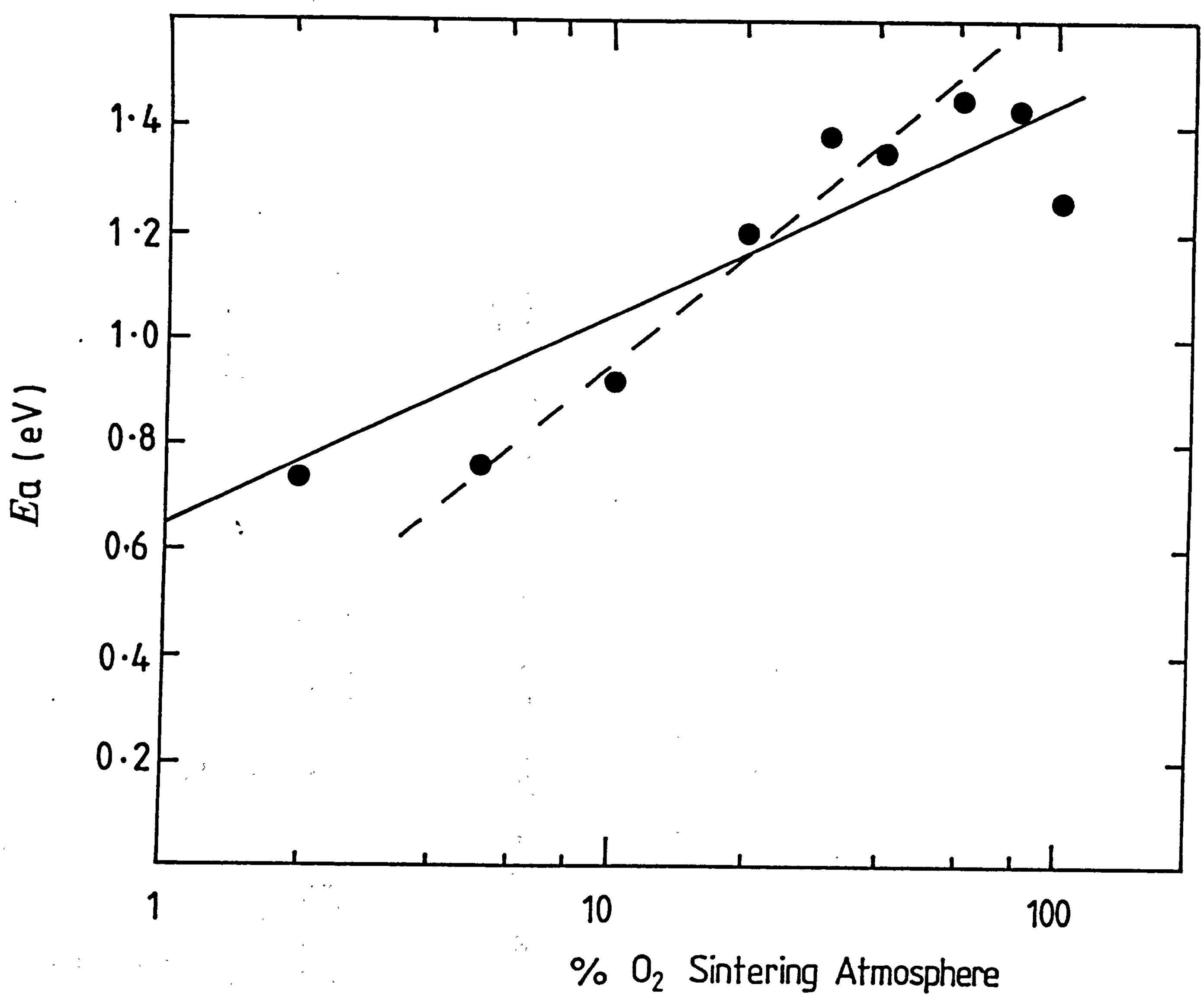

Figure 8.10 Effect of oxygen concentration on acceptor energy.

% O_2 Sintering Atmosphere	A	N_{ao} (cm^{-2})
100	66.45	9.35×10^{13}
80	70.82	9.65×10^{13}
60	67.48	9.42×10^{13}
40	53.96	8.42×10^{13}
30	50.71	8.16×10^{13}
20	42.06	7.44×10^{13}
10	40.12	7.26×10^{13}
5	29.99	6.28×10^{13}
2	22.04	5.38×10^{13}
1	19.68	5.09×10^{13}
0.5	18.84	4.98×10^{13}
0.25	11.48	3.88×10^{13}
0.18	9.72	3.57×10^{13}

TABLE 8.1

Slope of the Arrhenius plots of $\ln\rho$ versus $(T-\theta)/T$ and total ionized grain boundary acceptor state density, for all samples.

% O_2 Sintering Atmosphere	ϕ_o (max) (eV)	N_a(400°C) (cm^{-2})	N_d/N_{ao}	E_a (eV)
100	0.69	6.07×10^{13}	0.65	1.26
80	0.85	6.74×10^{13}	0.70	1.43
60	0.86	6.80×10^{13}	0.73	1.45
40	0.76	6.38×10^{13}	0.76	1.35
30	0.77	6.43×10^{13}	0.79	1.38
20	0.60	5.68×10^{13}	0.76	1.20
10	0.36	4.38×10^{13}	0.60	0.92
5	0.21	3.35×10^{13}	0.53	0.76
2	0.17	3.05×10^{13}	0.57	0.73
1	0.20	3.26×10^{13}	0.64	0.77

TABLE 8.2

Maximum grain boundary potential barrier height, acceptor state density at 400°C and acceptor energy, for samples sintered in >1% O_2.

CHAPTER NINE

SUMMARY AND CONCLUSIONS

Throughout this project the Heywang model has been utilized for the analysis of experimental results of electric and dielectric measurements on donor doped barium titanate ceramics, prepared in a number of different ways. This analysis has enabled the examination of the grain boundary layers, in particular, the acceptor state density and the acceptor energy, the two parameters which, according to Heywang, control the PTCR effect. The conclusions arrived at from each different part of this project are summarised below.

1. The magnitude and shape of the PTCR characteristic is strongly dependent on composition. As donor concentration was increased from 0.05 to 1.8 at%Ho, for samples sintered at 1460°C, normalised room temperature and maximum resistance described a broad minimum in value, between 0.4 and ~1.2 at%Ho. On the other hand, the temperature of the maximum described a broad maximum in value, around similar doping concentrations. A.c. impedance plots at room temperature indicated that the minimum in room temperature normalised resistance was due entirely to grain boundary effects.

Dielectric measurements revealed an increase of over an order of magnitude in the value of apparent relative permittivity on the incorporation of the smallest amounts of donor dopant. This was increased further, by an order of magnitude, as doping levels were raised towards ~0.5 at%Ho concentration. Apparant permittivity at room temperature and above the transition temperature was also found to describe a maximum in value, between 0.4 and ~1.0 at%Ho concentration. Assuming each grain boundary layer to consist of a parallel combination of resistance and capacitance, expressions for the impedance of the whole sam-

ple were used to describe the apparent permittivity in terms of grain boundary permittivity. It was then found that the effect of donor concentration was due entirely to modifications to the grain boundary layers with increasing doping and that the permittivity of the layers themselves was described by the Curie-Weiss law.

Analysis of the normalised resistance measurements in terms of the Heywang model resulted in the calculation of estimates of grain boundary potential barrier height and acceptor state density. Both were found to describe a broad minimum between 0.5 and ~1.0 at%Ho, in agreement with the results of the normalised resistance. Maximum grain boundary potential barrier height was estimated from the normalised resistance - temperature characteristics above the maximum, from which acceptor state density was obtained at a convenient temperature. Equation 2.6 was then utilized to estimate grain boundary acceptor energy. This was found to be 0.9 ±0.1eV for all samples, independent of donor concentration. This was in contrast to what was expected, since the nature of the acceptor states has always been believed, in the literature, to be affected by donor concentration.

As donor concentration was increased, the average grain size was reduced by approximately an order of magnitude, quickly at first, between 0.05 and ~0.3 at%Ho, then slowly above this doping level. It was found that, above 0.4 at%Ho concentration, the total surface charge per grain was dependent on the total surface area per grain, from which the increase in grain boundary acceptor state density was attributed to the supression of donor incorporation and grain growth at these higher doping levels.

2. Electric and dielectric results from samples containing donor concentrations between 0.05 and 0.8 at%Ho, sintered at a lower temperature (and found to have smaller grains) were observed to agree qualitatively with the results of the first set of samples, sintered at the higher temperature. The minima in normalised

resistance and the maximum in the temperature at which the normalised resistance maximum took place were present, but were more narrow and were shifted towards lower dopant concentrations, being centred around 0.3 - 0.4 at%Ho. The sample doped with 0.8 at%Ho had very high normalised room temperature resistance and described an NTCR characteristic with a flattened region between 110 and ~150°C. The characteristic belonging to the sample doped with 0.6 at%Ho was intermediate in shape between PTCR and NTCR, having a steep NTCR below the transition and a short, steep PTCR between T_c and ~160°C.

The dielectric measurements revealed a maximum in apparent permittivity below and above the transition temperaure, which was also shown to be due to the presence of the thin grain boundary layers. A.c. impedance measurements, like those of the previous samples, demonstrated the effect of donor concentration on the normalised room temperature resistivity to be entirely due to the grain boundaries.

Analysis of the permittivity and resistance measurements showed the minima in normalised resistance to be reflected in a mininum in the value of grain boundary acceptor state density. Normalised resistance above the maximum enabled the calculation of the maximum potential barrier height for each composition, from which the acceptor energy was eventually obtained. This was found, as for the previous samples, to be unaffected by donor concentration, at 0.85 ±0.1eV. The normalised resistance - temperature characteristics of the samples doped with 0.6 and 0.8 at%Ho were analysed and found to be due to high residual grain boundary potential barriers below the transition temperature. The sample containing 0.6 at%Ho had its NTCR behaviour between room temperature and T_c in accordance with an activation energy of 0.2eV, while the sample doped with 0.8 at%Ho had an activation energy of 0.5eV, due presumably to the presence of a very large number of acceptor states. Comparison of values of potential barrier estimated so far in the project showed that the sample containing 0.5eV had a residual grain

boundary potential barrier higher than many samples obtain at the maximum. Hence, any PTCR effect taking place at the grain boundaries was obscured. The sample containing 0.6 at%Ho had a sufficiently small residual potential barrier to enable the PTCR effect above T_c to be observed.

3. The addition of a small amount of manganese to a standard composition and incorporated into the $BaTiO_3$ lattice on Ti^{4+} sites with +2 valency, i.e. which acts as a acceptor, was found to increase the magnitude of the PTCR characteristic significantly. Room temperature resistivity was approximately doubled, maximum resistivity increased by nearly $1\frac{1}{2}$ orders of magnitude and the temperature of the maximum raised by ~40°C. A.c. impedance measurements at room temperature showed a doubling of grain boundary resistance and no change to the grain bulk resistance, demonstrating the effect of the Mn doping to be due entirely to the grain boundaries. It was thus assumed that all of the Mn ions were segregated to the grain boundaries. Apparant permittivity of the Mn-doped sample was lower than that of the Mn-free sample, below the transition, demonstrating the modification to the grain boundary layers.

Detailed analysis of the resistivity measurements in terms of the Heywang model revealed an increase in the value of grain boundary acceptor state density of ~25% after Mn-doping and an increase in the acceptor energy, from 1.0eV to 1.4eV. This was in line with the predictions of the Heywang model since an increase in the acceptor state density is expected to be reflected in maximum resistivity and the rise of resistivity with temperature between T_c and the maximum. An increase in acceptor energy causes the depopulation of the acceptor states to take place at higher temperatures, hence the resistivity maximum is also found at a higher temperature. The change in the value of acceptor energy demonstrated the nature of the Mn ions to be acceptor-like, since all samples used were prepared identically and therefore contained the same number of inherent impurities and

other acceptor states.

4. The magnitude and shape of the PTCR characteristic, for samples of the same composition, is dependent on the sintering conditions. This was intially apparent with samples doped with the same donor concentration, sintered at 1460 and 1420°C, particularly those containing 0.8 at%Ho. In addition to these observations, samples sintered in different amounts of oxygen exhibited PTCR characteristics, the magnitude and shape of which were dependent on the partial pressure of oxygen. As the oxygen concentration was reduced from 100 to 0.18%, the maximum resistivity of samples doped with 0.4 at%Ho fell by ~2 orders of magnitude and the temperature of the maximum gradually increased, both in accordance with $\ln p_{O_2}$. A.c. impedance plots revealed that the effect of the sintering atmosphere was exhibited only within the grain boundary layers. In addition, apparent permittivity rose with $\ln p_{O_2}$ as oxygen concentration was reduced, demonstrating the effect of sintering atmosphere on the grain boundary layers. It was also shown that the permittivity of the material within the grain boundary layers was unaffected by the sintering atmosphere.

Detailed analysis of the resistivity measurements revealed that the grain boundary acceptor state density was dependent on the partial pressure of oxygen during sintering and the following empirical relationship between N_{ao} and $\ln p_{O_2}$ was derived:

$$N_{ao}(p_{O_2}) = (7.52 + 0.608 ln(p_{O_2})) \times 10^{13}.$$

Above the resistivity maximum, the maximum potential barrier height was estimated and used to find values of acceptor energy, as usual. This was found to be unchanged by sintering atmosphere, remaining constant at 0.9 ±0.1eV. These results demonstrated the dominant nature of adsorbed oxgyen atoms on the grain boundary layer characteristics.

5. The PTCR characteristic was found to be dependent on sintering atmosphere in samples additionally doped with a small amount of Mn acceptor. As the amount of oxygen in the sintering atmosphere fell from 100% to 0.18%, the magnitude of the PTCR characteristic fell by 3 - 4 orders of magnitude and the temperature of the resistivity maximum gradually increased. At room temperature the resistivity of the samples was approximately twice that of the corresponding Mn-free samples, and the PTCR characteristic extended to higher resistivities and temperatures, in general agreement with the results of the initial Mn-doping study. Maximum resistivity fell and the temperature of the maximum increased in accordance with $\ln p_{O_2}$, in a similar manner to the Mn-free samples.

Analysis of the resistivity measurements led to an empirical relationship between the grain boundary acceptor state density and partial pressure of oxgyen:

$$N_{ao}(p_{O_2}) = (9.41 + 0.93ln(p_{O_2})) \times 10^{13},$$

showing the requirement for the presence of adsorbed oxygen in addition to the Mn ions, and the residual acceptor state density to be higher in the Mn-doped samples. Estimates of the acceptor energies revealed that the oxygen partial pressure affected the nature of the electron traps such that, as oxygen concentration was reduced, so was the acceptor energy. This was proposed to be due to interaction between the Mn ions and oxygen, possibly as a result of the need for the ions to be activated in some way by oxygen for the creation of the most effective acceptor states.

6. The nature of the grain boundary acceptor states in donor doped barium titanate ceramics is clearly dependent on the partial pressure of oxygen during sintering and the impurity concentration. The density of the acceptor states is dependent on these factors and the grain size. Where grain size was reduced in donor doped samples, by sintering at a lower temperature, the acceptor state density was increased slightly, presumably because of the larger total surface area

per grain but there was no effect on the acceptor energy, indicating no change to the nature of the electron traps. Incorporation of ions which act as acceptors, segregating to the grain boundaries, increases the acceptor state density and energy above that present naturally in the material, without affecting the grain size. Acceptor energy has been found only to be affected in samples additionally doped with acceptor ions and sintered in low concentrations of oxygen (<10%), where there is assumed not to be sufficient oxygen present to activate the Mn ions and to create the most effective and deep electron traps.

7. Investigation of the current - voltage characteristics above the transition temperature and below the resistivity maximum, of samples containing different donor concentrations was carried out to find the current conduction mechansim. This was found to be described most suitably by simple diffusion, in contrast to the prediction of Heywang who believed it to be thermionic emission. Where samples deviated from the simple ideal diffusion mechanism, it was assumed that the current passing across the grain boundary layers caused self-heating and inaccuracies in the measurements.

Finally, the work described in this thesis has shown the validity of the Heywang model to describe sufficiently accurately the PTCR effect in donor doped barium titanate ceramics. Samples containing different impurity concentrations (donor and acceptor), prepared in various ways, have been used to demonstrate the sensitivity of the PTCR characteristic on the preparation of the material. Grain boundary acceptor state density and energy were found for each type of sample and found also to be sensitive to sample preparation and composition. The control of these parameters by a suitable choice of composition and sintering regime is therefore necessary for the control of the PTCR characteristic.

UNIV DUNDEE